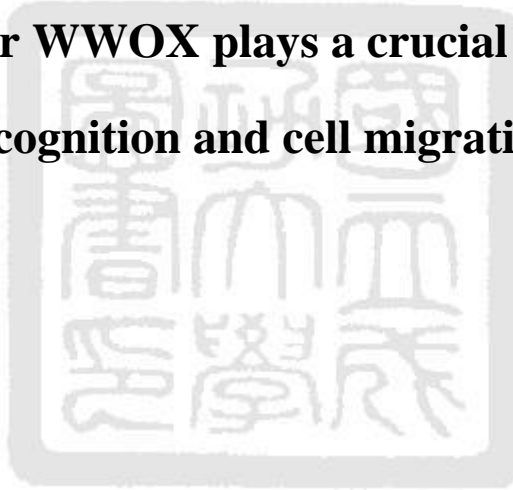


國立成功大學  
分子醫學研究所  
碩士論文

腫瘤抑制子 WWOX 在細胞間的識別與  
細胞移行中扮演重要的角色

**Tumor suppressor WWOX plays a crucial role in cell-to-cell  
recognition and cell migration**



研究生：陳俞安

指導教授：張南山 博士

中華民國一百零二年六月

國立成功大學

碩士論文

腫瘤抑制子WWOX在細胞間的識別與細胞移行中扮演  
重要的角色

Tumor suppressor WWOX plays a crucial role in  
cell-to-cell recognition and cell migration.

研究生：陳俞安

本論文業經審查及口試合格特此證明

論文考試委員：張名揚

劉校生

徐麗君

執行 賴明德

指導教授：張名揚

系(所)主管：張名揚

中華民國 102 年 7 月 15 日

## Abstract

Neurofibromatosis type 1 and 2 are very rare diseases. There are no curable treatments have been developed. Transforming growth factor beta (TGF- $\beta$ ) plays a critical role in tissue homeostasis. Excessive activity of TGF- $\beta$  tends to generate fibrosis. TGF- $\beta$  and growth factors control the growth and development of neurofibromas in Neurofibromatosis type 1 (NF1), as well as in neurodegeneration.

In this study, we determined that tumor suppressor WWOX/WOX1 is downregulated, and transforming growth factor  $\beta$  (TGFC-induced TIAF1, TRAPPC6A (TPC6A), and SH3GLB2 (or Bif-2), are upregulated in the NF1 tumors. Those proteins tended to undergo self-aggregation in cancer and formed a peritumor capsule which is benefit for cancer growth. We also demonstrated that aggregated TIAF1 inhibited SMAD4 promoter activity by binding with SMAD4 protein.

Importantly, we clarified how tumor suppressor WOX1 regulates cell migration and cell-to-cell recognition. Tumor suppressor WWOX is frequently deficient in metastatic cancer cells. *Wwox*<sup>-/-</sup> MEF cells migrated individually, however, wild type *Wwox*<sup>+/+</sup> MEF cells migrated collectively. Remarkably, when wild type *Wwox*<sup>+/+</sup> MEF cells met *Wwox*<sup>-/-</sup> MEF cells, they failed to recognize each other, the knockout cells stretched out with their pseudopodia to touch the wild type cells, and then move in a retrograde manner, followed by dividing immediately.

Molecular analysis also revealed that when cells overexpressing WWgre (WOX1 7-21), a short *N*-terminal segment of WWOX, and they attracted visiting cells. In contrast, if they overexpressed SDRrepl (WOX1 286-299), a short segment in the *C*-terminal SDR domain, they repelled the visiting cells. Specific antibodies against SDRrepl or WWgre blocked the WWOX-regulated cell recognition effects. FRET analysis showed that upon activation, WWOX may undergo conformational changes, thus leading to inter- or intra-molecular interactions via WW and/or SDR domain interaction or self-binding.

Accordingly, under the pressure of metastasis, surface WWOX disappears from cancer cells. These cells are no longer recognized by the parental cancer cells, and thus repelled from the cancer mass. These repulsed cells look for WWOX-negative sites in organs for docking and homing.

Abbreviation: NF1, TGF- $\beta$ , WWOX, WWgre, SDRrepl, retrograde

## 致謝

「莫忘初衷」猶如在耳，兩年前，我懷抱著憧憬與熱忱踏入成大校園，榕園的綠茵在陽光與水的滋潤下搖曳青翠，而我就像那小草望著大榕樹，期待著…發芽展枝！

研究是旅程，而實驗就像沿途的風景，走過的每一吋酸甜苦辣，都讓我回味無窮。感謝一路上知心的夥伴，教我在迷惘時蓄勢待發，不以物喜不以己悲。感謝一路上拔刀相助的貴人，助我克服面臨的艱難與無助。感謝一路上家人的愛與包容，照亮我在學海中每個風雨的黑夜。感謝動物老師們的犧牲奉獻，讓我了解到生命的真諦。

時光荏苒，在張南山教授的引領下，獲益良多，紮實的訓練與諄諄教誨，給予我迎向未來旅程的力量與勇氣。

畢業了，揹著滿載的感謝啟程了！

### 感謝

張南山老師實驗室成員：貞仔、永達、何歡、宇欣、Liz、榆文、沛宜、似蓉、Annie、婉嬪、若婷、秀汝、政璋、景雲、聖翔

徐麗君老師實驗室成員：映岑、瑞燕

### 感謝

財團法人罕見疾病基金會 頒予 2013 博碩士論文獎助

國立成功大學醫學院 頒予 2013 藥理生理與訊息傳遞組博碩士論文競賽 優勝

中華民國斐陶斐榮譽學會 頒予 榮譽會員

# Table of contents

<b>Abstract</b> .....	<b>I</b>
致謝.....	<b>II</b>
<b>Table of Contents</b> .....	<b>III</b>
<b>Index of Figures</b> .....	<b>VI</b>
<b>Abbreviation</b> .....	<b>IX</b>
<b>Introduction</b> .....	<b>1</b>
Neurofibromatosis.....	1
WW domain-containing oxidoreductase WWOX/WOX1 .....	2
WWOX suppresses tumorigenesis .....	4
Down-regulation of WWOX in cancer cells .....	6
WWOX is not just a tumor suppressor .....	8
TGF- $\beta$ 1-induced antiapoptotic factor (TIAF1).....	10
TRAPP Complex Subunit 6A .....	11
TGF $\beta$ signaling pathway and cancer progression.....	12
Cell migration and cancer metastasis.....	14
<b>Materials and Methods</b> .....	<b>18</b>
Cell lines and cell culture.....	18
Stable transfectants .....	19
cDNA constructs and electroporation.....	20
Chemicals and antibodies .....	21
Synthetic peptides and antibodies.....	21
Cell migration assay and time-lapse microscopy .....	22
Tissue microarrays and human cancer tissue sections.....	23

Immunofluorescent staining .....	24
Quantification of fluorescent images/Confocal Microscopy .....	25
Confocal Microscopy.....	25
Immunohistochemistry staining.....	26
Förster (Fluorescence) Resonance Energy Transfer (FRET).....	26
Cell cycle analysis.....	28
Soft agarose colony formation assay .....	28
2D invasion assay .....	29
Transwell invasion assay .....	29
UVB irradiation on hairless mouse skin .....	30
Animal experiment.....	31
Statistical analysis .....	31
<b>Results .....</b>	<b>32</b>
Expression of WOX1, TIAF1, TPC6A and Bif-2 in the cutaneous NF1 neurofibromas .....	32
TIAF1 aggregates in cancer cells.....	32
TIAF1-/Smad4-binding induces generation of amyloid precursor protein (APP) and A $\beta$ .....	34
TRAPPC6A (TPC6A) trafficking and intracellular self-aggregation.....	35
SH3GLB2/Bif-2 aggregation.....	36
Tumor suppressor WWOX in cell migration and cell-to-cell recognition .....	38
Molecular dissection of WWOX: two faces of WWOX in cell migration and cell-to-cell recognition.....	40
SDRrepl antibodies abolish SDRrepl function, and alter cell retrograde migration	42
TGF $\beta$ 1 induces WWOX and TGF- $\beta$ type II receptor (T $\beta$ RII) to relocate into cytoplasm and alters WWOX-mediated cell-to-cell recognition.....	44
Conformational alteration of WWOX may play a role in cell-to-cell recognition...	46
SDRrepl and TGF $\beta$ participate in the regulation of cell invasion .....	47
WWOX inhibits anchorage-independent cell growth of MDA-MB-231 breast cancer cells.....	48
WWOX regulates cancer cells metastasis <i>in vivo</i> .....	49
Self-polymerizing Zfra peptides elicit T cell-independent immune response for targeting cancer .....	50

**Discussions** ..... 52

**References** ..... 57

**Figures**..... 66



## Index of Figures

<b>Figure 1. Schematic diagram of WWOX structure and designed peptides .....</b>	<b>66</b>
<b>Figure 2. Expression of WOX1, TIAF1, TPC6A and Bif-2 in the cutaneous NF1 neurofibromas. ....</b>	<b>67</b>
<b>Figure 3. TIAF1 protein expression is significantly increased in prostate cancer. ....</b>	<b>68</b>
<b>Figure 4. TIAF1 colocalizes with Smad4 in prostate cancer. ....</b>	<b>71</b>
<b>Figure 5. TIAF1 overexpression, aggregation and super-induction of A<math>\beta</math>.....</b>	<b>72</b>
<b>Figure 6. TIAF1 self-association induces expression of Smad4.....</b>	<b>74</b>
<b>Figure 7. TIAF1-/Smad4-binding induces generation of amyloid precursor protein (APP) and A<math>\beta</math>. ....</b>	<b>75</b>
<b>Figure 8. TPC6A protein aggregation in subcellular compartment. ....</b>	<b>76</b>
<b>Figure 9. TGF-<math>\beta</math>1 induces Bif-2 aggregation.....</b>	<b>77</b>
<b>Figure 10. Bif-2 EM and 3D morphologies.....</b>	<b>78</b>
<b>Figure 11. WWOX senses extracellular cues.....</b>	<b>79</b>
<b>Figure 12. Cell migration assay. ....</b>	<b>81</b>
<b>Figure 13 Cell growth arrest in the assay for migration.....</b>	<b>82</b>
<b>Figure 14. WWOX suppresses cell migration... ..</b>	<b>83</b>
<b>Figure 15. Time-lapse microscopy of WWOX-deficient cells versus WWOX-expressing cells in migration assay. ....</b>	<b>84</b>

<b>Figure 16. MDA-MB-231 cell migration is accelerated by WWgre (WOX17-21) peptide but blocked by SDRrepl (WOX1286-299) peptide.....</b>	<b>86</b>
<b>Figure 17. Effect of WWgre and SDRrepl peptides on cell migration... ..</b>	<b>88</b>
<b>Figure 18. Treated peptides fail to cause cell death.....</b>	<b>90</b>
<b>Figure 19. Neutralization of WWgre and SDRrepl by specific antibodies.....</b>	<b>91</b>
<b>Figure 20. Specificities of WWgre and SDRrepl neutralizing antibodies. ....</b>	<b>93</b>
<b>Figure 21. SDR domain is critical in repelling cells.....</b>	<b>95</b>
<b>Figure 22. SDRrepl is retained in cell membrane area possessing an oxidoreductase activity .....</b>	<b>99</b>
<b>Figure 23. SDRrepl antibody abolishes the retrograde movement of WWOX-deficient MDA-MB-231 cells upon encountering WWOX-expressing L929 cells.....</b>	<b>100</b>
<b>Figure 24. SDRrepl antibody abolishes cell-to-cell repulsion between MDA-MB-231 cells and lung primary culture cells.....</b>	<b>103</b>
<b>Figure 25. WWgre and SDRrepl colocalize with cell membrane T<math>\beta</math>RII .....</b>	<b>107</b>
<b>Figure 26. TGF<math>\beta</math>1 alters the retrograde movement of WWOX-deficient cells upon encountering WWOX-expressing cells.....</b>	<b>109</b>
<b>Figure 27. TGF<math>\beta</math>1 induces WWOX and TGF-<math>\beta</math> type II receptor (T<math>\beta</math>RII) to relocate into the cytoplasm.....</b>	<b>115</b>
<b>Figure 28. TGF<math>\beta</math>1 alters bindings of intra-molecular and inter-molecular WWOX via WW and SDR domains... ..</b>	<b>116</b>
<b>Figure 29. SDRrepl participates in the regulation of cell invasion. ....</b>	<b>118</b>

**Figure 30. Design of environmental setting to allow SDRrepl to promote cancer cell invasion..... 119**

**Figure 31. WWOX, WWgre and SDRrepl inhibit MDA-MB-231 anchorage-independent cell growth and modulated cell migration..... 121**

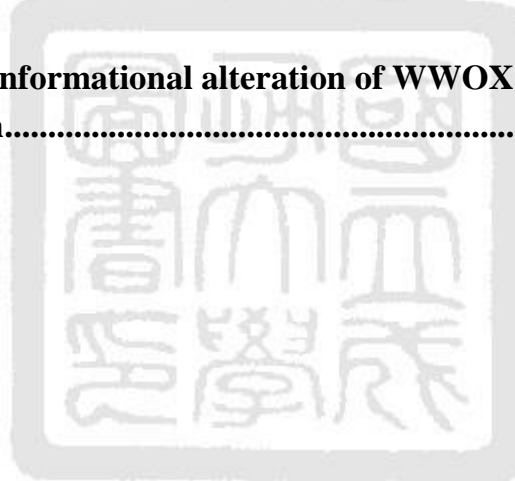
**Figure 32. WWOX suppresses tumor formation *in vivo* ..... 122**

**Figure 33. WWOX regulated cancer cells metastasis *in vivo*..... 123**

**Figure 34. Fig. 34. Zfra suppression of glioma and prostate cancer growth .. 125**

**Figure 35. Putative model of WOX1, TIAF1, TRAPPC6A, and SH3GLB2 in NF1 tumor growth ..... 126**

**Figure 36. Putative conformational alteration of WWOX and regulation of cell-to-cell recognition..... 127**



## Abbreviation

ADH/SDR: Short chain alcohol dehydrogenase/reductase

BSA: Bovine serum albumin

DMEM: Dulbecco's modified eagle medium

ECM: Extracellular matrix

FBS: Fetal bovine serum

Hyal-2: hyaluronoglucosaminidase 2

MEF: Mouse embryonic fibroblast

NF1: Neurofibromatosis 1

NLS: Nuclear localization sequence

NSYK motif: Asparagine-serine-tyrosine-lysine motif

PBS: Phosphate buffer saline

RPMI: Roswell Park Memorial Institute medium

SMAD4: Mothers Against Decapentaplegic Homolog 4

TGF $\beta$ 1: Transforming growth factor- $\beta$ 1

TIAF1: TGF- $\beta$ 1-induced antiapoptotic factor

T $\beta$ RII: TGF- $\beta$  receptor Type II

WWOX/WOX1: WW domain-containing oxidoreductase

# Introduction

## Neurofibromatosis

Neurofibromatosis type 1 and 2 are very rare diseases. No curable treatments have been developed yet. Transforming growth factor beta (TGF- $\beta$ ) plays a critical role in tissue homeostasis. Excessive activity of TGF- $\beta$  tends to generate fibrosis. TGF- $\beta$  and growth factors control the growth and development of neurofibromas in Neurofibromatosis type 1 (NF1) (McClatchey AI et al, 2007; Watanabe T et al, 2001), as well as in neurodegeneration (Yang FC et al, 2006).

*NF1*, encoding neurofibromin, is a common autosomal dominant disorder characterized by abnormalities affecting multiple tissues derived from the neural crest (Le MH et al,2010). Neurofibromin is a negative regulator of the ras signal transduction pathway. Non-tumor manifestations of *NF1*, including abnormal skin pigmentation (café-au-lait spots), learning disabilities, skeletal abnormalities, and visual anomalies, cause disfiguring or disabling (Le MH et al,2010). Neurofibromas develop on or around the peripheral nerves. They are encapsulated dermal and subcutaneous masses, whereas plexiform neurofibromas are often congenital and can develop deep within the body near the nerve roots (McClatchey AI et al, 2007).

## **WW domain-containing oxidoreductase WWOX/WOX1**

WW domain-containing oxidoreductase, also known as WWOX, FOR or WOX1, is composed of two *N*-terminal WW domains (containing conserved tryptophan residues), a *C*-terminal short-chain alcohol dehydrogenase (SDR)/alcohol dehydrogenase (ADH) domain and a D3 region (Bednarek et al., 2000; Chang et al., 2001; Ried et al., 2000). A nuclear localization sequence (NLS) locates between the two WW domains. WWOX also possesses a mitochondrial binding region in the ADH domain. There is an NSYK (Asn-Ser-Tyr-Lys) motif on the ADH domain as well (Chang et al., 2003) (Figure 1).

*WWOX* is a putative tumor suppressor gene that spans approximately a 1 Mb genomic region, and human *WWOX* gene is located on the second most common fragile site *FRA16D* on chromosome ch16q23.3-24.1 (Bednarek et al., 2000; Drusco et al., 2011; O'Keefe and Richards, 2006). There are several conserved phosphorylation sites of WWOX have been found, including Tyrosine 33 (Tyr33), Serine 14 (Ser14), and Tyrosine 287 (Tyr287).

WWOX recognizes a proline-rich PPXY motif via the first WW domain physically interacts with protein containing PPXY motif (P is proline, X means any amino acid, and Y is tyrosine). Many WW domain-containing proteins are involved

in signal transduction via their WW domains. These binding proteins include p73, AP-2 $\gamma$ , ErbB4, Ezrin, SIMPLE, c-Jun, and RUNX2 (Chang et al., 2010; Chang et al., 2007; Kurek et al., 2010; Lin et al., 2013; Yang and Zhang, 2008).

WWOX physically interacts with many proteins through phosphorylation at Tyr33 ((Bednarek et al., 2001; Chang et al., 2001). Stress stimuli, such as UV light, anisomycin, etoposide, and hypoxic stress rapidly induced phosphorylation of p53 at Ser46 and WWOX at Tyr33. Tyr33-phosphorylated WWOX physically interacts with Ser46-phosphorylated p53 and regulates apoptosis. Knock-down of WWOX by antisense mRNA abolishes p53-mediated apoptosis. (Chang et al., 2005a). WWOX binds Disheveled protein (Dvl), which are the key components of Wnt/ $\beta$ -catenin signaling pathway. WWOX inhibits Dvl-mediated Wnt/ $\beta$ -catenin pathway by inhibition of Dvl import to nucleus (Boutelle et al., 2009).

In addition, WWOX possesses an NSYK (Asn-Ser-Tyr-Lys) motif which are able to bind to hormones, supporting that WWOX is also a candidate hormone receptor (Aqeilan et al., 2009; Chan et al., 2009; Chang et al., 2005b). Substantial evidence reveals that WWOX acts as a molecular sensor of extracellular signals, as a portion of this protein is anchored on the cell surface (Hsu et al., 2009). In stomach parietal cells, WWOX is localized in the apical area and binds cytoskeletal

Ezrin (Jin et al., 2006). In certain cells, WWOX can also stay in the membrane/cytoskeleton area by associating with membrane Hyal-2 (hyaluronoglucosaminidase 2) (Hsu et al., 2009). In response to TGF $\beta$ , the membrane WWOX/Hyal-2 complex translocates to nucleus and enhances SMAD4-driven promoter activity (Chang et al., 2010; Ghebrehiwet et al., 2012; Hong et al., 2007; Hsu et al., 2009; Jin et al., 2006).

### **WWOX suppresses tumorigenesis**

The most well-known role of WWOX is its role in apoptosis. Tumor necrosis factor alpha (TNF- $\alpha$ ), transforming growth factor beta (TGF- $\beta$ ), staurosporine, UV irradiation, complement C1q, and sex steroid hormones estrogen and androgen, phosphorylate WWOX at Tyr33. Stress stimuli induce activation of WWOX, which results in translocation of WWOX to the mitochondria or nuclei (Chang, 2002b; Chang et al., 2001; Chang et al., 2005b; Chen et al., 2005; Hong et al., 2009).

Mitochondrial WWOX enhances the cytotoxic function of tumor necrosis factor (TNF- $\alpha$ ) by upregulating p53 and downregulating anti-apoptotic Bcl-2 and Bcl-xL (Chang, 2002a; Chang et al., 2001). Ectopic WWOX and p53 stimulate apoptosis synergistically. WWOX colocalizes with p53 in the cytosol and binds to

the proline-rich region of p53 via its WW domains. Phosphorylated WWOX at Tyr33 enables binding with activated pS46-p53 and forming p53/WWOX complex, which then translocates to the mitochondria and the nuclei to mediate apoptosis (Chang et al., 2003; Chang et al., 2005a; Chen et al., 2005; Lai et al., 2005). Knock-down of the expression of WWOX abolishes p53 proapoptotic function as well (Chang et al., 2005a; Chang et al., 2001).

In addition, WWOX participates in many extracellular stimuli-mediated apoptosis as well. Complement C1q induces WWOX phosphorylation at Tyr33, causing destabilizing of cell adhesion, and leads to apoptosis of prostate cancer cells (Hong et al., 2009). PMA treatment induces Jurkat T-cell apoptosis through dissociating MEK1/WWOX complex, which is regarded as a master on/off switch for apoptosis in leukemia T cells (Lin et al., 2011). WWOX also interacts with p73 in the cytoplasm mediating apoptosis of leukemia cells (Aqeilan et al., 2004b; Lin et al., 2013).

In cervical cancer, WWOX expression is decreased. Reconstitution of WWOX induces apoptosis of cervical cancer cells (Qu et al., 2013). Moreover, domain-negative mutation tumor suppressor p53 are frequently found in glioblastomas (GBMs), and this may result in resistance to temozolomide (TMZ)

and therapeutic drugs (Chiang et al., 2013). Overexpressed *WWOX* induces glioblastomas apoptosis via a mechanism independent of the intrinsic apoptotic pathway, thus offering a new strategy to overcome drug resistances (Chiang et al., 2013; Chiang et al., 2012; Sze et al., 2013).

In normal tissue, *WWOX* is preferentially expressed in secretory epithelial cells of reproductive, endocrine and exocrine organs, as well as in ductal epithelial cells of urinary system. Significant *WWOX* protein expressions are also observed in various cell types of neural origin including neurons, ependymal cells and astrocytes (Nunez et al., 2006). Unfortunately, in cancer cells, especially metastatic cancer cells are essentially devoid of tumor suppressor *WWOX* expression, and this appears to be associated with their enhanced migration. (Abdeen et al., 2011; Chang et al., 2007; Fabbri et al., 2005; Lewandowska et al., 2009; Pluciennik et al., 2006).

### **Down-regulation of *WWOX* in cancer cells**

Inactivation of *WWOX* is due, in part, to loss of heterozygosity (LOH) of human *WWOX* gene. Loss of heterozygosity (LOH) and chromosome of rearrangement of *WWOX* have been reported in many cancer types, including human extrahepatic cholangiocarcinoma, multiple myeloma, hepatocellular

carcinoma, and gastric carcinoma (Aqeilan et al., 2004a; Guo et al., 2013b; Jenner et al., 2007; Park et al., 2004; Ramos and Aldaz, 2006).

Human *WWOX* gene is composed of 9 exons. There are at least eight alternatively spliced mRNAs. In several *WWOX* isoforms, the SDR domain encoded by exons 4-8 is often deleted (Bednarek et al., 2000; Chang et al., 2001; Ried et al., 2000). In several cancer cell lines and in more than 30% of breast cancer cells, preference of aberrant *WWOX* mRNA transcripts has been shown with deletions of exons 4-8, which encode the large portion of the enzymatic SDR domain (Bednarek et al., 2001; Ludes-Meyers et al., 2004; Yang and Zhang, 2008; Zhou et al., 2005).

Moreover, epigenetic modification of *WWOX* gene promoter plays a key role in disappearance of protein expression (Guo et al., 2013a; Nakayama et al., 2009; Yan et al., 2011). Hypermethylation of promoter and exon occurs in esophageal squamous cell carcinoma cells (Guo et al., 2013b). In gastric cancer, *H. pylori* infection promotes methylation of *WWOX* gene and causes tumorigenicity (Yan et al., 2011). In breast cancer, *WWOX* mRNA and protein expression is significantly reduced due to hypermethylated *WWOX* CpG islands (Wang et al., 2009). Certain

aggressive breast cancer cell lines, e.g. MDA-MB-231, are especially devoid of WWOX expression caused by hypermethylation of the gene.

In a previous report, WWOX suppresses tumorigenicity and regulates peritoneal dissemination of ovarian cancer cells by modulating apoptosis in detached cells (Gourley et al., 2009). WWOX gene restoration prevents lung cancer growth through activation of the intrinsic apoptotic caspase cascade by promoting cancer cells to undergo apoptosis (Fabbri et al., 2005). In animal models, targeted deletion of the *Wwox* gene in the mouse have higher risk to acquire spontaneous and chemically induced cancer (Aqeilan and Croce, 2007; Driouch et al., 2002; Suzuki et al., 2009; Yang et al., 2010; Zhou et al., 2005)).

### **WWOX is not just a tumor suppressor**

Supporting evidence indicates that WWOX is not only a tumor suppressor, but also participates in regulation of many other physical functions. *Wwox*<sup>-/-</sup> mice with exon1 or exon2-4 ablation are significantly reduced in size, die at the age of 2-3 weeks, and suffer from metabolic disorder with delayed skeleton development and abnormal steroidogenesis (Aqeilan et al., 2007a; Aqeilan et al., 2009; Aqeilan et al., 2008). Intriguingly, *lde/lde* rat which is characterized by dwarfism, postnatal

lethality, male hypogonadism, and epilepsy, has no detectable *Wwox* expression in testes and hippocampi (Suzuki et al., 2009).

Also, in neuronal injury, WWOX inhibits the neuroprotective CREB and enhances NF-kappaB promoter activation which leads to eventual neuronal death (Li et al., 2009). Down-regulation of WWOX is observed in neurons of Alzheimer's disease patients' brain. Knock-down of WWOX expression by small interfering RNA in neuroblastoma cells spontaneously induces Tau phosphorylation at Thr212/Thr231 and Ser515/Ser516, enhances phosphorylation of glycogen synthase kinase 3 $\beta$  (GSK-3 $\beta$ ) and ERK, and also increases binding of phospho-GSK-3 $\beta$  with phospho-Tau, finally enhances neurofibrillary tangles (NFT) formation (Sze et al., 2004; Teng et al., 2012, 2013). Additionally, dopaminergic neurotoxin 1-methyl-4-phenyl-pyridinium (MPP<sup>+</sup>) treatment induces animals to develop Parkinson's disease (PD)-like symptoms. WWOX protein is upregulated and phosphorylation at Tyr33, which ultimately results in neuronal death (Lo et al., 2008).

WWOX also participates in with embryonic development. WWOX is differentially expressed in early dividing cells from all three germ layers from embryonic to perinatal stages (Chen et al., 2004).

## **TGF- $\beta$ 1-induced antiapoptotic factor (TIAF1)**

TGF- $\beta$ 1-induced antiapoptotic factor (TIAF1) is a 12-kDa TGF- $\beta$ 1-induced antiapoptotic factor, which protects murine L929 fibroblasts from apoptosis by tumor necrosis factor (TNF) and overexpressed TNF receptor adaptor proteins in the presence of actinomycin D, an inhibitor of DNA transcription (Chang NS et al, 1998; Khera S et al, 2003). Transiently overexpressed TIAF1 supports fibroblast growth, which is similar to the effect of TGF- $\beta$ 1. Also, like TGF- $\beta$ 1, ectopic TIAF1 suppresses cell growth and induces apoptosis of monocytic U937 and many non-fibroblast cells. TIAF1 increases the expression of p53 and Cip1/p21 and suppresses ERK phosphorylation in U937 cells, thereby inhibiting cell growth and inducing apoptosis. Ectopic TIAF1 upregulates the expression of tumor suppressor p53, and both proteins mediate cell death in either a cooperative or an antagonistic manner. Suppression of TIAF1 expression by small interfering RNA (siRNA) prevents UV irradiation-mediated p53 phosphorylation and nuclear translocation.

Expression of TIAF1 is significantly increased in activated helper T lymphocytes (TH2) in patients with chronic kidney and liver allograft rejection (Pfoertner S et al, 2006; van der Leij J et al, 2003). Regulatory T cells (Treg) have a significantly increased expression of TIAF1 (Pfoertner S et al, 2006; van der Leij J

et al, 2003). Whether TIAF1 controls the differentiation and activation-induced death of Treg and TH2 cells is unknown. TIAF1 is also associated with Hirschsprung's disease, a congenital complex disorder of intestinal innervations (Pfoertner S et al, 2006; van der Leij J et al, 2003).

TIAF1 physically interacts with Smad4, and blocks SMAD-dependent promoter activation when overexpressed. Knockdown of TIAF1 by siRNA induces spontaneous accumulation of Smad proteins in the nucleus and activation of the promoter governed by the SMAD complex (Chang JY et al, 2012). Notably, TGF- $\beta$ 1 and environmental stress (e.g. alterations in pericellular environment) cause TIAF1 self-aggregation in a type II TGF- $\beta$  receptor (T $\beta$ RII)-independent manner in cells. Hippocampal TIAF1 aggregation is shown at ages 40–70, which occurs before the generation of amyloid  $\beta$  (A $\beta$ ) plaques in Alzheimer's disease at 75–90-years (Lee MH et al, 2009).

## **TRAPP Complex Subunit 6A**

TRAPPC6A is a subunit of trafficking protein particle complex, which transport vesicles to the cis-Golgi membrane (Gwynn B et al, 2006). It is very important on ER-to-Golgi, intra-Golgi, and post-Golgi vesicle trafficking. There are

many alternatively spliced transcript variants have been determined (Sacher M et al, 2008).

## **TGF $\beta$ signaling pathway and cancer progression**

Transforming growth factor- $\beta$  (TGF- $\beta$ ) regulates a diverse range of processes, such as cell proliferation, differentiation, apoptosis and tumourigenesis. The roles of TGF- $\beta$  are distinct in different cell types. TGF $\beta$  superfamily of secreted factors including activins, nodals, bone morphogenetic proteins (BMPs), and growth and differentiation factors (GDFs), control diverse functions among different tissues (Weiss and Attisano, 2013). TGF- $\beta$  and the members of TGF- $\beta$  superfamily control the earliest stages of development and throughout the lifetime of animals. This indicates a large range of cellular functions such as embryonic stem cell self-renewal, gastrulation, differentiation, organ morphogenesis, and adult tissue homeostasis (Weiss and Attisano, 2013).

During signaling, TGF $\beta$  protein binds TGF $\beta$  receptor type II (TGF $\beta$ RII), followed by recruiting either TGF $\beta$ R type I or II to form a complex, which transduces downstream signaling (Heldin et al., 1997; Kretschmar and Massague, 1998). TGF- $\beta$  inhibits mammary epithelial cell growth. In contrast, TGF- $\beta$  is

frequently overproduced in invasive cancer cells to promote growth and metastasis (Imai et al., 2013; Muraoka-Cook et al., 2005; Quan et al., 2013).

Cumulative evidences have demonstrated that TGF- $\beta$  is associated with tumorigenesis and metastasis. In lung cancer, TGF- $\beta$ 1 expression is significantly stronger in minimally invasive adenocarcinoma (MIA) with fibrous stromal invasion than adenocarcinoma in situ (AIS) (Imai et al., 2013). In hepatoma, hepatitis C virus (HCV) induces TGF- $\beta$ 1 to promote invasion (Presser et al., 2013). In oral cancer, TGF- $\beta$ 1 induces epithelial-mesenchymal transition and promotes bone invasion via enhanced activity of osteoclasts (Quan et al., 2013). In breast cancer, TGF- $\beta$ 1 induces matrixmetalloproteinase-9 (MMP-9) and invasion through the TGF- $\beta$ /Smad and TGF- $\beta$ /ERK signaling (Mo et al., 2012).

Epithelial mesenchymal transition (EMT) is considered to be responsible for cancer invasion and metastasis. In many reports, TGF- $\beta$  has been shown to induce the expression of several transcription factors ultimately responsible for initiating and maintaining the EMT program (Larocca et al., 2013). Hypoxia stimulates the overproduction of TGF $\beta$ , which then promotes EMT of gastric cancer cells through autocrine TGF $\beta$  signaling (Matsuoka et al., 2013).

Intriguingly, cancer cells can also affect tumor-associated macrophages through TGF $\beta$ /BMP signal pathway, and finally promote angiogenesis and gastric cancer cells invasion (Shen et al., 2013a; Shen et al., 2013b). Another pathway, TGF- $\beta$ 1 binds cell surface hyaluronidase Hyal-2 on microvilli and recruits WWOX to form Hyal-2/WWOX complexes for relocation to the nuclei. Hyal-2/WWOX signaling is important in controlling growth and death of type II TGF- $\beta$  receptor-deficient cells (Hsu et al., 2009).

### **Cell migration and cancer metastasis**

In certain cells, WWOX is retained in the membrane/cytoskeleton area by associating with cytoskeletal Ezrin or membrane Hyal-2 (Hsu et al., 2009). In previous studies, knock-down of WWOX in basal cell carcinoma increases cancer cell migration activity and promotes lymphatic vessels invasion. Other group's study, miR-134 targets *WWOX* gene promoting cell invasion and metastasis results in poor survival rate (Liu et al., 2013). Up-regulation of migratory activity is observed in malignant metastatic cancer cell (Friedl, 2009; Sleeman and Steeg, 2010).

Cell migration is a highly regulated physiological event. Cells migration is important for morphologies, tissue vascularize action, wound healing, and immune response. Apparently, every tumor cells can also migrate and invade surrounding tissues, even dissemination.

Certain cells migrate as individuals, while others migrate collectively in a tightly or loosely associated manner. Cells migration is a complicated biological behavior regulated by many signal pathways, and may be varied depending upon cell types and microenvironment (Rorth, 2009). In general, cell migration can be classified in five steps: (1) extension of the leading edge which is driven by actin polymerization; (2) adhesion of extracellular matrix (ECM) (Sengbusch et al., 2002); (3) contraction of the cytoplasm; (4) release from contact sites; and (5) recycling of membrane receptors from the rear to the front of the cell (Sheetz et al., 1999).

Precisely, migrating cell protrudes its leading edge touching the extracellular matrix (ECM). The contact between cell and ECM is driven by many adhesion molecules (Reticker-Flynn et al., 2012). One of the major adhesion molecules is integrin. Integrin contacts with adhesion receptors and recruits proteases to degrade ECM components. Cell forms stress fibers and cortical actin by assemblage and elongation of actin filament. Then, cell moves forward with the cycle of detachment

of rear edge from ECM and attachment of leading edge (Wolf and Friedl, 2011). Three types of actin filament are connected with cell motility, including lamellipodia, filopodia, and actin stress fibers (Naumanen et al., 2008). Both protrusive and contractile actin filament structures operate cell migration and morphogenesis. lamellipodial and filopodial actin filament provide the force for plasma membrane protrusions through actin filament treadmilling (Tojkander et al., 2011).

In a large part of cancers, migration is believed to be an initial step of invasion and metastasis, which are major cause of poor prognosis and high mortality rate (Friedl, 2009; Sleeman and Steeg, 2010). The interaction between pro-metastatic cancer cells and stroma or environment also plays the key role of metastasis (Bradbury et al., 2012; Bravo-Cordero et al., 2012; Chang et al., 2012; Gangadhara et al., 2012; Gourley et al., 2009; van Zijl et al., 2011; Vortnikov, 2011). Breast cancer cells alter their microenvironment in part through the production of protumor molecules, which influence macrophages via inhibiting chemotactic factors such as tumor necrosis factor alpha (TNF- $\alpha$ ) to recruit macrophage and stimulate the cytotoxic/tumor cell killing macrophage phenotype during tumor progression and metastasis (Rego et al., 2013). Many inflammatory

cytokines within the tumor microenvironment are also linked to cancer progression. Interleukin- 19 (IL- 19) secreted by monocytes, B cells and several types of tumor cells is correlated with increased advanced tumor stage and higher metastasis (Chen et al., 2013). In peritumor areas, TGF- $\beta$ -induced antiapoptotic factor 1 (TIAF1) controls tumor progression, metastasis, and regulation of cell death in an aggregation-dependent manner (Chang et al., 2012).

In addition, it has reported that microRNAs (miRNAs) are important regulators in carcinogenesis. Rescent study indicates that, in head and neck squamous cell carcinoma (HNSCC), miR-134 targeted *WWOX* gene promoting cell invasion and metastasis (Liu et al., 2013). Therefore, clarifying cell migration and cell-cell interaction is helpful for preventing cancer metastasis.

# Materials and Methods

## Cell lines and cell culture

Cell lines used in this study were human breast cancer MDA-MB-231 cells, human lung NCI-H1299 cells, human neuroblastoma SK-N-SH cells, human prostate DU145 cells (American Type Culture Collections, Manassas, VA, USA), mouse L929 fibrosarcoma, mouse skin melanoma B16F10, mouse syngeneic breast cancer 4T1, squama cell carcinoma SCC9 and SCC15, and monkey kidney fibroblasts Cos7. MDA-MB-231, DU145, 4T1, SCC-9, SCC-15 and Cos7 were cultured with DMEM medium (Thermo), supplemented with 10% heat-inactivated fetal bovine serum (FBS) (Gibco) according to the instruction of ATCC (American Type Culture Collection). SK-N-SH, NCI-H1299, L929 and B16F10 were maintained in RPMI-1640 medium (Sigma) containing 10% heat-inactivated FBS.

*Wwox*-knock out and wild type mouse embryonic fibroblast (MEF) were acquired from Dr. Hsu. *Wwox*-knockout MEF cells were from *Wwox* exon-1 ablation transgenic mice. To generate *Wwox*-knockout mice, an insertion of LoxP sites to vector for targeting exon1 was designed. Cre-regulated recombination of sequences flanked by LoxP site was performed in embryonic stem cells (ESCs). The

targeted ESC clones were chosen and injected into blastocysts to generate chimeric mice. Then, the chimeric mice were crossed with C57BL/6 mice to acquire germline transmission of the target allele. Heterozygous mice were interbred to generate  $Wwox^{+/+}$ ,  $Wwox^{+/-}$ , and  $Wwox^{-/-}$  mouse embryos. MEF cells were obtained from around E16.5 mouse fetuses. MEF cells were maintained in RPMI-1640 medium supplemented with 10% heat-inactivated FBS.

Primary lung cells were isolated from 11 weeks old of NOD.CB17-Prkdcscid/NcrCrl (NOD-SCID) mouse. Lung tissue was placed in RPMI medium containing 10% FBS, then minced, and filtered through a 200-bore metal mesh to remove clumps. The single cell suspensions were centrifuged at 200g for 5 min, and resuspended in RPMI-1640 medium contained 10% heat-inactivated FBS. The freshly isolated cells were plated into a 10cm<sup>2</sup> culture dish at  $1 \times 10^5$  cells/ml and incubated at 37°C with 5% CO<sub>2</sub>/95% air. After 72 hours, non-adherent cells were removed and the medium was replaced. At 80% confluence, cells were harvested with 0.25% trypsin–0.02% EDTA for 2min at 37°C, replanted and examined.

### **Stable transfectants**

cDNA constructs were transfected into cells by electroporation. After electroporation, cells were incubated at 37°C with 5% CO<sub>2</sub>/95% air for 24 hours. The next day, the standard medium was replaced with medium containing 300 µg/ml G418 (Life Technologies, Inc.). Over time, this selected for cells that have stably expressed pEGFP-C1 or pDsred2-C1 plasmid. After several days, colonies were picked and transferred to 3.5 cm<sup>2</sup> dishes with 1 ml media containing G418 in each dish. When the dishes were confluent, cells were trypsinized and transferred into 5cm<sup>2</sup> dishes. Immunofluorescent microscopy was used to screen colonies which should be put down and which were worth keeping. Colonies were treated G418 continuously. When the colonies had been selected, lower amount of G418 was treated for maintenance. The expression of interested proteins were confirmed by immunofluorescent staining and western blotting.

### **cDNA constructs and electroporation**

The WWOX full length, WW domain, SDR domain, WOX1<sub>7-21</sub> construct, and TIAF1 were generated. All the constructs made in pEGFP-C1, pDsred2-C1, pECFP-C1 or pEYFP-C1 vector (Clontech). Constructs were transfected into cells by electroporation with BTX ECM 830 Square Wave Electroporator; Genetronics,

San Diego, CA).

## **Chemicals and antibodies**

TGF $\beta$ 1 were purchased from Preprotech. Polyclonal antibody against T $\beta$ RII was purchased from Cell signal. Polyclonal antibody against GFP was purchased from Santa Cruz Biotechnology. G418 was purchased from Life Technologies, Inc.

## **Synthetic peptides and antibodies**

WVOX peptides (amino acids 7-21: CAGLDDTDSEDELPPG, phosphorylation form of amino acids 7-21 at Ser14: CAGLDDTD-pS-EDELPPG, amino acids 11-20: DTDSEDELPP, amino acid 28-42: CKDGWVYYANHTEEKT, phosphorylation form of amino acids 28-42 at Tyr33: CKDGWV-pY-YANHTEEKT, amino acids 286-299: DYWAMLAYNRSKLC, phosphorylation form of amino acids 286-299 at Tyr287: D-pY-WAMLAYNRSKLC, scramble amino acids 7-21: DETEPDGLDAGPSLD, and scramble amino acids 286-299: CAYKRDNALYSMWL) were synthesized by Genemed Biotechnologies, Inc. (San Francisco, CA) and conjugated with keyhole limpet hemocyanin for antibody production in rabbits using the Pierce antibody production kit. Rabbits were injected with synthetic peptides subcutaneously 3 times for 3 weeks. Then, the blood was

collected from ear veins. After the blood clotted, the plasma was separated by centrifugation at 5000 rpm in microfuges. The selected WWOX sequence is identical between human and mouse.

### **Cell migration assay and time-lapse microscopy**

Cell migration assay was performed by Culture-insert (Ibidi). We placed a culture insert into a 3.5cm<sup>2</sup> dish and seeded equal number of cells (3X10<sup>5</sup> cells, 70μl) into two wells of the insert. After overnight incubation at 37°C with 5% CO<sub>2</sub>/95% air, the insert was gently removed by tweezers and the medium was replaced by medium containing 2% FBS. NIKON TE2000-U microscope was used to observe the cell migration. For time-lapse migration analysis, cells were maintained in medium containing 2% FBS and performed with Olympus IX83 fully-motorised and automated inverted microscope system and xcellence software. Cell migration rate was measured by cell migration distance. Single cell migratory path was tracked by image J manual tracking and chemotaxis. Autocorrelation Function (VACF) was calculated to confirm the treatment actually affected cell migration each self's initial condition. The formula of calculation was:

The velocity can be express as  $\vec{v}(t) = \frac{[\vec{R}(t + \delta) - \vec{R}(t)]}{\delta}$

The velocity autocorrelation function can be define as  $R(\tau) = \langle \vec{v}(t+\tau) \cdot \vec{v}(t) \rangle$   
 $\vec{R}(t)$  means the position of a single cell tracking center.  $\tau$  means the time interval of the normal diffusion.  $\delta$  means the time interval of each frame. The maximum correlation value is 1. Lower the value is means more uncorrelated. We used the temporal correlation of the velocity to randomly analyzed 10 cells the behavior of each cell migration. The Autocorrelation Function (VACF) is calculated by the aforementioned formula (Campos et al., 2010; Tkachenko et al., 2011; Weber et al., 2012).

### **Tissue microarrays and human cancer tissue sections**

Prostate cancer tissue microarray slides (T-RP-2D), containing 75 samples each for control and cancer groups, respectively, were obtained from the Tissue Array Research Program, National Cancer Institute (Bethesda, MD, USA). In addition, human cancer tissue sections were obtained from the Department of Pathology, University of Colorado Health Sciences Center (by Dr. CI Sze, before 2005). IRB approval was waived. Informed consents were obtained from the family members of the deceased patients. Also, cancer tissue sections were obtained from the MacKay Memorial Hospital, Taipei, Taiwan (by Dr. MF Chiang) with IRB approval.

## **Immunofluorescent staining**

$3 \times 10^5$  cells were seeded on to 15mm X 15mm coverglass. After overnight culture to wait for cell attachment, cells were fixed with 4% paraformaldehyde for 15 min and permeabilized with 0.25% triton-X-100 in PBS for 5 min. Cells were washed three times by PBS and blocked with 4% BSA overnight at 4 °C. Cells then incubated with primary antibody in PBS containing 2% BSA for 2hr at room temperature. Cells were washed three times and then incubated with fluorescence conjugated secondary antibody (Donkey anti-rabbit Alexa Flour 488, Donkey anti-goat Alexa Flour 549, or Goat anti-mouse Texas Red, Invitrogen) in PBS containing 2% BSA for 1hr at room temperature. Cells were washed three times and then stain with DAPI for 15 min at room temperature. Cells were mounted with mounting solution. NIKON TE2000-U microscope was used to observe the images.

For non-permeabilized cell surface staining, cells were not permeabilized with Triton X-100. Primary Cells were incubated with primary antibody at 4 °C with 0.1% sodium azide for 1hr. Cells were washed three times with cold PBS. Then cells were incubated with fluorescence conjugated secondary antibody at 4 °C for 1hr. Finally, cells were fixed with 4% paraformaldehyde for 10 min and stain with DAPI for 15 min. In the negative controls, no primary antibodies were used.

## **Quantification of fluorescent images**

Fluorescent or immunofluorescent microscopy was performed using a NIKON TE2000-U microscope (Nikon, Tokyo, Japan), as described. For prostate cancer tissue microarray slides, the relative extent of protein expression in each section was quantified using the histogram tool of the Nikon's EIS Elements BR3.2 software (Nikon). Each slide was quantified independently by two laboratory researchers. For cultured cell images, the relative fluorescence intensities of whole cells or individual punctates were quantified by Photoshop (under the Histogram and Marquee or Quick Selection tools, Adobe Photoshop CS5) and by Nikon's software. For each control or experiment, 20–100 cells were examined in 3–5 experiments. Presented data were from analyses by Photoshop.

## **Confocal Microscopy**

Confocal microscopy analysis was performed to determine the interaction of WW domain and SDR domain. Cos7 cells were transfected with GFP tagged-WW domain and RFP tagged-SDR domain. In this study, Nikon C1-Si Laser Scanning Confocal Microscope was used to capture the confocal images. 457/488/514 nm laser were used.

## **Immunohistochemistry staining**

Formalin-fixed paraffin embedded sections were cut into 5 $\mu$ m tissue slices. Before staining, slides were deparaffinized and rehydrated followed by antigen retrieval. Slides then blocked by 4% BSA in PBS at 4 $^{\circ}$ C overnight. After washed three times, tissues were incubated with primary antibody in PBS containing 2% BSA for 2hr. Slides were washed three times with cold PBS. Then cells were incubated with DAB conjugated secondary antibody at room temperature for 1hr. Finally, add chromogenic substrate purchased from Dako. NIKON TE2000-U microscope was used to observe the expression level of target proteins.

## **Förster (Fluorescence) Resonance Energy Transfer (FRET)**

The WW domain and SDR domain were constructed in-frame with EGFP and pDsRed2 expression vectors (Clontech). Cos7 cells were transfected with constructs by electroporation and cultured for 24–48 hours. FRET analysis was performed with inverted fluorescence NIKON TE2000-U microscope. Cells were stimulated with an excitation wavelength 488 nm. FRET signals were detected at an emission wavelength 549nm. The FRET images were corrected for background fluorescence from an area free of cells and spectral bleed-through.

TIAF1si, scrambled RNA and stable L929 cell transfectants were prepared as previously described. TIAF1 and Smad4 were tagged with enhanced green fluorescence protein (EGFP; in pEGFP-C1, Clontech, Mountain View, CA, USA), ECFP in pECFP-C1 (Clontech) or DsRed in pDsRed (Clontech). These are mammalian expression plasmids. Additional mammalian expression plasmids were WOX1, p53, dominant-negative TIAF1 (E22/23A), dnJNK1 and dnWOX1. Where indicated, L929, MCF7, NCI-H1299 cells or other indicated cells were electroporated with the above constructs (200 V, 50 msec; Square Wave BTX ECM830, Genetronics, San Diego, CA, USA), cultured overnight and then treated with TGF- $\beta$ 1 for indicated times. Alternatively, the cells were transfected with the aforementioned DNA constructs using liposome-based GeneFactor (Venn Nova). Whole cell lysates were prepared in the presence of a cocktail of protease inhibitors (Sigma). The extent of protein expression was determined using indicated specific antibodies in each indicated experiment. FRET analysis for bimolecular interactions was carried out as described. Briefly, cells were stimulated with an excitation wavelength of 440 nm. FRET signals were detected at an emission wavelength of 535 nm. ECFP and EYFP were used as donor and acceptor fluorescent molecules, respectively.

The spectrally corrected FRET concentration (FRET<sub>c</sub>) was calculated by

Youvan's equation (using a software program Image-Pro 6.1, Media Cybernetics):

$$\text{FRETc} = [\text{fret} - \text{bk}(\text{fret})] - \text{cf}(\text{don}) \times [\text{don} - \text{bk}(\text{don})] - \text{cf}(\text{acc}) \times [\text{acc} - \text{bk}(\text{acc})],$$

where fret = fret image, bk = background, cf = correction factor, don = donor image, and acc = acceptor image. The equation normalizes the FRET signals to the expression levels of the fluorescent proteins.

### **Cell cycle analysis**

Cells were collected into 2ml eppendorff followed by precipitated by centrifugation at 5000 rpm for 15 minutes and gently washed once, then fixed with equal volume of PBS and 100% ethanol for overnight at -20°C. Following fixation with ethanol and precipitation (centrifugation at 5000 rpm in microfuges), the cells were stained with propidium iodide solution (2 µg/mL, containing 10 µg/mL RNase A) for 30 minutes at room temperature in dark place. The DNA contents were analyzed by flow cytometry (Becton Dickinson, Franklin Lakes, NJ).

### **Soft agarose colony formation assay**

0.8% low-melting point agarose in medium with 0.5M HEPES and antibiotics was prepared.  $3 \times 10^4$  cells were mixed with 0.8% low-melting point agarose in medium. Then the mixture was transferred into  $3.5 \text{cm}^2$  followed by Incubation for 3

weeks.

## **2D invasion assay**

MDA-MB-231 cells expressing EGFP and L929 cells expressing DsRed2 transfectants were established. Equal number of two stable transfectants ( $3 \times 10^5$  cells, 70 $\mu$ l) were seeded into two wells of the insert. After overnight incubation at 37°C with 5% CO<sub>2</sub>/95% air, the insert was gently removed by tweezers and the medium was replaced by medium containing 2% FBS. After culture for 4 days, NIKON TE2000-U microscope was used to observe the images. Image J software was used to count the invasive MDA-MB-231 cells in the L929 cell mass.

## **Transwell invasion assay**

The Transwell invasion assay was performed with Corning Transwell permeable supports kit.  $1 \times 10^5$  lung primary cultured cells were seeded in lower well followed by incubation at 37°C waiting for cell attachment. At the same time, 100 $\mu$ l 0.1% gelatin (in water) was added into apical chamber coating for 2 hours at room temperature. Then 3500 MDA-MB-231 cells were mixed with 100 $\mu$ l 0.1% gelatin (in serum free medium). Then 3500 MDA-MB-231-stable transfectants (egfp

or SDR domain in 100ul serum free medium) were added into the apical chamber gently as well. Then the medium in the lower well was replaced with 500ul fresh medium containing 10% FBS. And the apical chamber was then putted onto the well followed by 18 hours incubation. The non-invasive cells were removed by swabs. The invasive cells were stained with staining solution (40% methanol ∨ 10% glacial acetic acid ∨ 0.1% coomassie brilliant blue) followed by destaining with destaining solution (40% methanol ∨ 10% glacial acetic acid). The cell number were counted and analysis by microscopy.

#### **UVB irradiation on hairless mouse skin**

The *in vivo* experiments were performed, as described.<sup>15</sup> An approved protocol for animal use was obtained from the Institutional Animal Care and Use Committee of the National Cheng Kung University Medical College. Briefly, hairless SKH-hr1 female mice, 6-week-old, were obtained from Charles River Laboratories (Wilmington, MA, USA). The mice were housed in individual cages in a room with a constant temperature and humidity and an alternating 12-h light and dark cycle, and fed ad libitum with a commercial diet and water. To examine acute response, three mice were exposed to UVB (2.16 kJ/m<sup>2</sup>; 312 nm) once using a

BLE-8T312 UV lamp (Spectronics, Westbury, NY, USA), and the mice were killed 1 day later. To determine chronic response, mice were exposed to UVB thrice per week (Monday, Wednesday and Friday) starting with 0.36 kJ/m<sup>2</sup>, respectively, for 1 and 5 months (n=3), followed by increasing 100% weekly. After week 10, a consistent dose of UVB irradiation (2.16 kJ/m<sup>2</sup>) was given over the next 8 weeks. In a control group, mice received no UVB irradiation. Skin tissue sections were prepared and processed for IHC staining using TIAF1(R48-2) antibody.

### **Animal experiment**

BALB/C mice were used in this study. 2X10<sup>6</sup> tumor cells and WWOX peptides were subcutaneously injected in different site separately. Tumor sizes and weight were measured every other day. After sacrifice, organs were fixed by 4% paraformaldehyde immediately. Then the tissue sections were embedded with paraffin followed by section slice and immunohistochemistry staining.

### **Statistical analysis**

Data were analyzed by Student's *t* test using Microsoft excel. Data were expressed as mean±standard deviation p<0.05 was considered significant.

## Results

### **Expression of WOX1, TIAF1, TPC6A and Bif-2 in the cutaneous NF1 neurofibromas.**

In previous study, the protein levels of tumor suppressor WOX1, isoform WOX2, and Tyr33-phosphorylated forms are significantly decreased in the hippocampal neurons of individuals with AD. This down-regulation significantly induces activation of tau kinases (e.g., GSK-3 $\beta$ , cdk5, JNK, p38, ERK) and promotes tau hyperphosphorylation, along with increased tau tangle formation in the neuronal cells. At the first of this study, we performed immunohistochemistry staining to determine the expression levels of target proteins that are present in the NF1 tumors and encapsulate the neurofibromas. Tumor suppressor WWOX/WOX1 is downregulated, and transforming growth factor  $\beta$  (TGF- $\beta$ )-induced TIAF1, TRAPPC6A (TPC6A, and SH3GLB2 (or Bif-2), are upregulated in the NF1 tumors (Figure 2). Data indicated that the presence of significantly increased levels of TIAF1/TPC6A/Bif-2 complex is likely to support NF1 tumor progression.

### **TIAF1 aggregates in cancer cells.**

In prostate tissue microarray slides, TIAF1 levels are significantly increased in prostate cancer, compared with normal controls, as determined using both

TIAF1(R48-2 homemade antibody) and the commercial antibodies for fluorescence microscopy (Figure 3A; 75 samples for control and cancer groups and damaged samples excluded). Immunofluorescent and immunohistochemistry staining also confirmed the expression of TIAF1 in prostate cancer compared with control (Figure 3B, C). Upregulation of TIAF1 and Smad4 is shown in the prostate cancer tissues (Figure 3D).

TIAF1 physically interacts with Smad4, and knockdown of TIAF1 expression induces spontaneous accumulation of Smad proteins in the nuclei. By immunofluorescence microscopy, TIAF1 colocalized with Smad4 in the cytosol and prostatic concretions in the lumens of glandular ducts (Figure 4). Both TIAF1 and Smad4 proteins are colocalized and appear as aggregates (Figure 4). Similarly, expression of TIAF1 and Smad4 proteins is significantly increased ( $P < 0.05$ ) in colon cancer cells, as compared with controls (Figure 3D).

TIAF1 aggregates are present in the hippocampi of both non-demented humans and patients with Alzheimer's disease. Co-expression of TIAF1 and A $\beta$  aggregates was found in the metastatic cancer in the brain (Figure 5). Conceivably, when metastatic small-cell lung cancer cells relocated to the brain, TIAF1 aggregates were deposited in the interface between cancer and brain cells or within the tumors

(Figures 5A, B). Fluoro-Jade C stain demonstrated the presence of degenerating neurons (Figures 5A, B). Similarly, co-expression of the aggregates for TIAF1 and  $A\beta$  was shown for the metastatic lung cancer, nasopharyngeal carcinoma (NPC) and colon cancer in the brain (Figures 5B). Despite the presence of  $A\beta$ , no apparent apoptosis was observed in the cancer cells.

Compared with TIAF1, WOX1 expression is relatively low in neurofibromatosis NF1 (Figures 6C, D). TIAF1 is overexpressed in the peritumor area (Figure 5D). Alteration of environmental cues induces TIAF1 expression and aggregation. Presence of fibrous aggregation of TIAF1 is shown in the peritumor coat of NF1 (Figure 5C, D, E), and prostate cancer (Figure 5F).

### **TIAF1-/Smad4-binding induces generation of amyloid precursor protein (APP) and $A\beta$ .**

In agreement with our previous observations, ectopic expression of TIAF1 tagged with ECFP or EYFP (ECFP-TIAF1 or EYFP-TIAF1) in breast MCF7 cells resulted in an increased self-binding, as determined by FRET (Förster resonance energy transfer) analysis (Figure 6A). The TIAF1 self-binding led to an increased expression of Smad4, and both Smad4 and TIAF1 colocalized in the cytoplasm and

cellular protrusion (Figure 6B). TGF- $\beta$ 1 marginally reduced the effects (Figure 6). p53-deficient NCI-H1299 cells were transiently overexpressed with ECFP-Smad4 and EYFP-TIAF1. The cells were treated with TGF- $\beta$ 1 for 24 h, which resulted in an increased generation of APP and A $\beta$  (Figure 7). By FRET analysis, TGF- $\beta$ 1 increased the binding of Smad4 and TIAF1 (Figure 7).

### **TRAPPC6A (TPC6A) trafficking and intracellular self-aggregation.**

We also determine whether TRAPPC6A protein that significantly upregulated in NF1 exhibits self-aggregation ability. Endogenous TPC6A in the cytoplasm is a monomer (17-20 kDa), and becomes a trimeric protein in the nuclei (~70 kDa and larger) in cutaneous basal cell carcinoma BCC cells (Figure 8A). Exposure of BCC cells to UV irradiation rapidly induced formation of a trimer in 10 min and larger aggregates of > 200 kDa in 60-120 min in the cytoplasm. In the nucleus, aggregate formation occurred in 40 min post UV exposure, followed by disappearance of the large size aggregates (Figure 8A). The aggregates are metabolically degradable and notably no ubiquitination was observed in these proteins. Similarly, TGF- $\beta$ 1 induced aggregation of Ser35-phosphorylated TPC6A, including formation of dimeric, trimeric and so on in melanoma B16F10 cells (Figure 8B). TGF- $\beta$ 1 increased the formation of polymerized TPC6A in the nucleus

of SK-N-SH cells (Figure 8C). TGF- $\beta$ 1 causes relocation of TPC6A to the mitochondria, and the protein occurs as a dimeric form.

### **SH3GLB2/Bif-2 aggregation**

Previous study had determined that isolated Bif-2 as a binding protein of TIAF1 by using yeast two-hybrid screen. When overexpressed in COS7 cells, EGFP-Bif-2 or monomeric DsRed-Bif-2 underwent polymerization to a crescent or “wormy” fiber (Figure 9A). TGF- $\beta$ 1 increased the formation of a large size horseshoe or “C” shape fiber assembled surrounding the nuclei (Figure 9B). When TIAF1 was knocked down by siRNA, aggregation of Bif-2 was blocked (Figure 9C). Normally, a large wormy fiber chased a small one and then both became merged, followed by further merging with another fiber and migrating to the perinuclear area (Figure 9D). We have determined that the mean velocity of migration is  $\sim 1.0926 \mu\text{m}/\text{sec}$ . While TGF- $\beta$ 1 induces Bif-2 aggregation in 24 hr and longer, the aggregation process can be accelerated by staurosporine (for causing mitochondrial stress) and thapsigargin (for ER stress) in 4 hr. That is, subcellular compartments, when subjected to stress, may lead to aggregation of Bif-2. FRET analysis showed that there is an initial increase in the binding of Bif-2 with TIAF1 in response to TGF- $\beta$ , followed by reduction (Figure 9E).

Aggregation of TIAF1 and TPC6A is probably related with generation of cross- $\beta$ -sheet accumulation. Bif-2 self-assembly is likely caused by binding among helical segments, according to the assembly model of Bif-1. When overexpressed in smaller neuroblastoma SK-N-SH or colon HCT116 cells, Bif-2 turned into a long, thin, coiled rope, as revealed in 3D imaging with an average diameter of  $\sim 7 \mu\text{m}$  (Figure 10A). Three-dimensional stimulated emission depletion microscopy (STED) shows the assembly of tiny fibrils or tubules to become a rope (Figure 9B). By electron microscopy (EM), aggregated Bif-2 is found at the perinuclear area, and forms hollow tubes or tubules (Figures 9C, D). The wall of each tube is also composed of many small hollow tubules of  $\sim 100 \text{ nm}$  in diameter (Figure 9D). By high-resolution three-dimensional structured illumination microscopy (SIM), each hollow Bif-2 fiber is composed of many small hollow tubules in the wall ( $\sim 200 \text{ nm}$  in diameter; Figure 4E). A few single or double tubules are also shown (Figure 9F). Bif-2 fends off apoptotic stress caused by a mitochondrial apoptosis-inducing chemical CCCP (carbonyl cyanide 3-chlorophenylhydrazone) (Figure 9G), suggesting that Bif-2 is a prosurvival protein. The Y77F Bif-2 mutant did not undergo polymerization and still blocked the mitochondrial apoptosis.

## Tumor suppressor WWOX in cell migration and cell-to-cell recognition

Substantial evidences reveal that WWOX suppresses tumor formation through inhibiting cancer cell migration. To further elucidate the underlying molecular mechanism, we utilized wild type MEF (mouse embryonic fibroblasts)  $Wwox^{+/+}$  and knockout  $Wwox^{-/-}$  cells to perform cell migration assay.  $Wwox^{-/-}$  MEF cells migrated significantly faster than the wild type  $Wwox^{+/+}$  cells (Figure 14A). Intriguingly, we also observed that the migratory morphologies were very different between these two cells. Wild type cells migrated collectively, but the knockout cells migrated individually (Figure 14B).

To simulate the migration of metastatic cancer cells to target organs, we seeded knockout cells and wild type  $Wwox$  cells in each chamber of a culture-insert respectively (Figure 15). After overnight incubation and waiting for cells attachment, the insert was gently removed by a tweezers. Cells were then cultured in medium containing 2% FBS to block cell proliferation (~30% Go/G1 phase of the cell cycle) (Figure 13). When the  $Wwox^{-/-}$  knockout cells were migrating close to the wild type cells, the knockout cells extended their pseudopodia to touch the wild type cells. Knockout cells then turned around and moved toward the opposite direction or divided rapidly (Figure 15A). A triple-negative MDA-MB-231 breast cancer cell

line, which lacks estrogen receptor (ER), progesterone receptor (PR), and HER2 expression was used. This cell line has epigenetically inactivated *WWOX* gene. When the *WWOX*-deficient MDA-MB-231 cells confronted *WWOX*-positive L929 fibroblasts, MDA-MB-231 also underwent retrograde migration (Figure 15B).

In general, the observations are true for *WWOX*-deficient cells encountering *WWOX*-expressing cells (Figure 15C). Actually, *WWOX*-deficient cells could sense the presence of *WWOX*-expressing cells from a distance. These cells directly migrated in a retrograde manner. Alternatively, few cells migrated forward to probe the *WWOX*-positive cells with cells pseudopodia. Again, these cells turned back to their parental cell population. However, when the same cells (two chambers of culture-insert were seeded the same cell line ) met each other, they move forward steadily and aligned nicely without retrograde movement. The observations suggest that either *WWOX*-positive or -negative cells may release cytokines to alert each other, and regulate the migration of *WWOX*-deficient cells indirectly. Overall, based upon the aforementioned observations, 3 fundamental questions are raised: 1) how does *WWOX* regulate cell-to-cell recognition? 2) Why are there only few *WWOX*-negative cells coming out of the parental mass to face the *WWOX*-positive cells? And 3) how do these *WWOX*-negative cells know their home base to move back?

## **Molecular dissection of WWOX: two faces of WWOX in cell migration and cell-to-cell recognition**

WWOX is composed of a nuclear localization sequence (NLS), two *N*-terminal WW domains (containing conserved tryptophan residues), a *C*-terminal short-chain alcohol dehydrogenase/reductase (SDR) domain and a D3 region. To elucidate how WWOX regulates cell migration, we designed 10 peptides, WOX17-21, pS14-WOX17-21, WOX111-20, WOX128-42, pY33-WOX128-42, WOX1286-299, pY287-WOX1286-299, WOX17-21 scramble, and WOX1286-299 scramble, according to the surface-exposure regions and phosphorylation sites of a simulated 3-dimensional structure of WWOX (Figure 16A).

A WWOX peptide was coated onto one chamber of the culture insert, and were seeded cells MDA-MB-231 in the other side (Figure 16A). Cell migration was then carried out. We determined two most potent peptides, which regulated cell migration. WOX17-21, also designated WWgre (greeting signal in WW domain) accelerated cell migration, whereas WOX1286-299, named SDRrepl (repellence signal in the SDR domain), suppressed cell migration.. When SDRrepl (WOX1286-299) peptide was coated onto the culture dish surface, MDA-MB-231 cells became highly resistant to migrate over to the peptide-coated area (Figure 16B). That means the peptide epitope repelled the upcoming cells. However,

phosphorylation of SDRrepl at Tyr287 abolished the repellence functions. In contrast, WWgre (WOX17-21) was shown to greet the visiting MDA-MB-231 cells, and that phosphorylation of Ser14 also reduced the cell attraction (Figure 16B). The coating efficiency of peptides were confirmed by Enzyme-linked immunosorbent assay (Figure 16C).

In parallel experiments, MDA-MB-231 cells were pre-treated with the WWgre and SDRrepl peptides at 20  $\mu$ M for 4 hr, followed by washing and running time-lapse microscopy. When cells were treated with the SDRrepl peptide (20  $\mu$ M) for 4 hr, these cells strongly resisted the untreated visiting cells (Figure 17). The visiting cells hesitated to migrate forward and underwent retrograde migration (Figure 17A, D). In contrast, WWgre greeted the visiting cells, and the cell migratory activity of visitors were accelerated (Figure 17A, C). By cell cycle analysis, the peptide-treated peptides did not cause cell death (Figure 18).

These results indicated that both WWgre and SDRrepl peptides participate in cell-to-cell recognition, and they are probably retained on cell surface to be recognized by visiting cells. We have generated antibodies against WWgre, SDRrepl, and their phosphorylation forms. The neutralizing antibodies were used to detect the presence of these peptides in non-permeabilized cells.

By immunofluorescent staining, we determined these peptides can be retained on cell surface to participate in cell-to-cell recognition (Figure 24). The specificity of these antibodies were tested by migration assay (Figure 19) and immunofluorescent staining (Figure 20). We neutralized these peptides coated on the plastic surface by the generated specific antibodies, which resulted in abrogation of WWgre and SDRrepl functions in controlling cell migration (Figure 19). These confirmed the specific function of WWgre and SDRrepl in regulating cell migration and recognition.

### **SDRrepl antibodies abolish SDRrepl function, and alter cell retrograde migration**

To further confirm the aforementioned observations, we established stable transfectants of MDA-MB-231 cells expressing EGFP-tagged WWOX (full length), SDR domain, WOX17-21, and EGFP only) (Figure 21A). By fluorescence microscopy, we confirmed that the SDRrepl segment in WWOX was localized in the plasma membrane area, and possessed oxidoreductase activities (Figure 22).

When EGFP-SDR-expressing MDA-MB-231 cells encountered un-transfected control cells, the EGFP-SDR-expressing cells repelled the visiting MDA-MB-231 control cells to undergo retrograde migration from a distance without contact at all

(Figure 21B, C, D ), suggesting that cytokines secreted by the SDR-expressing cells are capable of fending off WWOX-deficient cells. However, when an aliquot of antiserum against the SDR domain was added to the co-culture, anterograde movement of the cells from both fields was restored (Figure 21F), again indicating the critical role of SDR domain in conferring cell repellence. Non-immune serum and pY287-SDRrepl antiserum had no effect (Figure 21E, G). The results are in parallel with the observations that phosphor-SDRrepl has no effect on cell migration (Figure 16B).

The similar repellence effect was also observed when WWOX-deficient MDA-MB-231 cells encountered WWOX-expressing L929 cells. Again, the SDR antiserum treatment suppressed retrograde movement of MDA-MB-231 cells migrating toward L929 cells (Figure 23).

To further analyze the cell migration. We also use Velocity Autocorrelation Function (VACF) analysis to determine the movement of MDA-MB-231 when they encountered MDA-MB-231-expressing SDR domain of WWOX (Figure 23 C, D, E). In the random process, the correlation function reflects how smooth or wiggly a process is.

The velocity of MDA-MB-231 under SDRrepl antiserum treatment was lower than control (Figure 23C, D). Total velocity autocorrelation function was also

significantly lower than control. With the treatment, MDA-MB-231 cells took much time to become uncorrelated to the initial condition (Figure 23C, E). Anterograde and retrograde movement were significantly decreased with SDRrepl antiserum treatment (Figure 23D). That is SDRrepl antiserum blocked the repellence function of MDA-MB-231-expressing SDR domain of WWOX, so they could relatively recognize each other without repulsion. (Figure 23). The treatment reduced the sensitivities of cells upon encountering foreign cells. The results clearly indicate that SDRrepl is the segment in SDR domain of WWOX which is accountable for repelling visiting cells.

To simulate WWOX-deficient MDA-MB-231 cells encountered WWOX-expressing tissue, we utilize MDA-MB-231 and lung cell primary culture to perform time-lapse migration assay (Figure 24). As expected, MDA-MB-231 had a retrograde movement when encountered lung cells (Figure 24B, C, E). However, SDRrepl antibody treatment abolished the retrograde movement of MDA-MB-231 cells (Figure 24B, D, E).

### **TGF $\beta$ 1 induces WWOX and TGF- $\beta$ type II receptor (T $\beta$ RII) to relocate into cytoplasm and alters WWOX-mediated cell-to-cell recognition**

By fluorescence microscopy, WWgre and SDRrepl peptides can be retained on

cell surface and in part colocalized with T $\beta$ RII (TGF $\beta$  receptor Type II) (Figure 25). Confirm the observation by confocal microscope, we determined WWgre and SDRrepl peptides physically interacted with T $\beta$ RII in the plasma membrane of MDA-MB-231 cells (Figure 24). It has reported that a portion of cytosolic WWOX localizes on the membrane/cytoskeleton area, as determined by immunoelectron microscopy (Hsu et al., 2009) (Figure 11). In the cell membrane, WWOX may exist by itself as multi-molecular aggregates, and binds Hyal-2, Ezrin (Hsu et al., 2009; Jin et al., 2006).

Transforming growth factor beta (TGF- $\beta$ ) family proteins regulate multiple biological functions, such as cell growth, extracellular matrix protein synthesis, and immune cell functions. In previous studies, TGF- $\beta$  plays a dual role in cell growth and tumorigenesis. TGF- $\beta$  inhibits mammary epithelial cell growth, and promotes epithelial-to-mesenchymal transition (EMT). Invasive cancer cells frequently overproduce TGF- $\beta$  to promote growth and metastasis (Bachman and Park, 2005; Muraoka-Cook et al., 2005; Tirino et al., 2013).

To simulate the TGF $\beta$ 1 overproduction of metastatic cancer cells, we added 10ng/ml TGF $\beta$ 1 in co-culture. In this experiment, we determined that TGF- $\beta$ 1 abolished the retrograde movement of WWOX-deficient MDA-MB-231 cells when they encountered WWOX-expressing L929 cells (Figure 26A-G). The similar result

was observed when MDA-MB-231 cells encountered primary lung cells as well (Figure 26H-N). It suggested that metastatic cancer cells may overcome the repellence of WWOX-expressing normal tissue by TGF $\beta$ 1 overproduction.

We also utilized *Wwox*<sup>+/+</sup> MEF cells as a model to assess the correlation of membrane WWOX and T $\beta$ RII when WWOX-expressing cells encountered TGF $\beta$ 1 stimulation. By non-permeabilized fluorescence staining, SDRrepl physically interacted with T $\beta$ RII in the plasma membrane of *Wwox*<sup>+/+</sup> cells. TGF $\beta$ 1 treatment resulted in the decrease of SDRrepl and T $\beta$ RII expression in the plasma membrane (figure 27). The reduction of SDRrepl and T $\beta$ RII expression in the plasma membrane offer an explanation for retard of SDRrepl caused retrograde movement by TGF $\beta$ 1 treatment (figure 26). This maybe SDRrepl and T $\beta$ RII were internalized by the cells. In the future, we will determine whether the internalization of SDRrepl and T $\beta$ RII involve in TGF- $\beta$  signaling regulating cell-to-cell recognition (figure 36).

### **Conformational alteration of WWOX may play a role in cell-to-cell recognition**

We examined whether there is a binding between WW and SDR in WWOX via either an intramolecular- or intermolecular-dependent manner. By FRET (Förster resonance energy transfer) analysis, we determined that the WW domain bound the SDR domain (Figure 28A). Also, WW or SDR domain can undergo self-binding

(Figure 28A). In addition, we also validate TGF $\beta$ 1 increased the binding level between WW and SDR domain in 15min post-treatment, and then decreased slowly. (Figure 28B). These suggested that WWOX may be a sentry alert to the extracellular stimulation and transduce signaling by conformational alteration.

### **SDRrepl and TGF $\beta$ participate in the regulation of cell invasion**

To determine whether SDRrepl regulates cell invasion, we perform 2D invasion assay (Figure 29). We established stable transfectants of MDA-MB-231 cells expressing EGFP and stable transfectants of L929 cells expressing DsRed2. Then these two stable transfectants were seeded in two side of culture insert separately. After overnight incubation and waiting for cells attachment, the insert was gently removed by tweezers. The co-cultures were cultured at 37°C with 5% CO<sub>2</sub> for 4 days. Image J software was used to count the invasive MDA-MB-231 cells in the L929 cell mass. Compare to control and normal rabbit serum, the number of invasive cells was significant increased when we added SDRrepl antibody and TGF $\beta$ 1 into co-culture (Figure 29). We also performed transwell assay (Figure 30A) to mimic the beginning of cancer cell metastasis. We pre-seeded primary lung cells in lower well. The apical chamber was seeded with MDA-MB-231 cells with or without the coculture of cells-expressing SDRrepl.

Significantly, MDA-MB-231 cocultured with cells-expressing SDRrepl in apical chamber had an increased invasive activity. SDR Ab and TGF $\beta$ 1 treatment in lower well also increased the number of invasive MDA-MB-231 cell number (Figure 30B).

### **WWOX inhibits anchorage-independent cell growth of breast cancer cells.**

WWOX suppress tumorigenicity, a likely scenario is that it suppress tumor formation by inhibiting cancer cell migration. To determine the regulation of WWOX in anchorage-independent cell growth, we utilized established stable transfectants of MDA-MB-231 cells expressing EGFP-tagged WWOX (full length), SDR domain, WOX1 7-21, and EGFP only) to perform with soft agarose assay (figure 31). This data showed that WWOX stable transfectants, WWgre, SDR domain and full length, had the lower number and smaller size of colonies compared to control and GFP (figure 31). Intriguingly, we also observed the cell-to-cell junctions of stable transfectant-expressing SDR domain were looser than control and GFP sets and there seemed some cells migrating out (figure 31). However, cells closed tightly in WWgre set (figure 31). The observation agreed with the aforementioned results. Here, we confirmed WWgre and SDRrepl

participate in cell-to-cell recognition and migration in anchorage-independent 3D culture.

### **WWOX regulates cancer cells metastasis *in vivo***

We use BALB/C mice, and subcutaneous inject WWOX peptides and B16F10 melanoma cells in different site separately. Control mouse died due to enormous tumor and metastasis in 3 months post injection, however mice with WWOX peptide injection did not observed tumor formation (Figure 32). Then we inoculated mouse syngeneic breast cancer 4T1 cells into mice those had injected with WWOX peptides subcutaneously. 3 weeks post tumor inoculation, these mice were sacrificed, and the organs were fixed. Significantly, there was no lung or liver metastasis in mouse treated with WWgre (Figure 33). That is the injected WWgre peptide may induce immunoreaction of BALB/c mouse to generate anti-WWgre antibodies which reduced the WWgre expression of lung and liver. Lack of the WWgre, cancer cells cannot metastasize to target organs successfully. However, WWgre with phosphorylation at Ser14 failed to inhibit metastasis. Remarkably, the mouse treated with SDRrepl had the largest tumor size, and the most serious metastasis (Figure 33). That is injected SDRrepl peptide may induce the production of anti-SDRrepl antibodies to block the SDRrepl expression of lung and liver, and

result in target organs lost the repellence signals. The SDRrepl with phosphorylation at Tyr287 reduced the metastasis of SDRrepl. The underlying mechanism is still remained to uncover. In the future, we will use  $Wwox^{+/+}$  and  $Wwox^{-/-}$  mice to proceed the following research.

### **Self-polymerizing Zfra peptides elicit T cell-independent immune response for targeting cancer**

A novel immune response in targeting skin, breast, and many other cancer cells can be elicited by using self-polymerizing peptides. Zfra, a 31-amino-acid zinc finger-like protein that regulates apoptosis, is a WOX1-binding protein. Synthetic Zfra peptide undergoes self-polymerization in degassed enzyme-free solutions. Pre-injection of the full length Zfra1-31, or truncated Zfra4-10, via tail veins (<40 micromoles) protects nude mice from growing human prostate DU145, glioma U87-MG (Figure 34), many other cancer cells such as lung cancer NCI-H1299, breast cancer MDA-MB-231, basal cell carcinoma BCC, melanoma B16F10, glioma 13-06-MG, and so on. Alteration of Ser8 to Gly resulted in failure of self-polymerization and cancer suppression, suggesting that Ser8 is central to the function of Zfra both *in vivo* and *in vitro*. When spleen cells from Zfra-treated nude mice were transferred to naïve nude mice, these mice became resistant to the growth of implanted cancer cells (50-78% suppression), suggesting that non-T “memory”

cells are involved in blocking cancer growth. NOD-SCID mice, which are defective in innate T and B cells, failed to generate anticancer response upon pretreatment with Zfra peptides. The observations suggest non-T immune cells are involved in anticancer response.



## Discussion

Our breakthrough finding is the presence of significantly increased levels of TIAF1/TPC6A/Bif-2 complex in the NF1 tumor. Previous study shows that the protein complex is likely to support NF1 tumor progression. WOX1/WWOX is downregulated in the NF1 tumors, and this appears to lead to upregulation of TIAF1, TPC6A and Bif-2 and their aggregation. How these proteins control the growth of NF tumors is unknown and will be established in this proposed study. Our *Wwox*<sup>-/-</sup> MEF cells are susceptible to TGF- $\beta$ 1-induced protein aggregation. It is reasonable to hypothesize that WOX1 homeostatically stabilizes cellular proteins.

While synthetic zfra peptides are capable of eliciting T-cell independent immune response to block many types of cancer cell growth in vivo. Designing self-polymerizing peptides based upon the sequences of TIAF1, TPC6A and Bif-2 is likely to induce a similar response to blocking NF1 tumor growth.

Metastasis is believed as the major problem to cause poor cancer prognosis and low survival rate. In here, we also demonstrated that WWOX actually regulate cell migration and cell-to-cell recognition. *Wwox*<sup>-/-</sup> MEF cells migrate significantly faster than wild type *Wwox*<sup>+/+</sup> cells (Figure 14A). By time-lapse microscopy, we observed that wild type cells migrate collectively, however the knockout cells migrate individually (Figure 14B). The other tested WWOX-deficient cancer cells also migrate under an individual manner. These observations suggest that WWOX participates in cell shape control and migratory regulation.

In previous studies, overexpression of WWOX suppresses cell migration (Gourley et al., 2009). WWOX is considered as a tumor suppressor, in mouse,

targeted deletion of *Wwox* results in spontaneous tumor formation.(Aqeilan et al., 2007b). Thus, WWOX probably prevent tumorigenesis not only by inhibiting tumor growth but also suppression of cancer cells migration. There are studies indicate that WWOX can interact with Ezrin at membrane area, which is an intermediate between the cytoplasm membrane and the actin (Jin et al., 2006). Evidence also shows that WWOX can retain in cell membrane/cytoskeleton area interacting with Hyal-2 (Hsu et al., 2009). WWOX can interact with many other membrane area proteins including C1q binding protein (C1qBP) and Dishevelled protein (Dvl), the key components of Wnt/ $\beta$ -catenin signaling pathway (Bouteille et al., 2009; Hong et al., 2009). These finding suggest that WWOX can act as a sensor of extracellular cue.

We also observed when *Wwox*<sup>-/-</sup> knockout cells encountered wild type cells, the *Wwox*<sup>-/-</sup> knockout cells extended their pseudopodia to touch the wild type cells. *Wwox*<sup>-/-</sup> knockout cells then turned around and moved toward the opposite direction or divided rapidly (Figure 15A). The phenomena could also be observed in many WWOX-deficient cells encountered WWOX-expressing cells (Figure 15B, C). It means that WWOX participates in cell-to-cell recognition as well. For many cancers, migration is believed to be an initial step of invasion and metastasis (Friedl, 2009; van Zijl et al., 2011).

A variety of cancer cells can modulate their microenvironment and immune cells or tumor stroma cells (Rego et al., 2013; Shen et al., 2013a). A large part of cancer cells are highly devoid the expression of WWOX, either result from loss of heterozygosity (LOH) or promoter hypermethylation (Gourley et al., 2005; Yan et al., 2011).

In here, we further determined that WWOX regulates cell migration and cell-to-cell recognition by two segments which play distinct functions. SDRrepl epitope strongly fends off WWOX-deficient cells, whereas WWgre welcomes cells. (Figure 16,17). We also observed that EGFP-SDR-expressing MDA-MB-231 cells cause the visiting MDA-MB-231 control cells migration in a significant retrograde manner (Figure 21B, D). When an aliquot of antiserum against the SDR domain is added to the co-culture, anterograde movement of cells is restored (Figure 21B, F). The similar neutralized function was also observed when *WWOX*-deficient cells encountered WWOX-expressing cells (Figure 23, 24). We also determined TGF $\beta$ 1 can restore the anterograde movement of WWOX-deficient cancer cells when they encountered WWOX-expressing cells (Figure 26).

Many studies have mentioned that TGF- $\beta$  is frequently overproduced in invasive cancer cells, promoting epithelial mesenchymal transition (EMT), growth and eventual metastasis (Larocca et al., 2013; Tirino et al., 2013). In our study, we assay that TGF $\beta$ 1 can induce T $\beta$ RII and WWOX to translocate to cytoplasm (Figure 25, 27). So, maybe that is why the retrograde movement is disappeared under TGF $\beta$ 1 treatment.

We think conformational alterations of WWOX probably play a crucial role in determining cell-to-cell recognition. By Förster (Fluorescence) Resonance Energy Transfer (FRET), we determined that WWOX possesses intra-molecular and inter-molecular domain-domain interaction (Figure 28). TGF $\beta$ 1 also affects the domain-domain binding of WWOX (Figure 28). It supports our scenario that WWOX regulates migration and cell-to-cell-recognition by conformational alterations. Tumor suppressor WWOX is frequently deficient in metastatic cancer

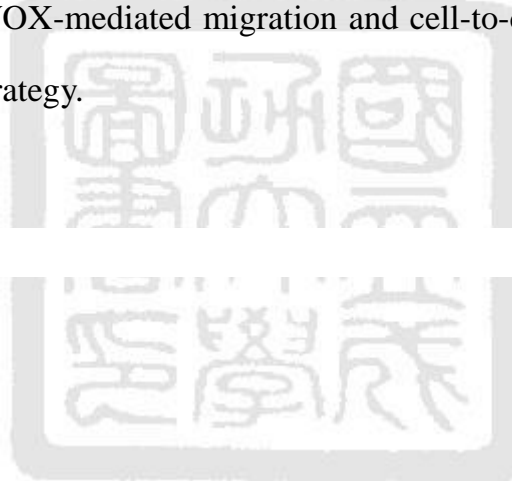
cells. We propose that when WWOX is not activated via Tyr33 (Chang et al., 2003, 2007; Chang et al., 2010), the protein is folded via WW/SDR domain interactions (a closed form) (Fig. 36A). As such, the C-terminal SDRrepl is concealed and the N-terminal WWgre is exposed and thereby attracts cells. When WWOX becomes activated via phosphorylation at Tyr33 (Chang et al., 2003, 2005, 2007), its SDRrepl is phosphorylated at Tyr287 and becomes exposed onto the cell surface (open form) (Fig. 36A). Concurrently, WWgre is hidden via binding with WW domain or D3 tail (Fig. 36A).

For example, serum-stimulated cells are frequently Tyr33-phosphorylated and the phosphorylation can be further increased by stress stimuli (Chang et al., 2003, 2005, 2007). Upon stimulation of these cells with TGF- $\beta$ 1 or specific antibody, internalization of T $\beta$ RII and SDRrepl occurs and thereby reduces the capability of the cells in fending off WWOX-negative cells. Metastatic cancer cells frequently secrete high levels of TGF- $\beta$  to enhance their proliferation. Conceivably, TGF- $\beta$ -induced loss of WWOX in cancer cells increases their metastatic potential.

By 2D invasion assay and trans well invasion assay, we determined the inhibition function of SDRrepl and the promotion of TGF $\beta$  in cell invasion (Figure 29, 30). In addition, *in vivo*, there is no lung or liver metastasis in mouse treated with WWgre (Figure 32, 33). That is the injected WWgre peptide induces immunoreaction of BALB/c mouse to generate anti-WWgre antibodies which reduces the WWgre expression of lung and liver. However, other peptides, SDRrepl, pSDRrepl and pWWgre all fail to suppress tumor metastasis.

From *in vivo* observations, we have demonstrated that when cancer cells start to metastasize, expression of WWOX/Wwox disappears gradually (Lai et al., 2005).

It is likely that, in initiation of metastasis, the WWOX of parental cancer cells are phosphorylated at Tyr287. The metastatic cells apparently become foreign to the parental tumor cells and are forced to migrate out of the tumor mass. These cells look for WWOX-negative or WWgre-exposed cells in the blood or lymphatic capillaries as friendly docking sites, so as to adhere, penetrate, and grow in target organs (Fig. 36C). We designate this as a “WOXin” model. The metastatic cells turn away from the WWOX-positive cells as “WOXout”. Regarding “WOXaway”, the metastatic cells dock with WWOX-negative or WWgre-expressing cells but run away when WWgre turns to SDRrepl on the cell surface (Fig. 36B). Thus, clarifying the mechanism of WWOX-mediated migration and cell-to-cell recognition offers a potential therapeutic strategy.



## References

- Abdeen, S.K., Salah, Z., Maly, B., Smith, Y., Tufail, R., Abu-Odeh, M., Zanesi, N., Croce, C.M., Nawaz, Z., and Aqeilan, R.I. (2011). Wwox inactivation enhances mammary tumorigenesis. *Oncogene* 30, 3900-3906.
- Aqeilan, R.I., Kuroki, T., Pekarsky, Y., Albagha, O., Trapasso, F., Baffa, R., Huebner, K., Edmonds, P., and Croce, C.M. (2004). Loss of WWOX expression in gastric carcinoma. *Clin Cancer Res* 10, 3053-3058.
- Aqeilan, R.I., Pekarsky, Y., Herrero, J.J., Palamarchuk, A., Letofsky, J., Druck, T., Trapasso, F., Han, S.Y., Melino, G., Huebner, K., *et al.* (2004b). Functional association between Wwox tumor suppressor protein and p73, a p53 homolog. *PNAS* 101, 4401-4406.
- Aqeilan, R.I., Trapasso, F., Hussain, S., Costinean, S., Marshall, D., Pekarsky, Y., Hagan, J.P., Zanesi, N., Kaou, M., Stein, G.S., *et al.* (2007). Targeted deletion of Wwox reveals a tumor suppressor function. *PNAS* 104, 3949-3954.
- Aqeilan, R.I., and Croce, C.M. (2007). WWOX in biological control and tumorigenesis. *J Cell Physiol* 212, 307-310.
- Aqeilan, R.I., Hagan, J.P., Aqeilan, H.A., Pichiorri, F., Fong, L.Y., and Croce, C.M. (2007a). Inactivation of the Wwox gene accelerates forestomach tumor progression in vivo. *Cancer Res* 67, 5606-5610.
- Aqeilan, R.I., Hassan, M.Q., de Bruin, A., Hagan, J.P., Volinia, S., Palumbo, T., Hussain, S., Lee, S.H., Gaur, T., Stein, G.S., *et al.* (2008). The WWOX tumor suppressor is essential for postnatal survival and normal bone metabolism. *J Biol Chem* 283, 21629-21639.
- Aqeilan, R.I., Hagan, J.P., de Bruin, A., Rawahneh, M., Salah, Z., Gaudio, E., Siddiqui, H., Volinia, S., Alder, H., Lian, J.B., *et al.* (2009). Targeted ablation of the WW domain-containing oxidoreductase tumor suppressor leads to impaired steroidogenesis. *Endocrinology* 150, 1530-1535.
- Bachman, K.E., and Park, B.H. (2005). Dual nature of TGF- $\beta$  signaling: tumor suppressor vs. tumor promoter. *Curr Opin Oncol* 17, 49-54.
- Bednarek, A.K., Laflin, K.J., Daniel, R.L., Liao, Q., Hawkins, K.A., and Aldaz, C.M. (2000). WWOX, a novel WW domain-containing protein mapping to human chromosome 16q23.3-24.1, a region frequently affected in breast cancer. *Cancer Res* 60, 2140-2145.
- Bednarek, A.K., Keck-Waggoner, C.L., Daniel, R.L., Laflin, K.J., Bergsagel, P.L., Kiguchi, K., Brenner, A.J., and Aldaz, C.M. (2001). WWOX, the FRA16D gene, behaves as a suppressor of tumor growth. *Cancer Res* 61, 8068-8073.

- Bouteille, N., Driouch, K., Hage, P.E., Sin, S., Formstecher, E., Camonis, J., Lidereau, R., and Lallemand, F. (2009). Inhibition of the Wnt/beta-catenin pathway by the WWOX tumor suppressor protein. *Oncogene* 28, 2569-2580.
- Bradbury, P., Fabry, B., and O'Neill, G.M. (2012). Occupy tissue: the movement in cancer metastasis. *Cell Adh Migr* 6, 424-432.
- Bravo-Cordero, J.J., Hodgson, L., and Condeelis, J. (2012). Directed cell invasion and migration during metastasis. *Curr Opin Cell Biol* 24, 277-283.
- Campos, D., Mendez, V., and Llopis, I. (2010). Persistent random motion: uncovering cell migration dynamics. *J Theor Biol* 267, 526-534.
- Chan, W., Tian, R., Lee, Y.F., Sit, S.T., Lim, L., and Manser, E. (2009). Down-regulation of active ACK1 is mediated by association with the E3 ubiquitin ligase Nedd4-2. *The J Biol Chem* 284, 8185-8194.
- Chang, J.Y., He, R.Y., Lin, H.P., Hsu, L.J., Lai, F.J., Hong, Q., Chen, S.J., and Chang, N.S. (2010). Signaling from membrane receptors to tumor suppressor WW domain-containing oxidoreductase. *Exp. Med. Biol* 235, 796-804.
- Chang, J.Y., Chiang, M.F., Lin, S.R., Lee, M.H., He, H., Chou, P.Y., Chen, S.J., Chen, Y.A., Yang, L.Y., Lai, F.J., *et al.* (2012). TIAF1 self-aggregation in peritumor capsule formation, spontaneous activation of SMAD-responsive promoter in p53-deficient environment, and cell death. *Cell Death Dis* 3, e302.
- Chang, N.S., Pratt, N., Heath, J., Schultz, L., Sleve, D., Carey, G.B., and Zevotek, N. (2001). Hyaluronidase induction of a WW domain-containing oxidoreductase that enhances tumor necrosis factor cytotoxicity. *J Biol Chem* 276, 3361-3370.
- Chang, N.S. (2002a). A potential role of p53 and WOX1 in mitochondrial apoptosis (review). *Int J Mol Med* 9, 19-24.
- Chang, N.S. (2002b). Transforming growth factor-beta1 blocks the enhancement of tumor necrosis factor cytotoxicity by hyaluronidase Hyal-2 in L929 fibroblasts. *BMC cell biol* 3, 8.
- Chang, N.S., Doherty, J., Ensign, A., Lewis, J., Heath, J., Schultz, L., Chen, S.T., and Oppermann, U. (2003). Molecular mechanisms underlying WOX1 activation during apoptotic and stress responses. *Biochem Pharmacol* 66, 1347-1354.
- Chang, N.S., Doherty, J., Ensign, A., Schultz, L., Hsu, L.J., and Hong, Q. (2005a). WOX1 is essential for tumor necrosis factor-, UV light-, staurosporine-, and p53-mediated cell death, and its tyrosine 33-phosphorylated form binds and stabilizes serine 46-phosphorylated p53. *J Biol Chem* 280, 43100-43108.
- Chang, N.S., Schultz, L., Hsu, L.J., Lewis, J., Su, M., and Sze, C.I. (2005b). 17beta-Estradiol upregulates and activates WOX1/WWOXv1 and WOX2/WWOXv2 in vitro: potential role in cancerous progression of breast and

- prostate to a premetastatic state in vivo. *Oncogene* 24, 714-723.
- Chang, N.S., Hsu, L.J., Lin, Y.S., Lai, F.J., and Sheu, H.M. (2007). WW domain-containing oxidoreductase: a candidate tumor suppressor. *Trends Mol Med* 13, 12-22.
- Chen, S.T., Chuang, J.I., Wang, J.P., Tsai, M.S., Li, H., and Chang, N.S. (2004). Expression of WW domain-containing oxidoreductase WOX1 in the developing murine nervous system. *Neuroscience* 124, 831-839.
- Chen, S.T., Chuang, J.I., Cheng, C.L., Hsu, L.J., and Chang, N.S. (2005). Light-induced retinal damage involves tyrosine 33 phosphorylation, mitochondrial and nuclear translocation of WW domain-containing oxidoreductase in vivo. *Neuroscience* 130, 397-407.
- Chen, Y.Y., Li, C.F., Yeh, C.H., Chang, M.S., and Hsing, C.H. (2013). Interleukin-19 in breast cancer. *Clin Dev Immunol* 2013, 294320.
- Chiang, M.F., Yeh, S.T., Liao, H.F., Chang, N.S., and Chen, Y.J. (2012). Overexpression of WW domain-containing oxidoreductase WOX1 preferentially induces apoptosis in human glioblastoma cells harboring mutant p53. *Biomed Pharmacother* 66, 433-438.
- Chiang, M.F., Chou, P.Y., Wang, W.J., Sze, C.I., and Chang, N.S. (2013). Tumor Suppressor WWOX and p53 Alterations and Drug Resistance in Glioblastomas. *FONC* 3, 43.
- Driouch, K., Prydz, H., Monese, R., Johansen, H., Lidereau, R., and Frengen, E. (2002). Alternative transcripts of the candidate tumor suppressor gene, WWOX, are expressed at high levels in human breast tumors. *Oncogene* 21, 1832-1840.
- Drusco, A., Pekarsky, Y., Costinean, S., Antenucci, A., Conti, L., Volinia, S., Aqeilan, R.I., Huebner, K., and Zanesi, N. (2011). Common fragile site tumor suppressor genes and corresponding mouse models of cancer. *J Biomed Biotechnol* 2011, 984505.
- Fabbri, M., Iliopoulos, D., Trapasso, F., Aqeilan, R.I., Cimmino, A., Zanesi, N., Yendamuri, S., Han, S.Y., Amadori, D., Huebner, K., *et al.* (2005). WWOX gene restoration prevents lung cancer growth in vitro and in vivo. *PNAS* 102, 15611-15616.
- Friedl, P. (2009). Dynamic imaging of cancer invasion and metastasis: principles and preclinical applications. *Clin Exp Metastasis* 26, 269-271.
- Gangadhara, S., Barrett-Lee, P., Nicholson, R.I., and Hiscox, S. (2012). Pro-metastatic tumor-stroma interactions in breast cancer. *Future oncology* 8, 1427-1442.
- Ghebrehiwet, B., Hosszu, K.K., Valentino, A., and Peerschke, E.I. (2012). The C1q family of proteins: insights into the emerging non-traditional functions. *Fimmu* 3.
- Gourley, C., Paige, A.J., Taylor, K.J., Scott, D., Francis, N.J., Rush, R., Aldaz, C.M., Smyth, J.F., and Gabra, H. (2005). WWOX mRNA expression profile in epithelial ovarian cancer supports the role of WWOX variant 1 as a tumour suppressor, although the

- role of variant 4 remains unclear. *Int J Oncol* 26, 1681-1689.
- Gourley, C., Paige, A.J., Taylor, K.J., Ward, C., Kuske, B., Zhang, J., Sun, M., Janczar, S., Harrison, D.J., Muir, M., *et al.* (2009). WWOX gene expression abolishes ovarian cancer tumorigenicity in vivo and decreases attachment to fibronectin via integrin alpha3. *Cancer Res* 69, 4835-4842.
- Guo, W., Dong, Z., Dong, Y., Guo, Y., Kuang, G., and Yang, Z. (2013a). Genetic and epigenetic alterations of WWOX in the development of gastric cardia adenocarcinoma. *Environ Mol Mutagen* 54, 112-123.
- Guo, W., Wang, G., Dong, Y., Guo, Y., Kuang, G., and Dong, Z. (2013b). Decreased expression of WWOX in the development of esophageal squamous cell carcinoma. *Mol Carcinogenesis* 52, 265-274.
- Gwynn B, Smith RS, Rowe LB, Taylor BA, Peters LL (2006) A mouse TRAPP-related protein is involved in pigmentation. *Genomics* 88, 196-203
- Heldin, C.H., Miyazono, K., and ten Dijke, P. (1997). TGF- $\beta$  signalling from cell membrane to nucleus through SMAD proteins. *Nature* 390, 465-471.
- Hong, Q., Kuo, E., Schultz, L., Boackle, R.J., and Chang, N.S. (2007). Conformationally altered hyaluronan restricts complement classical pathway activation by binding to C1q, C1r, C1s, C2, C5 and C9, and suppresses WOX1 expression in prostate DU145 cells. *Int J Mol Med* 19, 173-179.
- Hong, Q., Sze, C.I., Lin, S.R., Lee, M.H., He, R.Y., Schultz, L., Chang, J.Y., Chen, S.J., Boackle, R.J., Hsu, L.J., *et al.* (2009). Complement C1q activates tumor suppressor WWOX to induce apoptosis in prostate cancer cells. *PLoS one* 4, e5755.
- Hsu, L.J., Schultz, L., Hong, Q., Van Moer, K., Heath, J., Li, M.Y., Lai, F.J., Lin, S.R., Lee, M.H., Lo, C.P., *et al.* (2009). Transforming growth factor beta1 signaling via interaction with cell surface Hyal-2 and recruitment of WWOX/WOX1. *J Biol Chem* 284, 16049-16059.
- Imai, K., Minamiya, Y., Goto, A., Nanjo, H., Saito, H., Motoyama, S., Sato, Y., Kudo, S., Takashima, S., Kawaharada, Y., *et al.* (2013). Bronchioloalveolar invasion in non-small cell lung cancer is associated with expression of transforming growth factor-beta1. *World J Microb Biot* 11, 113.
- Jenner, M.W., Leone, P.E., Walker, B.A., Ross, F.M., Johnson, D.C., Gonzalez, D., Chiecchio, L., Dachs Cabanas, E., Dagrada, G.P., Nightingale, M., *et al.* (2007). Gene mapping and expression analysis of 16q loss of heterozygosity identifies WWOX and CYLD as being important in determining clinical outcome in multiple myeloma. *Blood* 110, 3291-3300.
- Jin, C., Ge, L., Ding, X., Chen, Y., Zhu, H., Ward, T., Wu, F., Cao, X., Wang, Q., and Yao, X. (2006). PKA-mediated protein phosphorylation regulates ezrin-WWOX

- interaction. *Biochem Biophys Res Commun* 341, 784-791.
- Kretzschmar, M., and Massague, J. (1998). SMADs: mediators and regulators of TGF- $\beta$  signaling. *Curr Opin Genet Dev* 8, 103-111.
- Kurek, K.C., Del Mare, S., Salah, Z., Abdeen, S., Sadiq, H., Lee, S.H., Gaudio, E., Zanasi, N., Jones, K.B., DeYoung, B., *et al.* (2010). Frequent attenuation of the WWOX tumor suppressor in osteosarcoma is associated with increased tumorigenicity and aberrant RUNX2 expression. *Cancer Res* 70, 5577-5586.
- Lai, F.J., Cheng, C.L., Chen, S.T., Wu, C.H., Hsu, L.J., Lee, J.Y., Chao, S.C., Sheen, M.C., Shen, C.L., Chang, N.S., *et al.* (2005). WOX1 is essential for UVB irradiation-induced apoptosis and down-regulated via translational blockade in UVB-induced cutaneous squamous cell carcinoma in vivo. *Clinical cancer research : an official journal of the American Association for Cancer Res* 11, 5769-5777.
- Larocca, C., Cohen, J.R., Fernando, R.I., Huang, B., Hamilton, D.H., and Palena, C. (2013). An autocrine loop between TGF- $\beta$ 1 and the transcription factor Brachyury controls the transition of human carcinoma cells into a mesenchymal phenotype. *Mol Cancer Ther.*
- Lee MH, Lin SR, Chang JY, Schultz L, Heath J, Hsu LJ, Kuo YM, Hong Q, Chiang MF, Gong CX, Sze CI, Chang NS (2010) TGF- $\beta$  induces TIAF1 self-aggregation via type II receptor-independent signaling that leads to generation of amyloid  $\beta$  plaques in Alzheimer's disease. *Cell Death & Dis* 1, e110.
- Lewandowska, U., Zelazowski, M., Seta, K., Byczewska, M., Pluciennik, E., and Bednarek, A.K. (2009). WWOX, the tumour suppressor gene affected in multiple cancers. *J Physiol Pharmacol* 1, 47-56.
- Li, M.Y., Lai, F.J., Hsu, L.J., Lo, C.P., Cheng, C.L., Lin, S.R., Lee, M.H., Chang, J.Y., Subhan, D., Tsai, M.S., *et al.* (2009). Dramatic co-activation of WWOX/WOX1 with CREB and NF-kappaB in delayed loss of small dorsal root ganglion neurons upon sciatic nerve transection in rats. *PloS one* 4, e7820.
- Lin, D., Cui, Z., Kong, L., Cheng, F., Xu, J., and Lan, F. (2013). p73 participates in WWOX-mediated apoptosis in leukemia cells. *Intl J Mol Med* 31, 849-854.
- Lin, H.P., Chang, J.Y., Lin, S.R., Lee, M.H., Huang, S.S., Hsu, L.J., and Chang, N.S. (2011). Identification of an In Vivo MEK/WOX1 Complex as a Master Switch for Apoptosis in T Cell Leukemia. *Genes & cancer* 2, 550-562.
- Liu, C.J., Shen, W.G., Peng, S.Y., Cheng, H.W., Kao, S.Y., Lin, S.C., and Chang, K.W. (2013). miR-134 induces oncogenicity and metastasis in head and neck carcinoma through targeting WWOX gene. *Int J Cancer*.
- Lo, C.P., Hsu, L.J., Li, M.Y., Hsu, S.Y., Chuang, J.I., Tsai, M.S., Lin, S.R., Chang, N.S.,

- and Chen, S.T. (2008). MPP<sup>+</sup>-induced neuronal death in rats involves tyrosine 33 phosphorylation of WW domain-containing oxidoreductase WOX1. *Eur J Neuroscience* 27, 1634-1646.
- Ludes-Meyers, J.H., Kil, H., Bednarek, A.K., Drake, J., Bedford, M.T., and Aldaz, C.M. (2004). WWOX binds the specific proline-rich ligand PPXY: identification of candidate interacting proteins. *Oncogene* 23, 5049-5055.
- Matsuoka, J., Yashiro, M., Doi, Y., Fuyuhiko, Y., Kato, Y., Shinto, O., Noda, S., Kashiwagi, S., Aomatsu, N., Hirakawa, T., *et al.* (2013). Hypoxia Stimulates the EMT of Gastric Cancer Cells through Autocrine TGFbeta Signaling. *PloS one* 8, e62310.
- McClatchey AI (2007) Neurofibromatosis. *Annu Rev Pathol* 2, 191-216. Review.
- Mo, N., Li, Z.Q., Li, J., and Cao, Y.D. (2012). Curcumin inhibits TGF- $\beta$ 1-induced MMP-9 and invasion through ERK and Smad signaling in breast cancer MDA-MB-231 cells. *APJCP* 13, 5709-5714.
- Muraoka-Cook, R.S., Dumont, N., and Arteaga, C.L. (2005). Dual role of transforming growth factor beta in mammary tumorigenesis and metastatic progression. *Clin Cancer Res* 11, 937s-943s.
- Nakayama, S., Semba, S., Maeda, N., Matsushita, M., Kuroda, Y., and Yokozaki, H. (2009). Hypermethylation-mediated reduction of WWOX expression in intraductal papillary mucinous neoplasms of the pancreas. *Br J Cancer* 100, 1438-1443.
- Naumanen, P., Lappalainen, P., and Hotulainen, P. (2008). Mechanisms of actin stress fibre assembly. *J. Microsc.* 231, 446-454.
- Nunez, M.I., Ludes-Meyers, J., and Aldaz, C.M. (2006). WWOX protein expression in normal human tissues. *J Mol Histol* 37, 115-125.
- O'Keefe, L.V., and Richards, R.I. (2006). Common chromosomal fragile sites and cancer: focus on FRA16D. *Cancer letters* 232, 37-47.
- Park, S.W., Ludes-Meyers, J., Zimonjic, D.B., Durkin, M.E., Popescu, N.C., and Aldaz, C.M. (2004). Frequent downregulation and loss of WWOX gene expression in human hepatocellular carcinoma. *Br J Cancer* 91, 753-759.
- Pluciennik, E., Kusinska, R., Potemski, P., Kubiak, R., Kordek, R., and Bednarek, A.K. (2006). WWOX--the FRA16D cancer gene: expression correlation with breast cancer progression and prognosis. *Eur J Surg Oncol* 32, 153-157.
- Presser, L.D., McRae, S., and Waris, G. (2013). Activation of TGF- $\beta$ 1 promoter by hepatitis C virus-induced AP-1 and Sp1: role of TGF- $\beta$ 1 in hepatic stellate cell activation and invasion. *PloS one* 8, e56367.
- Qu, J., Lu, W., Li, B., Lu, C., and Wan, X. (2013). WWOX induces apoptosis and inhibits proliferation in cervical cancer and cell lines. *Int J Mol Med* 31, 1139-1147.
- Quan, J., Elhousiny, M., Johnson, N.W., and Gao, J. (2013). Transforming growth

- factor-beta1 treatment of oral cancer induces epithelial-mesenchymal transition and promotes bone invasion via enhanced activity of osteoclasts. *Clin Exp Metastasis* 30, 659-670.
- Ramos, D., and Aldaz, C.M. (2006). WWOX, a chromosomal fragile site gene and its role in cancer. *Adv. Exp. Med. Biol.* 587, 149-159.
- Rego, S.L., Swamydas, M., Kidiyoor, A., Helms, R., De Piante, A., Lance, A.L., Mukherjee, P., and Dreau, D. (2013). Soluble Tumor Necrosis Factor Receptors Shed by Breast Tumor Cells Inhibit Macrophage J. *Interferon Cytokine Res.*
- Reticker-Flynn, N.E., Malta, D.F., Winslow, M.M., Lamar, J.M., Xu, M.J., Underhill, G.H., Hynes, R.O., Jacks, T.E., and Bhatia, S.N. (2012). A combinatorial extracellular matrix platform identifies cell-extracellular matrix interactions that correlate with metastasis. *Nature comm* 3, 1122.
- Rorth, P. (2009). Collective cell migration. *Annual review of cell and developmental biology* 25, 407-429.
- Sacher M, Kim YG, Lavie A, Oh BH, Segev N (2008) The TRAPP Complex: Insights into its Architecture and Function. *Traffic* 9, 2032-2042
- Sengbusch, J.K., He, W., Pinco, K.A., and Yang, J.T. (2002). Dual functions of  $\alpha 4\beta 1$  integrin in epicardial development: initial migration and long-term attachment. *J cell Biol* 157, 873-882.
- Sheetz, M.P., Felsenfeld, D., Galbraith, C.G., and Choquet, D. (1999). Cell migration as a five-step cycle. *Biochem Soci sympo* 65, 233-243.
- Shen, Z., Kauttu, T., Cao, J., Seppanen, H., Vainionpaa, S., Ye, Y., Wang, S., Mustonen, H., and Puolakkainen, P. (2013a). Macrophage coculture enhanced invasion of gastric cancer cells via TGF- $\beta$  and BMP pathways. *Scand J Gastroenterol* 48, 466-472.
- Shen, Z., Seppanen, H., Kauttu, T., Vainionpaa, S., Ye, Y., Wang, S., Mustonen, H., and Puolakkainen, P. (2013b). Vasohibin-1 Expression Is Regulated by Transforming Growth Factor-beta/Bone Morphogenic Protein Signaling Pathway Between Tumor-Associated Macrophages and Pancreatic Cancer Cells. *J Interferon Cytokine Res.*
- Sleeman, J., and Steeg, P.S. (2010). Cancer metastasis as a therapeutic target. *Eur J cancer* 46, 1177-1180.
- Suzuki, H., Katayama, K., Takenaka, M., Amakasu, K., Saito, K., and Suzuki, K. (2009). A spontaneous mutation of the Wwox gene and audiogenic seizures in rats with lethal dwarfism and epilepsy. *Genes Brain Behav* 8, 650-660.
- Sze, C.I., Su, M., Pugazhenthii, S., Jambal, P., Hsu, L.J., Heath, J., Schultz, L., and Chang, N.S. (2004). Down-regulation of WW domain-containing oxidoreductase induces Tau phosphorylation in vitro. A potential role in Alzheimer's disease. *J Biol Chem*

279, 30498-30506.

- Sze, C.I., Su, W.P., Chiang, M.F., Lu, C.Y., Chen, Y.A., and Chang, N.S. (2013). Assessing current therapeutic approaches to decode potential resistance mechanisms in glioblastomas. *FONC* 3, 59.
- Teng, C.C., Yang, Y.T., Chen, Y.C., Kuo, Y.M., and Sze, C.I. (2012). Role of WWOX/WOX1 in Alzheimer's disease pathology and in cell death signaling. *Front biosci* 4, 1951-1965.
- Teng, C.C., Yang, Y.T., Chen, Y.C., Kuo, Y.M., and Sze, C.I. (2013). Role of WWOX/WOX1 in Alzheimer's disease pathology and in cell death signaling. *Front biosci* 5, 72-85.
- Tirino, V., Camerlingo, R., Bifulco, K., Irollo, E., Montella, R., Paino, F., Sessa, G., Carriero, M.V., Normanno, N., Rocco, G., *et al.* (2013). TGF- $\beta$ 1 exposure induces epithelial to mesenchymal transition both in CSCs and non-CSCs of the A549 cell line, leading to an increase of migration ability in the CD133(+) A549 cell fraction. *Cell Death Dis* 4, e620.
- Tkachenko, E., Sabouri-Ghomi, M., Pertz, O., Kim, C., Gutierrez, E., Machacek, M., Groisman, A., Danuser, G., and Ginsberg, M.H. (2011). Protein kinase A governs a RhoA-RhoGDI protrusion-retraction pacemaker in migrating cells. *Nat Cell Biol* 13, 660-667.
- Tojkander, S., Gateva, G., Schevzov, G., Hotulainen, P., Naumanen, P., Martin, C., Gunning, P.W., and Lappalainen, P. (2011). A molecular pathway for myosin II recruitment to stress fibers. *Current biology : CB*. 21, 539-550.
- Van Zijl, F., Krupitza, G., and Mikulits, W. (2011). Initial steps of metastasis: cell invasion and endothelial transmigration. *Mutation research* 728, 23-34.
- Vorotnikov, A.V. (2011). Chemotaxis: movement, direction, control. *Biochemistry Mosc.* 76, 1528-1555.
- Wang, X., Chao, L., Jin, G., Ma, G., Zang, Y., and Sun, J. (2009). Association between CpG island methylation of the WWOX gene and its expression in breast cancers. *Tumour Biol* 30, 8-14.
- Watanabe T, Oda Y, Tamiya S, Masuda K, Tsuneyoshi M (2001) Malignant peripheral nerve sheath tumour arising within neurofibroma. An immunohistochemical analysis in the comparison between benign and malignant components. *J Clin Pathol* 54, 631-636.
- Weber, S.C., Thompson, M.A., Moerner, W.E., Spakowitz, A.J., and Theriot, J.A. (2012). Analytical tools to distinguish the effects of localization error, confinement, and medium elasticity on the velocity autocorrelation function. *Biophys J* 102, 2443-2450.

- Weiss, A., and Attisano, L. (2013). The TGFbeta Superfamily Signaling Pathway. Wiley Interdiscip Rev Dev Bio 2, 47-63.
- Wolf, K., and Friedl, P. (2011). Extracellular matrix determinants of proteolytic and non-proteolytic cell migration. Trends Cell Biol 21, 736-744.
- Yang FC, Chen S, Clegg T, Li X, Morgan T, Estwick SA, Yuan J, Khalaf W, Burgin S, Travers J, Parada LF, Ingram DA, Clapp DW (2006) Nf1+/- mast cells induce neurofibroma like phenotypes through secreted TGF-β signaling. Hum Mol Genet 15, 2421-2437.
- Yang, J., and Zhang, W. (2008). WWOX tumor suppressor gene. Histol Histopathol 23, 877-882.
- Yang, J., Cogdell, D., Yang, D., Hu, L., Li, H., Zheng, H., Du, X., Pang, Y., Trent, J., Chen, K., *et al.* (2010). Deletion of the WWOX gene and frequent loss of its protein expression in human osteosarcoma. Cancer letters 291, 31-38.
- Yan, J., Zhang, M., Zhang, J., Chen, X., and Zhang, X. (2011). Helicobacter pylori infection promotes methylation of WWOX gene in human gastric cancer. Biochem Biophys Res Commun 408, 99-102.
- Zhou, Y., Xu, Y., and Zhang, Z. (2005). Deletion and mutation of WWOX exons 6-8 in human non-small cell lung cancer. J. Huazhong Univ. Sci. Technol Med sci 25, 162-165.

# Figures

**Figure 1. Schematic diagram of WWOX structure and designed peptides.**

WW domain-containing oxidoreductase, also known as WWOX, FOR or WOX1, which is composed of two *N*-terminal WW domains, a nuclear localization sequence, a *C*-terminal alcohol dehydrogenase (ADH) domain and a D3 region. There are a nuclear localization sequence (NLS) between the WW domains, and a mitochondria-binding region in the SDR domain. WWOX possesses an NSYK (Asn-Ser-Tyr-Lys) motif, which is able to bind to sex steroid, supporting that WWOX is also a candidate hormone receptor. There are two conserved tyrosine phosphorylation sites, Tyr33 and Tyr287. Tyr6, Thr12, Ser14, Tyr61, Tyr293, and Thr393 are also predicted phosphorylation sites by NetPhos 2.0 Sever (Technical University of Denmark).

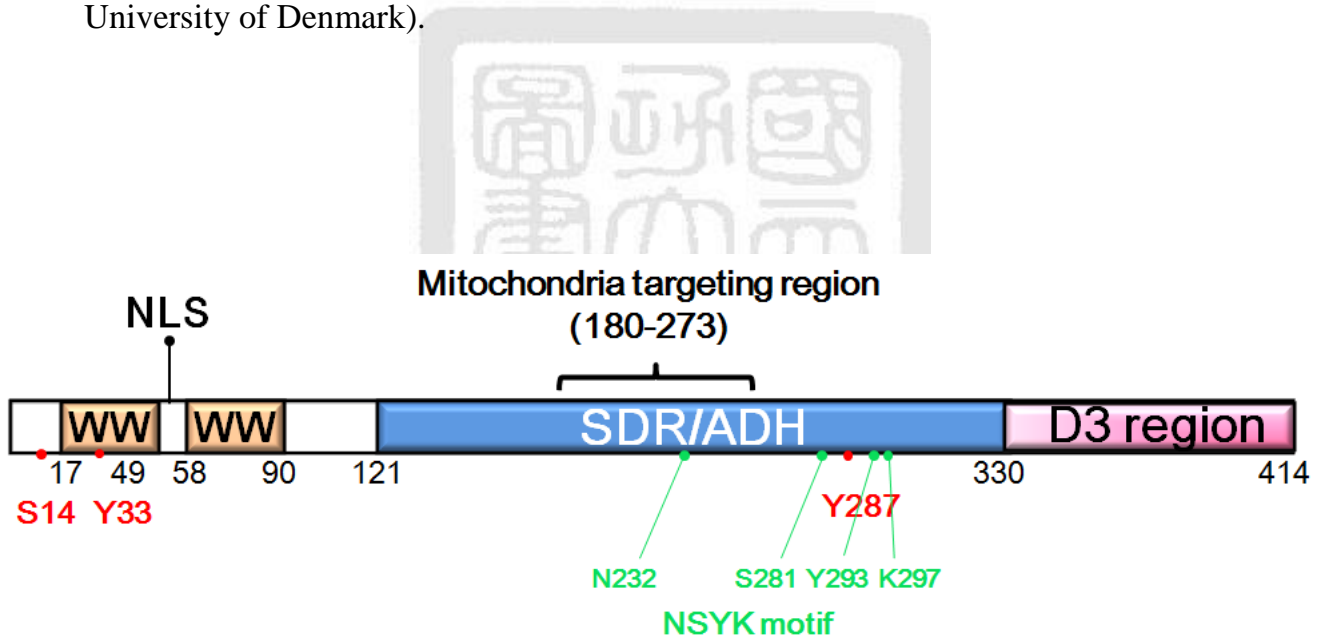


**Figure 2. Expression of WOX1, TIAF1, TPC6A and Bif-2 in the cutaneous NF1 neurofibromas.**

(A) Tumor sections from 3 patients with NF1 were stained with indicated antibodies and the whole tissue sections were scanned using a scanner. (B,C,D) By immunohistochemistry, the protein expression levels of the aforementioned proteins are shown to increase, whereas the WOX1 levels are low. (E) No signal is shown in the negative control. Non-immune serum was used.

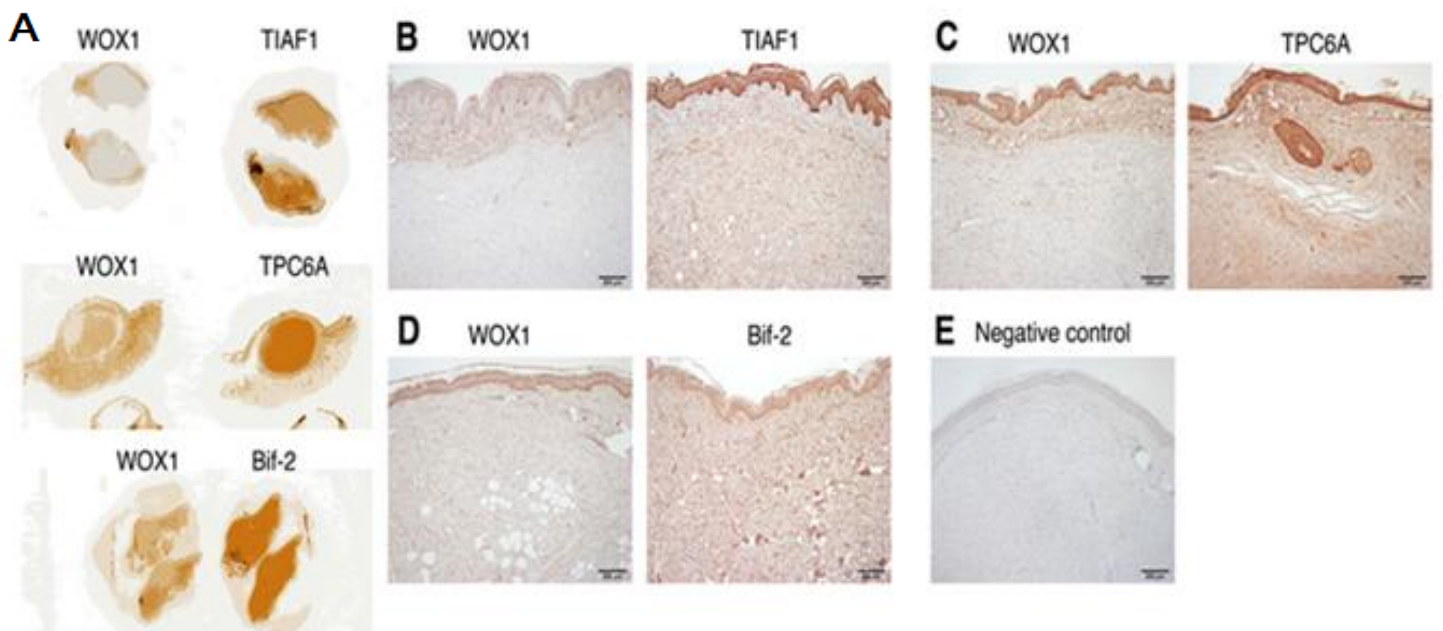
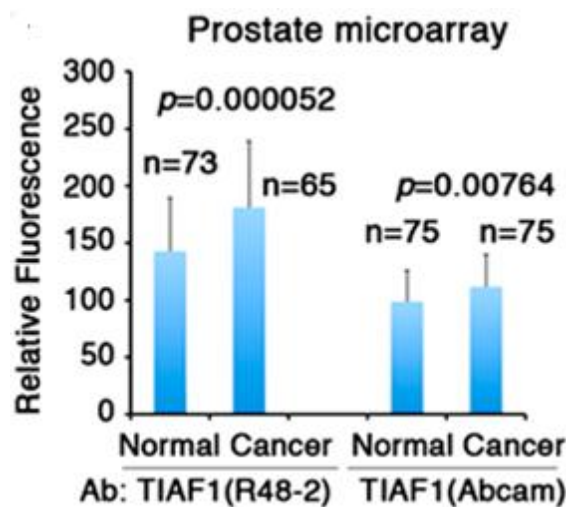


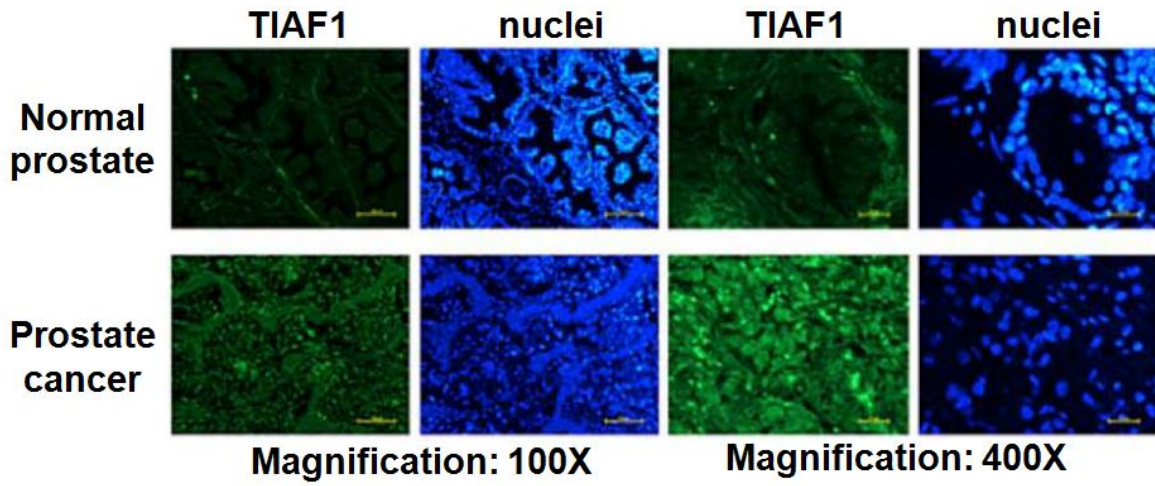
**Figure 3. TIAF1 protein expression is significantly increased in prostate cancer.**

(A) TIAF1 protein expression is significantly increased in prostate cancer, compared with normal controls, as determined using both the TIAF1(R48-2) homemade antibody (left panel) and a commercial TIAF1 antibody (right panel) for immunofluorescence microscopy in prostate tissue microarray slides from NCI (Student's *t*-test). (B) Compared to normal prostate, TIAF1 levels are increased by 50-120% in prostate cancer. Nuclei were stained with DAPI. Representative tissue sections were from staining 5 normal controls and 5 prostate cancer tissue sections. (C) In parallel with the above observations, TIAF1 has a higher level of expression in cancer, compared with the normal controls. Representative data is from 6 controls and 6 prostate cancers. Scale bar, 100  $\mu$ m at left column (200x magnification), and 50  $\mu$ m at right column (400x magnification). In negative controls, the R48-2 peptide was used to block the immunostaining. (D) TIAF1 (green) is significantly upregulated in colon cancer cells, as compared to age-matched controls. Also, the levels of Smad4 (red) are significantly increased in the colon cancer group compared with the normal controls. The number on top of each bar is the times for measuring a fixed square area in tissue sections from 5 samples or patients. Statistical analysis: normal versus cancer, Student's *t* test. In negative controls, fluorescent secondary antibodies were used only.

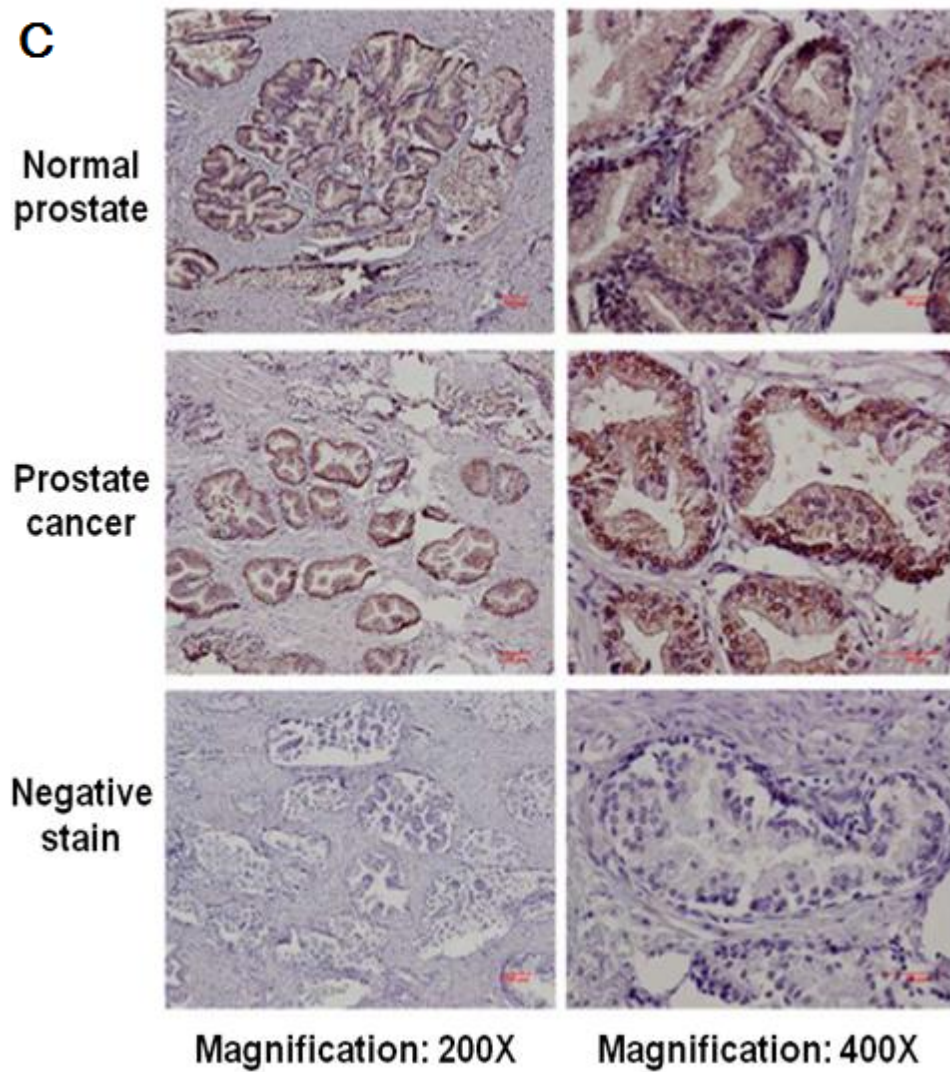
**A**



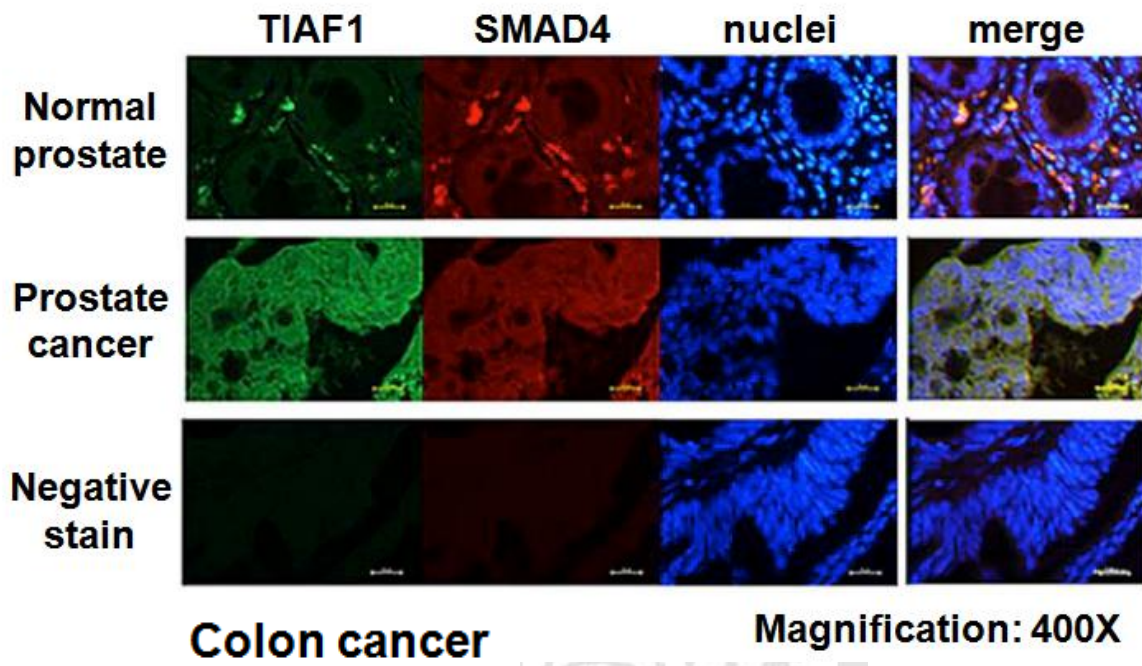
**B**



**C**

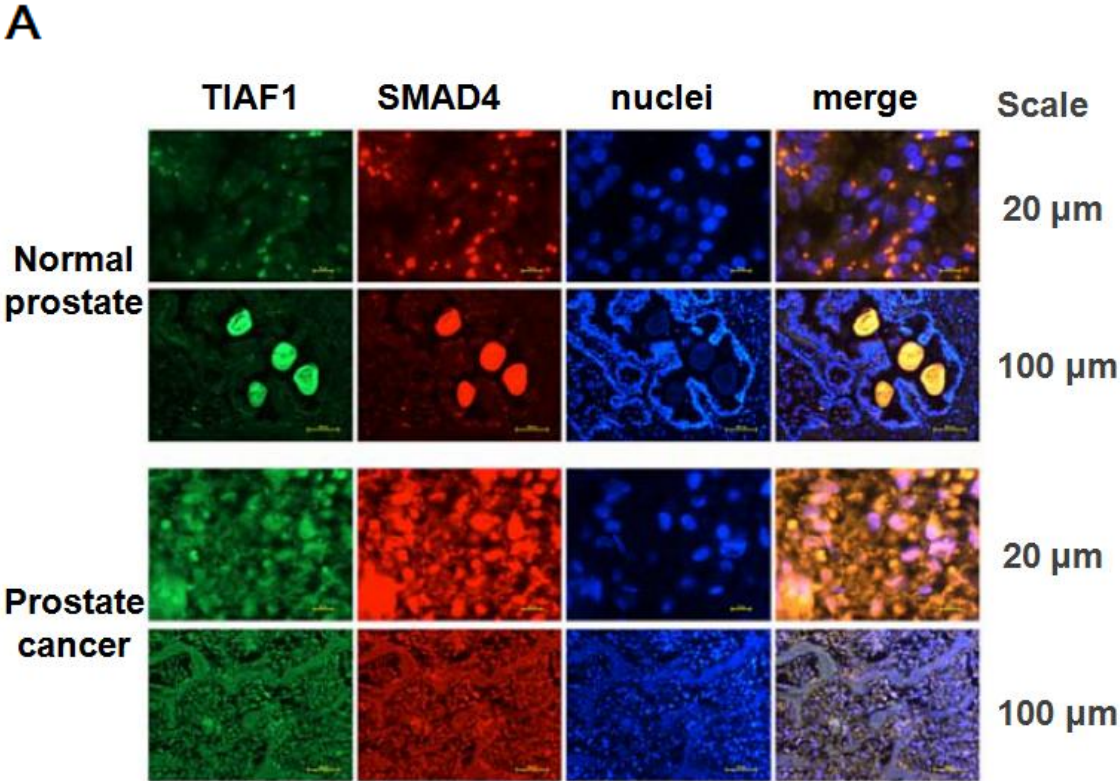


**D**



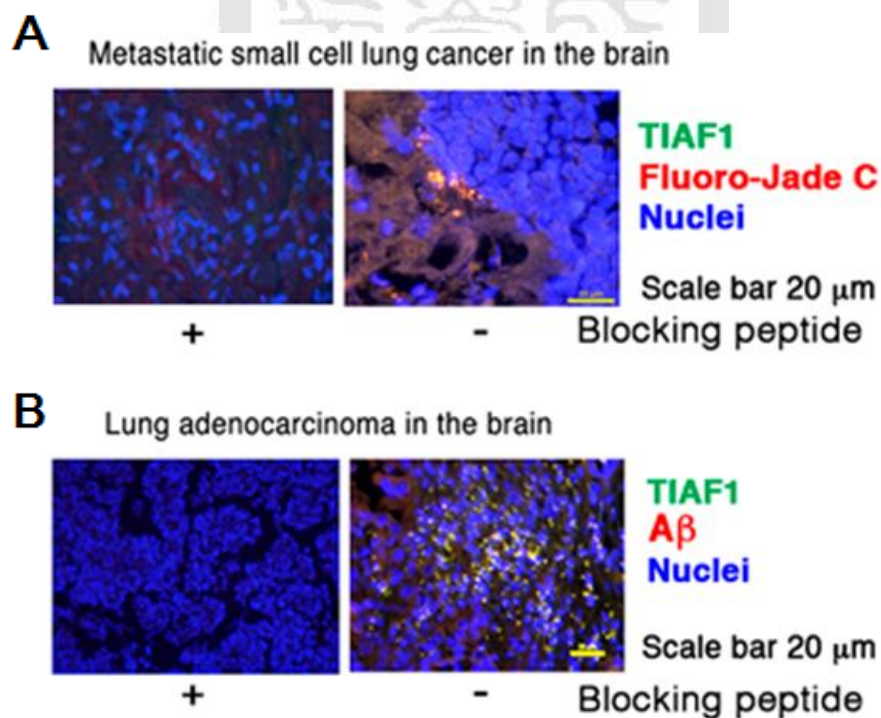
**Figure 4. TIAF1 colocalizes with Smad4 in prostate cancer.**

(A) TIAF1 co-localizes with Smad4 in the prostatic concretions in the lumens of prostatic glandular ducts. Both proteins are significantly upregulated in the non-metastatic prostate cancer. (B) Colocalization of TIAF1 and Smad4 is shown in the prostate gland cells.



### Figure 5. TIAF1 overexpression, aggregation and super-induction of A $\beta$ .

TIAF1 aggregation in the interface between metastatic cancer cells and the brain tissues. (A) Presence of aggregated TIAF1 in the dead neurons located in the interface between the brain tissue and the metastatic small-cell lung cancer. Degenerating neurons were stained with Fluoro-Jade C (red). Nuclei were stained with DAPI. Scale bar, 20  $\mu$ m;  $\times$  400 magnification. A merged image is of TIAF1 (green), Fluoro-Jade C (red) and DAPI (blue). (B) TIAF1/A $\beta$  aggregates are shown in a metastatic lung adenocarcinoma in the brain. Scale bar, 20  $\mu$ m;  $\times$  400 magnification. A merged image is of TIAF1 (green), A $\beta$  (red) and DAPI (blue). (C, D) In IHC staining, expression of WOX1 and TIAF1 is shown in neurofibromatosis NF1. TIAF1 is overexpressed in the peritumor area, but is less expressed in the tumor itself. Scale bar, 100  $\mu$ m. (E) Fibrous protein aggregates are shown in the peritumor coats of neurofibromas. TIAF1 is present in the fibrous aggregates (400X magnification). (F) Representative pictures are shown, which were taken surrounding the peritumor areas. TIAF1 fibrils are digitally magnified approximately 20-fold from the TIAF1 picture (lower left).



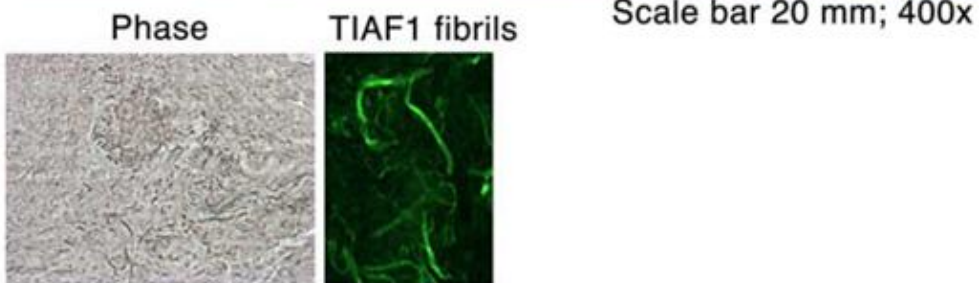
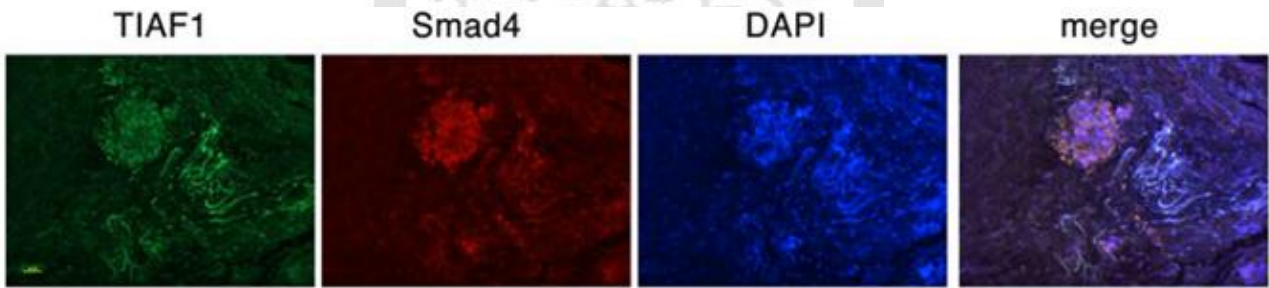
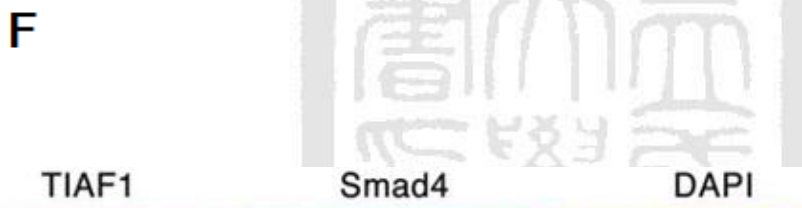
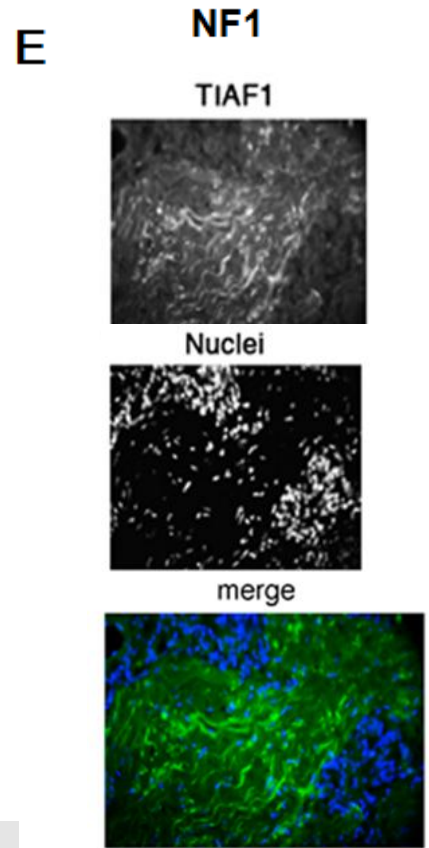
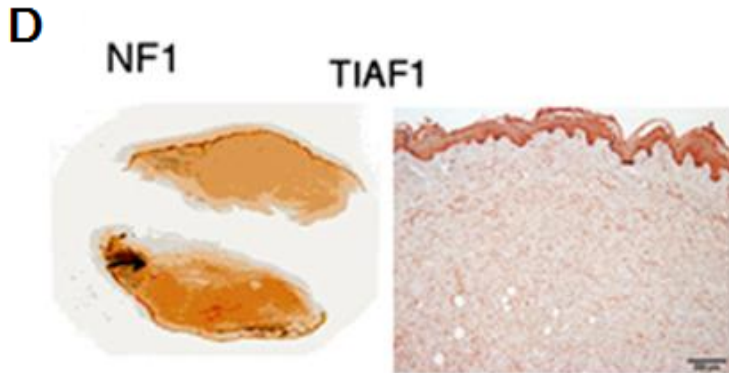
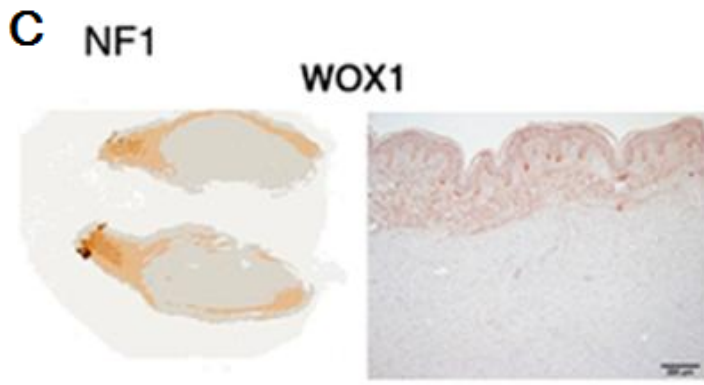


**Figure 6. TIAF1 self-association induces expression of Smad4 .**

(A) MCF7 cells were transiently transfected with ECFP and EYFP (C/Y) or ECFP-TIAF1 and EYFP-TIAF1 (Tc/Ty) by liposome. The cells were treated with or without TGF- $\beta$ 1 (5 ng/ml) for 24 h. TIAF1 self-binding was analyzed by FRET microscopy. FRETc shows the extent of protein/protein binding. TIAF1 self-binding led to Smad4 expression, as determined by immunofluorescence staining. Statistical analysis: all tests *versus* C/Y controls; Student’s *t*-test ( $n=6$ ). The induced Smad4 colocalized with TIAF1 in the cytoplasm and the spiny protrusion (400X magnification). (B) MCF7 cells were transiently transfected with ECFP-TIAF1 and EYFP-TIAF1 by liposome. The induced Smad4 (red) colocalizes with ECFP-TIAF1 (cyan) and EYFP-TIAF1 (yellow) in the cytoplasm and the spiny protrusion (400x magnification).

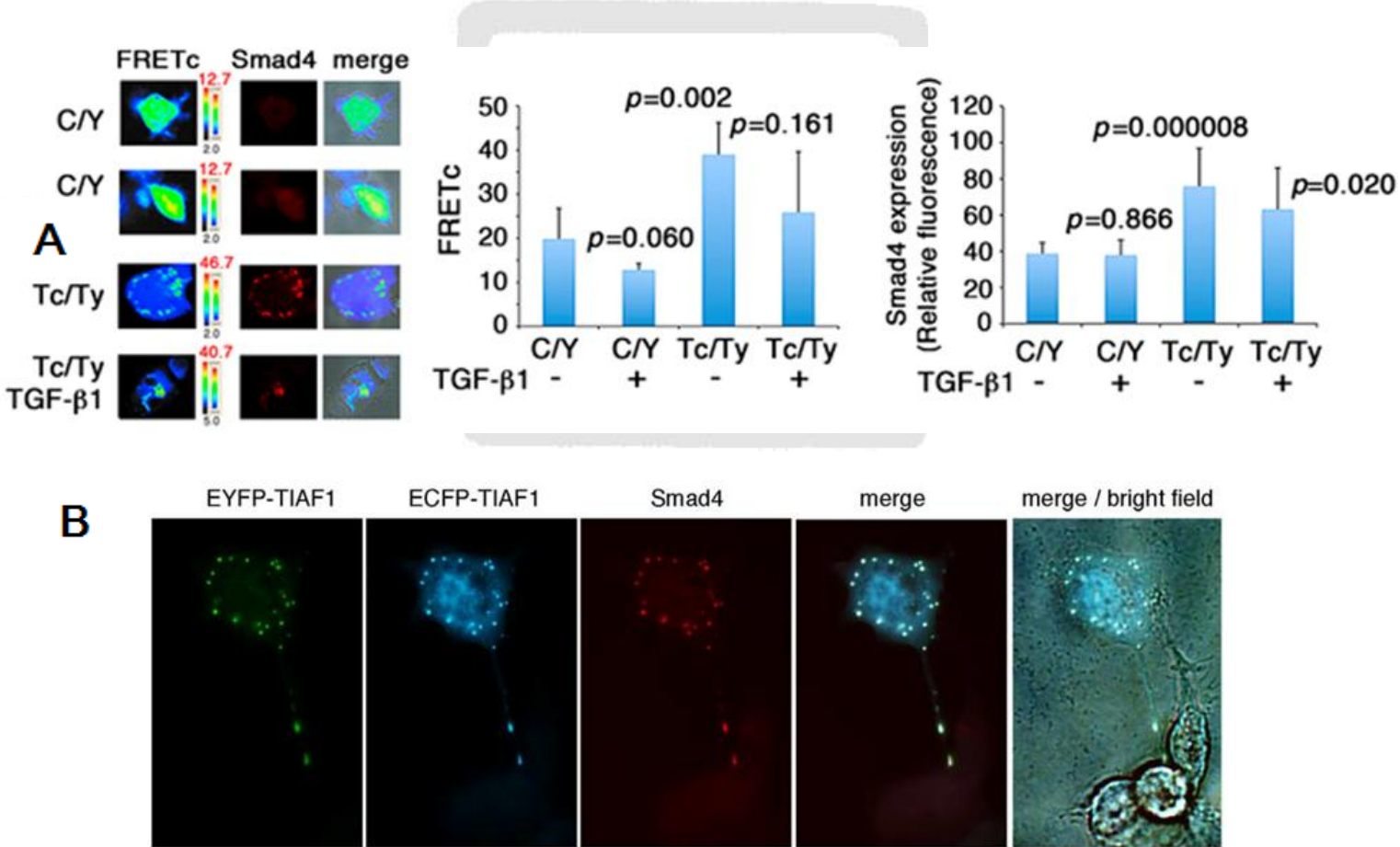


**Figure 7. TIAF1-/Smad4-binding induces generation of amyloid precursor protein (APP) and A $\beta$ .**

p53-deficient NCI-H1299 cells were transiently overexpressed with ECFP-Smad4 and EYFP-TIAF1. The cells were treated with TGF- $\beta$ 1 for 24 h, which resulted in an increased generation of APP and A $\beta$  (Figure 5e). By FRET analysis, TGF- $\beta$ 1 increased the binding of Smad4 and TIAF1 (Figure 5e).

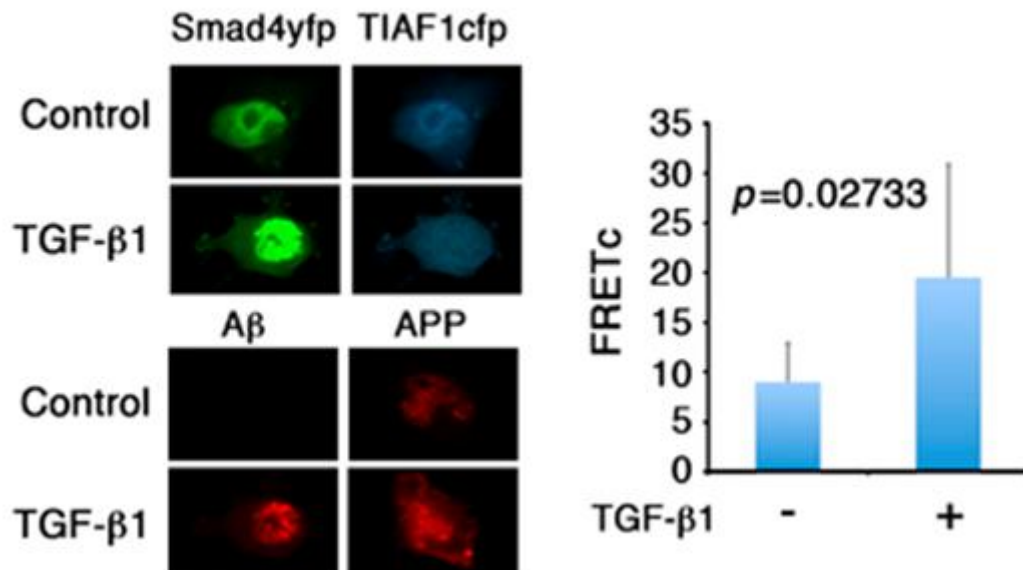


**Figure 8. TPC6A protein aggregation in subcellular compartment.**

(A) BCC cells were exposed to UV light, followed by incubation and then harvesting at indicated times. UV irradiation quickly induced trimer formation of endogenous TPC6A in both cytosol and nucleus in 10-20 minutes (reducing SDS-PAGE). (B) B16F10 melanoma cells were treated with TGF- $\beta$ 1 (5 ng/ml) for various durations. Presence of aggregates of TPC6A (with Ser35 phosphorylation) and TIAF1 is shown (non-reducing SDS-PAGE). No ubiquitin attachment to these proteins was observed (data not shown). Protein size markers are on the left column. Monomeric TIAF1 is 12 kDa and TPC6A is 17-20 kDa. (C) Similarly, SK-N-SH neuroblastoma cells were treated with or without TGF- $\beta$ 1 (5 ng/ml) for indicated times. An increased dimer formation of nuclear TPC6A is shown (reducing SDS-PAGE).

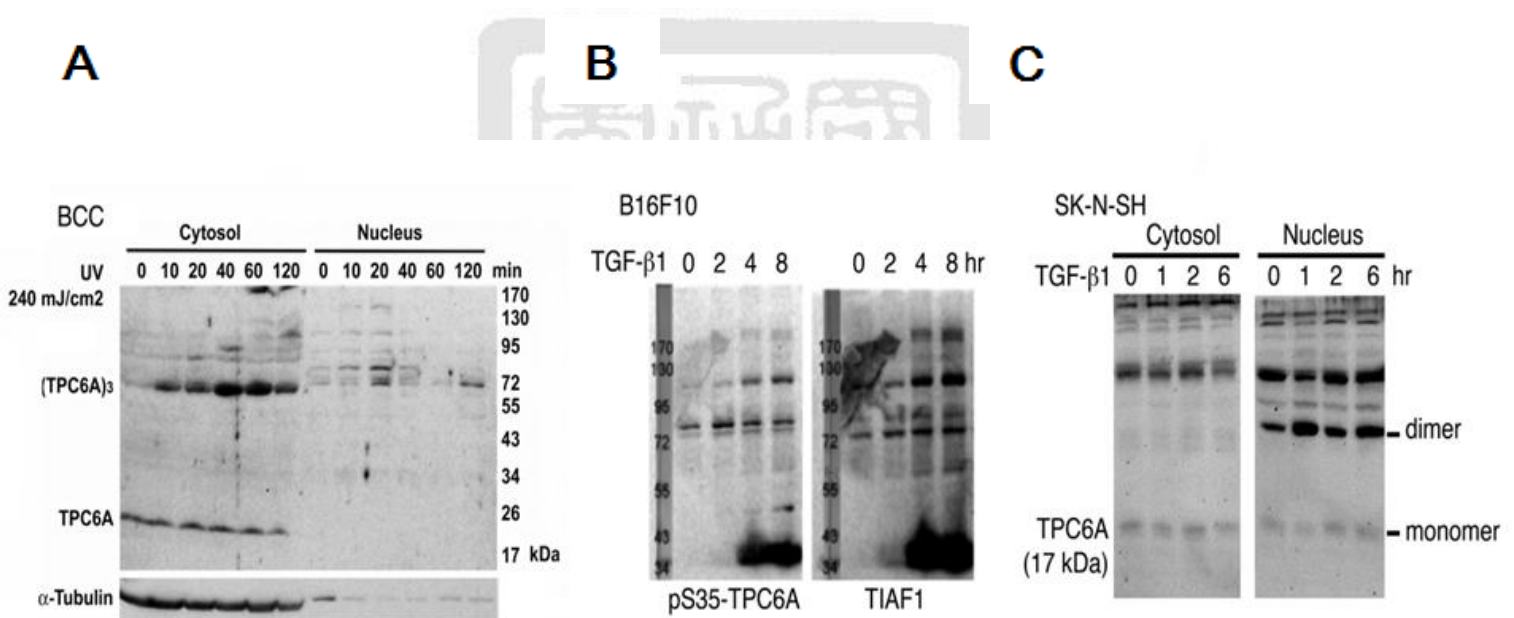


### Figure 9. TGF- $\beta$ 1 induces Bif-2 aggregation.

(A) Typical profiles of overexpressed Bif-2, tagged with EGFP, in cells. (B) TGF- $\beta$ 1 (5 ng/ml) induced EGFP-Bif-2 aggregation (10 min per frame, time-lapse microscopy). (C) When TIAF1 was knocked down by siRNA (TIAF1si), no Bif-2 aggregation was observed. (D) A large Bif-2 fiber hunted for a small fiber and both then became merged. (E) When co-expressed, a portion of TIAF1 binds Bif-2. TGF- $\beta$ 1 initially increased the binding, followed by reduction (see reducing red color or FRETc).

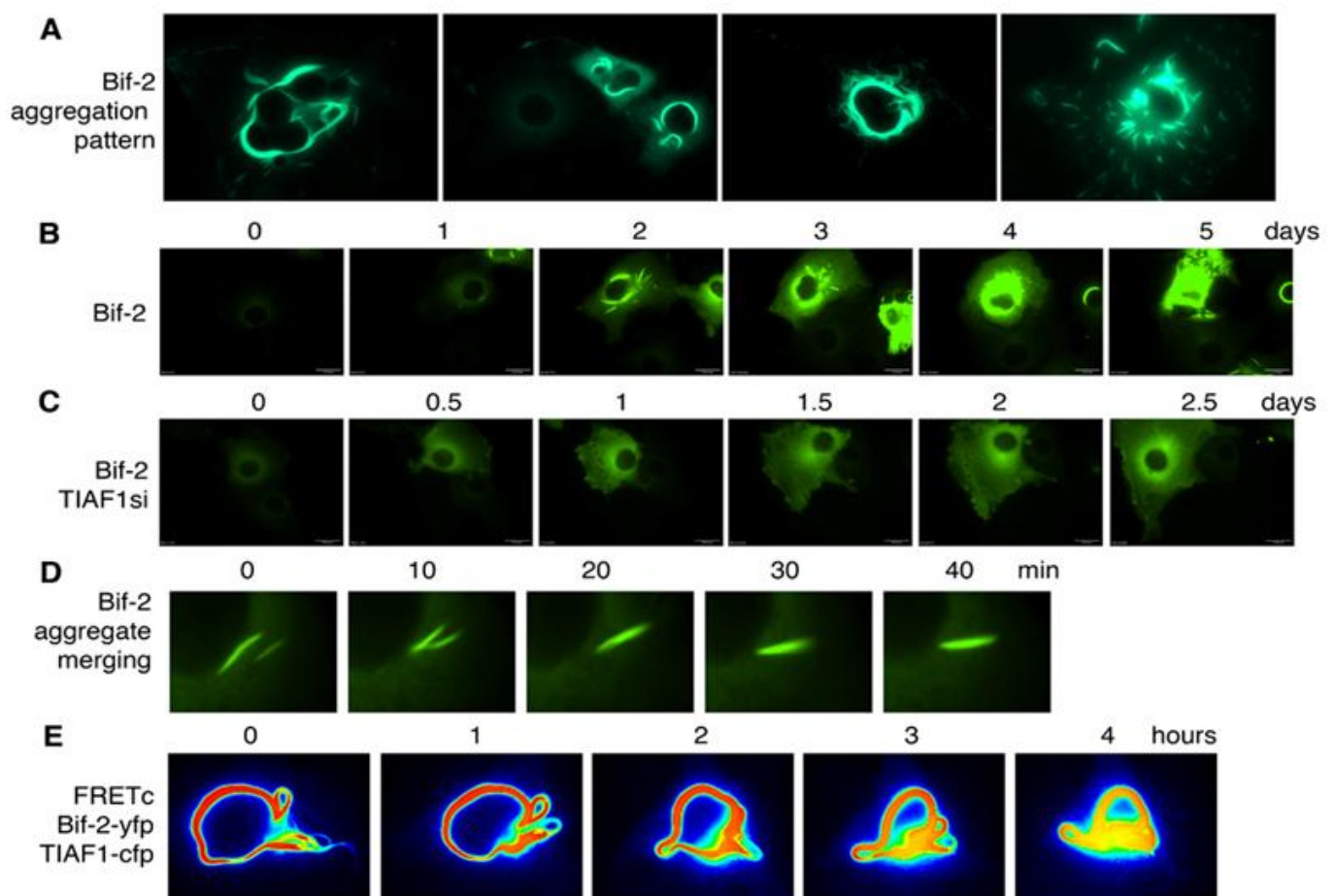


**Figure 10. Bif-2 EM and 3D morphologies.**

(A) High-speed laser scanning microscopy for EGFP-Bif-2 was carried out, and representative 3D graphs are shown. (B) STED microscopy (scale bar 5 nm). (C) Electron microscopy for EGFP-Bif-2 is shown. (D) An enlarged area (see box in B) shows hollow tubes or rings. SIM microscopy shows clusters (E) or single or double of rings (F). CCCP-induced mitochondrial apoptosis is blocked by wild type Bif-2 and Y77F mutant (G), as determined by cell cycle analysis. The mutant did not undergo polymerization. No ep = no electroporation. No ep = no electroporation.

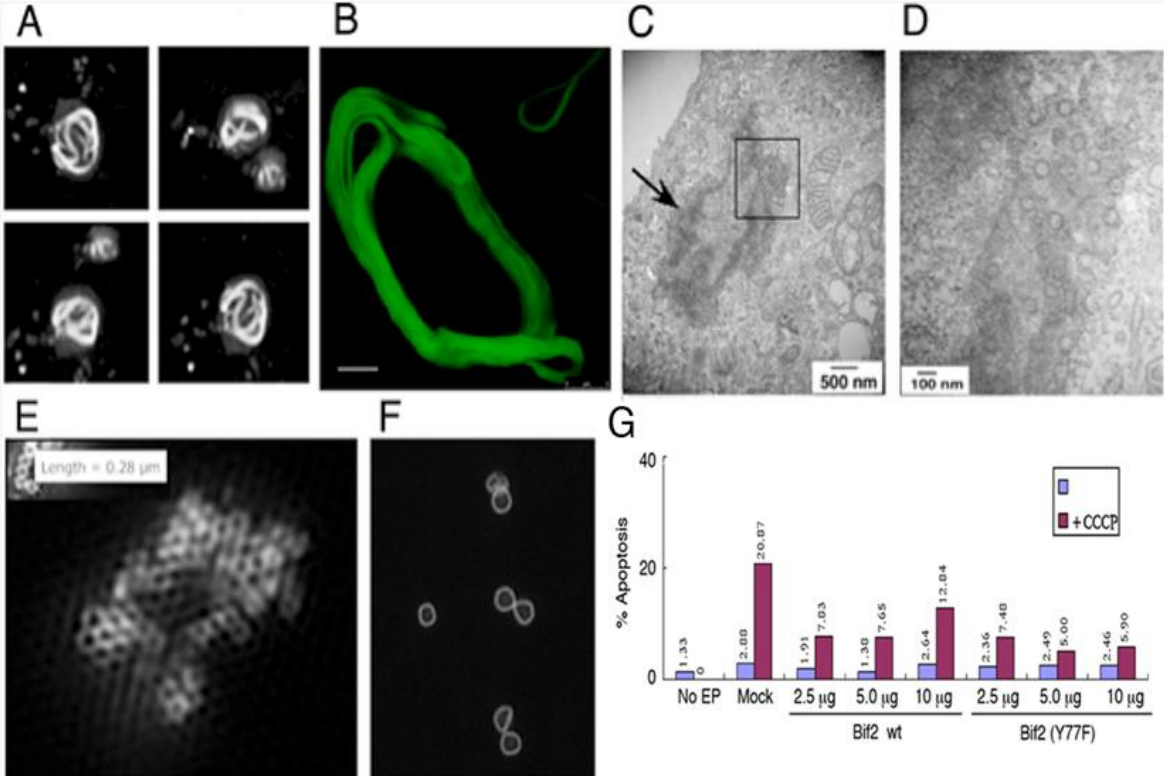


### **Figure 11. WWOX senses extracellular cues.**

Physical evidence shows that WWOX performs as a molecular sensor of extracellular signals. In certain cells, WWOX can be recruited to membrane area by association with cytoskeletal Ezrin, membrane Hyal-2 or C1qR staying in the membrane/cytoskeleton area. **Route 1:** WWOX binds Hyal2 and form WWOX/Hyal-2 complex. Then WWOX/Hyal-2 complex translocates to nucleus and enhances SMAD4-driven promoter activity. Various stress stimuli (e.g., TNF- $\alpha$ , TGF- $\beta$ , staurosporine, ultraviolet UV irradiation, complement C1q, PMA and sex steroid hormones estrogen and androgen) phosphorylate WWOX at Tyr33 in the first WW domain. **Route 2:** The activated WWOX interacts with phosphorylated p53 and translocates to the mitochondria and nucleus, and finally induces apoptosis. **Route 3:** WWOX binds PPXY motif containing transcriptional factors, such as RUNX2, c-Jun and ERBB4, via its first WW domains well; therefore inhibiting the activity of transcriptional factors by retaining them in the cytoplasm. **Route 4:** WWOX participates in the Wnt signal pathway. WWOX is physically associated with Dvl and inhibits the nuclear import of the Dvl. **Route 5:** In response to PMA stimulation, MEK/WWOX complex is dissociated, and released WWOX translocates to mitochondria causing cell death. **Route 6:** In many cancer cells, Ack1 was upregulated, which promoting the phosphorylation of WWOX at Tyr287, and leading WWOX undergo proteasomal degradation. **Route 7:** miR-134 targets *WWOX* gene promoting cell invasion and metastasis results in poor survival rate. Ack1, activated Cdc42-associated kinase 1; Hyal-2, hyaluronoglucosaminidase; CKI, casein kinase inhibitor; GSK, Glucogen synthase kinase; PKA, protein kinase A; PMA, phorbol myristate acetate.

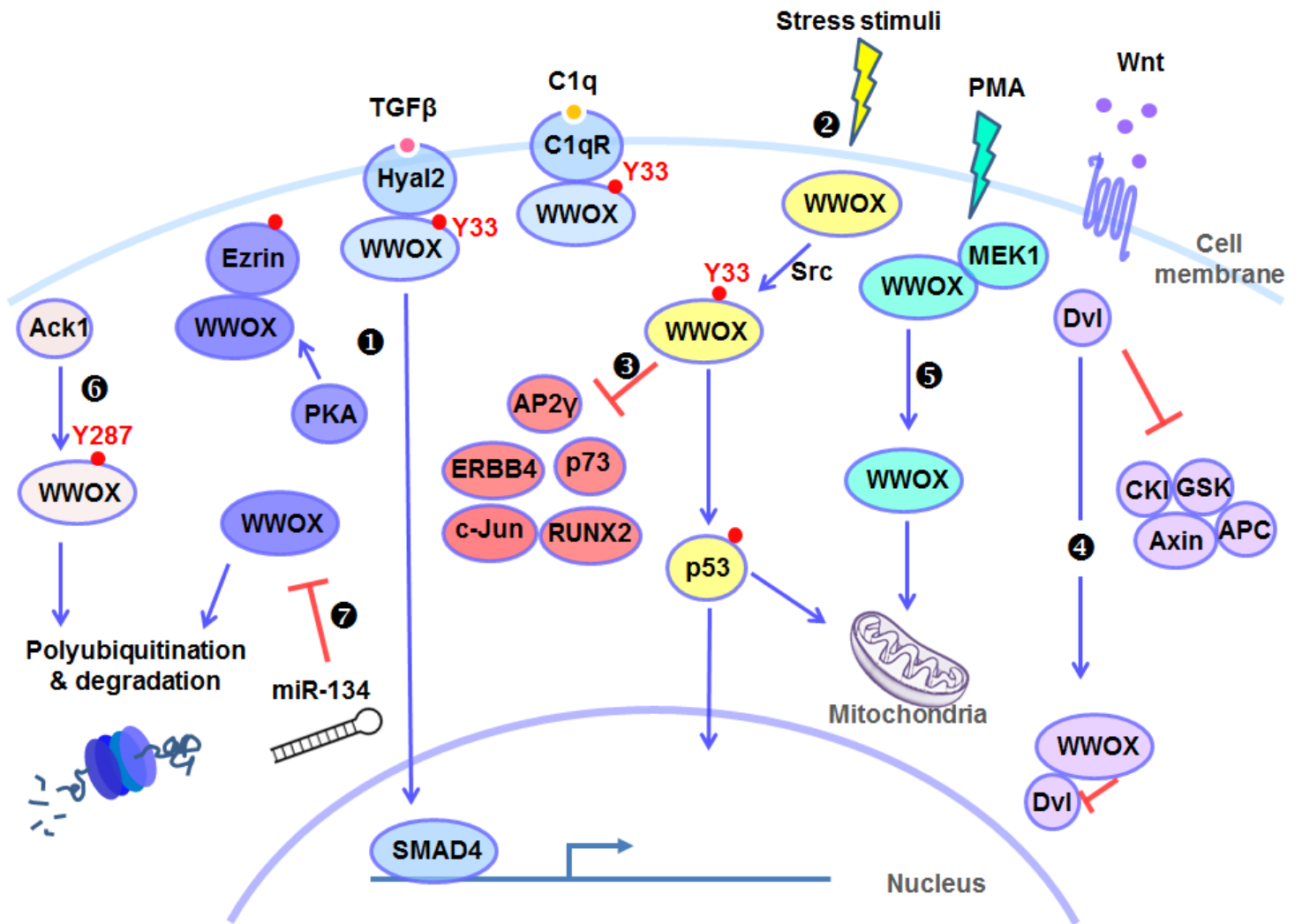


**Figure 12. Cell migration assay.**

A culture-insert (from ibidi) was placed on a petri dish, then seeded with indicated cells. After overnight cultures, the insert was removed gently, washed twice with PBS, and filled with 2% FBS culture medium. Time-lapse microscopy was carried out at 37°C with 5% CO<sub>2</sub>.

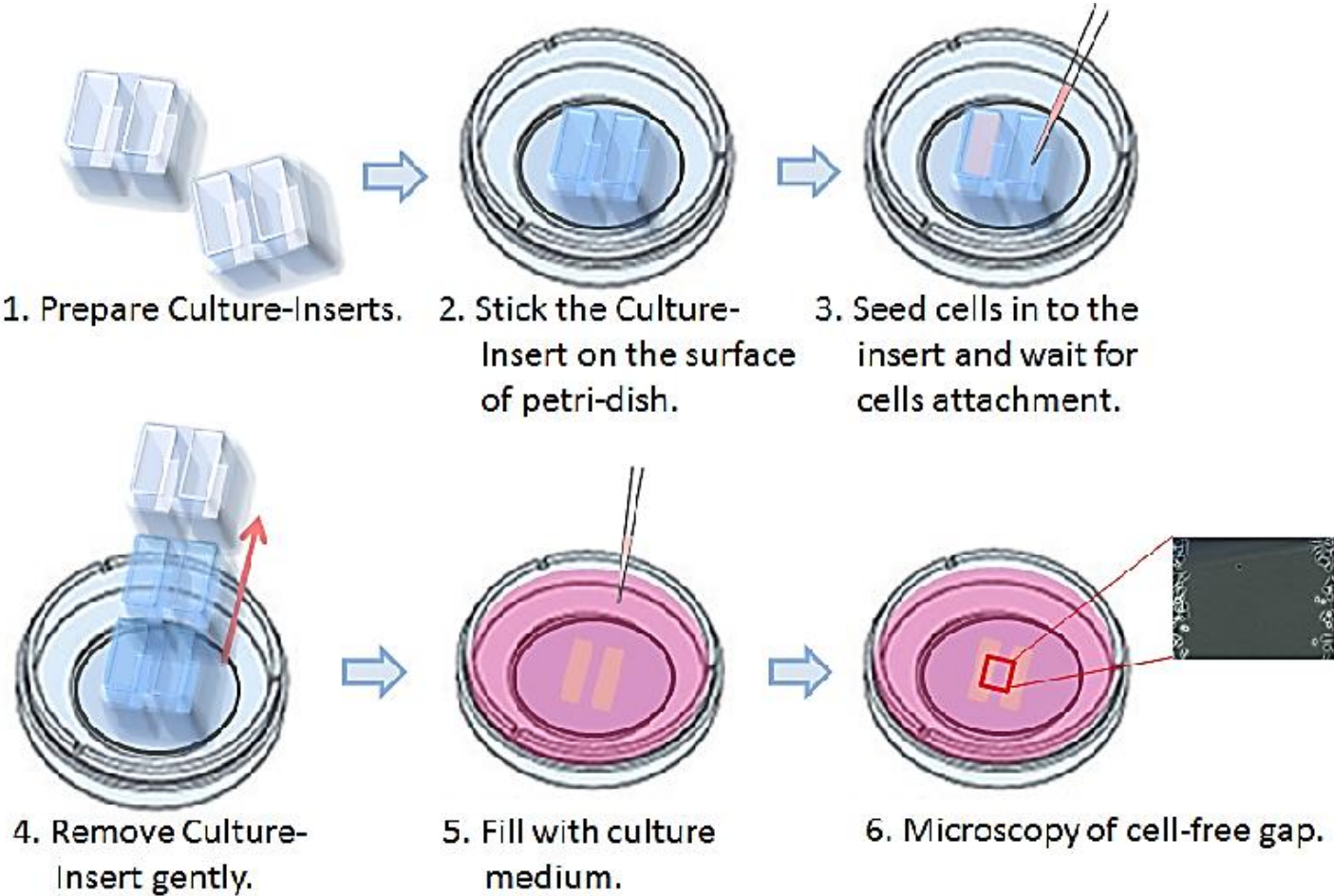


**Figure 13. Cell growth arrest in the assay for migration.**

To avoid the effect of cell proliferation on cell migration, all indicated cells were cultured on 2% FBS in DMEM or RPMI medium.  $2 \times 10^5$  MDA-MB-231 cells were seeded into  $3.5 \text{ cm}^2$  dishes cultured with medium containing 2% or 10% FBS for 1-3 days. Cells were harvested and stained with trypan blue and live cell numbers were counted. (mean  $\pm$  standard deviation;  $n=3$ ; Student's  $t$  test).

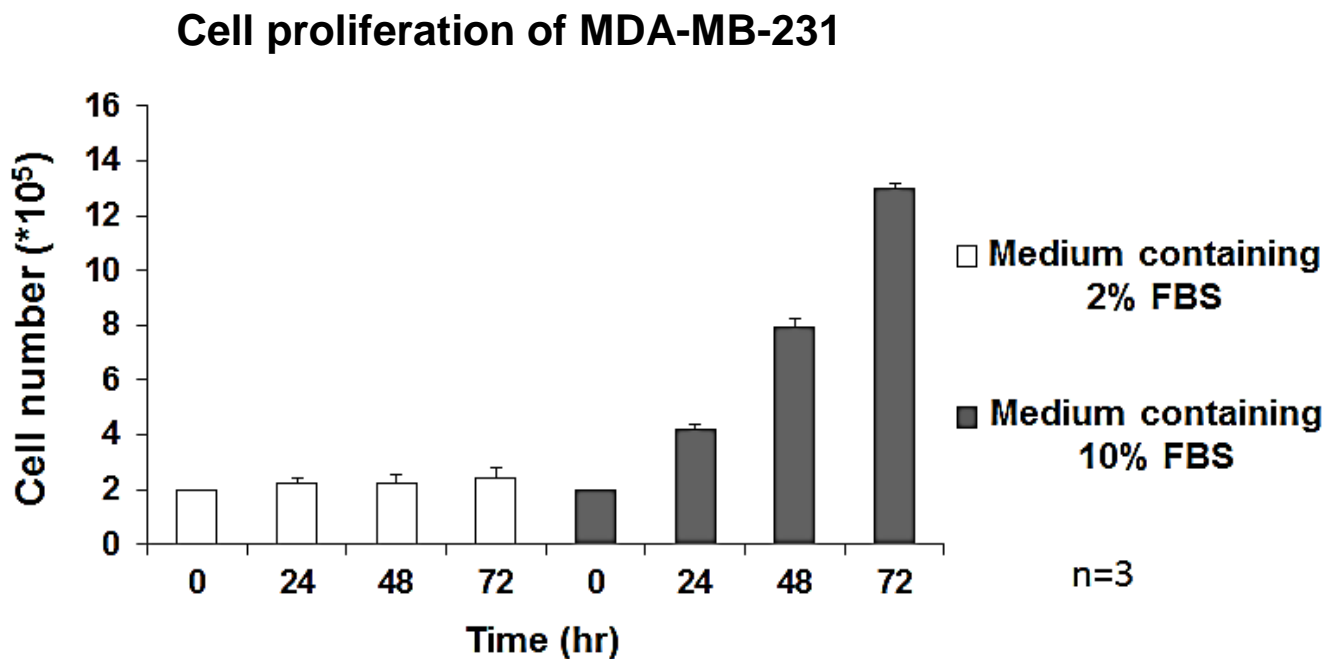


### Figure 14. WWOX suppresses cell migration.

Wild type and *Wwox*<sup>-/-</sup> MEF cells were co-cultured in migration assay. (A) *Wwox*<sup>-/-</sup> MEF cells migrated dramatically faster than the wild type cells. (B) The morphological features of these two cells were different. Wild type MEF cells tightly interact with each other and appear roundish and squamous, whereas knockout MEF cells appear elongated with few cell-cell contacts. Wild type cells migrated collectively, while the knockout cells migrated individually.

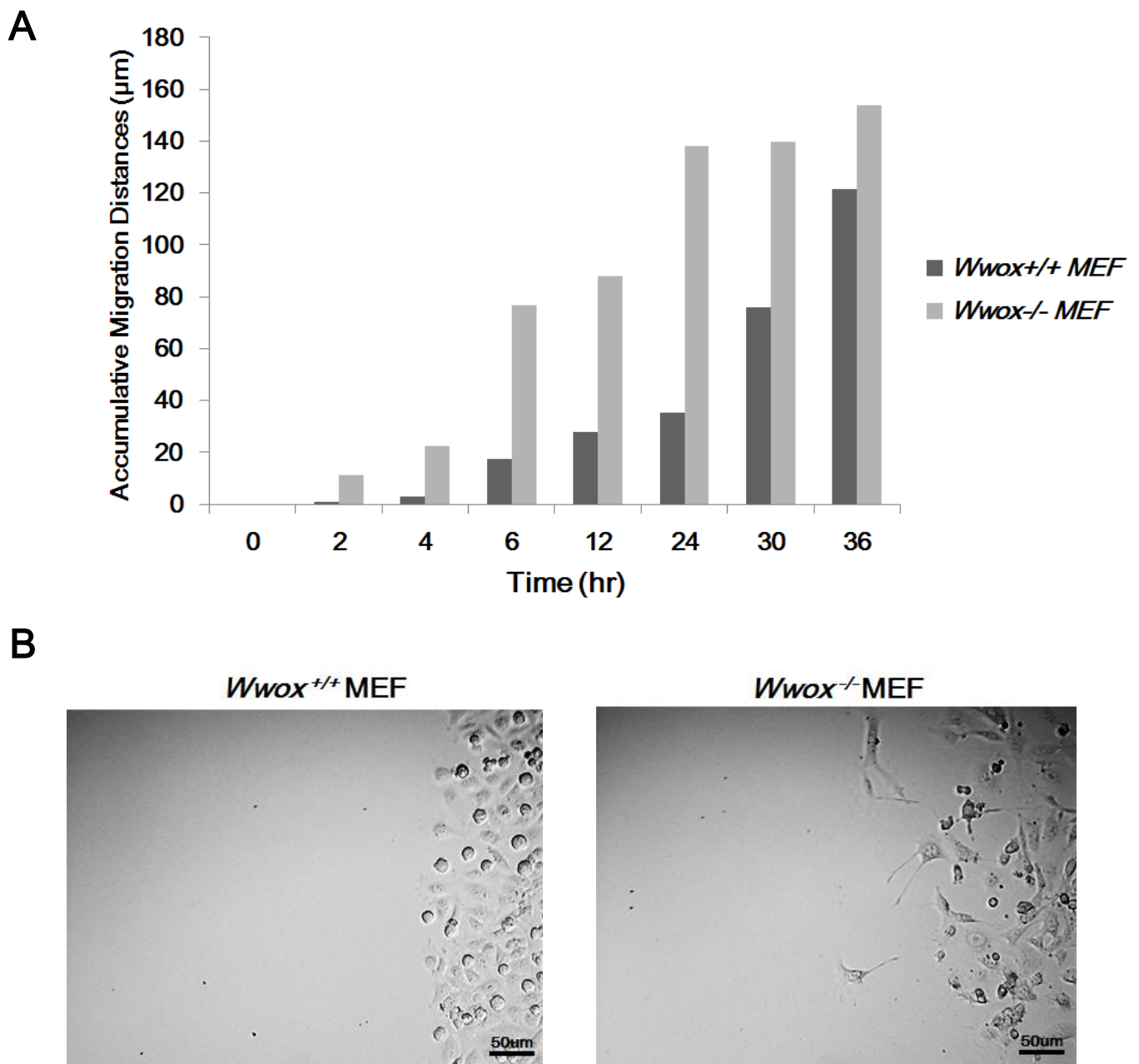


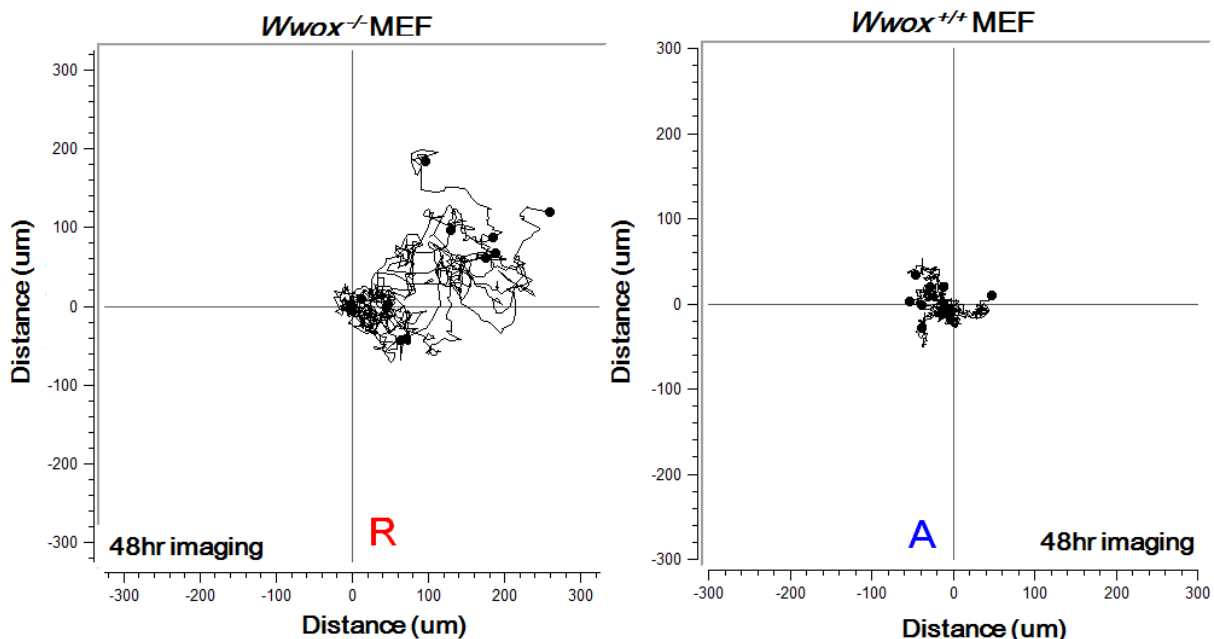
**Figure 15. Time-lapse microscopy of WWOX-deficient cells versus WWOX-expressing cells in migration assay.**

(A) *Wwox*<sup>-/-</sup> MEF cells (left) and *Wwox*<sup>+/+</sup> MEF cells (right) were seeded, respectively, in each side of the culture-insert (ibidi). After overnight incubation, time-lapse microscopy was carried out at 37°C with 5% CO<sub>2</sub>. When *Wwox*-knockout cells migrated forward with their stretched-out bodies with their dendrites upon touching the wild type cells, the knockout cells moved in a retrograde manner. (B) Similarly, when WWOX-negative MDA-MB-231 (left) migrated toward WWOX-positive L929 (right) cells, MDA-MB-231 cells moved in a retrograde manner upon touching. Without physical contacts, MDA-MB-231 cells undergo retrograde migration. Then, MDA-MB-231 cells divided rapidly. (C) The similar phenomenon was also observed when WWOX-deficient SCC9 cells encountered WWOX-expressing SCC15 cells. Each picture was taken every 10 min interval by time-lapse microscopy. A = anterograde movement; R = retrograde movement. (mean±standard deviation; n=10; Student's *t* test).

**A**

**A = anterograde movement**  
**R = retrograde movement**

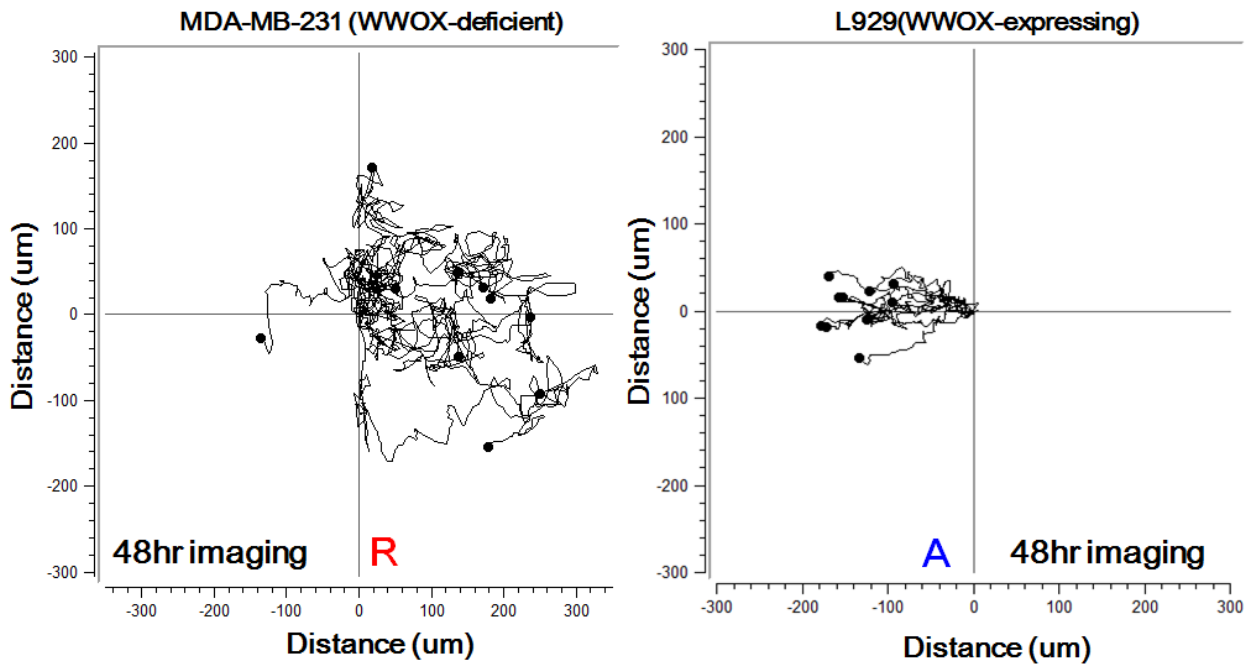
*Wwox*<sup>-/-</sup>MEF Vesus *Wwox*<sup>+/+</sup>MEF



A = anterograde movement  
R = retrograde movement

B

MDA-MB-231 Vesus L929



C

SCC9 Vesus SCC15

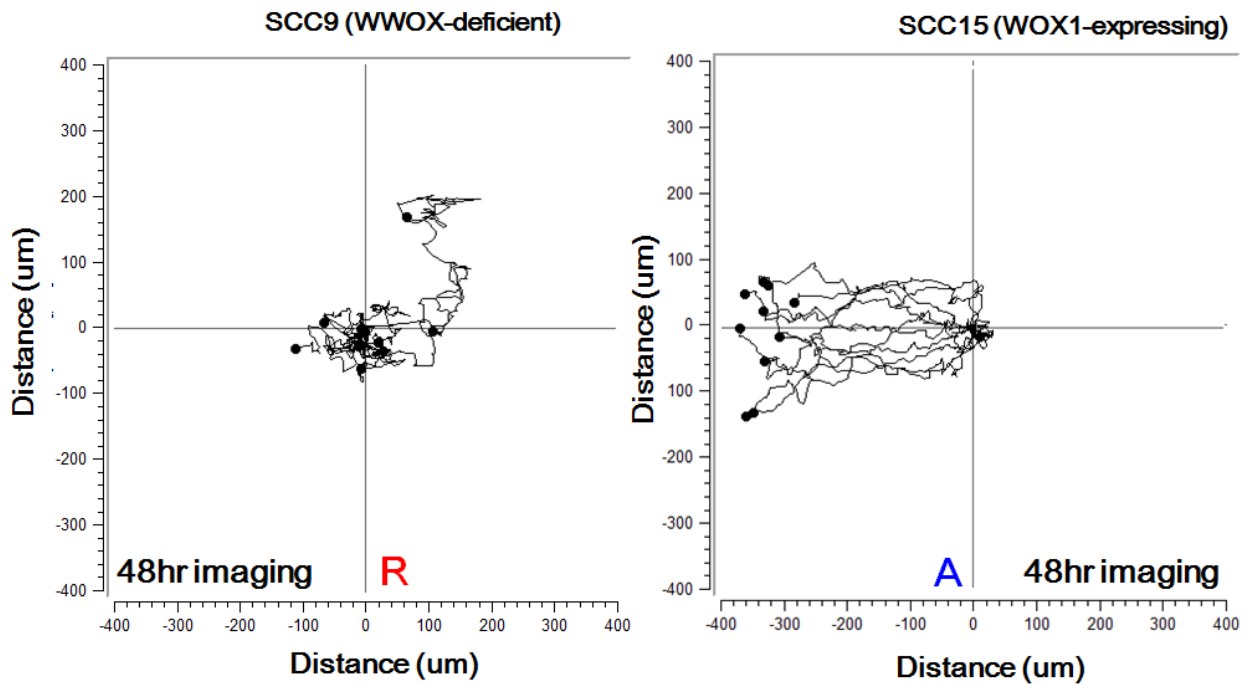
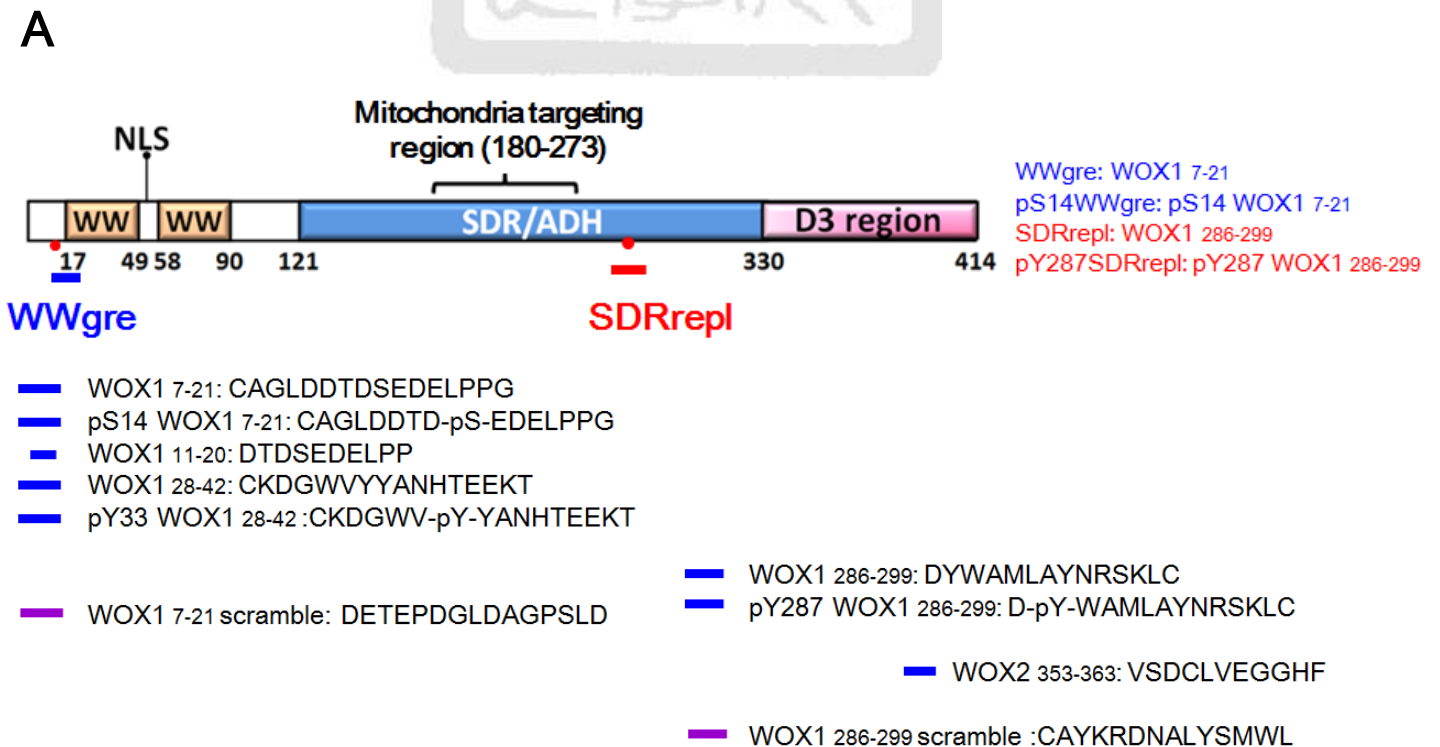
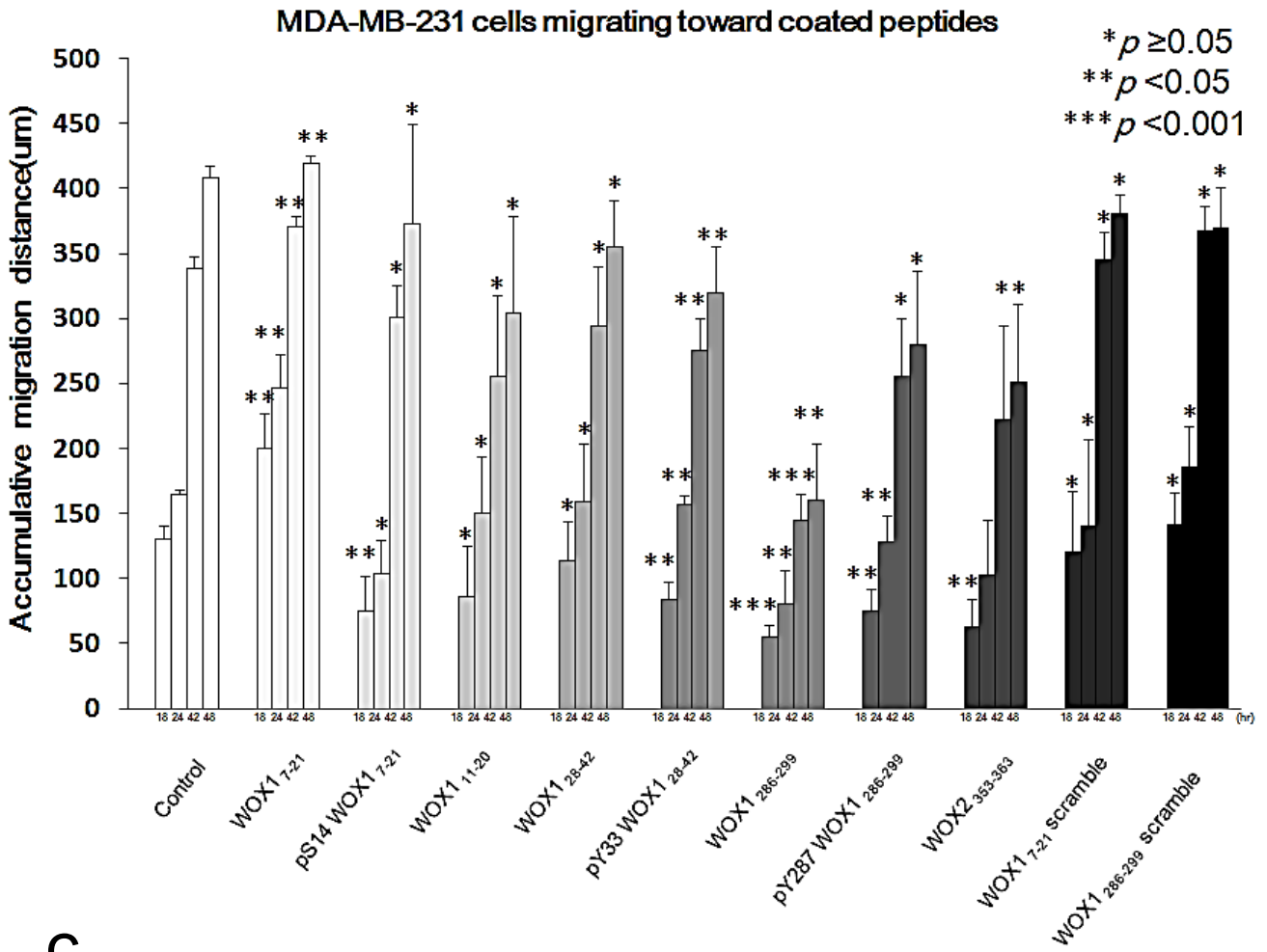


**Figure 16. MDA-MB-231 cell migration is accelerated by WWgre (WOX17-21) peptide but blocked by SDRrepl (WOX1286-299) peptide.**

(A) The primary structure of WWOX is shown. The locations of WWgre, SDRrepl are shown. 10 peptides (WOX17-21, pS14-WOX17-21, WOX111-20, WOX128-42, pY33-WOX128-42, WOX1286-299, pY287-WOX1286-299, WOX2353-363, WOX17-21 scramble and WOX1286-299 scramble) according to the surface-exposure regions and sites of phosphorylation of a simulated 3-dimensional structure of WWOX were synthesized. (B) One side of the culture-insert (ibidi) was coated with 200  $\mu$ M peptides (or conjugation buffer only) overnight, and the other side grown with cells. Migration of MDA-MB-231 cells to the indicated peptides was carried out, and the travel distance with time is shown. Pictures were taken at each indicated time point. WWgre significantly enhanced the cell migration from the very beginning. In contrast, SDRrepl significantly suppressed the cell migration. Phospho-peptides of WWgre and SDRrepl lost their activities. (C) Coating efficiency of WWgre, pWWgre, SDRrepl and pSDRrepl peptides were confirmed by Enzyme-linked immunosorbent assay (ELISA). 200uM peptides were coated onto ELISA microtiter plate by 37°C overnight incubation. Then indirect ELISA assay was perform with ELISA kit purchased from BD. (mean $\pm$ standard deviation;  $n=3$ ; Student's  $t$  test).



**B**



**C**

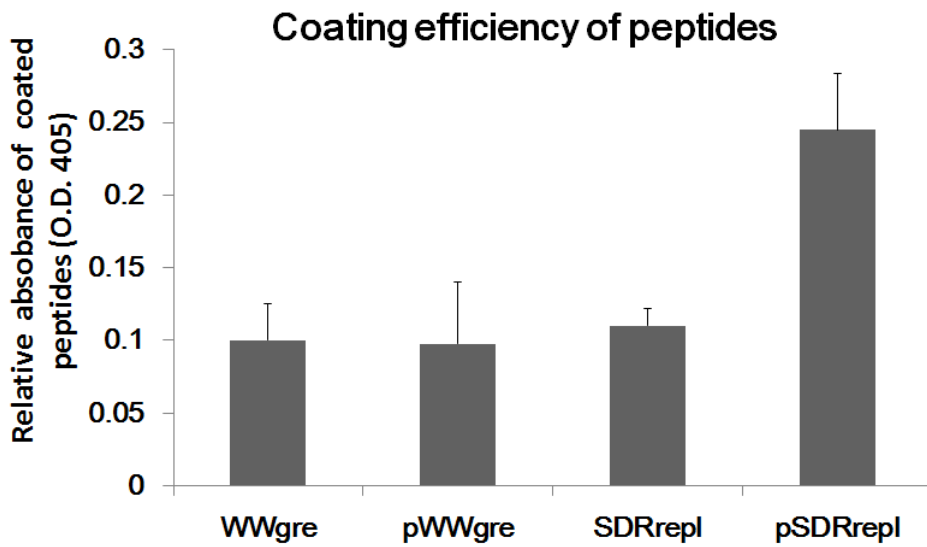
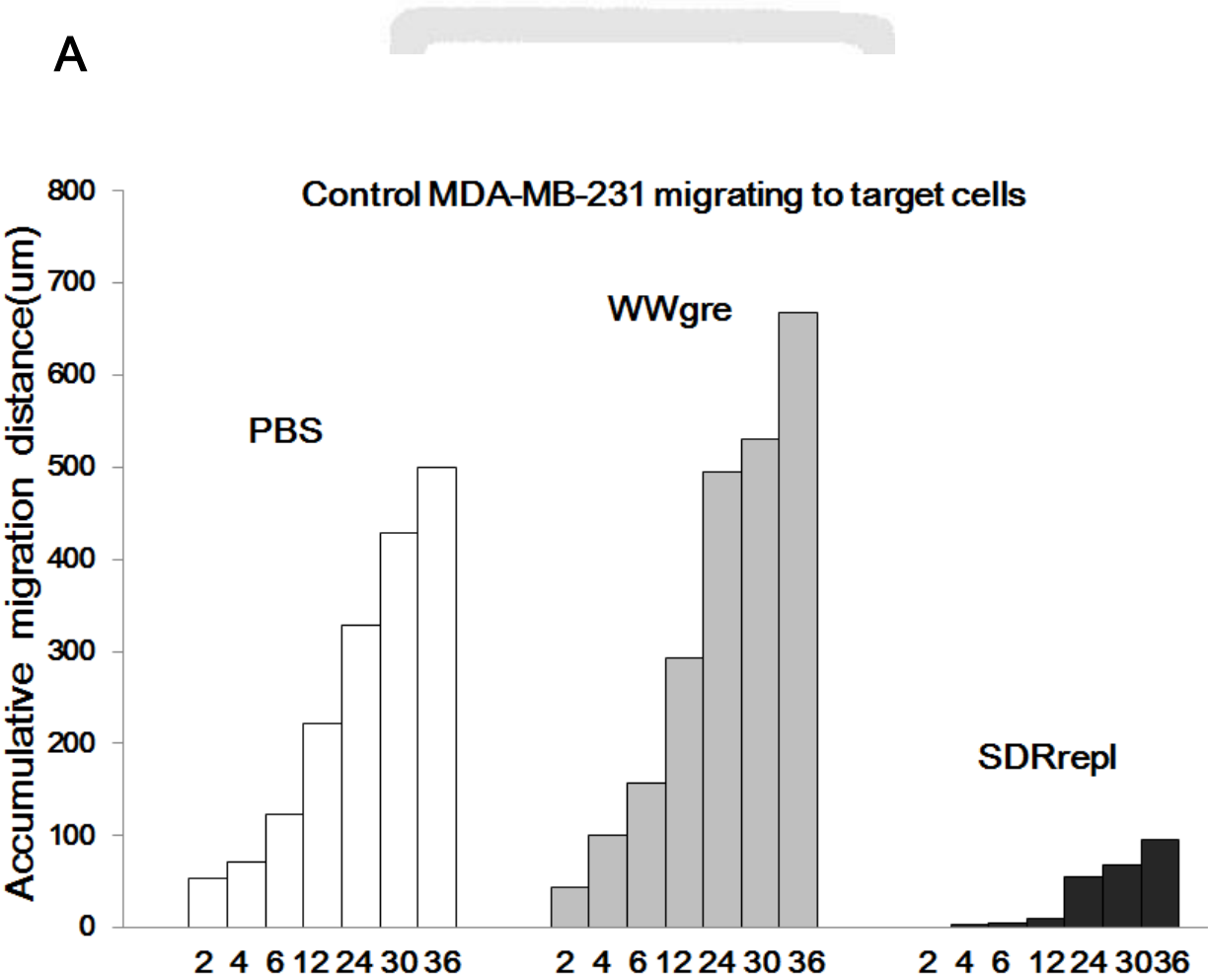


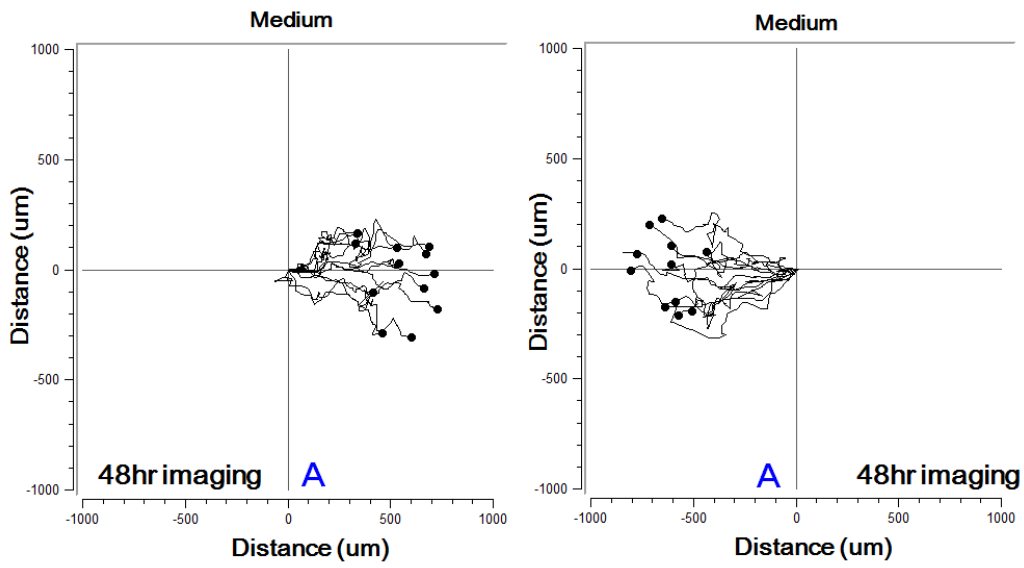
**Figure 17. Effect of WWgre and SDRrepl peptides on cell migration.**

(A) MDA-MB-231 cells in the left field were pretreated with WWgre or SDRrepl peptides (20 μM) for 4 hr at 37°C and washed to remove peptides. Untreated control cells were seeded at the right field and their migrating distance with time is shown. (B-D) Time-lapse microscopy was carried out to examine cell migration. The migration activity of control cells upon encountering WWgre-targeted cells was accelerated. These cells migrated strictly forward. In contrast, the migration activity of control cells underwent retrograde migration with a reduced speed upon facing SDRrepl-treated cells. The migratory paths was in a retrograde manner. A = anterograde movement; R = retrograde movement. Each picture was taken per 10 min. (mean±standard deviation; n=10; Student’s *t* test).

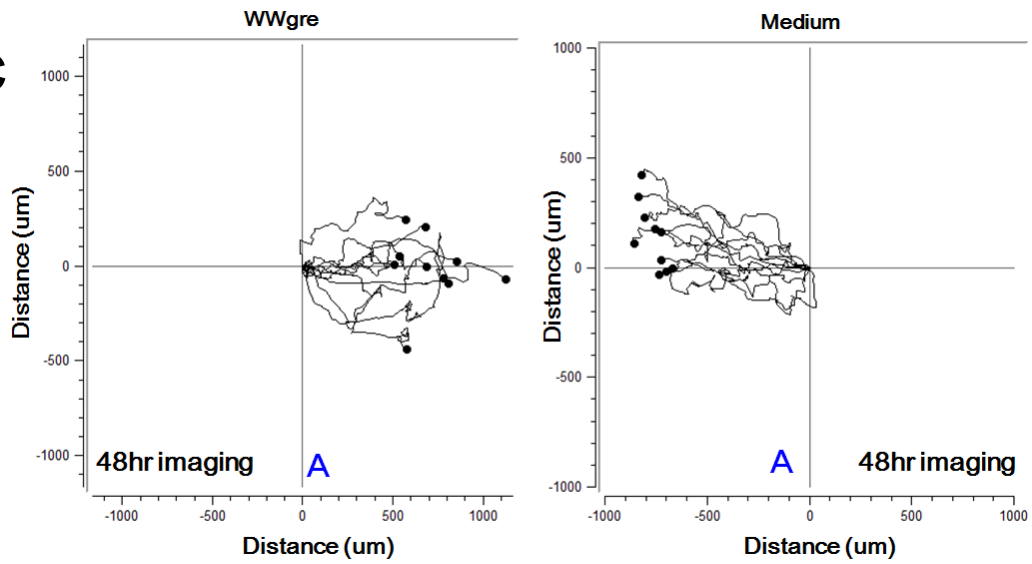


A = anterograde movement  
R = retrograde movement

B



C



D

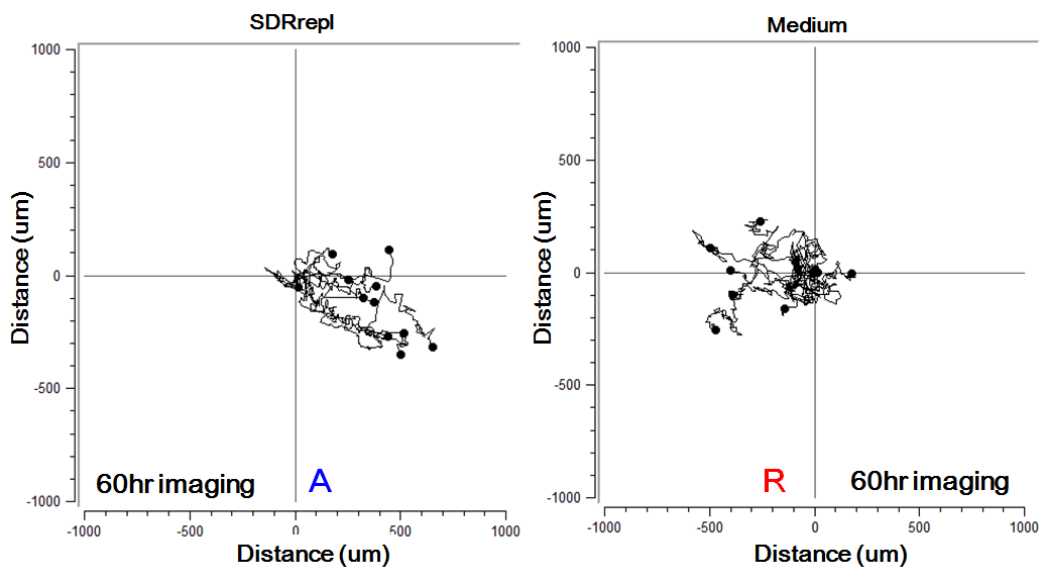


### Figure 18. Treated peptides fail to cause cell death.

MDA-MB-231 cells( $3 \times 10^5$ ) were grown in 2% FBS DMEM medium overnight, and treated with  $40 \mu\text{M}$  peptides at  $37^\circ\text{C}$  for 4 hr. Cell cycle analysis was then carried out. Cells were harvested by centrifugation at 5000 rpm for 15 minutes, then gently washed once, and finally fixed with an equal volume of PBS and 100% ethanol for overnight at  $-20^\circ\text{C}$ . The cells were stained with propanone iodine and DNA contents were analyzed by flow cytometry (Becton Dickinson, Franklin Lakes, NJ). No apparent cell death was observed during treatment for 4hr.

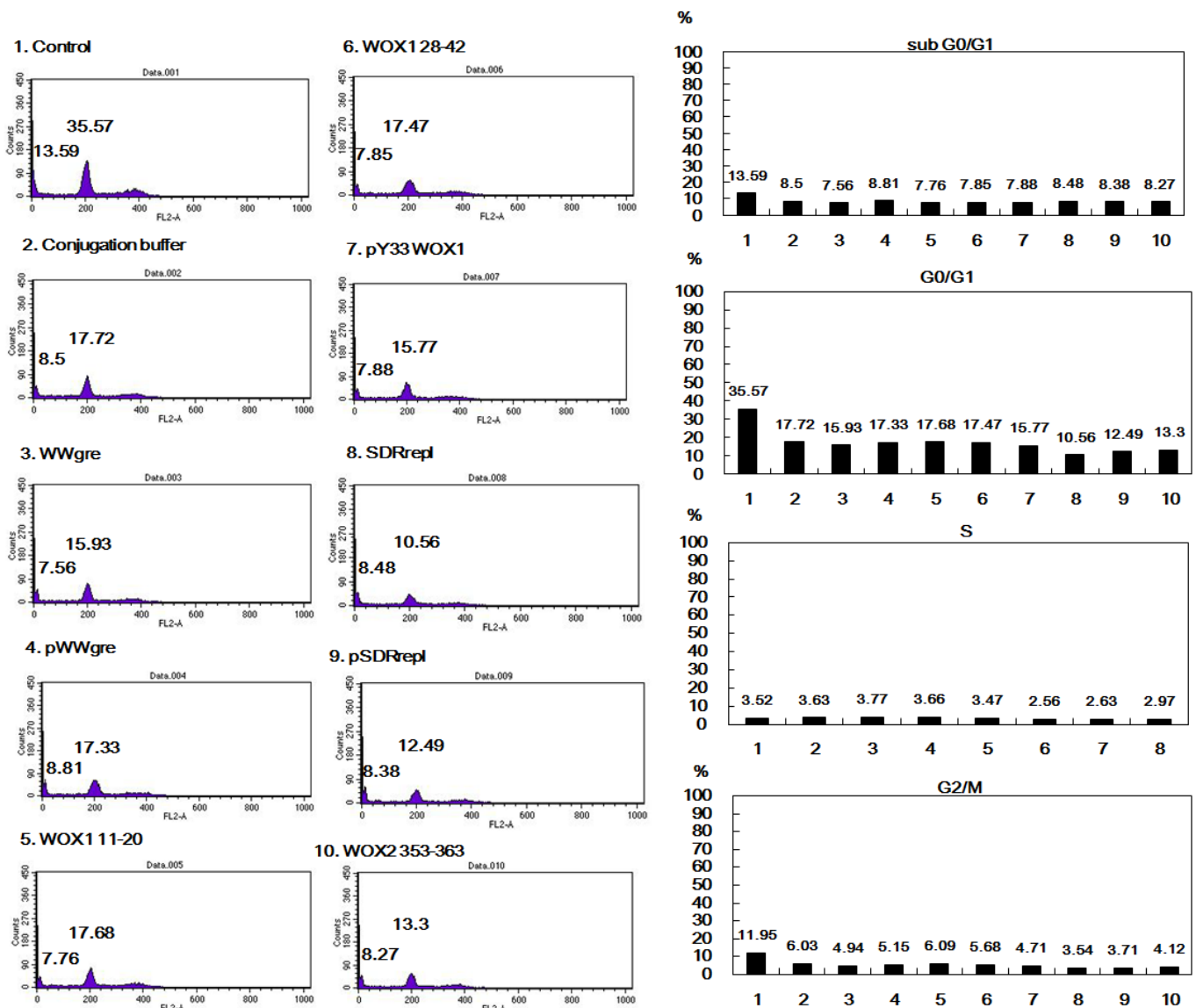
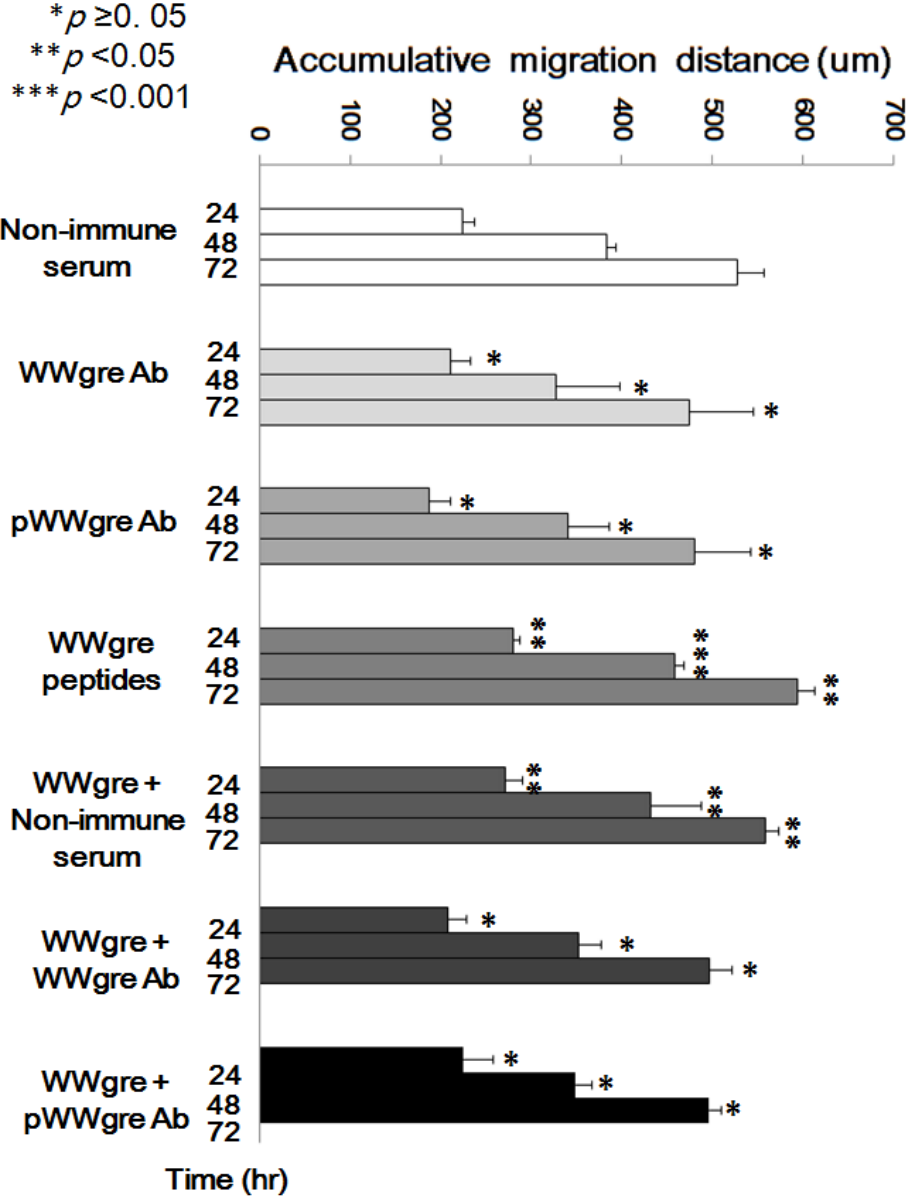


**Figure 19. Neutralization of WWgre and SDRrepl by specific antibodies.**

(A) WWgre and pS14WWgre peptides (200 μM) were coated onto the plastic surface, followed by washing and then treating with or without aliquots of diluted antisera (1:500). In controls, non-immune sera were used. Migration of MDA-MB-231 cells to each coated peptide area was imaged at indicated times. Student’s t tests were carried out for all experiments versus controls (mean±standard deviation; *n*=3; Student’s *t* test). (B) Similar experiments were carried out with the SDRrepl peptide. (mean±standard deviation; *n*=3; Student’s *t* test).

**A** **MDA-MB-231 migrating to coated WWgre peptides**  
**With or without antibody neutralization**



B

### MDA-MB-231 migrating to coated SDRrepl peptides With or without antibody neutralization

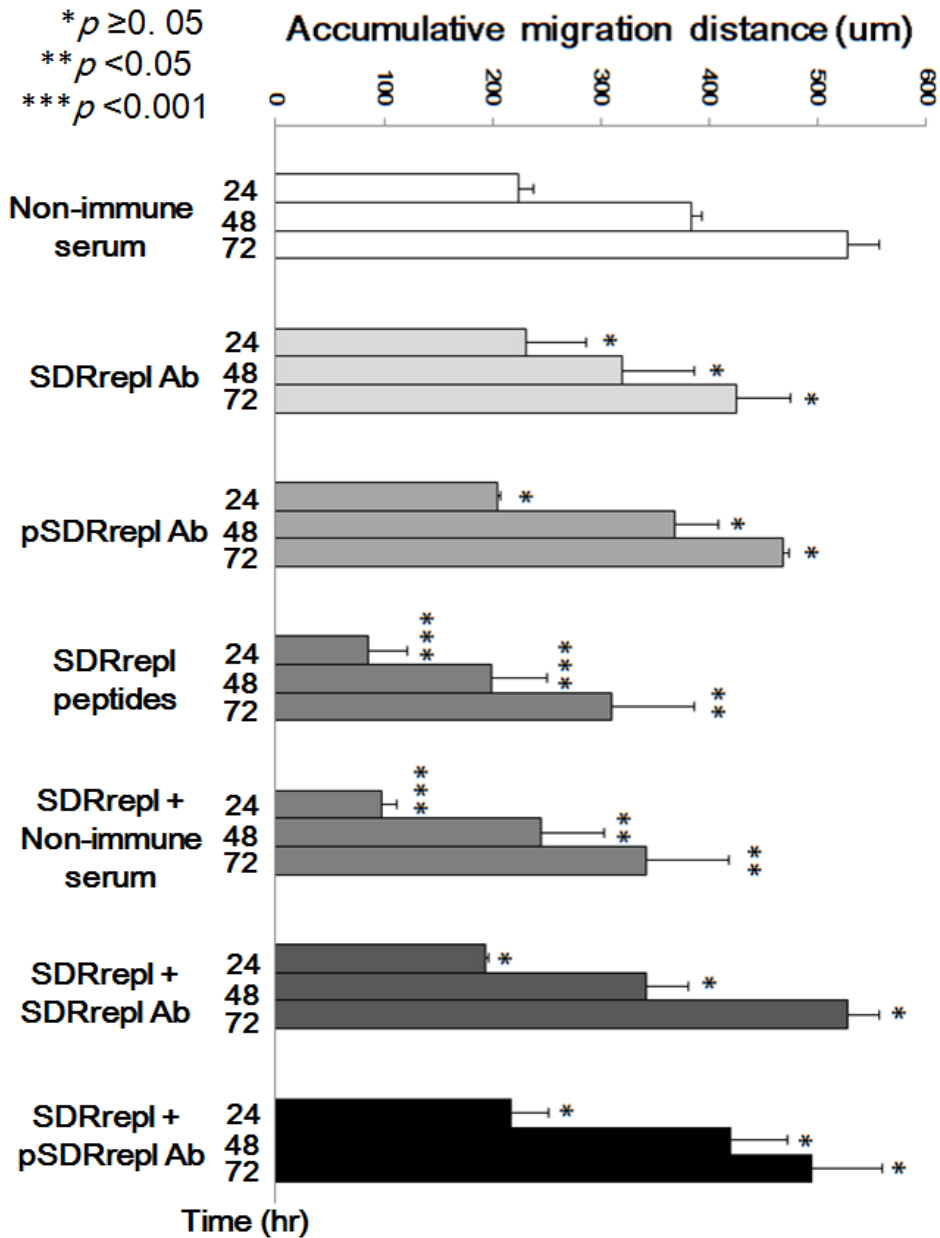
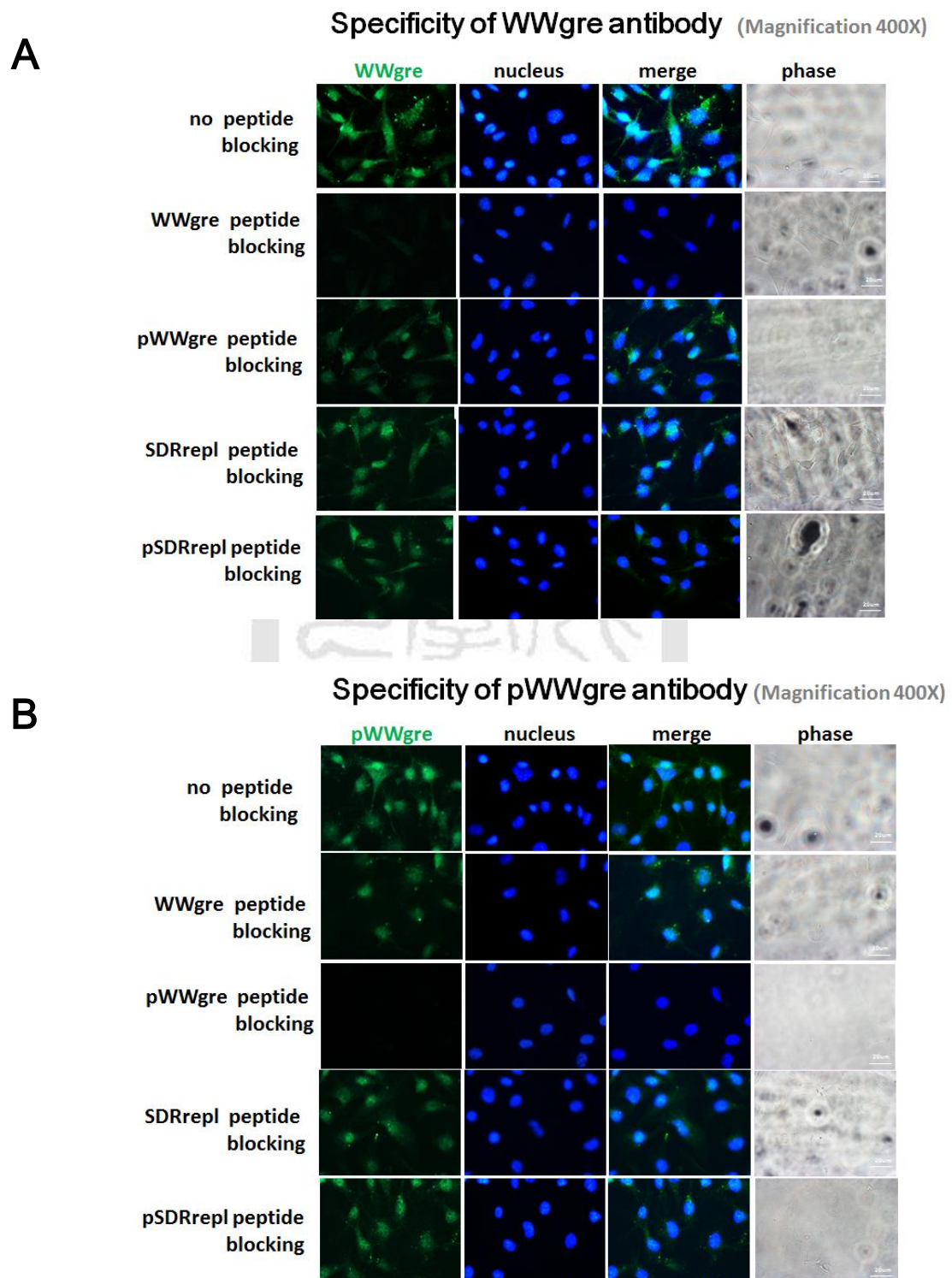


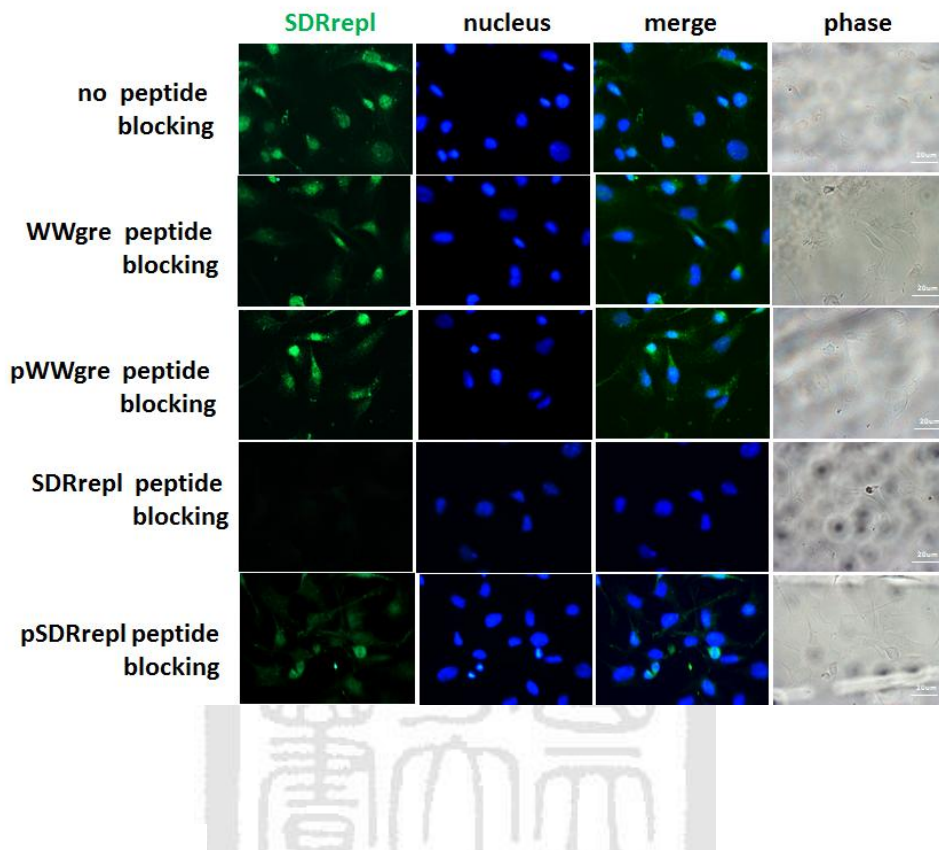
**Figure 20. Specificities of WWgre and SDRrepl neutralizing antibodies.**

$3 \times 10^5$  B16F10 cells were seeded on to coverglass overnight. Cells were fixed with 4% paraformaldehyde and permeabilized with 0.25% triton-X PBS. Prior to immunostaining, primary antibodies were pre-adsorbed with or without 1mM WWgre, pWWgre, SDRrepl, or pSDRrepl peptides for 1hr at room temperature.



C

Specificity of SDRrepl antibody (Magnification 400X)



D

Specificity of pSDRrepl antibody (Magnification 400X)

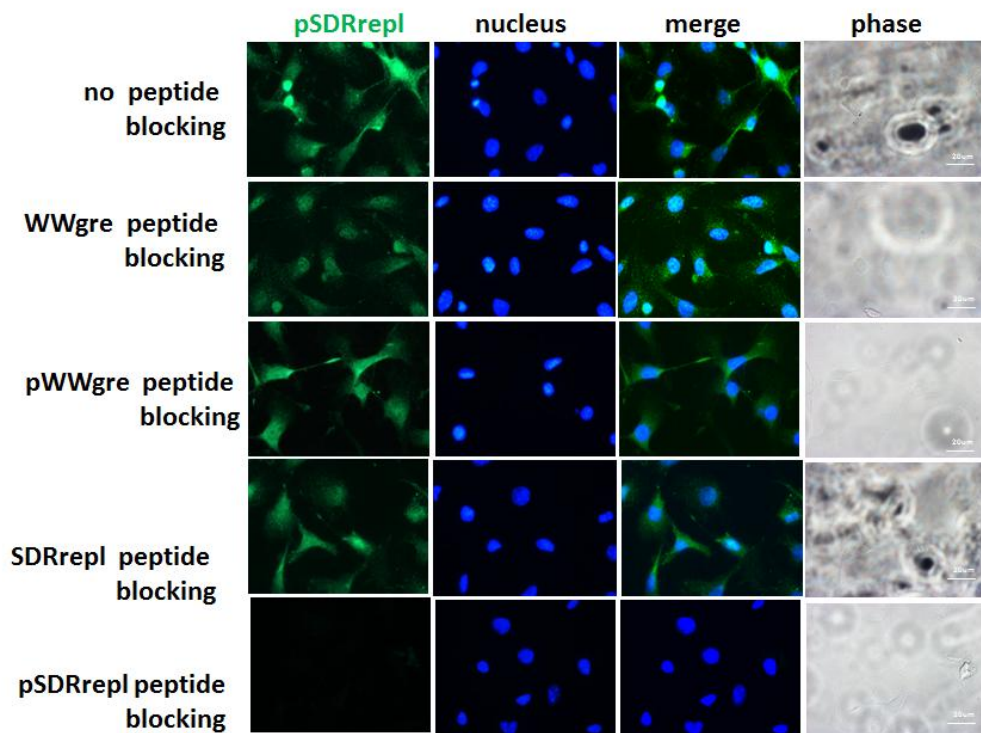
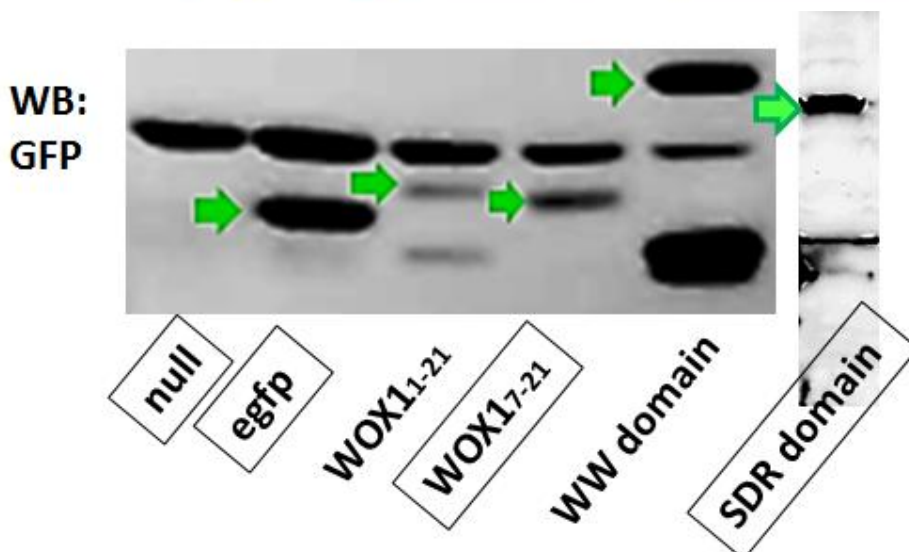
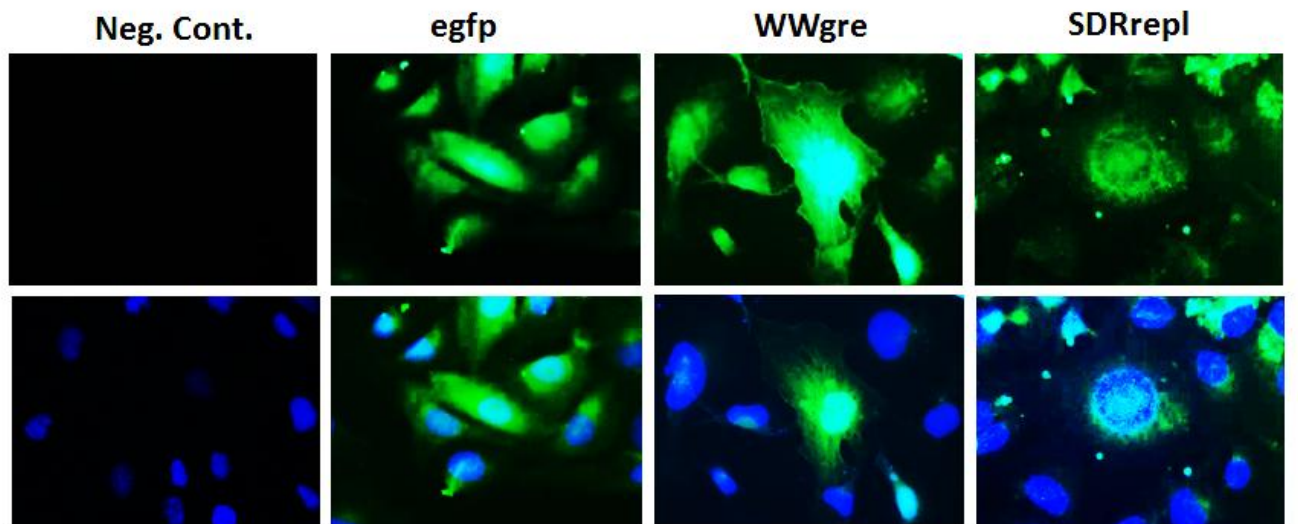


## Figure 21. SDR domain is critical in repelling cells.

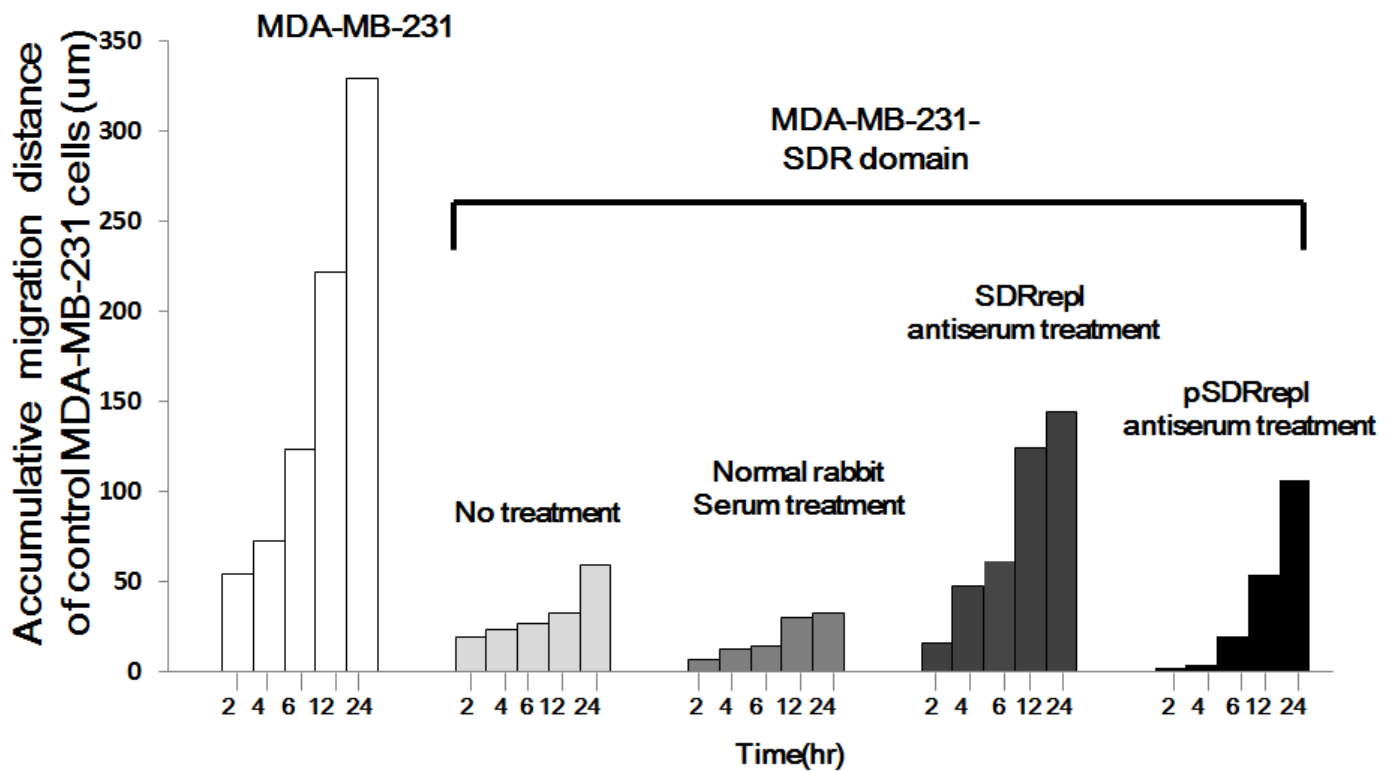
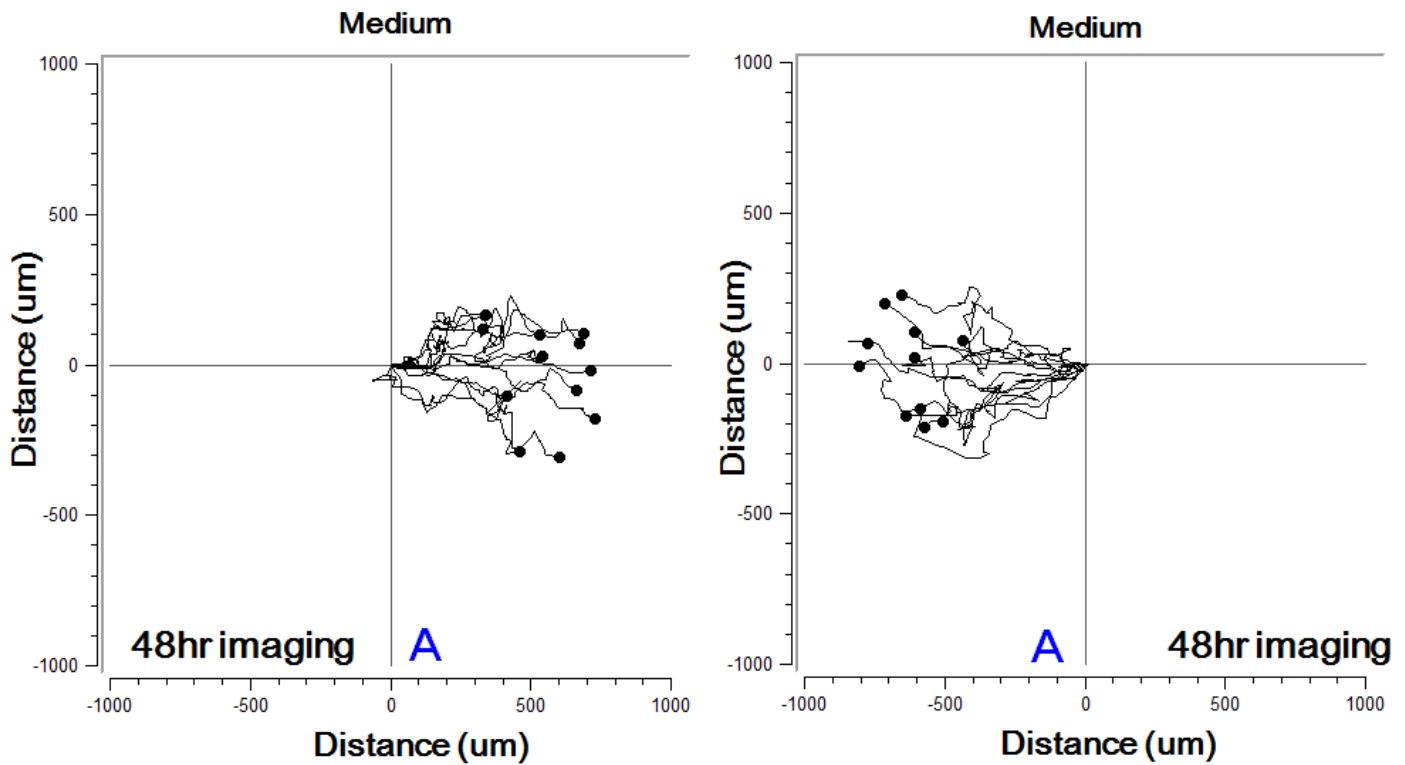
(A) Stable transfectants of MDA-MB-231 cells with EGFP or EGFP-SDR domain expression were established. Immunofluorescent staining and western blotting were performed to confirm the protein expression. (B-E) Stable transfectants of MDA-MB-231 cells with EGFP or EGFP-SDR domain (left) and MDA-MB-231 control cells (right) were seeded, respectively, in each side of the culture-insert (ibidi). After overnight incubation, time-lapse microscopy was carried out at 37°C with 5% CO<sub>2</sub>. SDR domain-expressing cells suppressed migration activity of control cell. Control cells migrated in a retrograde manner upon encountering SDR domain-expressing cells. (F, G) Antiserum against SDR domain (1:500 dilution) restored anterograde migration for both cells. The pSDRrepl antiserum had no effect. A = anterograde movement; R = retrograde movement. Each picture was taken per 10 min. (mean±standard deviation; *n*=10; Student's *t* test).

### A MDA-MB-231 Stable transfectant



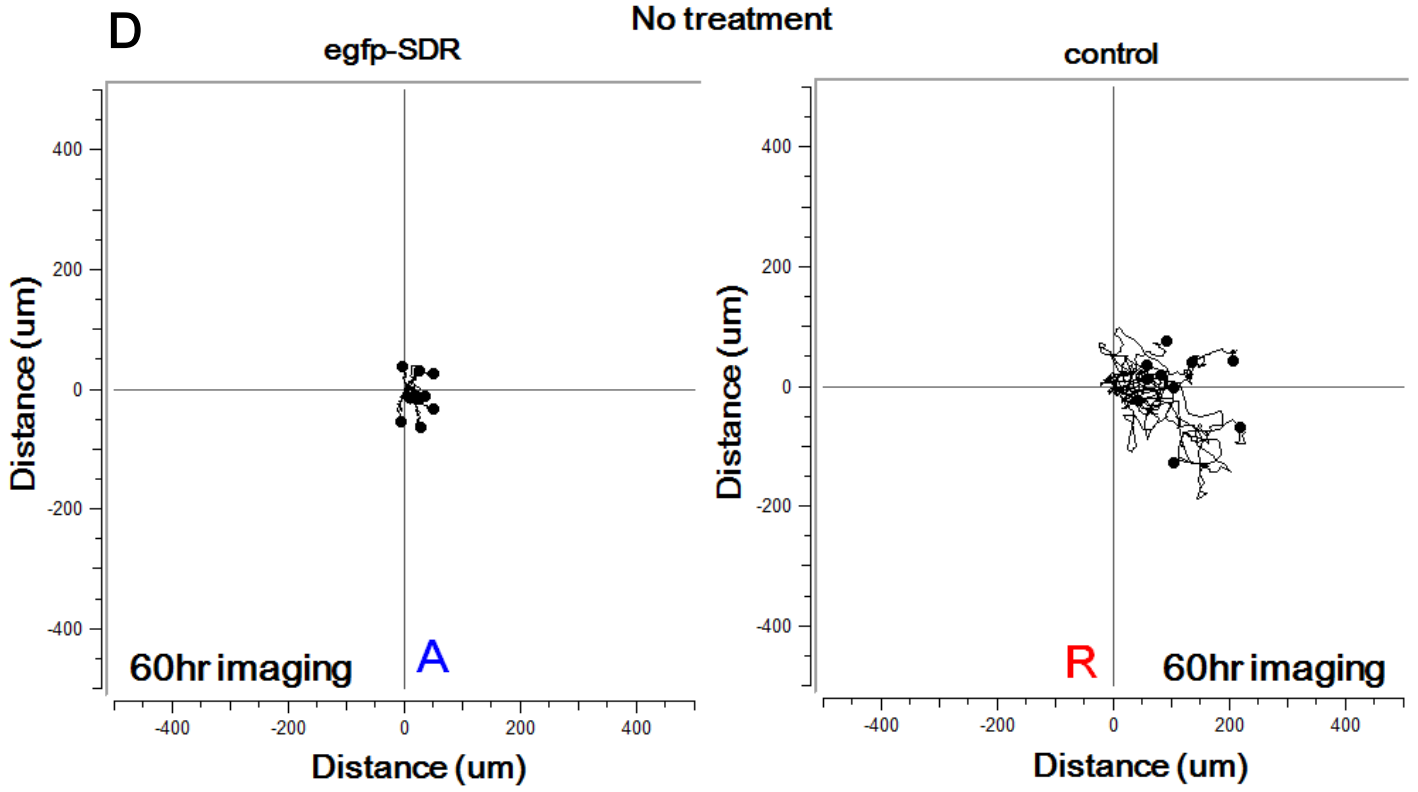
**B**

MDA-MB-231 migrating to MDA-MB-231-expressing SDR domain stable transfectant

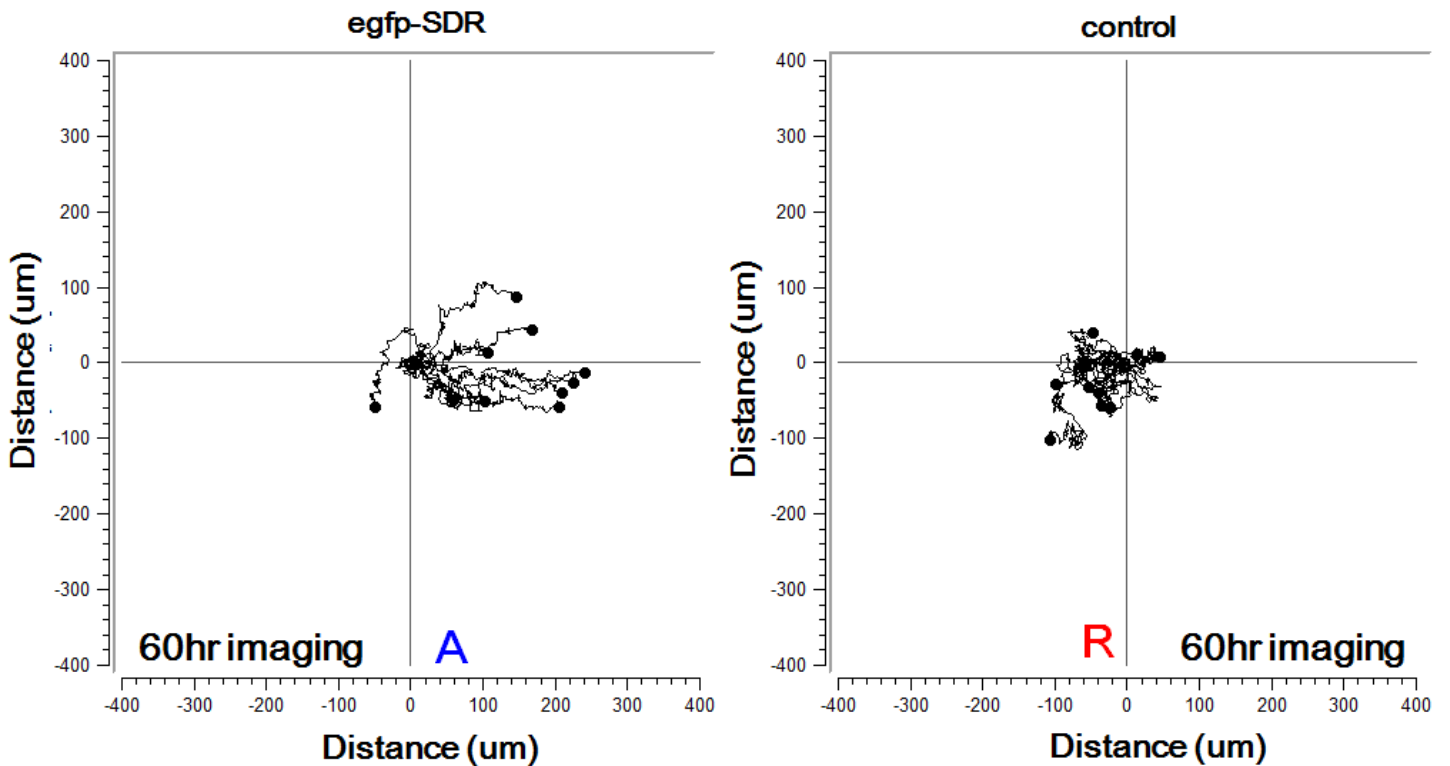
**C**

A = anterograde movement  
 R = retrograde movement

A = anterograde movement  
R = retrograde movement



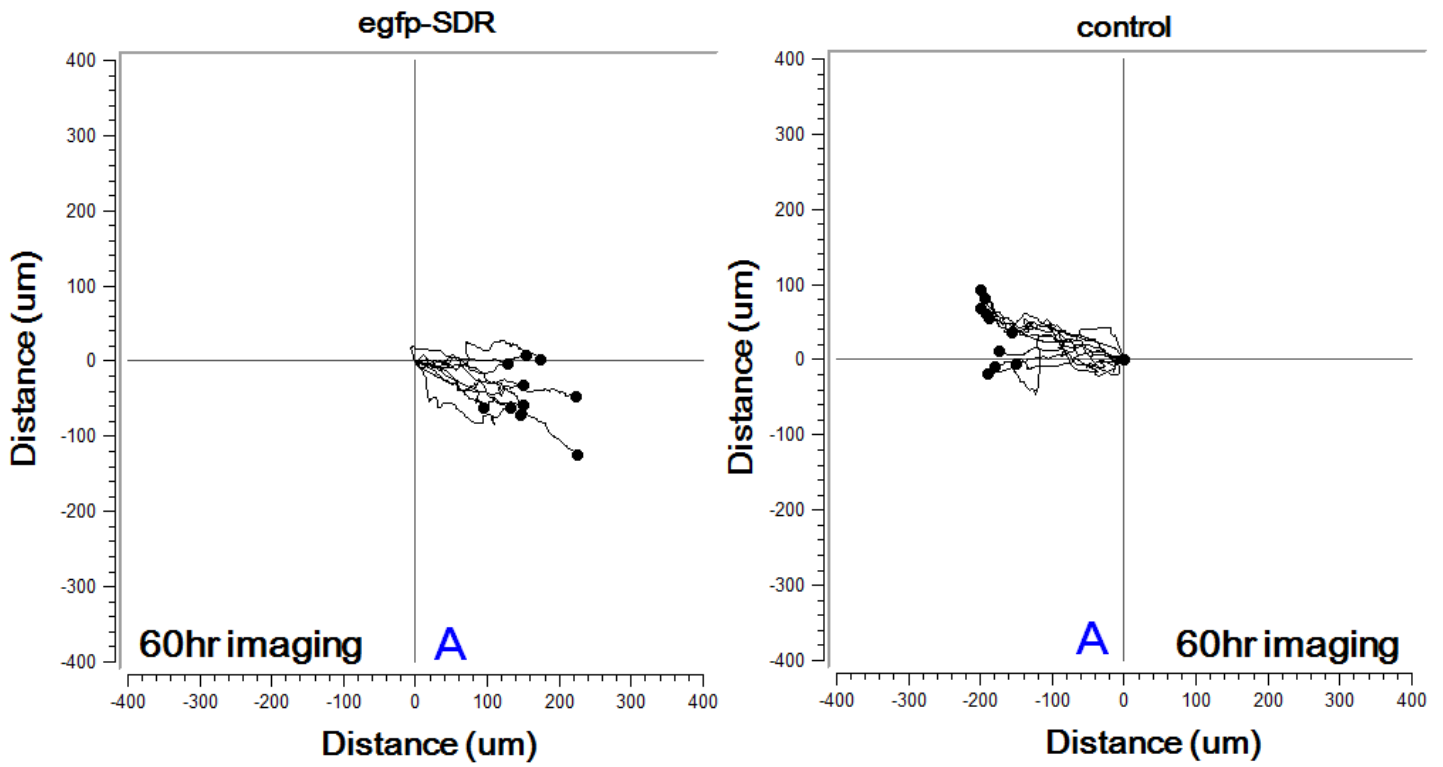
Normal rabbit serum treatment



A = anterograde movement  
R = retrograde movement

F

SDRrepl antiserum treatment



G

pSDRrepl antiserum treatment

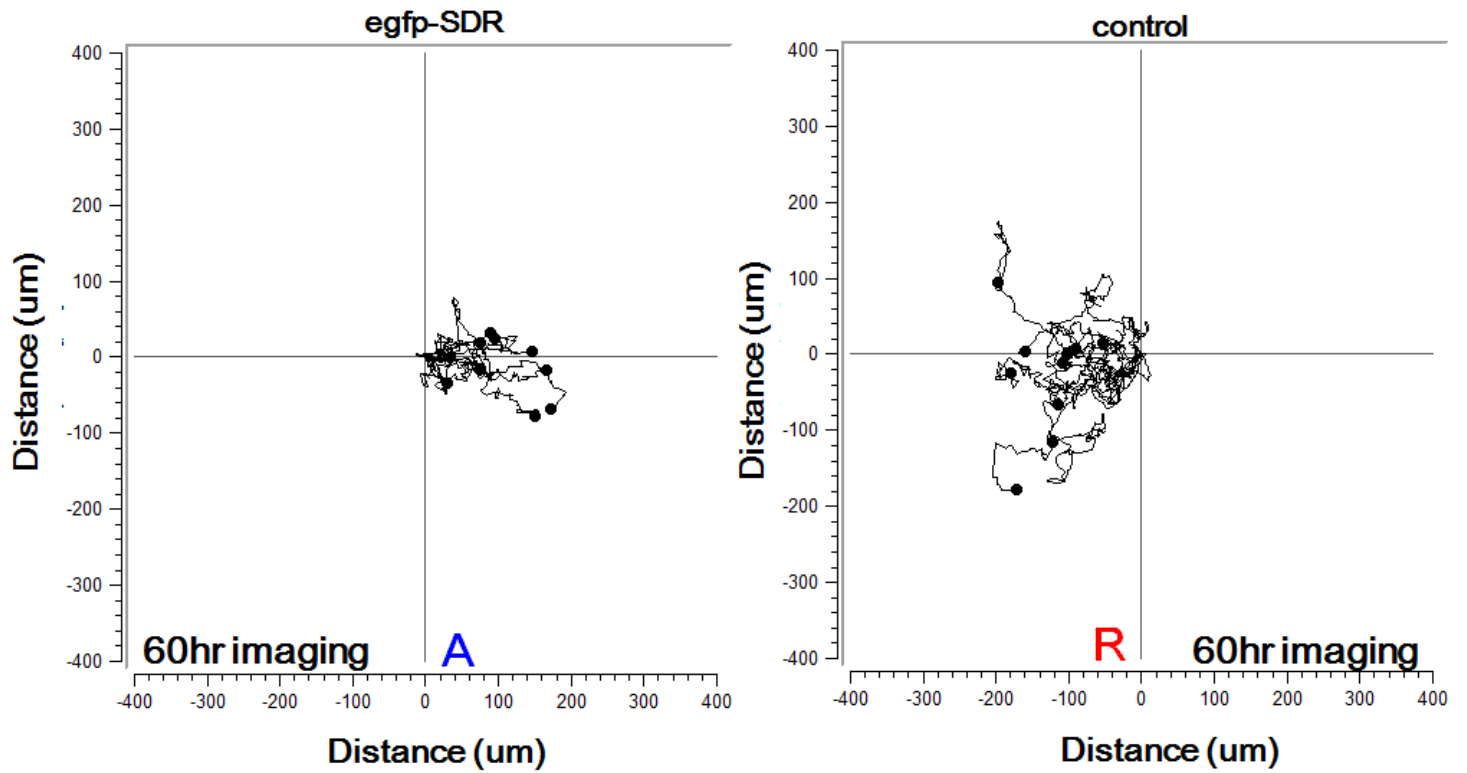
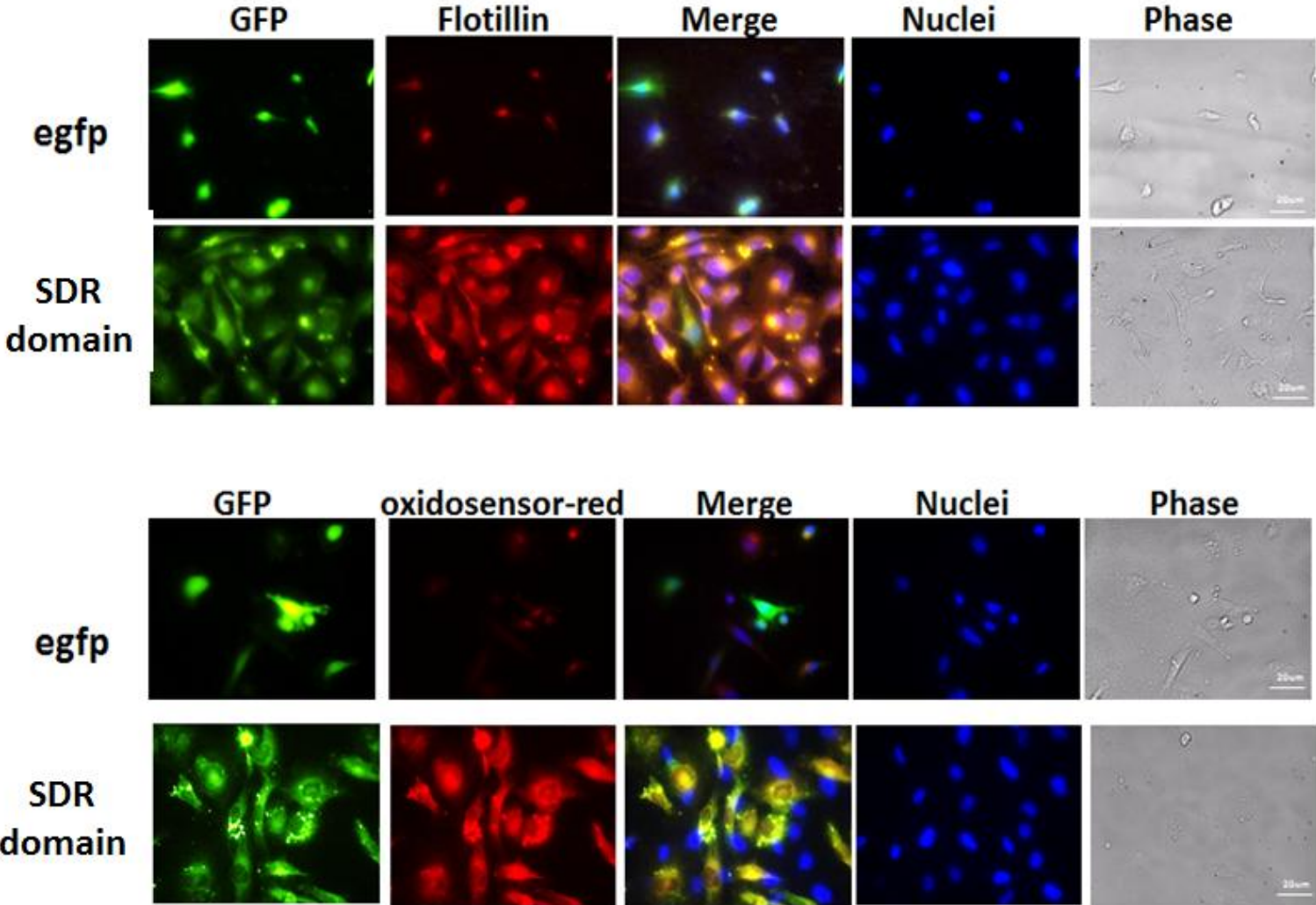


**Figure 22. SDRrepl is retained in cell membrane area possessing an oxidoreductase activity.**

MDA-MB-231-expressing SDR domain stable transfectant were seeded to process immunostaining. Cells were not permeabilized with Triton X-100. These cells were shown to colocalize with Flotillin-1 which is a caveolae-associated, integral membrane protein. The MDA-MB-231-expressing SDR domain stable transfectant was also oxidosensor-red positive.



(Magnification 400X)

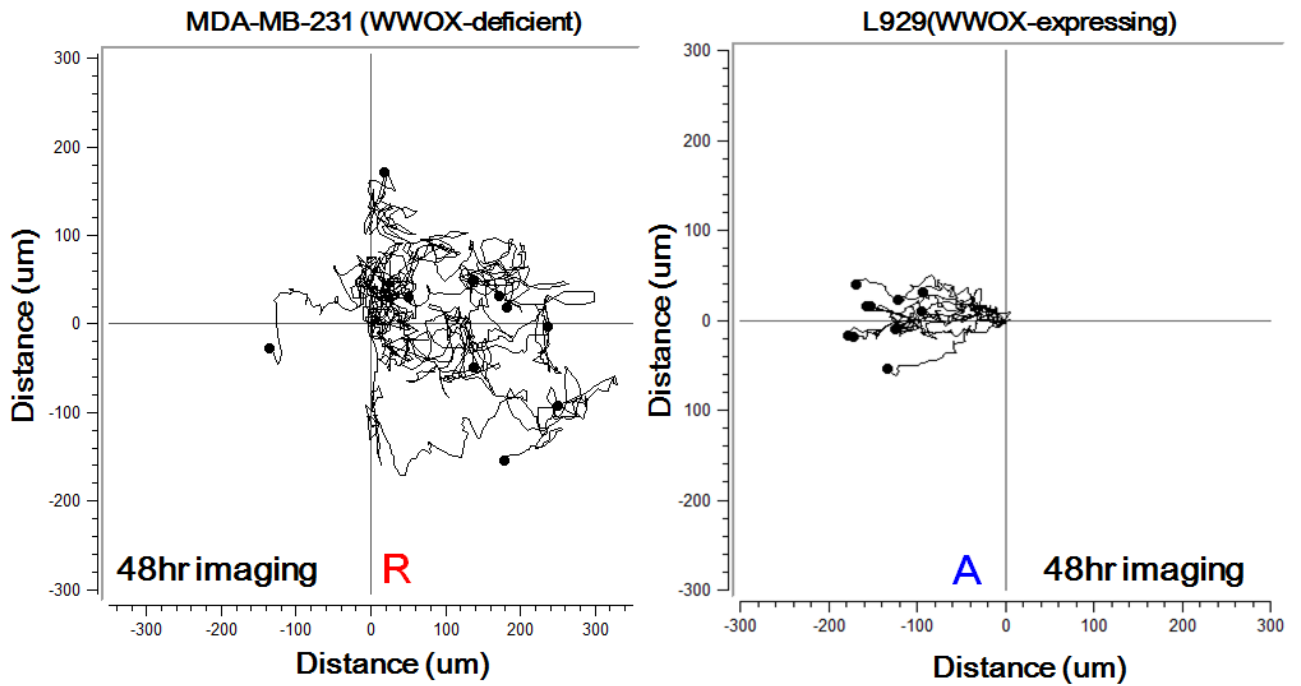
**Figure 23. SDRrepl antibody abolishes the retrograde movement of WWOX-deficient MDA-MB-231 cells upon encountering WWOX-expressing L929 cells.**

MDA-MB-231 cells (left) and L929 cells (right) were seeded, respectively, in each side of the culture-insert (ibidi). After overnight incubation, time-lapse microscopy was carried out at 37°C with 5% CO<sub>2</sub>. (A) WWOX-expressing L929 cells repelled the visiting WWOX-deficient MDA-MB-231 cells, which underwent retrograde migration. (B) Antiserum against SDR domain (1:500 dilution) abolished retrograde migration of MDA-MB-231 cells. (C) Temporal correlation of the velocity was performed to randomly analyze the migratory behavior of 10 cells. X, Y and total velocity were calculated. The velocities of cells in each time points were shown as peaks. The velocity of MDA-MB-231 under SDRrepl antiserum treatment was lower than control. The total velocity autocorrelation function was also lower than control. With the treatment, MDA-MB-231 cells took less time to become uncorrelated to the initial condition. It reflected that SDRrepl antiserum treatment altered the movement of MDA-MB-231 and reduced the sensitivities of cells upon sensing foreign cells. (D) Velocities of anterograde and retrograde movements were shown. SDRrepl Ab treatment also caused significant decrease of anterograde and retrograde movements. (E) The statistics and figures of total velocity autocorrelation function were shown. A = anterograde movement; R = retrograde movement. Each picture was taken per 10 min. (mean±standard deviation;  $n=10$ ; Student's  $t$  test).

A = anterograde movement  
R = retrograde movement

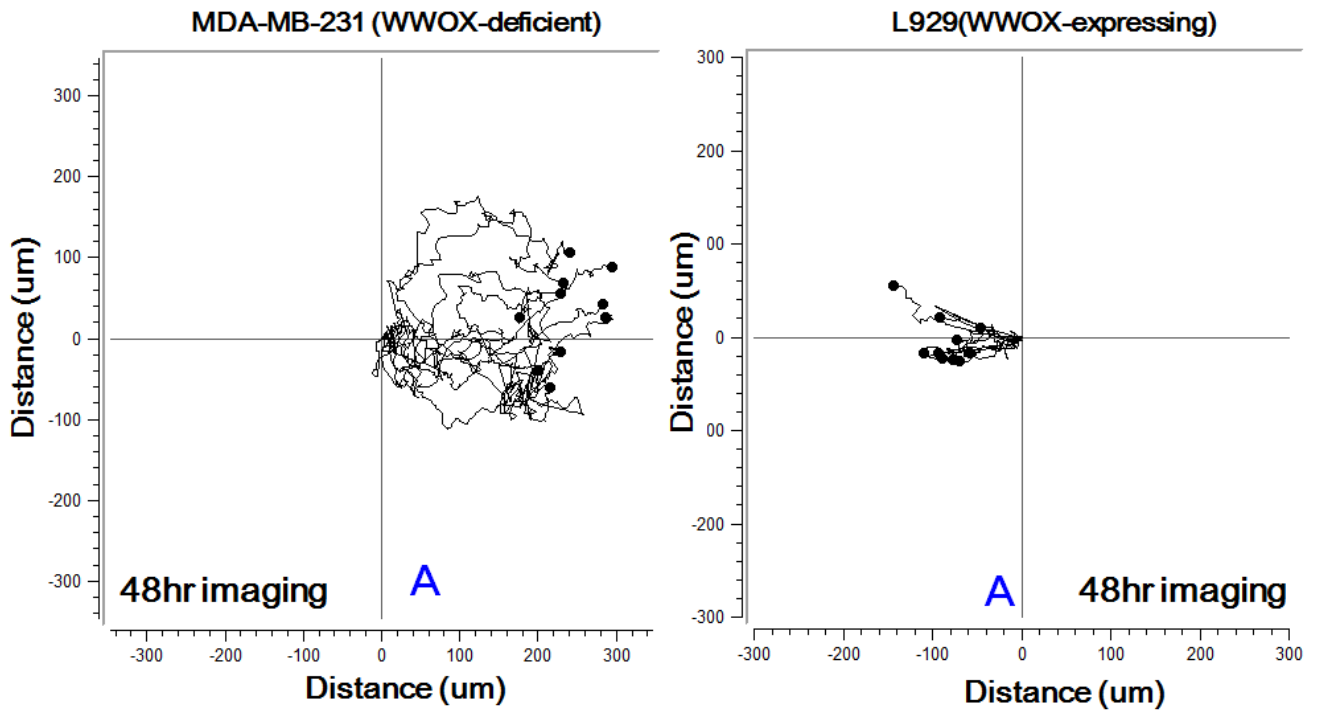
A

MDA-MB-231 Versus L929



B

SDRrepl antiserum treatment

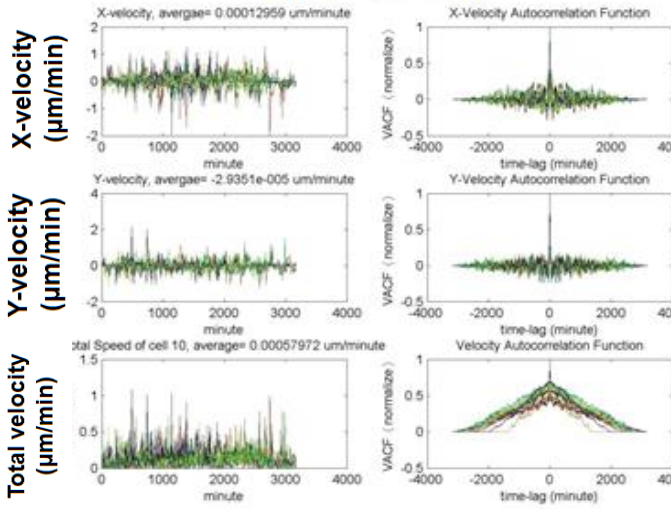


C

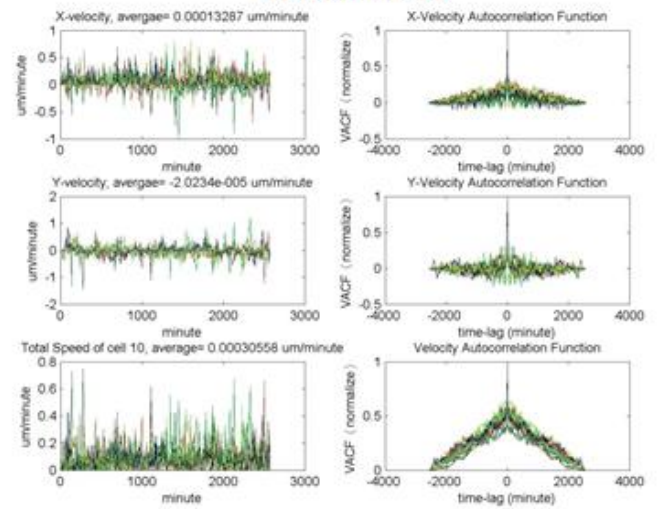
## MDA-MB-231 Versus L929

### Velocity of MDA-MB-231

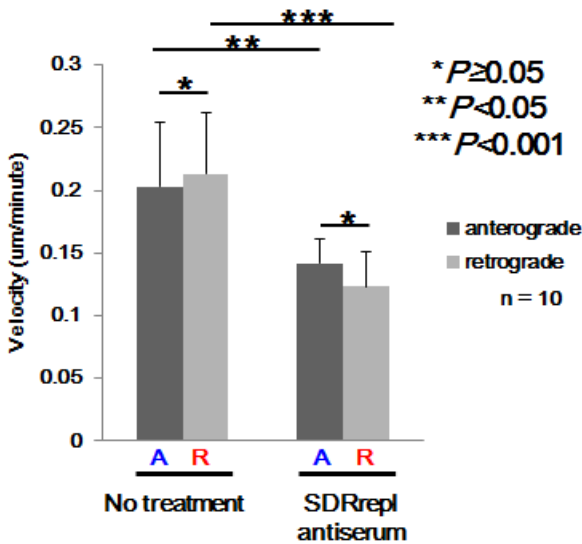
#### No treatment



### SDRrepl antiserum treatment



D



E



### Velocity Autocorrelation Function of MDA-MB-231

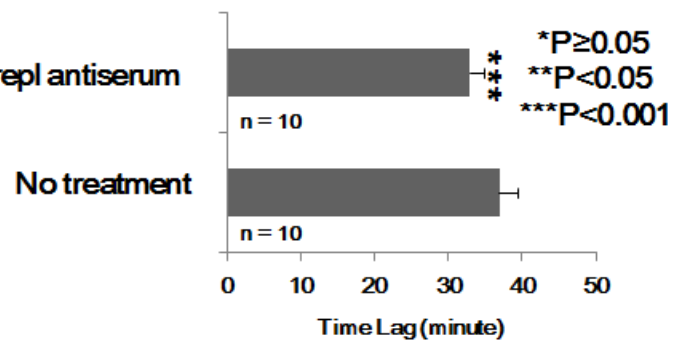
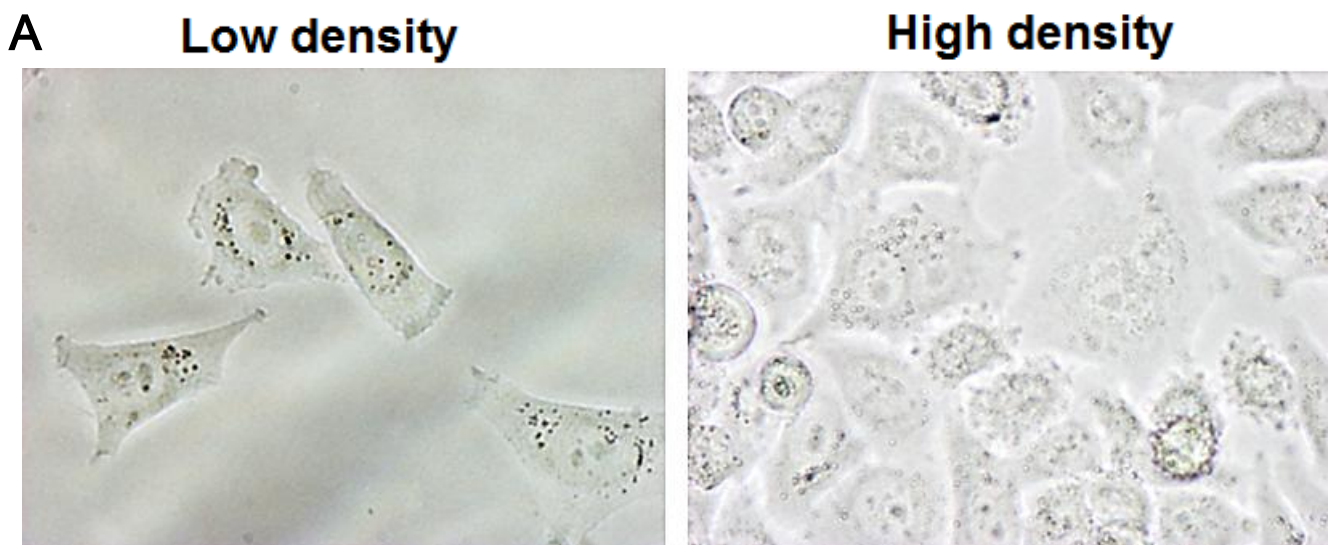
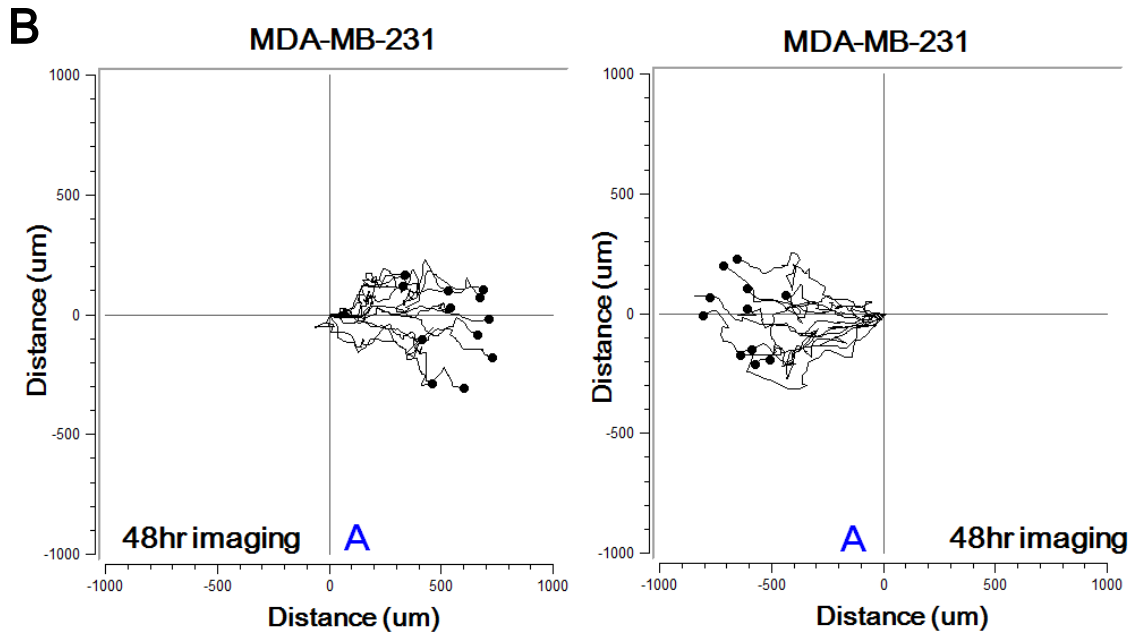


**Figure 24. SDRrepl antibody abolishes cell-to-cell repulsion between MDA-MB-231 cells and lung primary culture cells.**

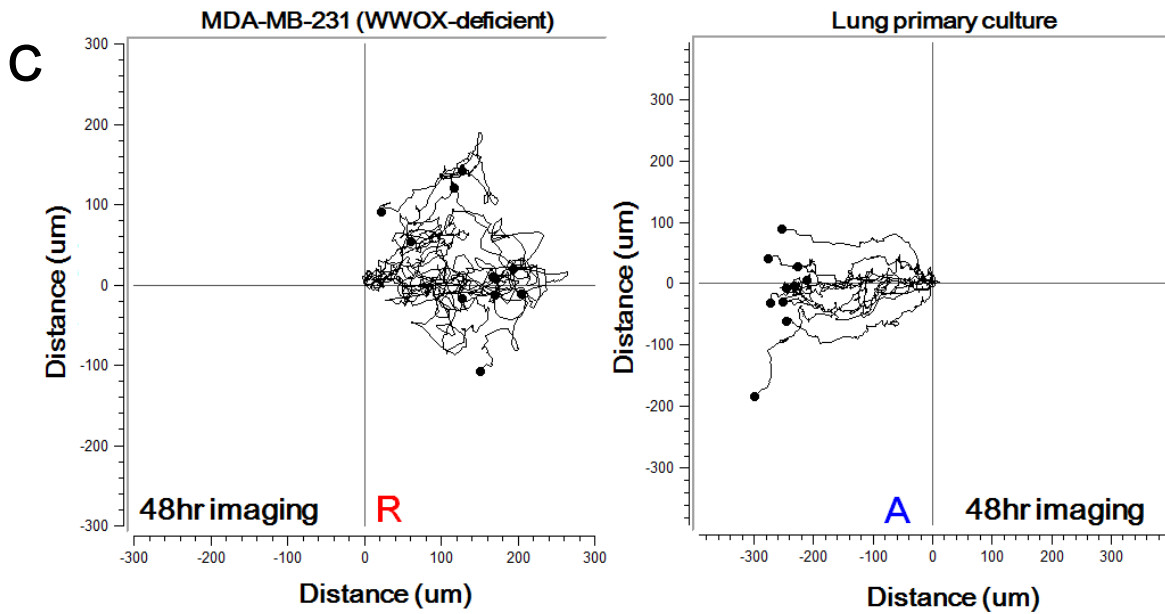
The lung cells were isolated from 11 weeks aged NOD-SCID mice. Tissue was put in RPMI medium containing 10% FBS, minced, and filtered through a 200-bore metal mesh to remove clumps. The single cells suspension were centrifuged at 200g for 5min to pellet the cells, and resuspended in 10%FBS RPMI. The freshly isolated cells were plated into a 10cm<sup>2</sup> culture dishes at 1×10<sup>5</sup>cells/ml and incubated at 37°C in 5% CO<sub>2</sub>/95% air. After 72h, non-adherent cells were removed and the medium was replaced. At 80% confluence, cells were harvested with 0.25% trypsin–0.02% EDTA for 2min at 37°C, replanted and examined. After 5 days culture, the adherent cells displayed epithelial, polygonal morphology. MDA-MB-231 cells (left) and lung cells (right) were seeded, respectively, in each side of the culture-insert (ibidi). After overnight incubation, time-lapse microscopy was carried out at 37°C with 5% CO<sub>2</sub>. (A) The cell morphology of primary lung cells in low cell density (left) and high cell density (right) were shown. (B) In control set, both well were seeded with MDA-MB-231 cells. Cells in the each side could recognize each other and migrated in a anterograde manner. (C) MDA-MB-231 migrated toward lung primary culture cells, MDA-MB-231 cells moved retrograde. (D) Antiserum against SDR domain (1:500 dilution) abolished retrograde migration of MDA-MB-231 cells. A = anterograde movement; R = retrograde movement. Each picture was taken per 10 min. (E) Their migrating distance with time is shown. (F) Average velocity of cell migration is shown. (G-I) The statistics and figure of total velocity autocorrelation function of MDA-MB-231 versus lung primary culture with or without SDRrepl antiserum treatment was shown. (mean±standard deviation; n=10; Student's *t* test).



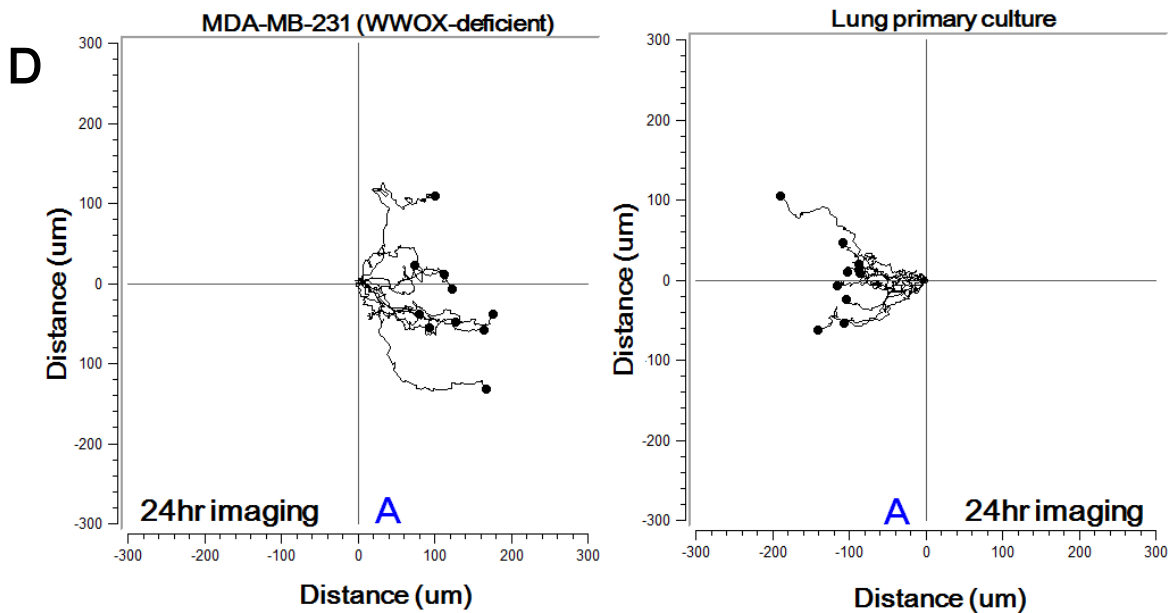
A = anterograde movement  
R = retrograde movement



MDA-MB-231 Versus Lung primary culture

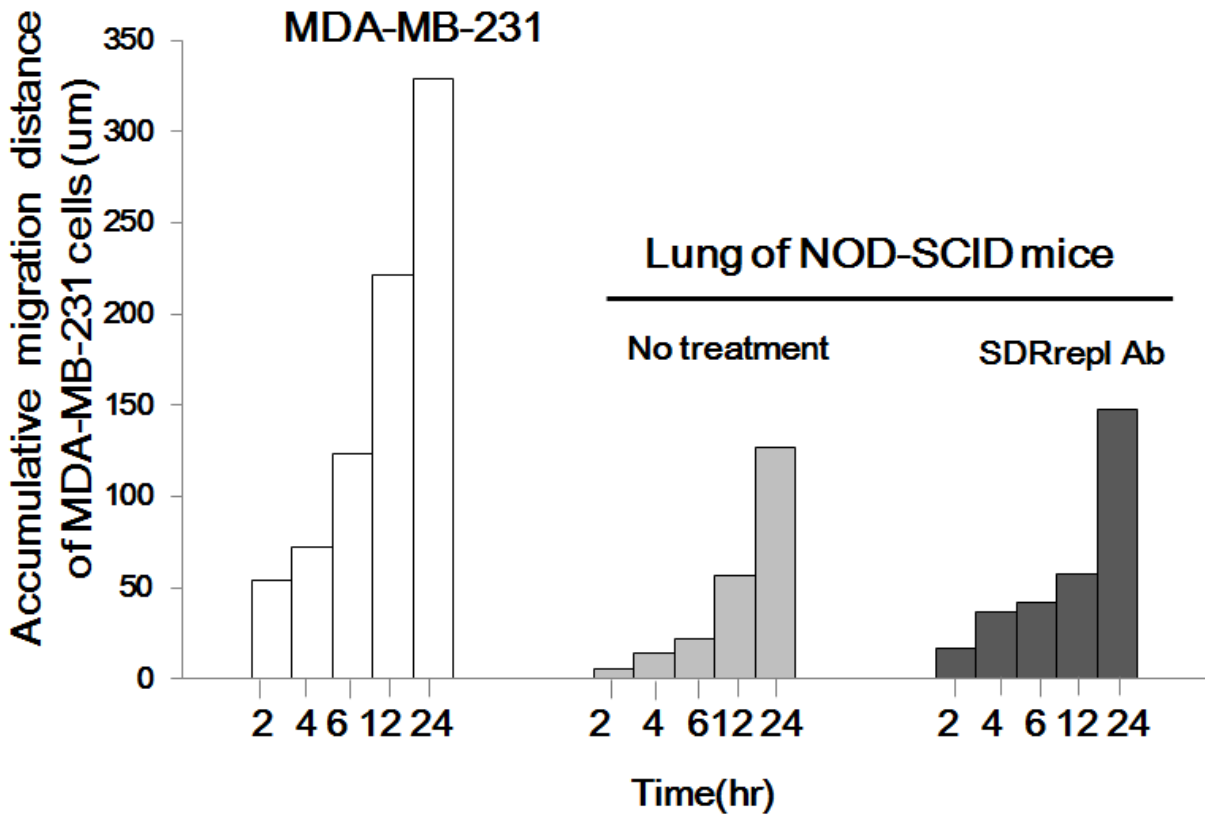


SDRrepl antiserum treatment

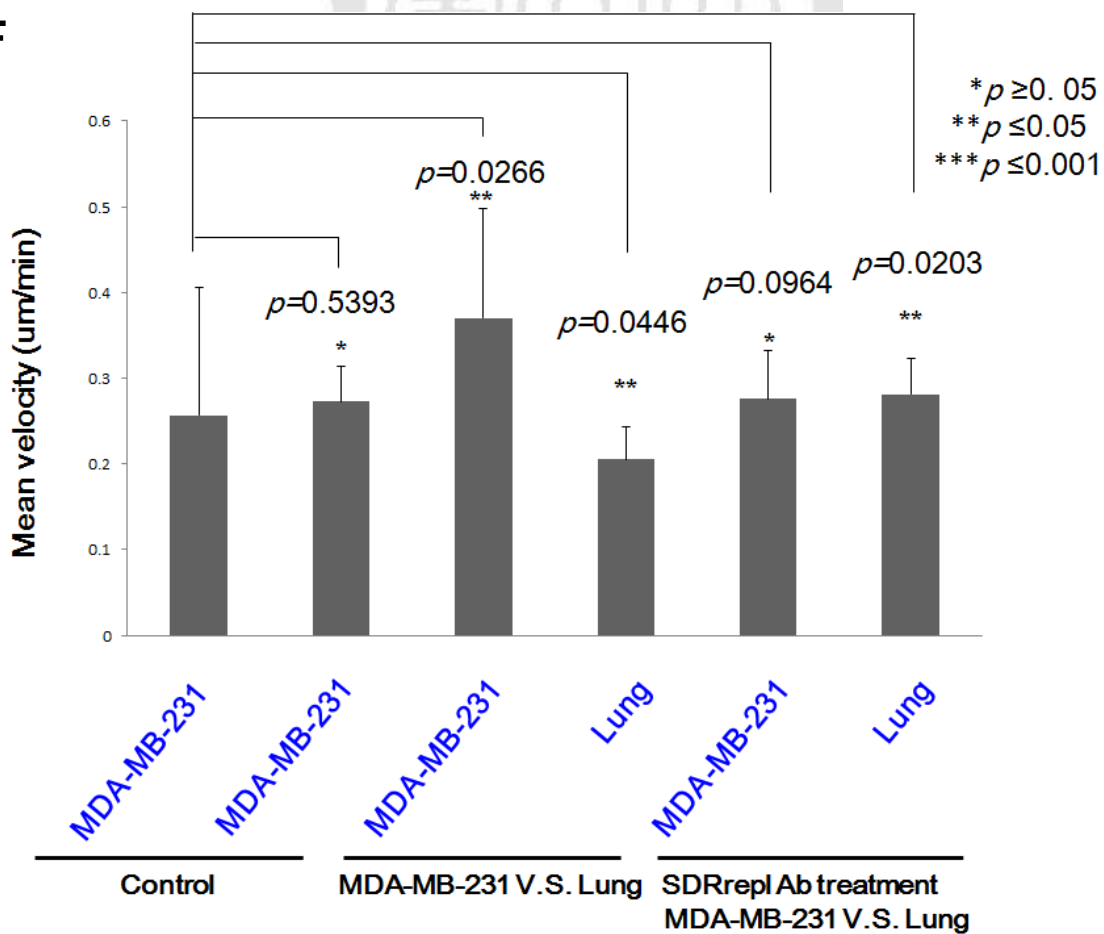


III

### MDA-MB-231 Versus Lung primary culture



IV



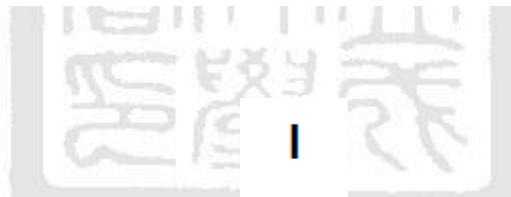
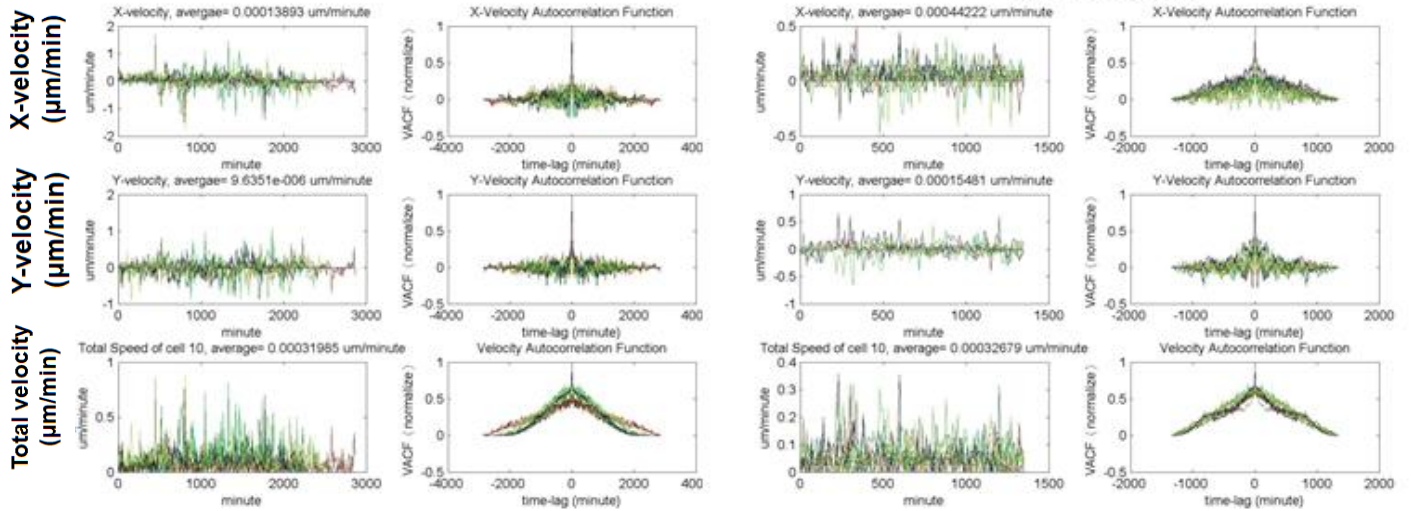
G

## MDA-MB-231 Versus Lung primary culture

### Velocity of MDA-MB-231

No treatment

### SDRrepl antiserum treatment



H

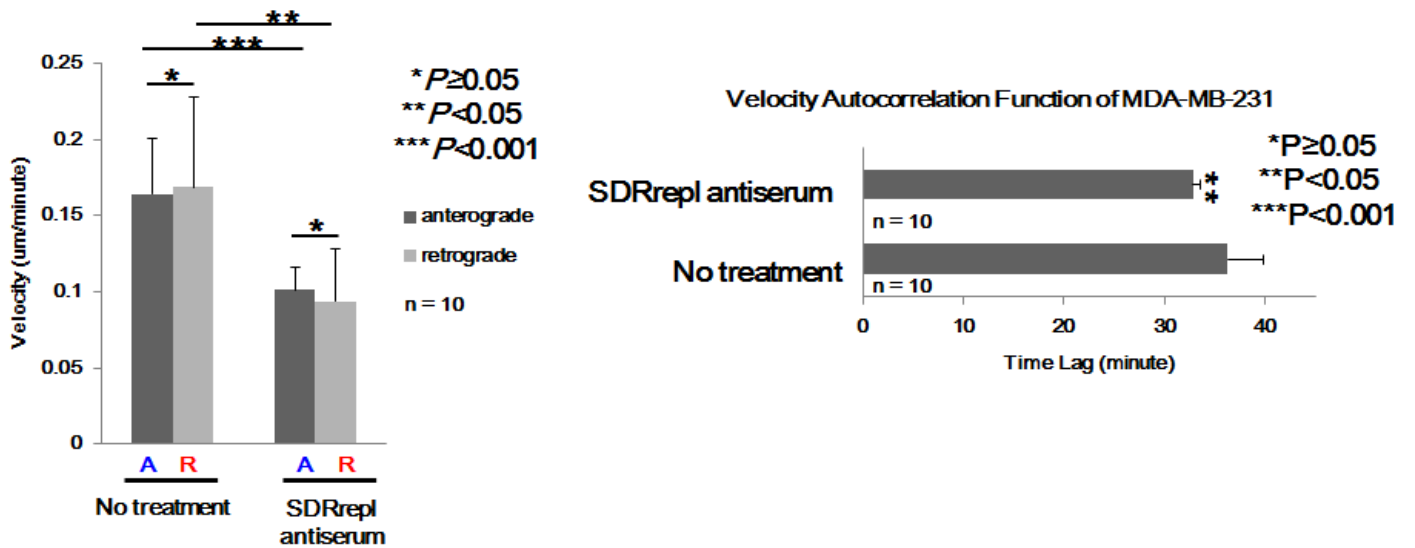
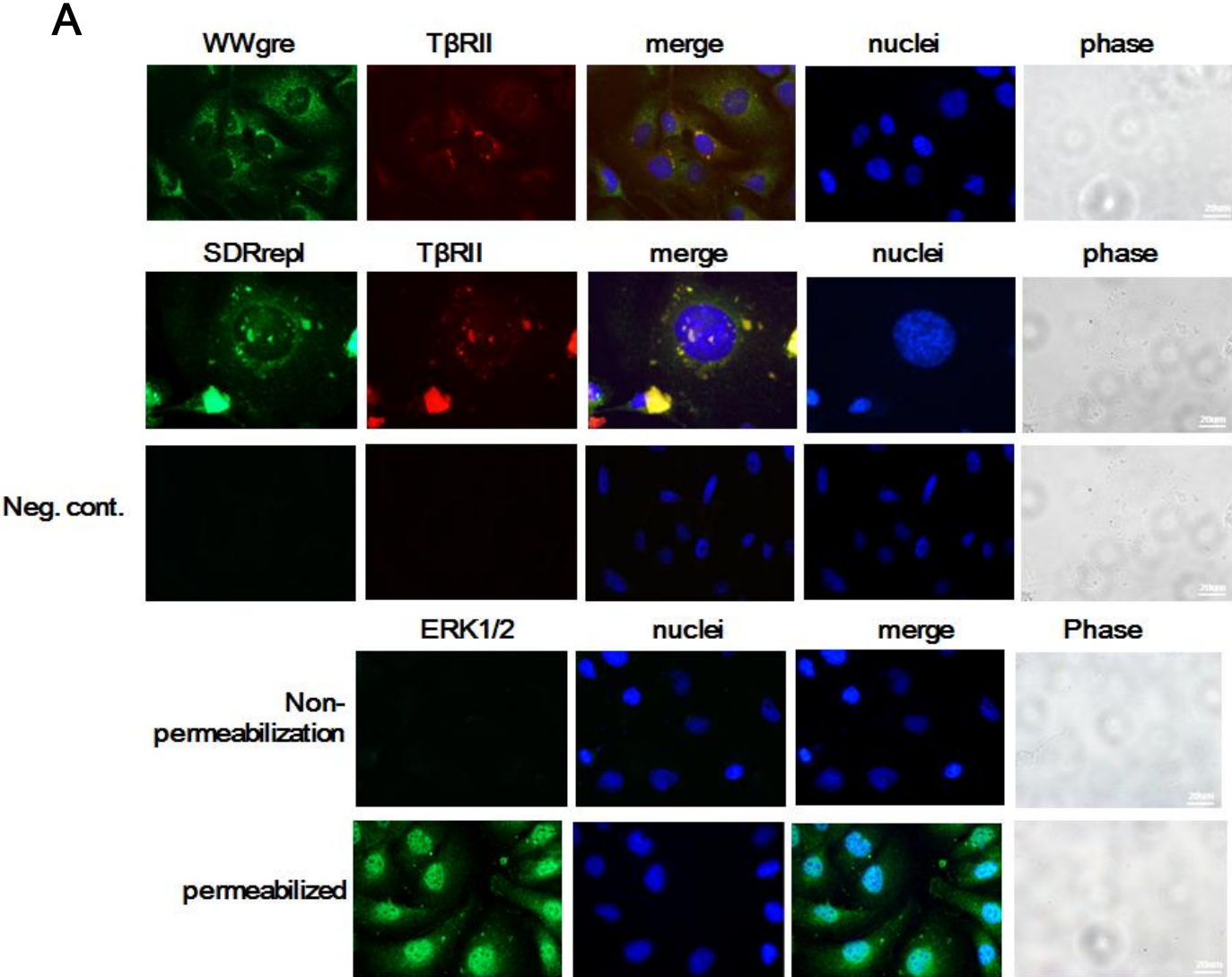


**Figure 25. WWgre and SDRrepl colocalize with cell membrane TβRII.**

(A) MDA-MB-231 cells were incubated with WWgre and SDRrepl peptides at 4°C for 30 min, followed by processing immunostaining using our generated peptide antibodies. These peptides were shown to colocalize with membrane TβRII. Cells were not permeabilized with Triton X-100. In the negative controls, no primary antibodies were used. In a control experiment, cells were stained for ERK1/2 to show its nuclear localization in Triton X-100-permeabilized cells. No signal was shown in non-permeabilized cells. (B) We also confirmed the colocalization between WWgre or SDRrepl and TβRII by confocal microscopy. (Magnification 400X)



B

## Confocal image

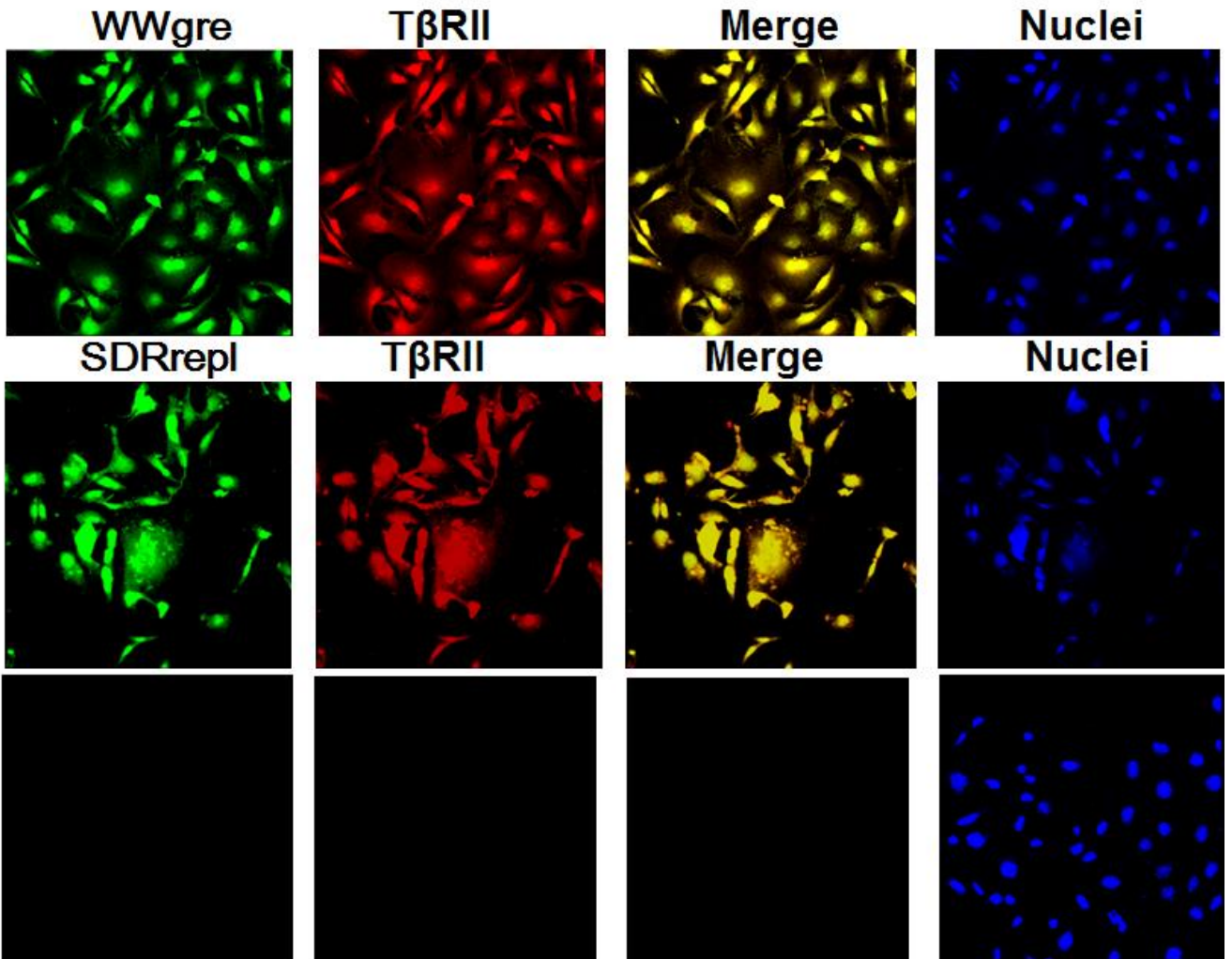
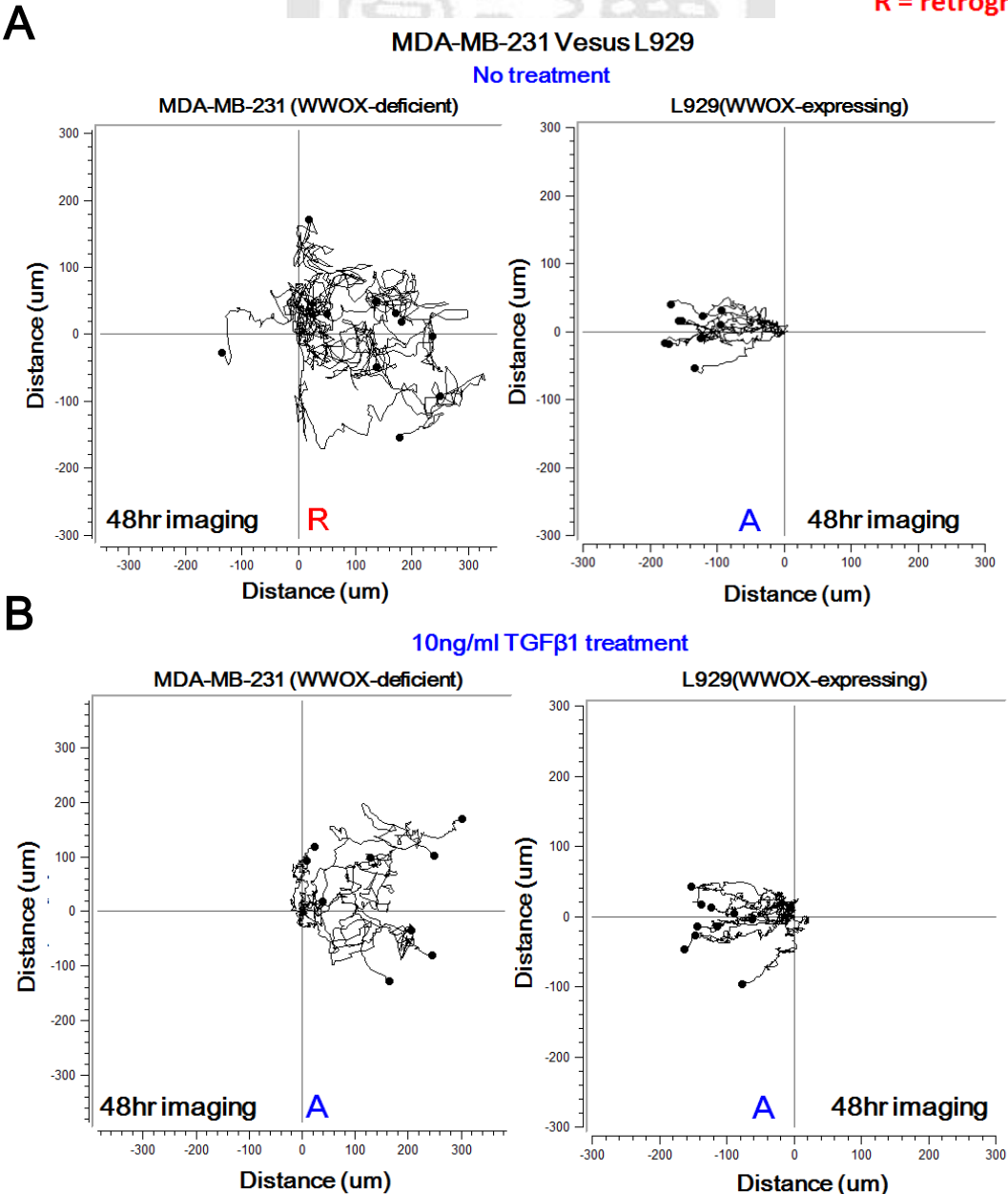


**Figure 26. TGFβ1 alters the retrograde movement of WWOX-deficient cells upon encountering WWOX-expressing cells.**

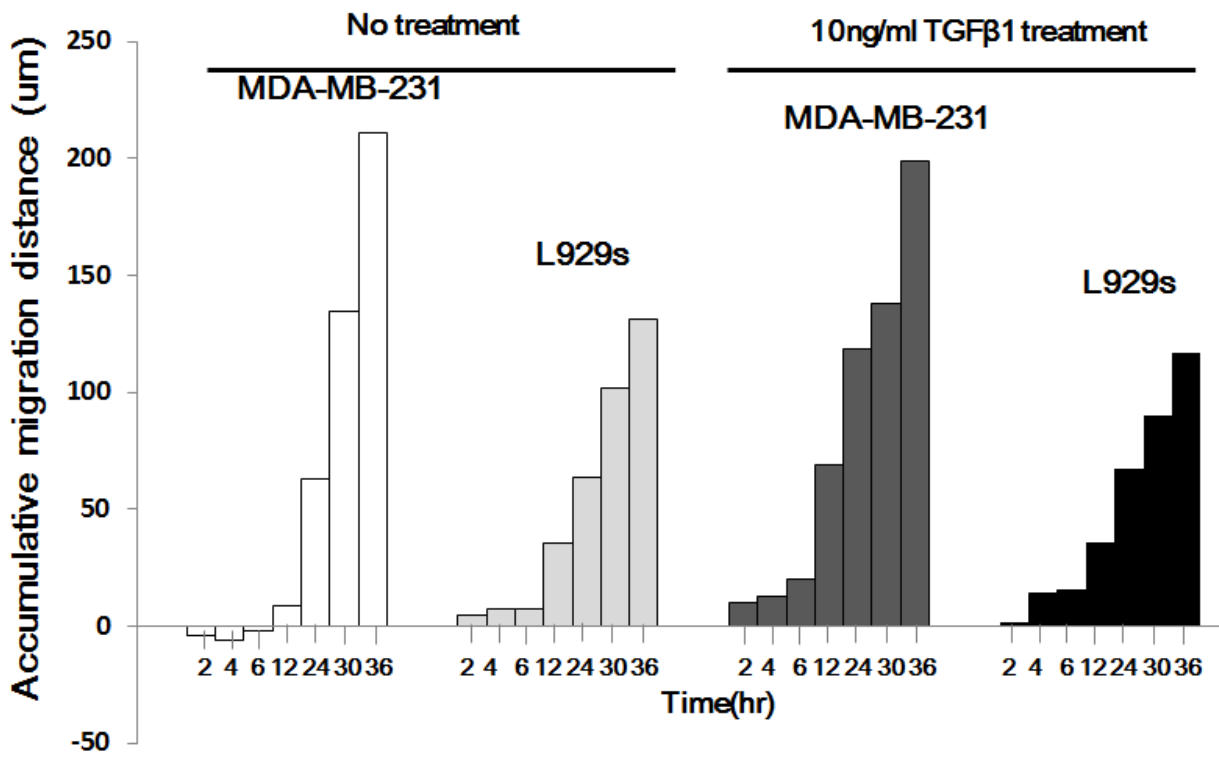
MDA-MB-231 cells (left) and L929 cells (right) were seeded, respectively, in each side of the culture-insert (ibidi). After overnight incubation, time-lapse microscopy was carried out at 37°C with 5% CO<sub>2</sub>. (A) WWOX-expressing L929 cells repelled the visiting WWOX-deficient MDA-MB-231 cells, which underwent retrograde migration. (B) 10ng/ml TGFβ1 treatment abolished retrograde migration of MDA-MB-231 cells. A = anterograde movement; R = retrograde movement. Each picture was taken per 10 min. (C) Their migrating distance with time is shown. (D) Average velocity of cell migration is shown. (E-G) The statistics and figures of total velocity autocorrelation function are shown. (H-N) The migration analysis of MDA-MB-231 versus lung primary culture with or without TGFβ1 treatment was shown. (mean±standard deviation; n=10; Student's *t* test).

A = anterograde movement  
R = retrograde movement



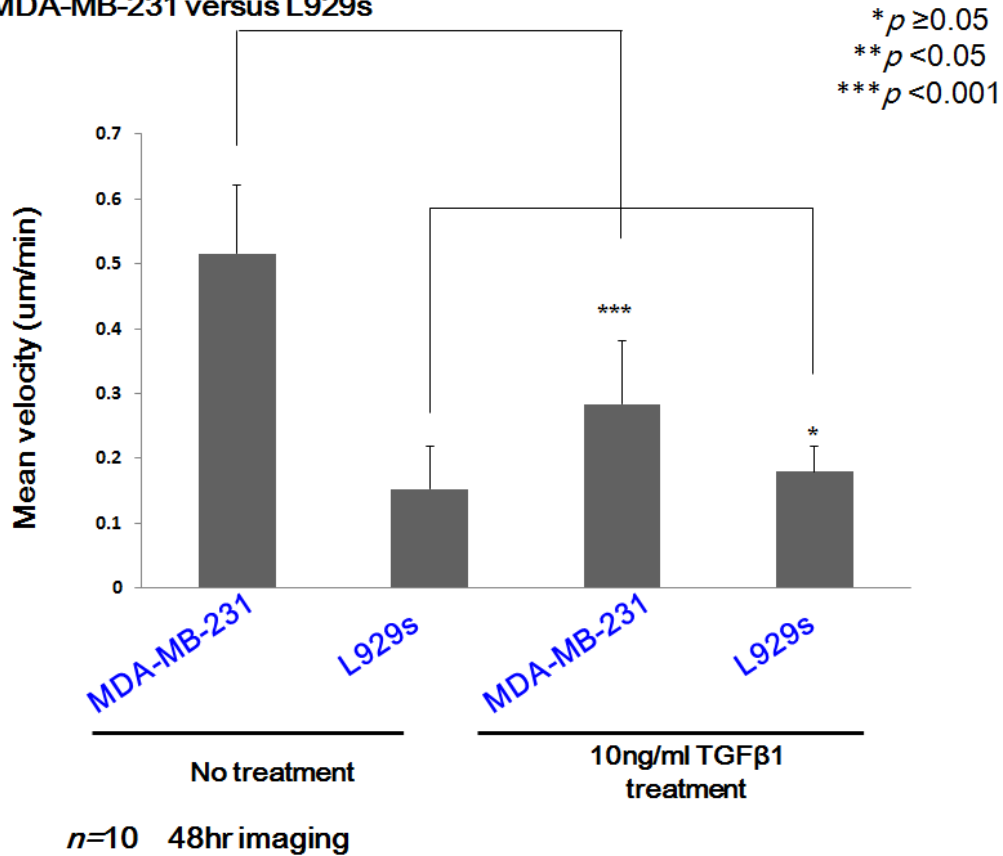
C

MDA-MB-231 versus L929



D

MDA-MB-231 versus L929s

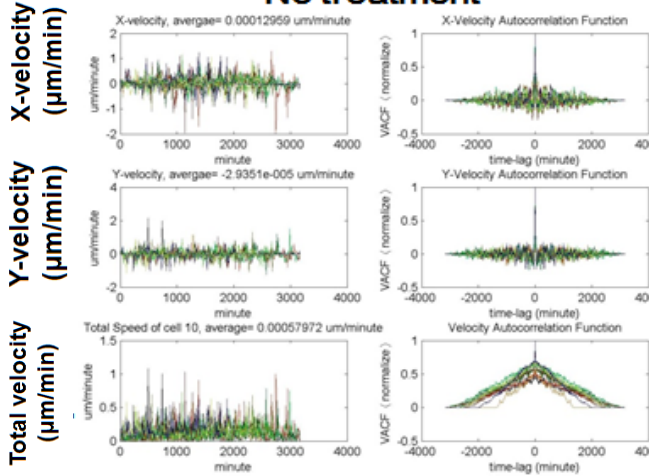


E

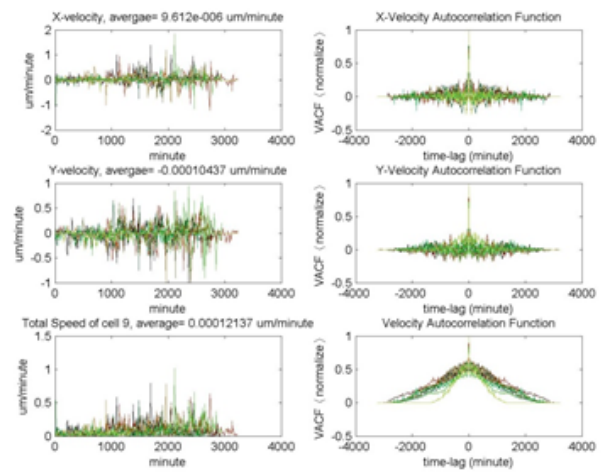
MDA-MB-231 Versus L929

Velocity of MDA-MB-231

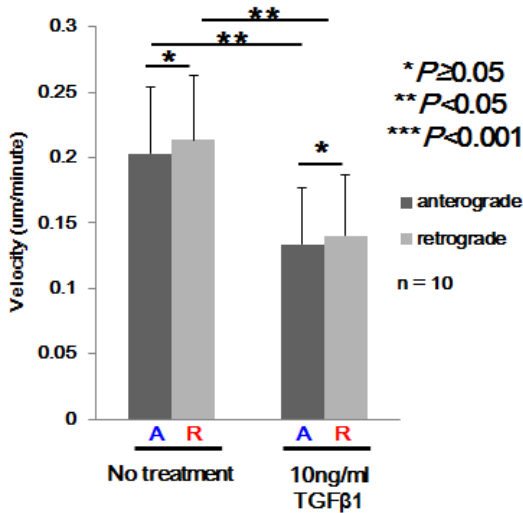
No treatment



10ng/ml TGFβ1 treatment

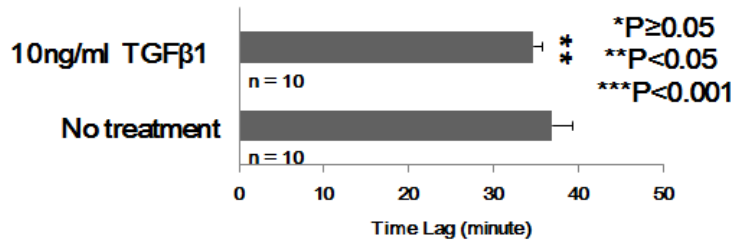


F



G

Velocity Autocorrelation Function of MDA-MB-231

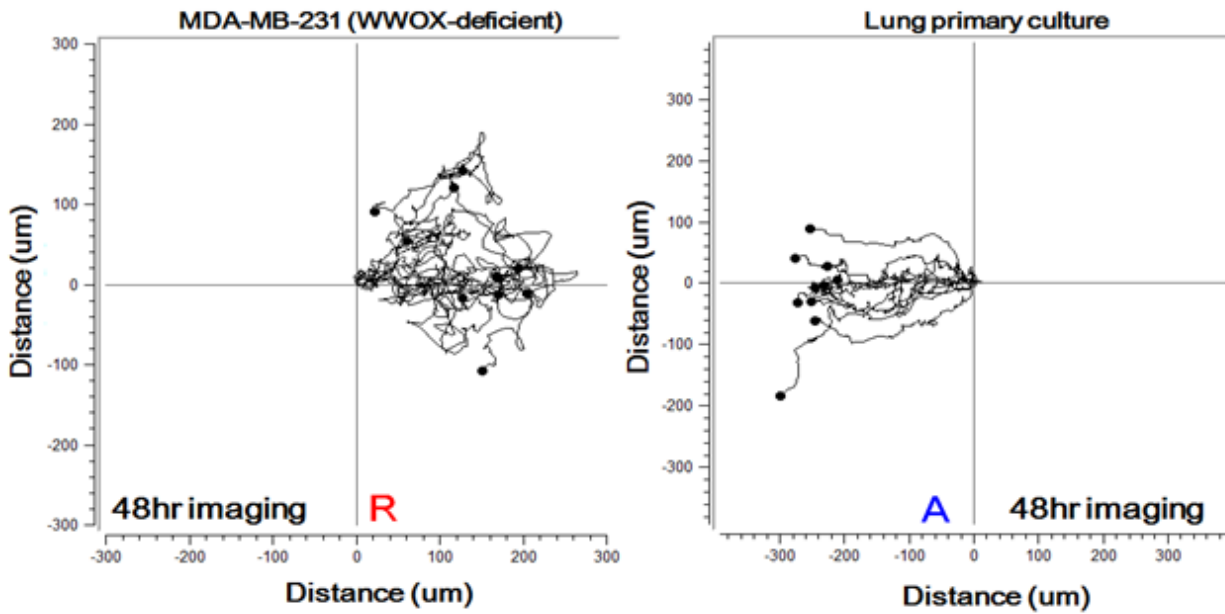


A = anterograde movement  
R = retrograde movement

H

### MDA-MB-231 Versus Lung primary culture

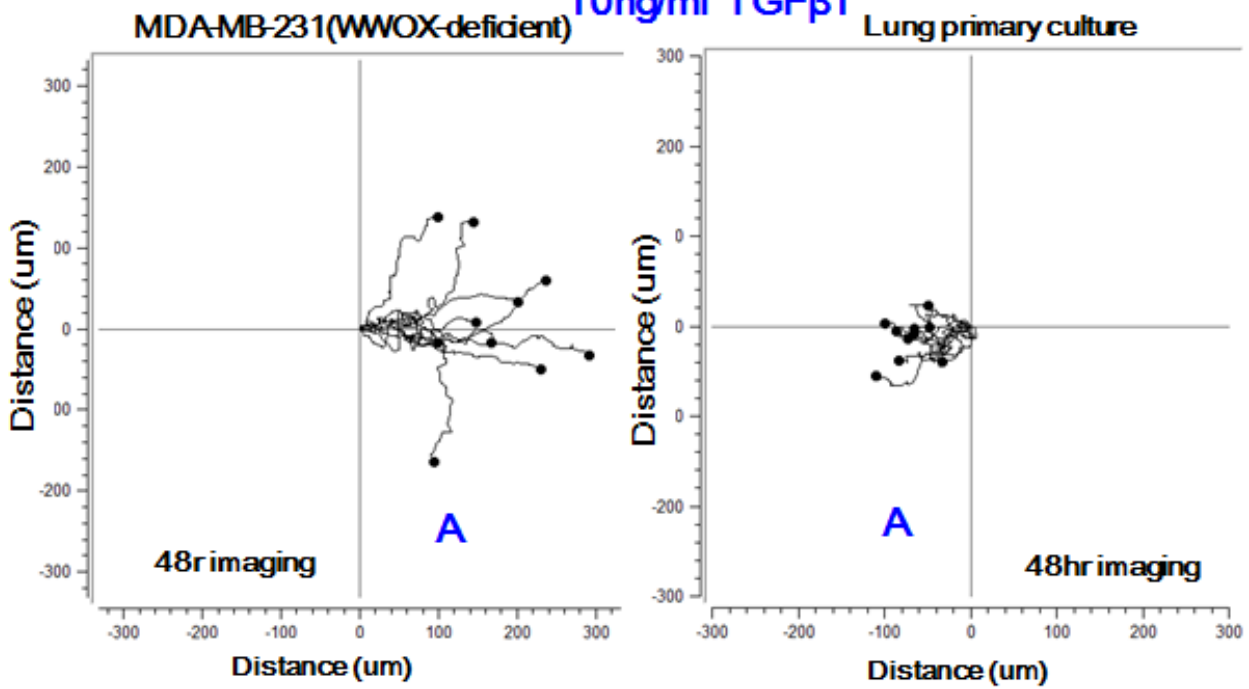
No treatment



I

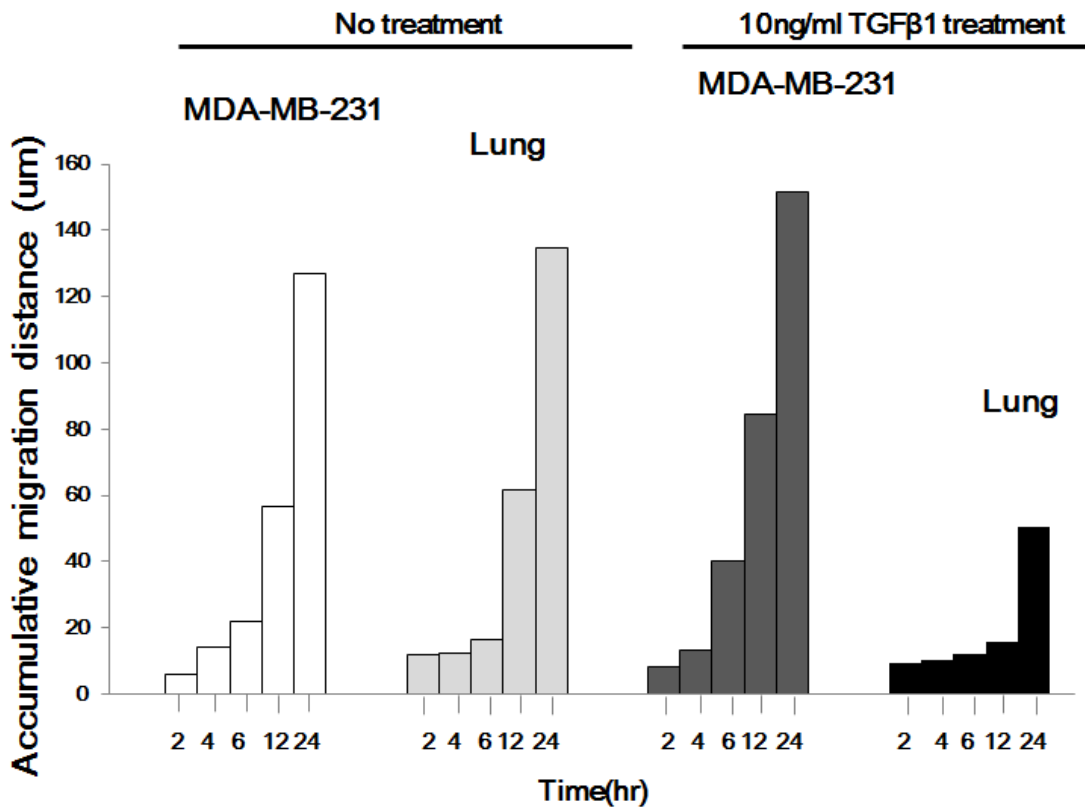


10ng/ml TGFβ1

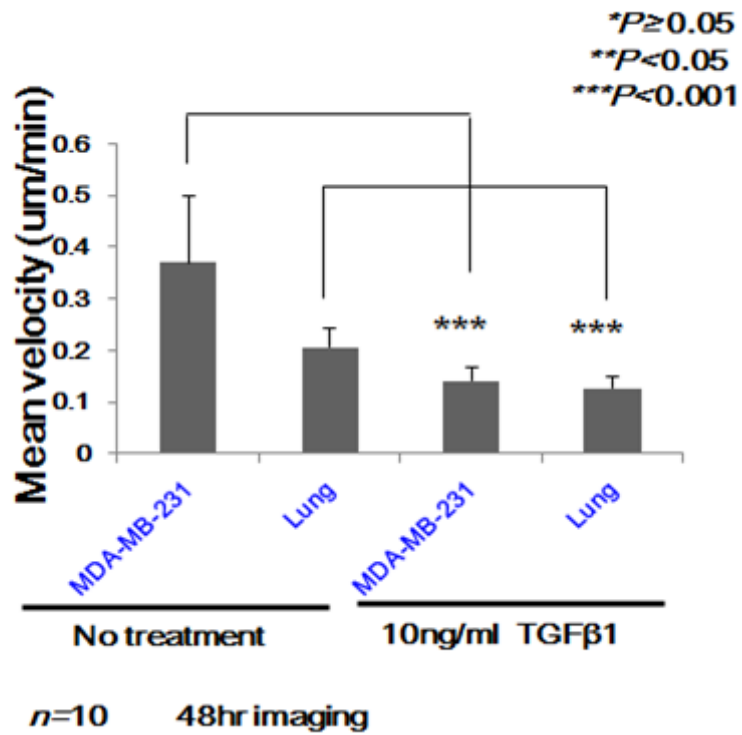


**J**

**MDA-MB-231 Versus Lung primary culture**



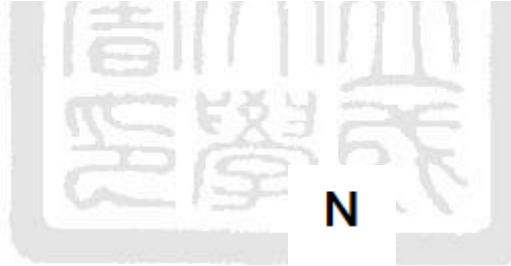
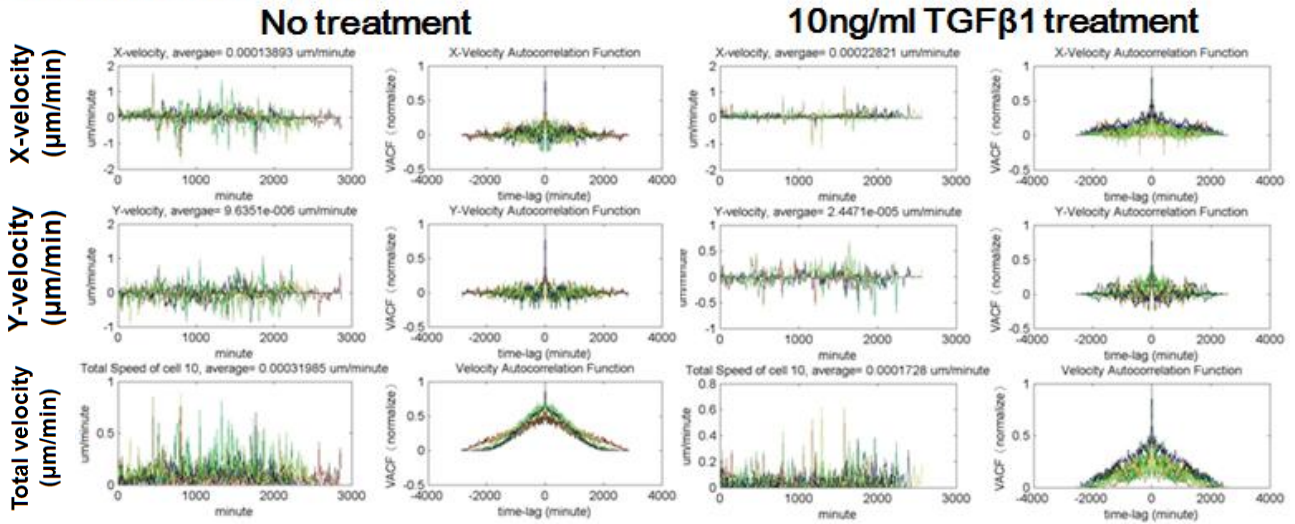
**K**



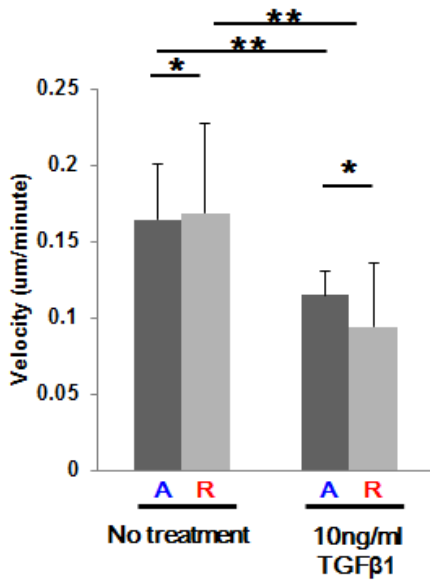
L

## MDA-MB-231 Versus Lung

### Velocity of MDA-MB-231



M

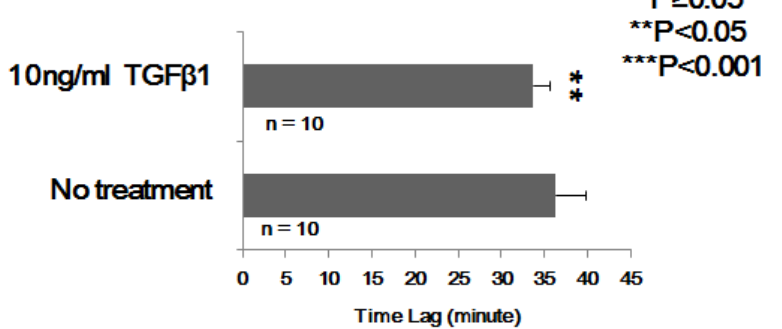


\*  $P \geq 0.05$   
 \*\*  $P < 0.05$   
 \*\*\*  $P < 0.001$

■ anterograde  
 ■ retrograde

n = 10

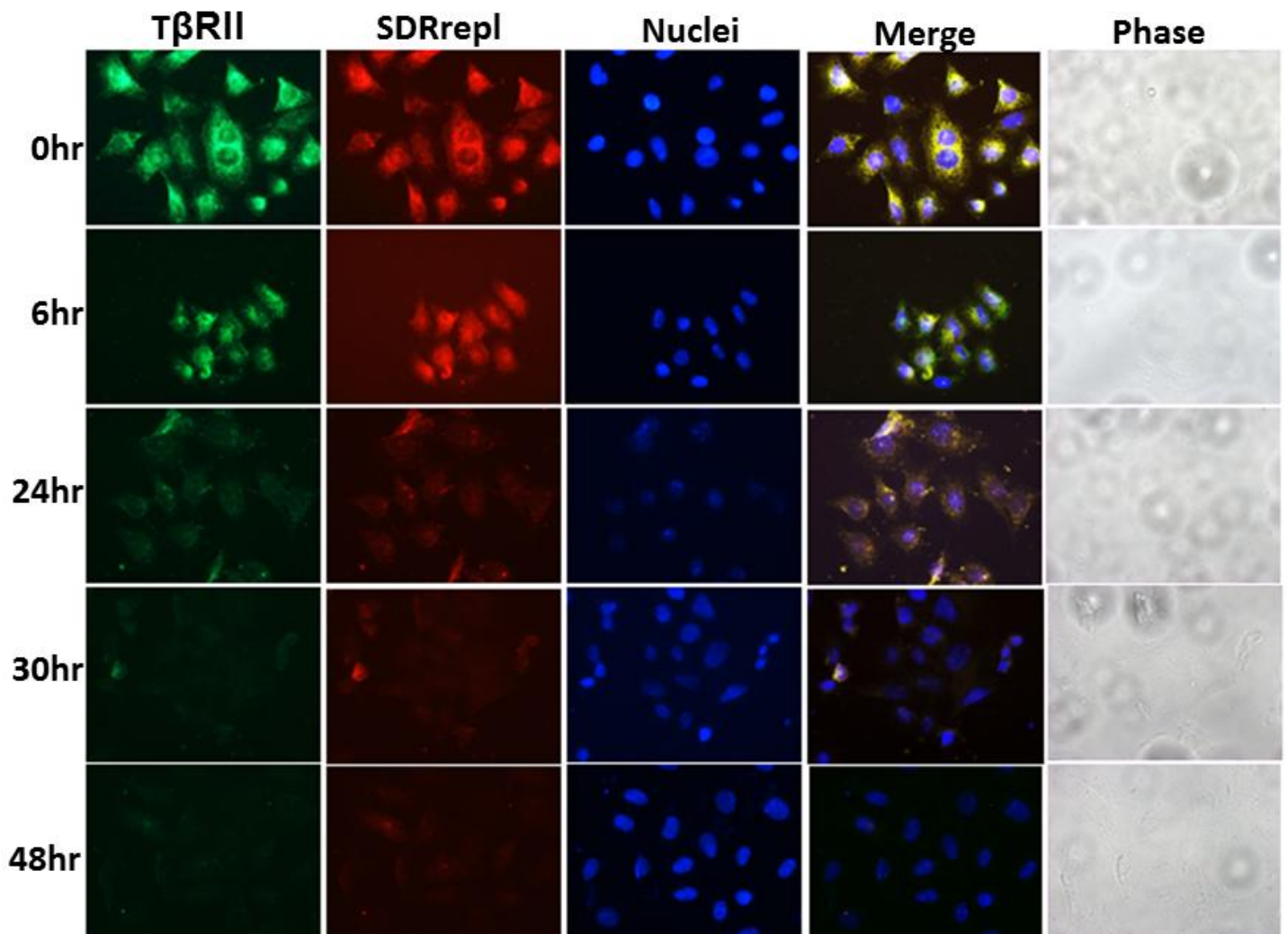
### Velocity Autocorrelation Function of MDA-MB-231



**Figure 27. TGFβ1 induces WWOX and TGF-β type II receptor (TβRII) to relocate into the cytoplasm..**

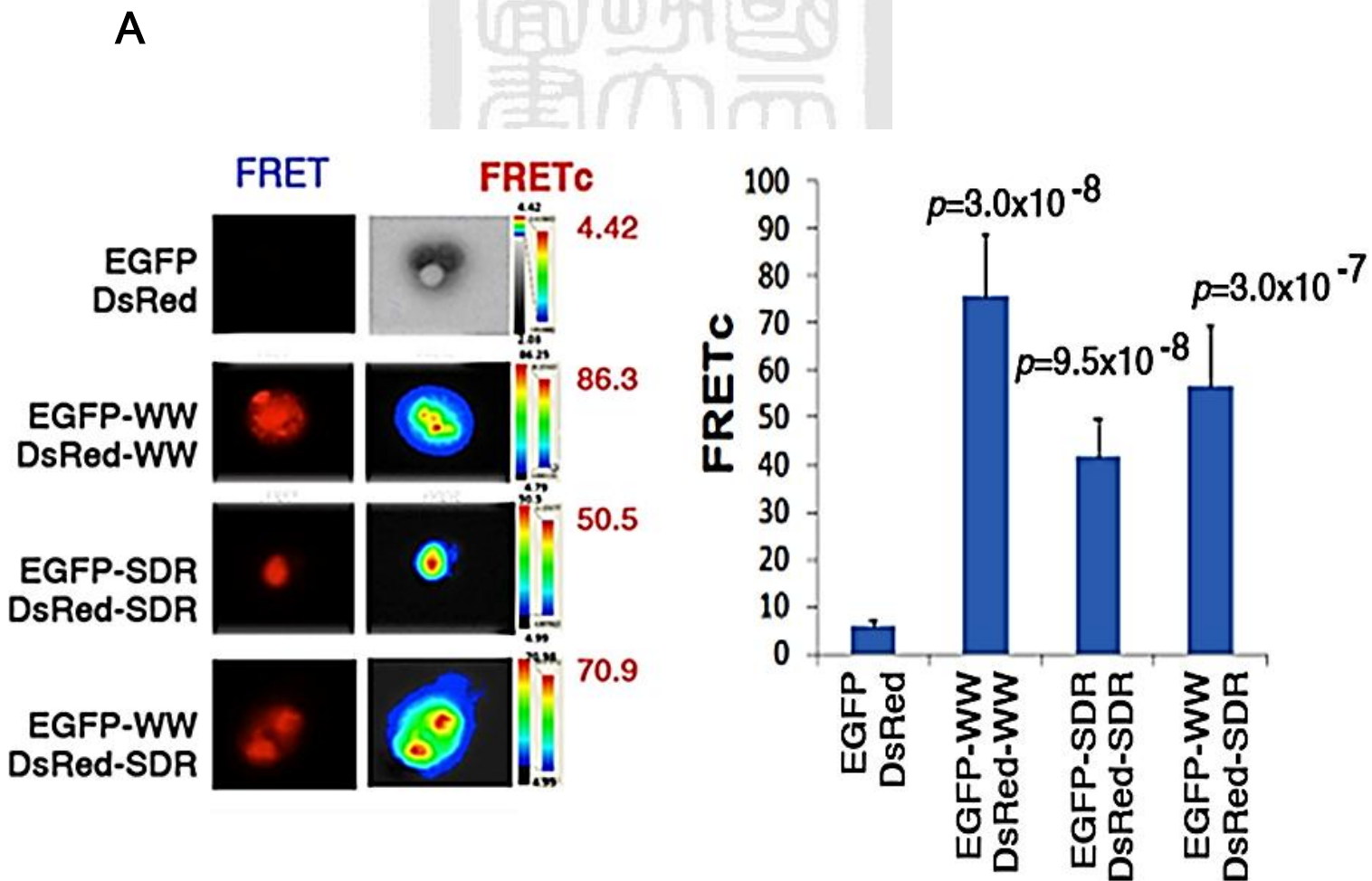
*Wwox* wild type MEF cells were utilized to perform non-permeabilized fluorescence staining. Cells were not permeabilized with Triton X-100. SDRrepl physically interacted with TβRII in the plasma membrane of *Wwox*<sup>+/+</sup> MEF cells. TGFβ1 treatment resulted in the decrease of SDRrepl and TβRII expression in the plasma membrane.

**MEF (*Wwox*<sup>+/+</sup>) treated with 10ng/ml TGFβ1 (Non-permeabilized, Magnification 400X)**



**Figure 28. TGFβ1 alters bindings of intra-molecular and inter-molecular WWOX via WW and SDR domains.**

(A) COS7 fibroblasts were co-transfected with a pair of expression constructs: 1) EGFP and DsRed, 2) EGFP-WW (*N*-terminal 1st and 2nd WW domains) and DsRed-WW; 3) EGFP-SDR and DsRed-SDR; 4) EGFP-WW and DsRed-SDR. FRET analysis was carried out. The extent of specific protein/protein interactions is calculated as FRET<sub>c</sub>. The spectrally corrected FRET concentration (FRET<sub>c</sub>) was calculated by Youvan's equation (using a software program Image-Pro 6.1, Media Cybernetics):  $FRET_c = [fret - bk(fret)] - cf(don) \times [don - bk(don)] - cf(acc) \times [acc - bk(acc)]$ , where *fret* = fret image, *bk* = background, *cf* = correction factor, *don* = donor image, and *acc* = acceptor image. (B) Upon treatment with TGFβ1, the binding affinity between WW and SDR domain was increased in 15min post-treatment, and then decreased slowly. (mean ± standard deviation; *n*=30; Student's *t* test).



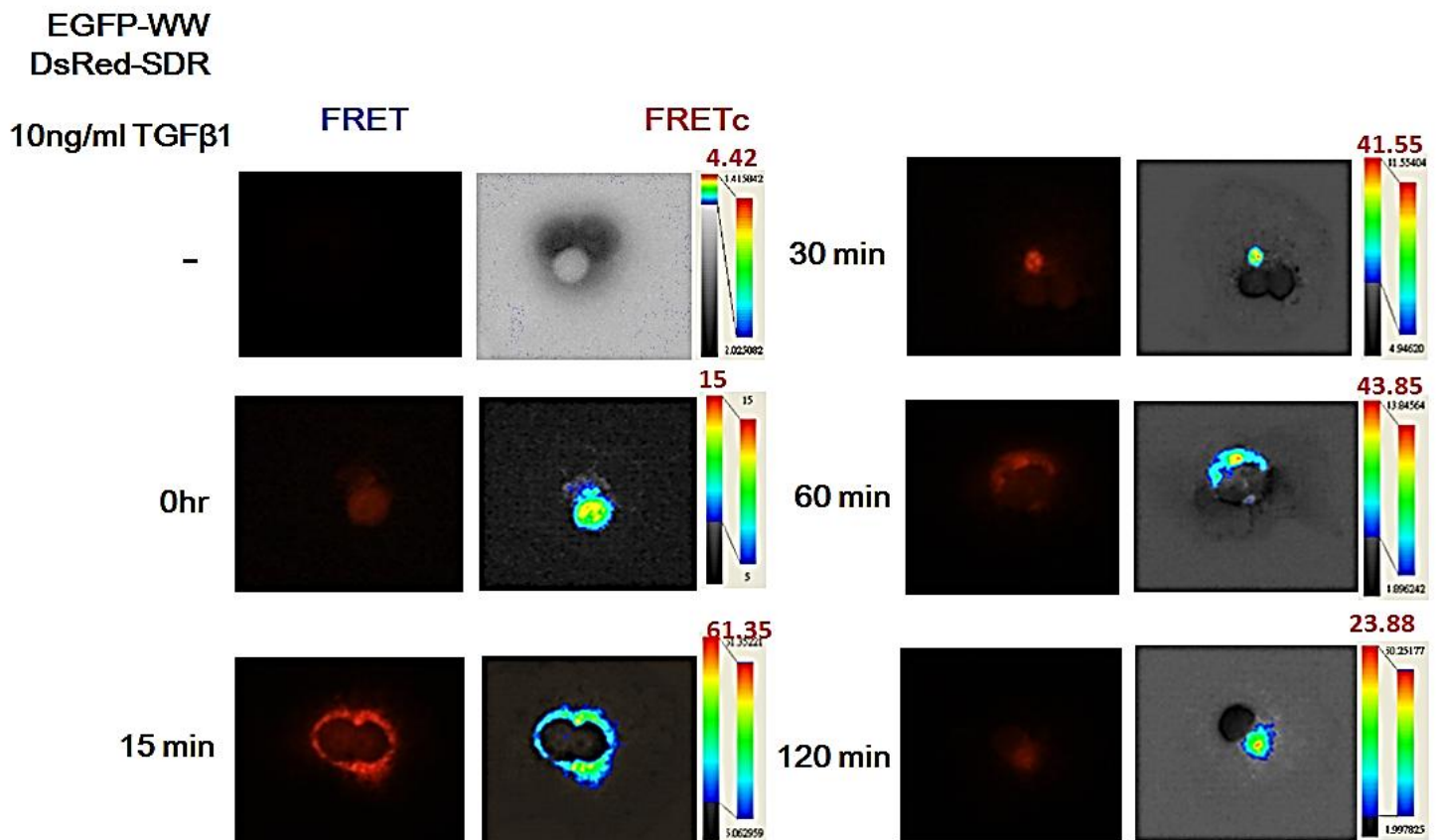
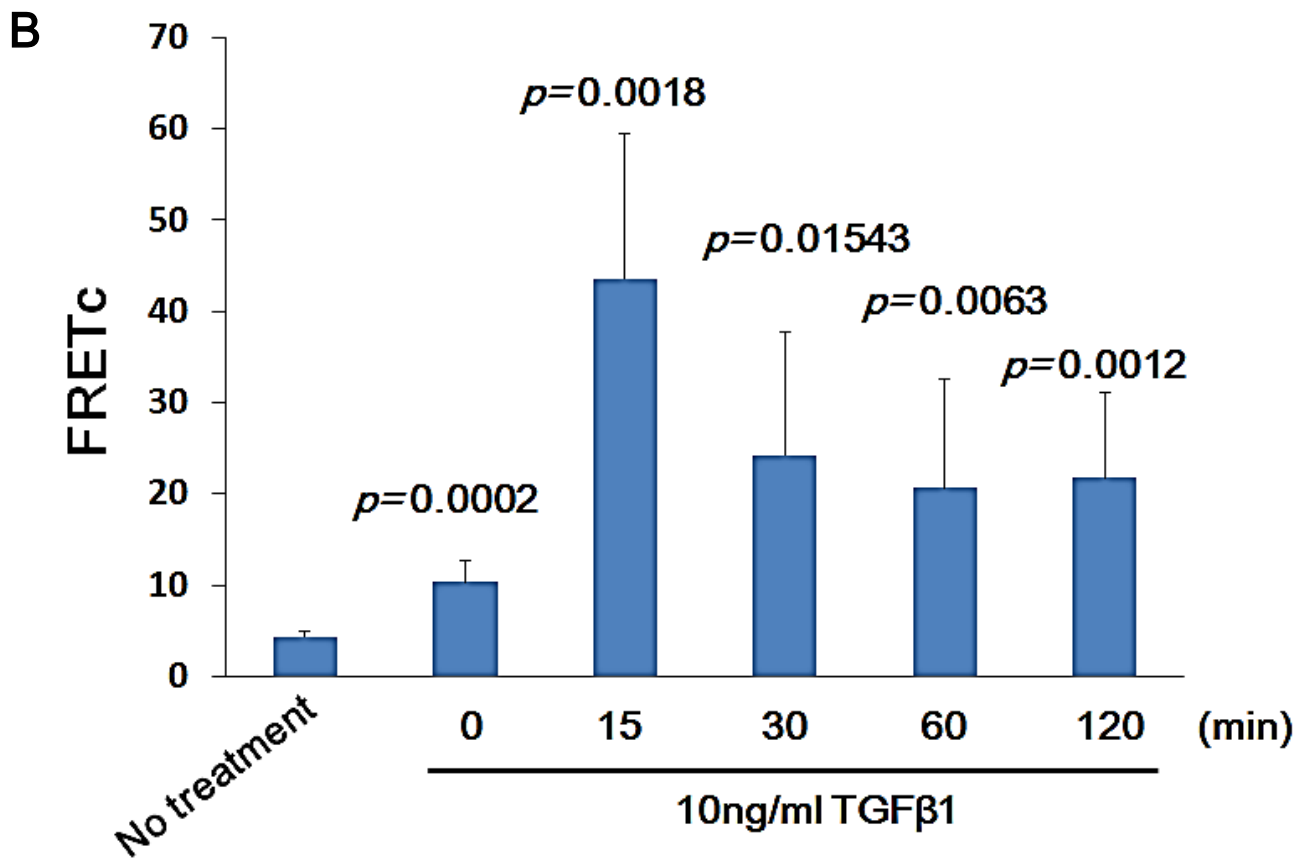


## Figure 29. SDRrepl participates in the regulation of cell invasion.

Two dimensional invasion assay was performed to determine whether SDRrepl regulates cell invasion. Stable transfectants of MDA-MB-231 cells expressing EGFP and stable transfectants of L929 cells expressing DsRed2 were established. These two stable transfectants were seeded in either side of the culture-insert (ibidi) separately. After overnight incubation and waiting for cells attachment, the insert was gently removed by a pair of tweezers. The cells were cultured at 37°C with 5% CO<sub>2</sub> for 4 days. Image J software was used to count the invasive MDA-MB-231 cells which invaded into the L929 cell mass. SDRrepl antiserum and TGFβ1 treatments significantly increased the number of invasive MDA-MB-231 cells. Non-immune serum treatment had no effect. (mean±standard deviation; *n*=4; Student's *t* test).

### SDRrepl participates in cells invasion

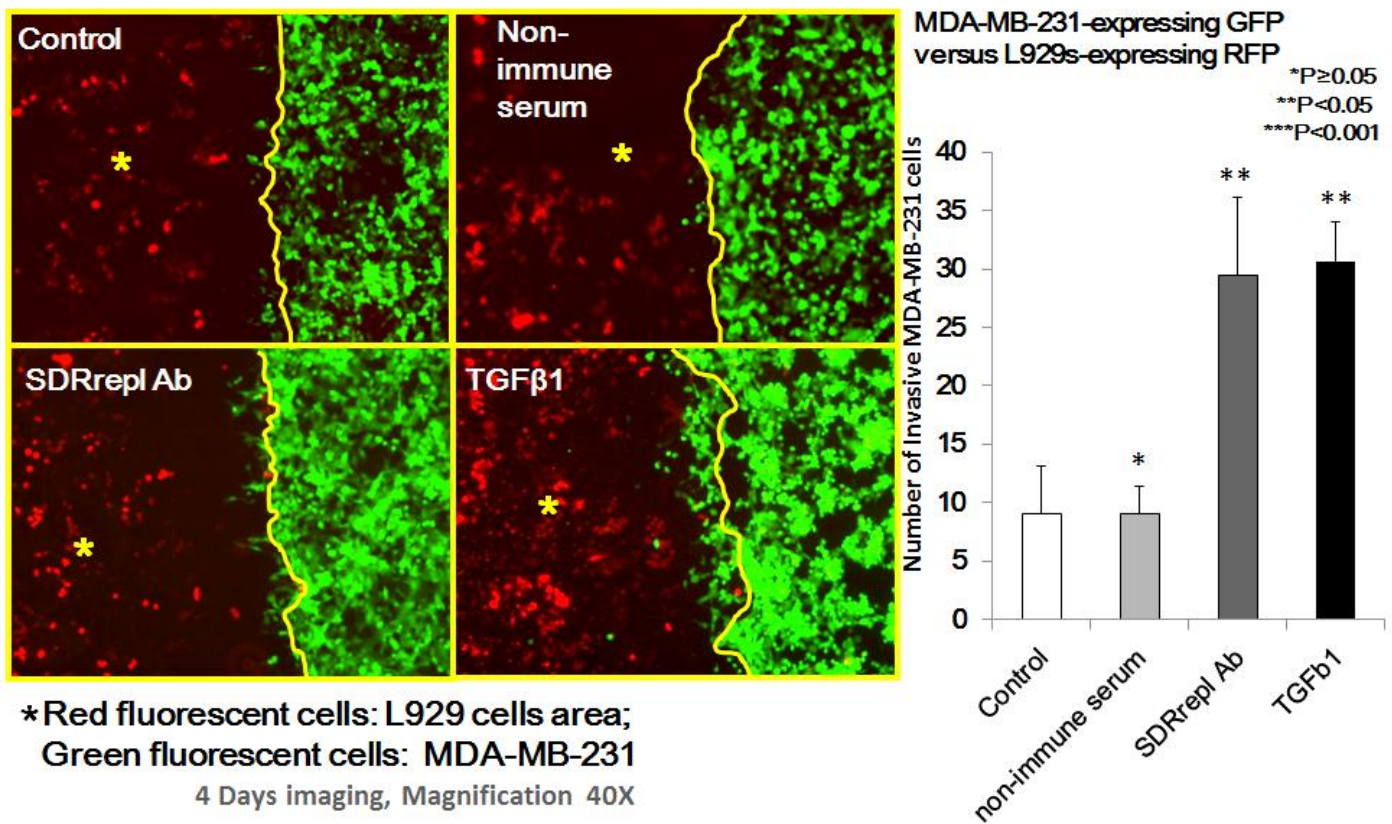
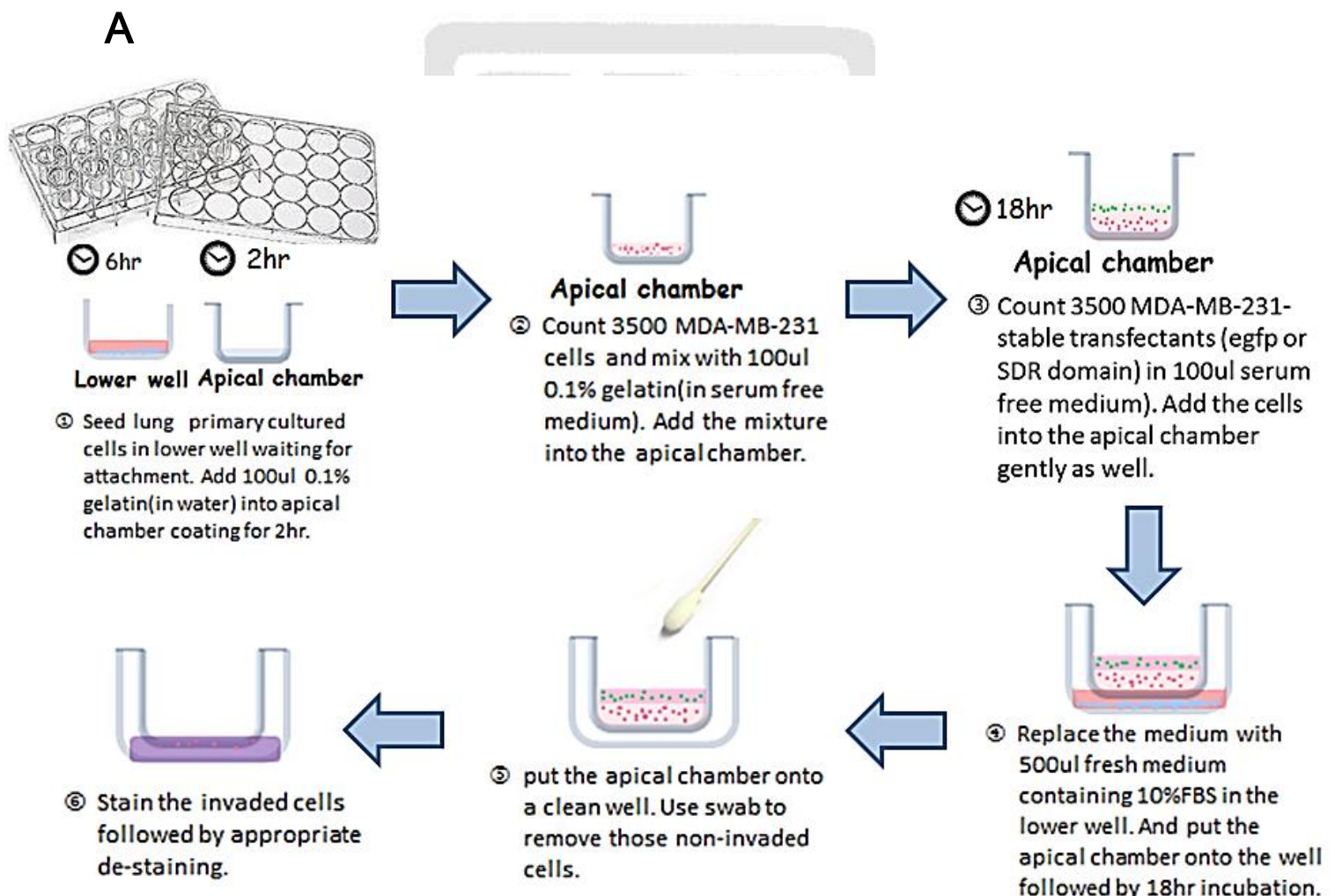
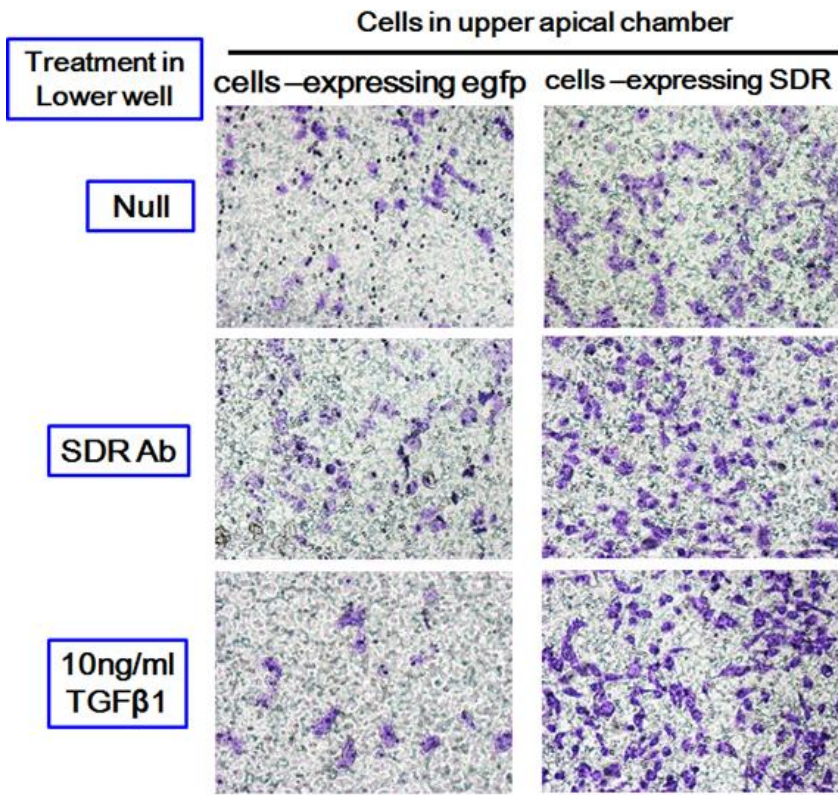
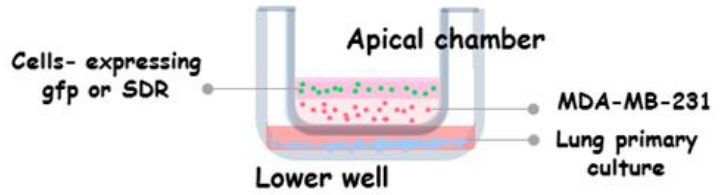


**Figure30. Design of environmental setting to allow SDRrepl to promote cancer cell invasion.**

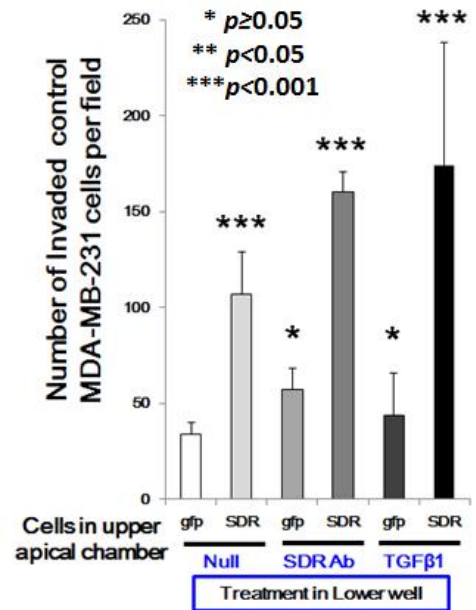
Transwell assay were performed to determine the regulation of SDRrepl in cancer cell invasion. (A) The experimental procedure is illustrated. (B) The invasive cells were stained with staining solution and performed with microscopy (Magnification 100X). MDA-MB-231 cocultured with cells-expressing SDRrepl in apical chamber had an increased invasive activity. SDR Ab and TGF $\beta$ 1 treatment in lower well also increased the number of invasive MDA-MB-231 cell number. (C) The 200X magnification was shown. (mean $\pm$ standard deviation;  $n=5$ ; Student's  $t$  test).



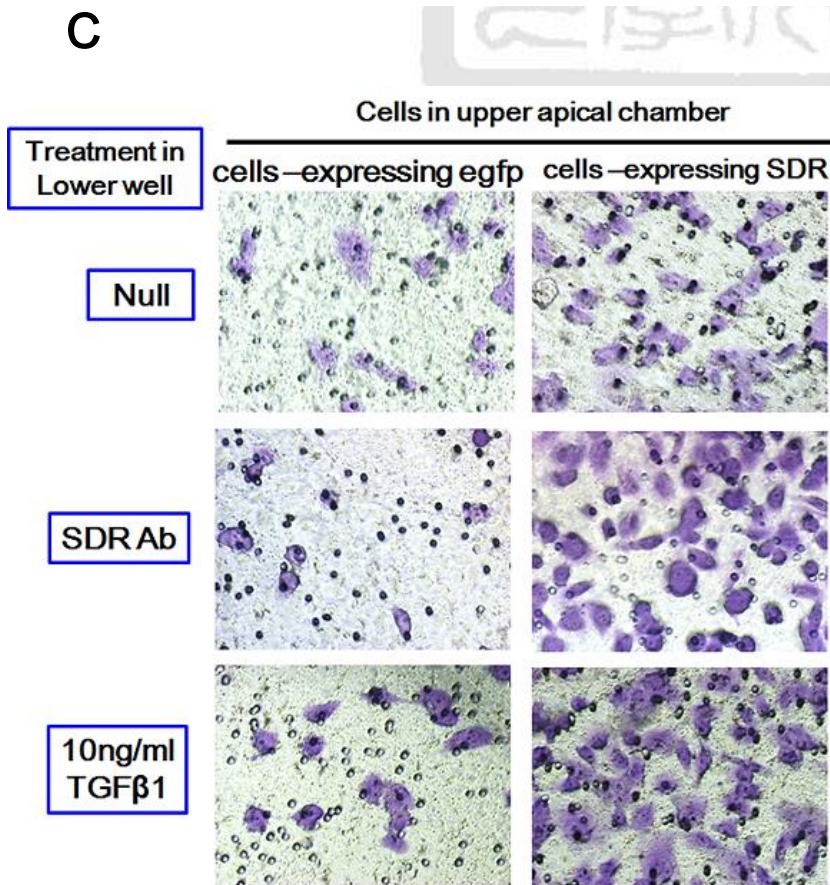
**B**



(Magnification 100X)



**C**



(Magnification 200X)

**Figure31. WWOX, WWgre and SDRrepl inhibit MDA-MB-231 anchorage-independent cell growth and modulated cell migration.**

(A) Soft agarose assay was performed to determine the anchorage-independent cell growth of WWOX stable transfectants. (A,B,C) Stable transfectants-expressing WWgre, SDR domain or WWOX full length, had the lower number and smaller size of colonies compared to control and GFP. Intriguingly, the cell-cell junctions of stable transfectant-expressed SDR domain were looser than control and GFP sets and there seemed some cells migrating out (red arrows indicated). However, cells closed tightly in WWgre set (blue arrow head indicated). Colony number and diameter had shown. (mean±standard deviation;  $n=3$ ; Student's  $t$  test).

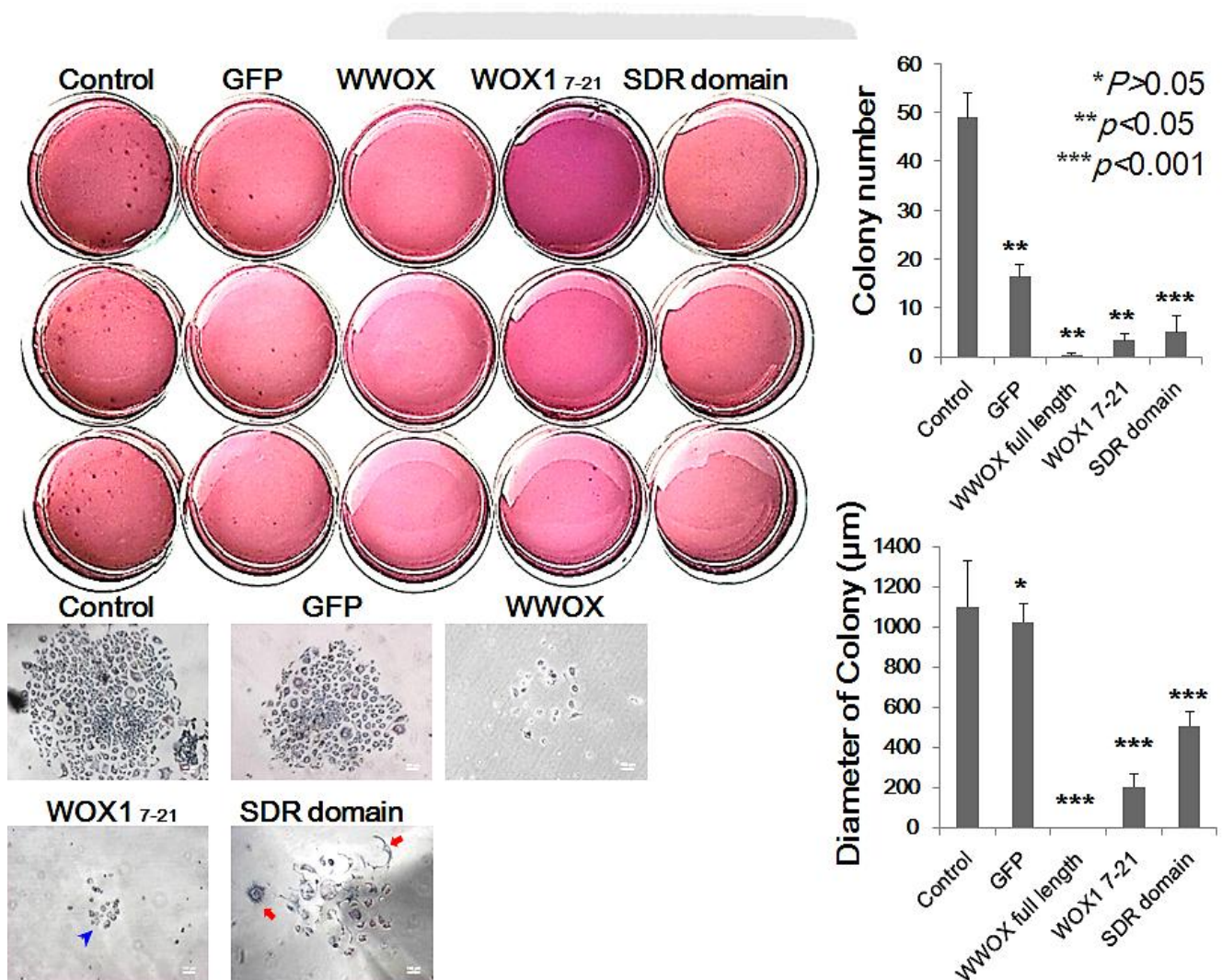
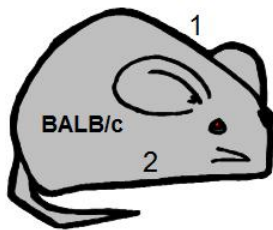


**Figure 32. WWOX suppresses tumor formation *in vivo*.**

BALB/C mice were used, and subcutaneously injected with WWOX peptides and B16F10 melanoma cells in different site separately. Control mouse died due to enormous tumor and metastasis in 3 months post injection, however mice with WWOX peptide injection did not observed tumor formation.

**A**



**Position 1:** WWOX peptides (2mM subcutaneous injection)

**Position 2:** B16F10 cells (subcutaneous injection)

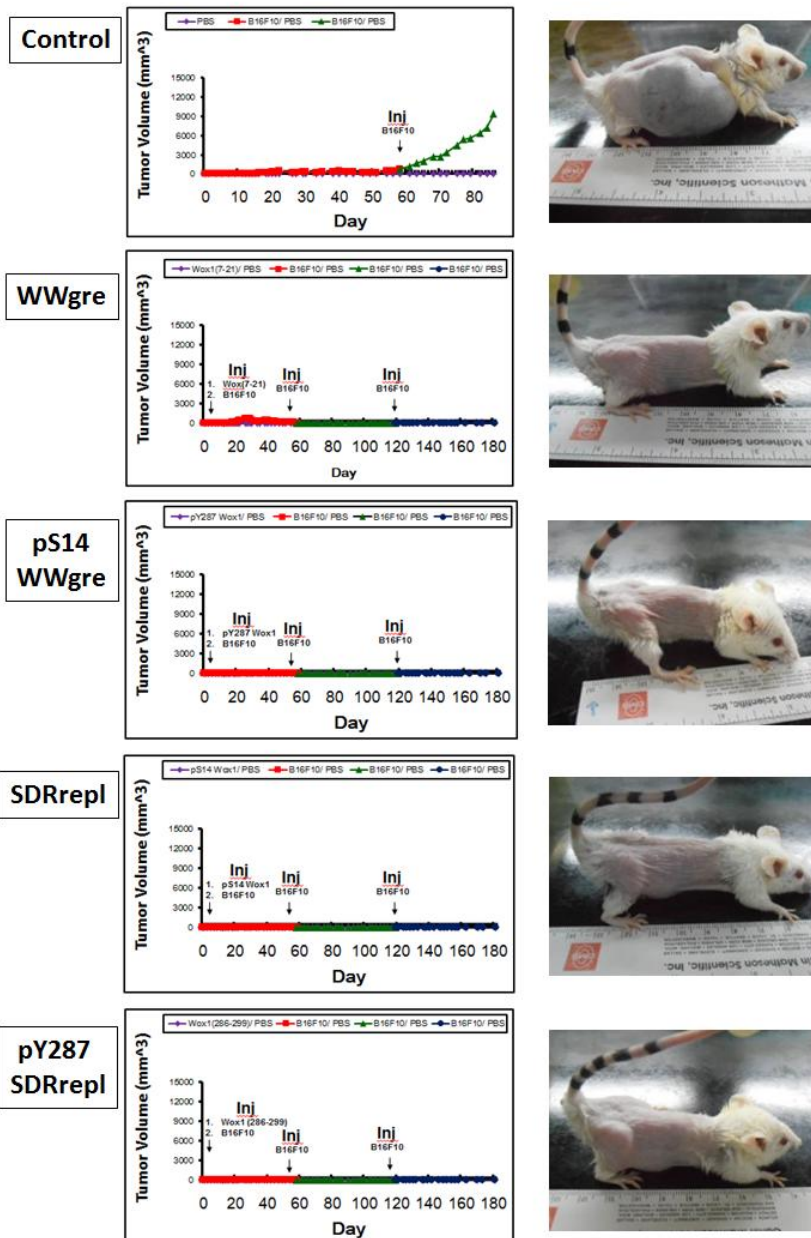
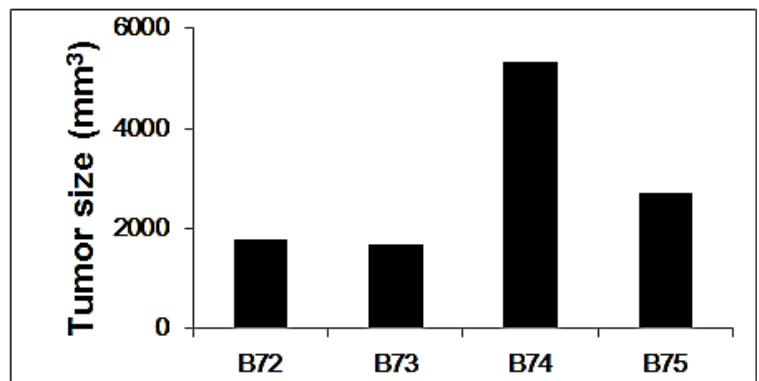
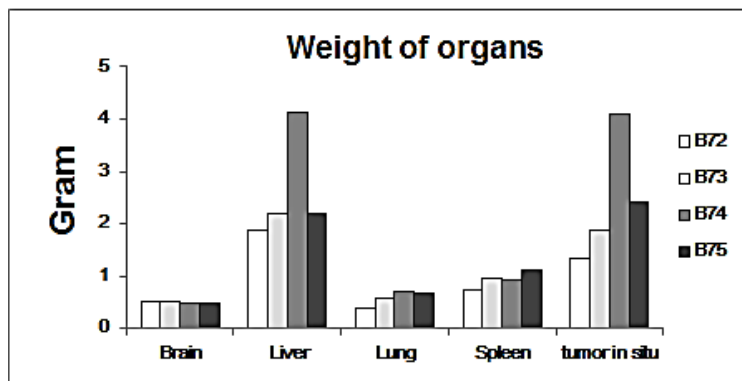
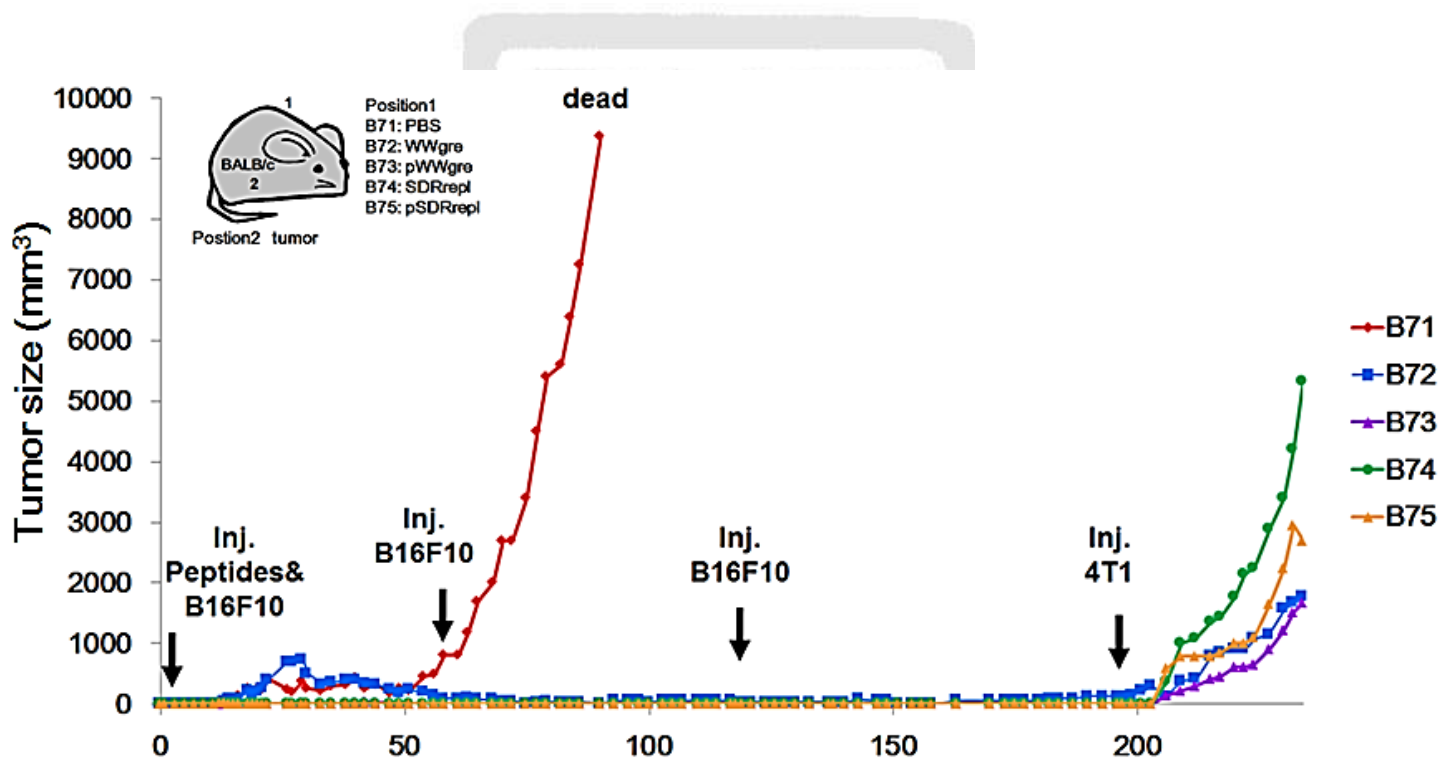


**Figure :**

**Figure 33. WWOX regulated cancer cells metastasis *in vivo*.**

As in the aforementioned experiments (Figure 23), mouse syngeneic breast cancer 4T1 cells were inoculated into BALB/C mice, which had previously injected with WWOX peptides subcutaneously. Post tumor inoculation for 5 weeks, these mice were sacrificed. (A) Experimental procedure and curves of tumor growth were illustrated. (B) Liver and lung were fixed to perform with immunohistological staining. Significantly, there was no lung or liver metastasis in mouse treated with WWgre. There were liver and lung metastasis observed in mice treated with pS14WWgre, SDRrepl, and pY287SDRrepl. Expression of WWgre in mouse treated with WWgre peptide was significant lower than mouse treated with pS14WWgre. Similarly, the expression of SDRrepl in mouse treated with SDRrepl peptide was also significantly lower than mouse treated with pY287SDRrepl.

**A**



**B**

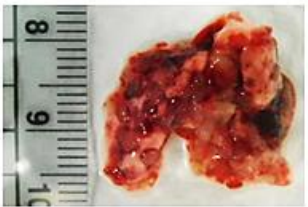
**WWgre-treated**



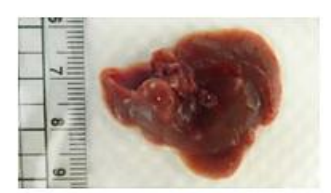
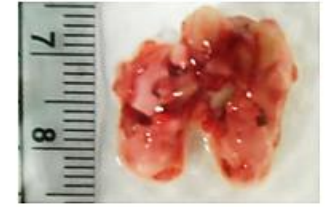
**pWWgre-treated**



**SDRrepl-treated**



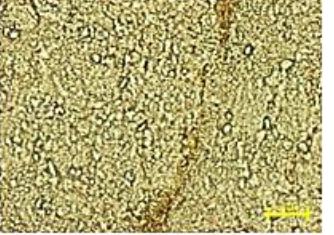
**pSDRrepl-treated**



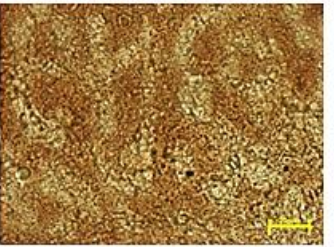
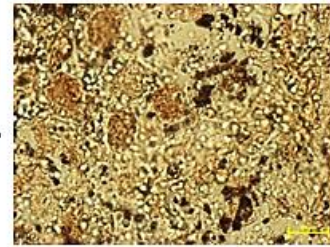
**WWgre-treated**



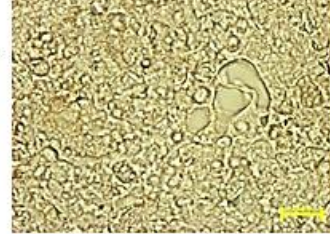
**pWWgre-treated**



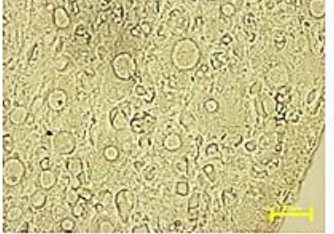
**Expression of WWgre**



**SDRrepl-treated**



**pSDRrepl-treated**



**Expression of SDRrepl**

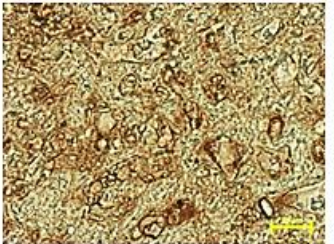
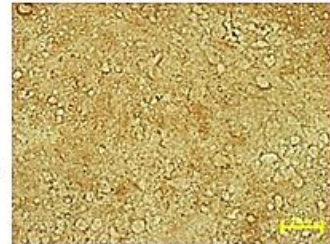


**Fig. 34. Zfra suppression of glioma and prostate cancer growth.**

(A) Nude mice were pre-injected with sterile MilliQ water or Zfra4-10 via tail veins in 3 consecutive weeks. A month later, the mice were inoculated with malignant glioma U87-MG cells (2 sites per mouse). (B) Nude mice were pre-injected with sterile MilliQ water or Zfra4-10 (4 mM in 100  $\mu$ l sterile water) in 3 consecutive weeks. Three months later, mice were inoculated with malignant prostate cancer DU145 cells (2 sites per mouse).

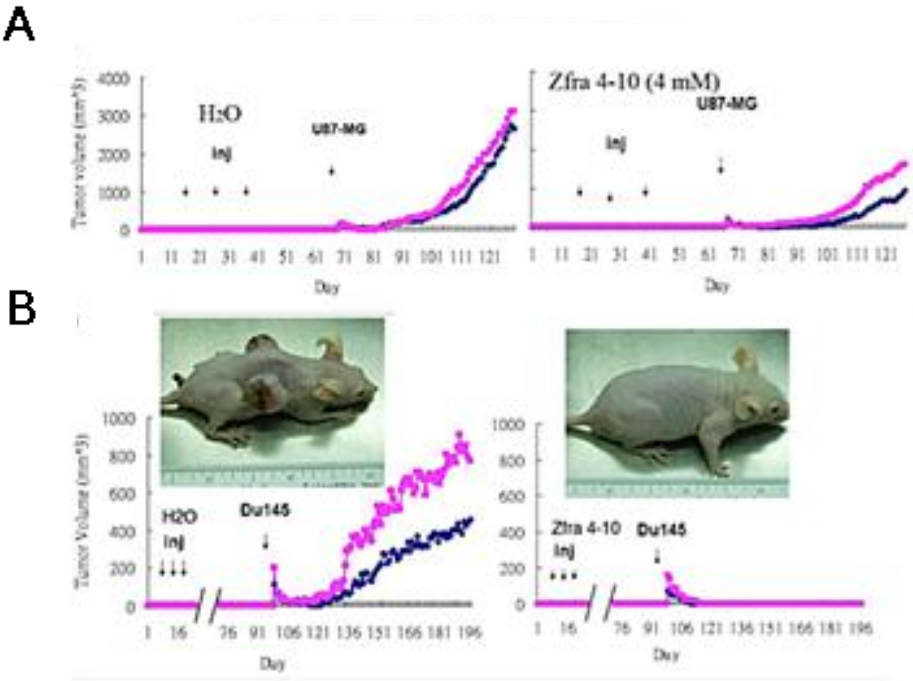


**Figure 35. Putative model of WOX1, TIAF1, TRAPPC6A, and SH3GLB2 in NF1 tumor growth.**

Downregulation of WWOX/WOX1 in NF1 neurofibromas significantly increases the expression of TIAF1, TRAPPC6A, and SH3GLB2/Bif-2, and the aggregated proteins form a peritumorcapsule, so as to provide growth advantages for cancer growth. TGF $\beta$ 1 also promote the aggregation of TIAF1, SH3GLB2, and TRAPPC6A. The self-aggregated TIAF1 binds to SMAD4, and inhibits SMAD4 promoter activation. During cancer progression, the expression level of WOX1 is down-regulated, and eventually promote cancer growth and metastasis.

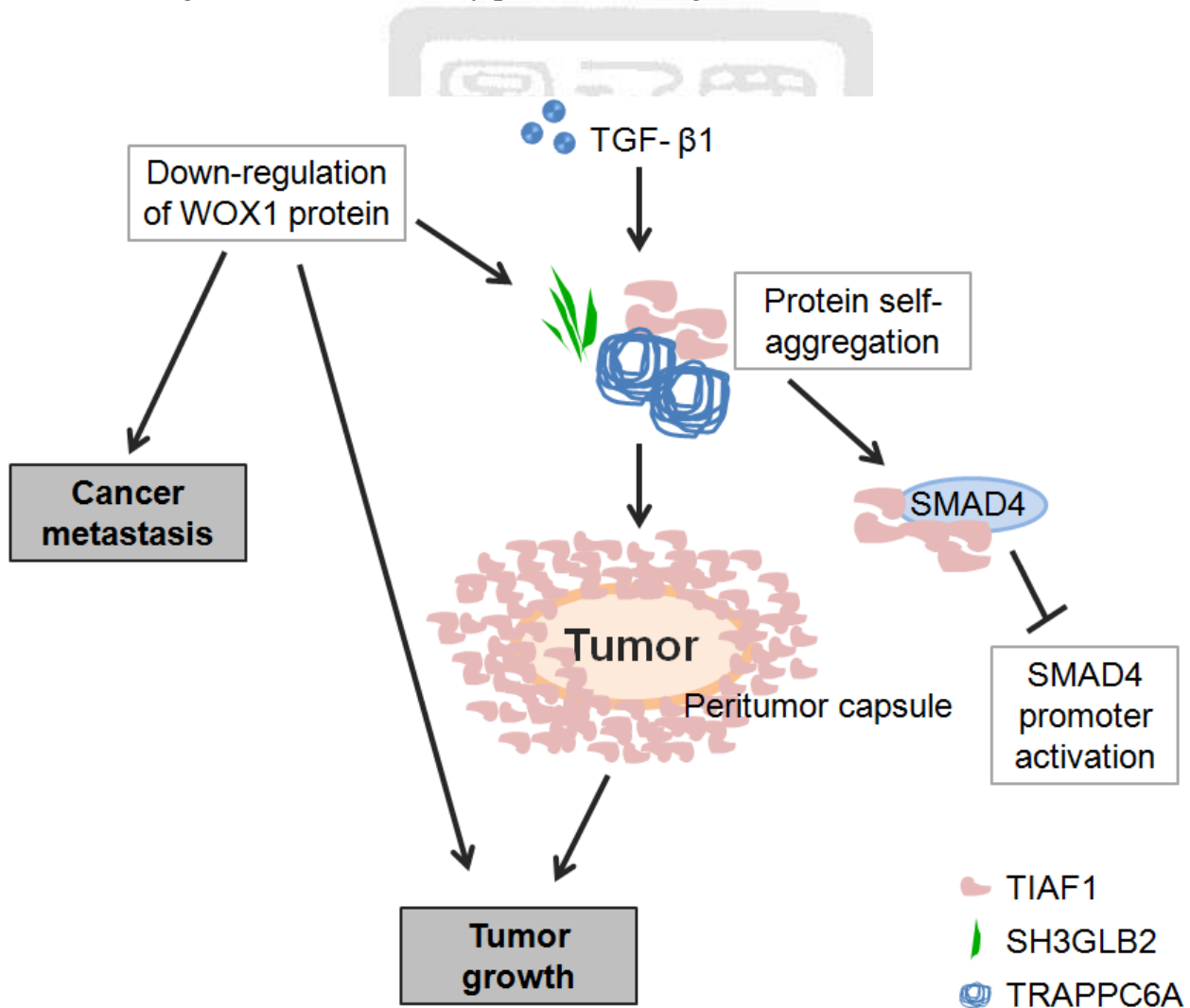
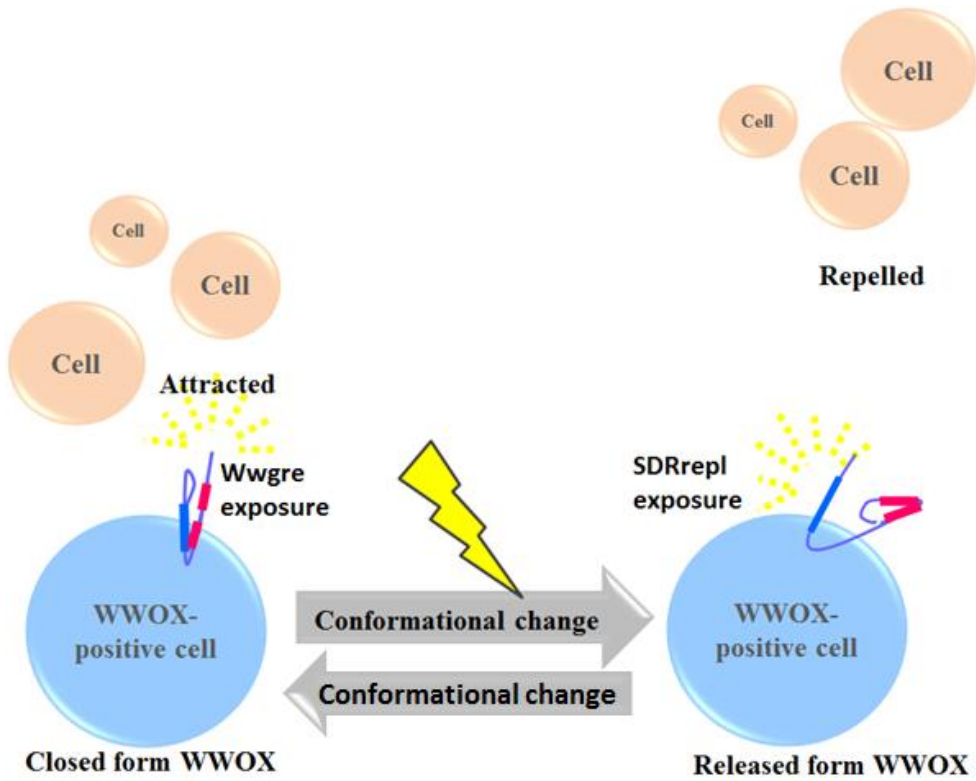


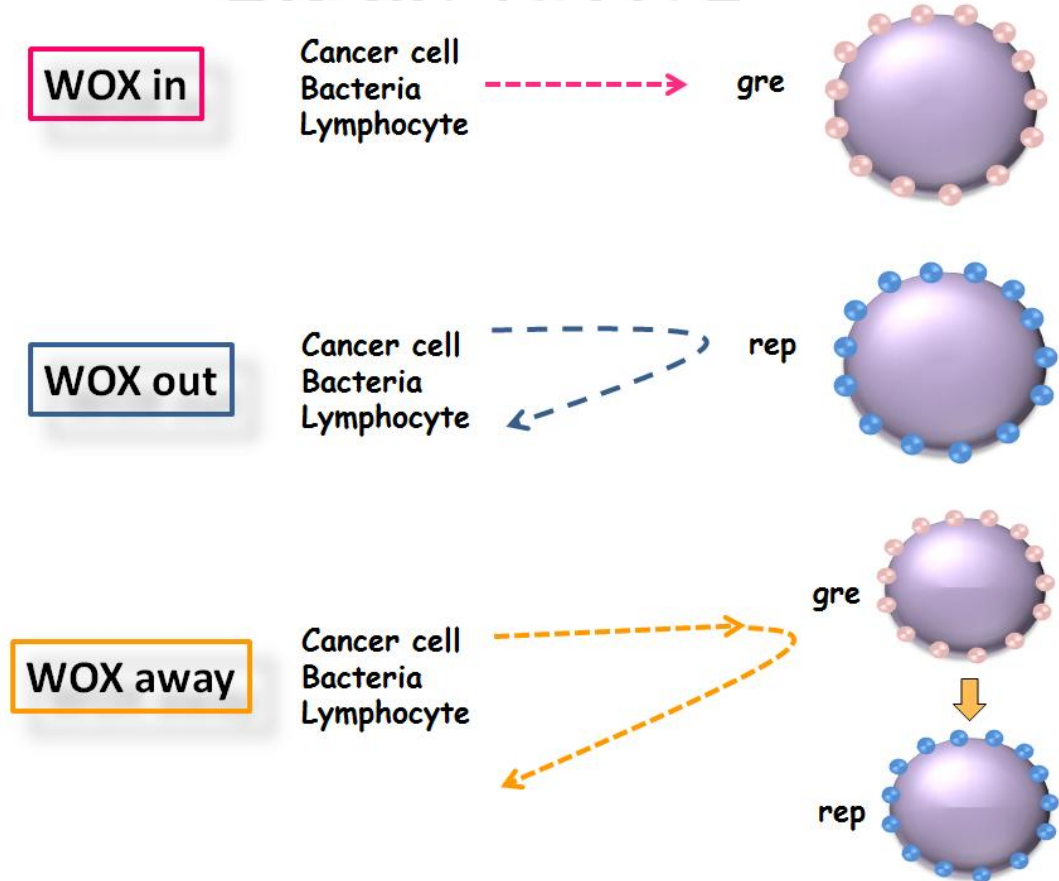
**Figure 36. Putative conformational alteration of WWOX and regulation of cell-to-cell recognition.**

(A) A putative conformational alteration of WWOX is illustrated. When WWOX protein is folded via WW/SDR domain interaction (a closed form), the SDRrepl is concealed and the *N*-terminal WWgre is exposed, thereby allowing cell attraction. On the other hand, when SDRrepl is exposed, cell repellence occurs. (B) Proposed models are shown for cell migration: 1) WOXin: WWOX-negative cells look for WWOX-negative or WWgre-exposed cells in the blood or lymphatic capillaries for docking; 2) WOXout: WWOX-negative cells turn away from the WWOX-positive cells; 3) WOXaway: WWOX-negative cells dock with WWgre-expressing cells, but walk away upon WWgre turning to SDRrepl. (C) When cancer cells start to metastasize, they start to lose WWOX. Accordingly, in situ WWOX-positive solid tumor no longer recognize and repel the metastatic cancer cells to depart from the parental tumor mass. These metastatic cells look for WWOX-negative cells in the blood or lymphatic capillaries as docking sites, so as to penetrate, dock and grow in target organs. TGF $\beta$  signaling or other cytokines probably participate in WWOX-mediated cell migration and cell-to-cell recognition.

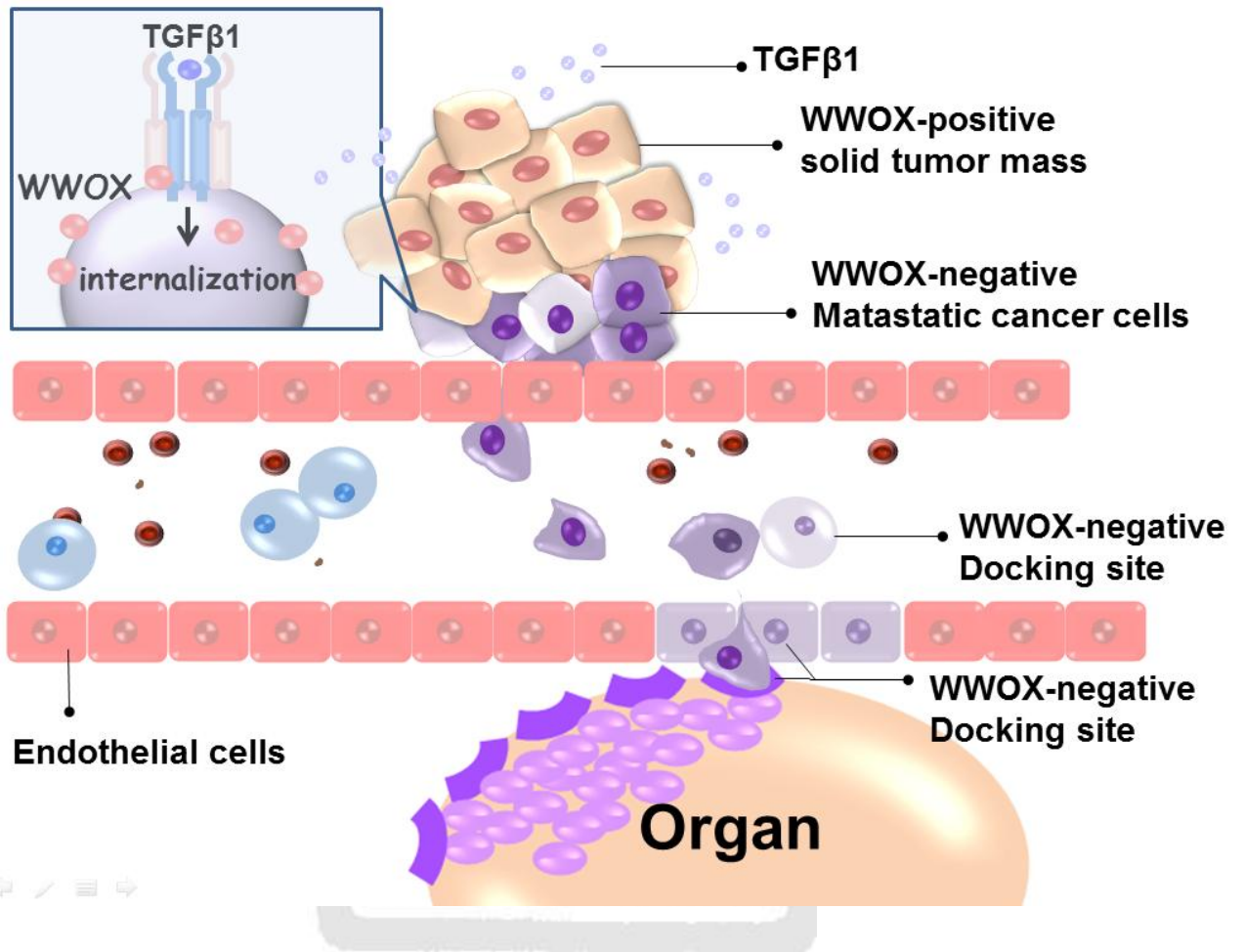
A



B



C



# TIAF1 self-aggregation in peritumor capsule formation, spontaneous activation of SMAD-responsive promoter in p53-deficient environment, and cell death

J-Y Chang<sup>1</sup>, M-F Chiang<sup>2</sup>, S-R Lin<sup>1</sup>, M-H Lee<sup>1</sup>, H He<sup>1</sup>, P-Y Chou<sup>1</sup>, S-J Chen<sup>1</sup>, Y-A Chen<sup>1</sup>, L-Y Yang<sup>1</sup>, F-J Lai<sup>3</sup>, C-C Hsieh<sup>3</sup>, T-H Hsieh<sup>4</sup>, H-M Sheu<sup>5</sup>, C-I Sze<sup>4</sup> and N-S Chang<sup>\*,1,2,6,7,8</sup>

Self-aggregation of transforming growth factor  $\beta$  (TGF- $\beta$ )-induced antiapoptotic factor (TIAF1) is known in the nondemented human hippocampus, and the aggregating process may lead to generation of amyloid  $\beta$  (A $\beta$ ) for causing neurodegeneration. Here, we determined that overexpressed TIAF1 exhibits as aggregates together with Smad4 and A $\beta$  in the cancer stroma and peritumor capsules of solid tumors. Also, TIAF1/A $\beta$  aggregates are shown on the interface between brain neural cells and the metastatic cancer cell mass. TIAF1 is upregulated in developing tumors, but may disappear in established metastatic cancer cells. Growing neuroblastoma cells on the extracellular matrices from other cancer cell types induced production of aggregated TIAF1 and A $\beta$ . *In vitro* induction of TIAF1 self-association upregulated the expression of tumor suppressors Smad4 and WW domain-containing oxidoreductase (WOX1 or WWOX), and WOX1 in turn increased the TIAF1 expression. TIAF1/Smad4 interaction further enhanced A $\beta$  formation. TIAF1 is known to suppress SMAD-regulated promoter activation. Intriguingly, without p53, self-aggregating TIAF1 spontaneously activated the SMAD-regulated promoter. TIAF1 was essential for p53-, WOX1- and dominant-negative JNK1-induced cell death. TIAF1, p53 and WOX1 acted synergistically in suppressing anchorage-independent growth, blocking cell migration and causing apoptosis. Together, TIAF1 shows an aggregation-dependent control of tumor progression and metastasis, and regulation of cell death.

*Cell Death and Disease* (2012) 3, e302; doi:10.1038/cddis.2012.36; published online 26 April 2012

**Subject Category:** Experimental Medicine

Transforming growth factor  $\beta$  (TGF- $\beta$ ) family proteins participate in a variety of biological events and diseases, including cell proliferation, immune response, apoptosis, oncogenesis and many physiological events.<sup>1,2</sup> TGF- $\beta$  has dual roles in cancer initiation and progression.<sup>3,4</sup> TGF- $\beta$  inhibits epithelial cell growth, and induces epithelial to mesenchymal transition (EMT). Cancerous cells are refractory to TGF- $\beta$ -mediated growth suppression, and produce autocrine TGF- $\beta$  for their growth and metastasis. The mechanism of this regard is largely unknown.

TGF- $\beta$ 1-induced antiapoptotic factor (TIAF1) is a 12-kDa TGF- $\beta$ 1-induced antiapoptotic factor, which protects murine L929 fibroblasts from apoptosis by tumor necrosis factor (TNF) and overexpressed TNF receptor adaptor proteins in the presence of actinomycin D, an inhibitor of DNA transcription.<sup>5,6</sup> Transiently overexpressed TIAF1 supports

fibroblast growth, which is similar to the effect of TGF- $\beta$ 1.<sup>6</sup> Also, like TGF- $\beta$ 1, ectopic TIAF1 suppresses cell growth and induces apoptosis of monocytic U937 and many non-fibroblast cells.<sup>6</sup> TIAF1 increases the expression of p53 and Cip1/p21 and suppresses ERK phosphorylation in U937 cells, thereby inhibiting cell growth and inducing apoptosis.<sup>6</sup> Ectopic TIAF1 upregulates the expression of tumor suppressor p53, and both proteins mediate cell death in either a cooperative or an antagonistic manner.<sup>7</sup> Suppression of TIAF1 expression by small interfering RNA (siRNA) prevents UV irradiation-mediated p53 phosphorylation and nuclear translocation.

Expression of TIAF1 is significantly increased in activated helper T lymphocytes (TH2) in patients with chronic kidney and liver allograft rejection.<sup>8</sup> Regulatory T cells (Treg) have a significantly increased expression of TIAF1.<sup>9</sup> Whether TIAF1 controls the differentiation and activation-induced death of

<sup>1</sup>Institute of Molecular Medicine, National Cheng Kung University College of Medicine, Tainan, Taiwan, ROC; <sup>2</sup>Department of Neurosurgery, Mackay Memorial Hospital, Graduate Institute of Injury Prevention and Control, Taipei Medical University, Taipei, Taiwan, ROC; <sup>3</sup>Department of Dermatology, Chi-Mei Medical Center, Tainan, Taiwan, ROC; <sup>4</sup>Department of Anatomy and Cell Biology, National Cheng Kung University College of Medicine, Tainan, Taiwan, ROC; <sup>5</sup>Department of Dermatology, National Cheng Kung University College of Medicine, Tainan, Taiwan, ROC; <sup>6</sup>Advanced Optoelectronic Technology Center, National Cheng Kung University College of Medicine, Tainan, Taiwan, ROC; <sup>7</sup>Center of Infectious Disease and Signal Research, National Cheng Kung University, Tainan, Taiwan, ROC and <sup>8</sup>Department of Neuroscience and Physiology, SUNY Upstate Medical University, Syracuse, NY, USA

\*Corresponding authors: N-S Chang, Institute of Molecular Medicine, National Cheng Kung University College of Medicine, 1 University Road, Tainan, Taiwan 70101, ROC. Tel: +88 66 235 3535 ext. 5592; Fax: +88 66 209 5845; E-mail: changns@mail.ncku.edu.tw

or F-J Lai, Department of Dermatology, Chi-Mei Medical Center, Tainan, Taiwan, ROC. Tel: +88 66 281 2811; Fax: +88 66 270 3706; E-mail: laifj@mail.ntin.edu.tw; or C-I Sze, Department of Anatomy and Cell Biology, National Cheng Kung University College of Medicine, 1 University Road, Tainan, Taiwan 70101, ROC.

Tel: +88 66 235 3535 ext. 5329; Fax: +88 66 209 3007; E-mail: szec@mail.ncku.edu.tw

**Keywords:** TIAF1; p53; WWOX; WOX1; TGF- $\beta$ ; Smad4

**Abbreviations:** TGF- $\beta$ , transforming growth factor  $\beta$ ; TIAF1, TGF- $\beta$ 1-induced antiapoptotic factor; A $\beta$ , amyloid  $\beta$ ; WWOX/WOX1, WW domain-containing oxidoreductase; Smad4, mothers against DPP homolog 4; TNF, tumor necrosis factor; FRET, Förster resonance energy transfer; IHC, immunohistochemistry

Received 15.8.11; revised 10.2.12; accepted 14.2.12; Edited by A Stephanou

Treg and TH2 cells is unknown. TIAF1 is also associated with Hirschsprung's disease, a congenital complex disorder of intestinal innervation.<sup>10</sup>

TIAF1 physically interacts with Smad4, and blocks SMAD-dependent promoter activation when overexpressed.<sup>11</sup> Knockdown of TIAF1 by siRNA induces spontaneous accumulation of Smad proteins in the nucleus and activation of the promoter governed by the SMAD complex.<sup>11</sup> Notably, TGF- $\beta$ 1 and environmental stress (e.g. alterations in pericellular environment) cause TIAF1 self-aggregation in a type II TGF- $\beta$  receptor (T $\beta$ RII)-independent manner in cells. Hippocampal TIAF1 aggregation is shown at ages 40–70, which occurs before the generation of amyloid  $\beta$  (A $\beta$ ) plaques in Alzheimer's disease at 75–90-years.<sup>11</sup> Here, we examined TIAF1 expression and aggregate formation in cancer cells and tissues, and determined the functional relationship between TIAF1 and tumor suppressors WW domain-containing oxidoreductase (designated WWOX, FOR or WOX)<sup>12–14</sup> and Smad4. TIAF1 control of SMAD-regulated promoter activation was examined.

## Results

### TIAF1 expression is upregulated in non-metastatic prostate cancer but is downregulated in breast cancer.

A synthetic TIAF1 peptide R48-2, which was originally used for the antibody production,<sup>5,11</sup> blocked the immunoreactivity in antibody staining, as determined in human melanoma (Supplementary Figure S1a), neurofibromatosis NF1 tumor (Supplementary Figure S1b), meningioma (Supplementary Figure S1c) and breast cancer (Figure 1a and Supplementary Figures S2g–i) and other tissue sections. The R48-2 peptide also blocked the immunoreactivity of a commercial antibody TIAF1(Abcam, Cambridge, MA, USA) (Supplementary Figure S1a). We generated another TIAF1(R48-1) antibody using a different peptide sequence. The TIAF1(R48-2) peptide failed to inhibit the immunoreactivity of TIAF1(R48-1) antibody (Supplementary Figure S1c).

TIAF1 expression is shown in normal human mammary gland cells, as determined by immunohistochemistry (IHC) (Figure 1a and Supplementary Figure S2). In breast adenocarcinoma, the levels of TIAF1 are significantly reduced (Figure 1a and Supplementary Figure S2). In negative controls, the R48-2 peptide blocked the immunoreactivity of TIAF1 antibody (Figure 1a).

In prostate tissue microarray slides, TIAF1 levels are significantly increased in prostate cancer, compared with normal controls, as determined using both TIAF1(R48-2) and the commercial antibodies for fluorescence microscopy (Figure 1b; 75 samples for control and cancer groups and damaged samples excluded). Both antibodies recognized essentially the same TIAF1 antigen, as both images appear to colocalize (Supplementary Figure S1a). Similar results were observed using the TIAF1(R48-2) antibody in IHC (data not shown). We further confirmed these findings by using normal prostate and prostate cancer sections in immunofluorescence microscopy and IHC (Figure 1c, Supplementary Figures S3a and S4). Compared with age-matched normal controls, there were significant increases (50–120%) in the expression of TIAF1 in prostate cancer tissues (Supplementary Figures S3a

and S4). In negative controls, R48-2 peptide blocked the immunoreactivity (Supplementary Figure S4).

**TIAF1 aggregates in cancer cells.** TIAF1 physically interacts with Smad4, and knockdown of TIAF1 expression induces spontaneous accumulation of Smad proteins in the nuclei.<sup>11</sup> By immunofluorescence microscopy, TIAF1 colocalized with Smad4 in the cytosol and prostatic concretions in the lumens of glandular ducts (Supplementary Figures S3b and S3c). Upregulation of TIAF1 and Smad4 is shown in the prostate cancer tissues (Figure 1c, Supplementary Figures S3 and S4). Both TIAF1 and Smad4 proteins are colocalized and appear as aggregates (Supplementary Figures S3b and S3c). Notably, expression of both TIAF1 and Smad4 are significantly downregulated in metastatic prostate cancer cells (Figure 1c and Supplementary Figure S5). Similarly, expression of TIAF1 and Smad4 proteins is significantly increased ( $P < 0.05$ ) in colon cancer cells, as compared with controls (Supplementary Figure S6). IHC staining of prostate with the TIAF1(R48-2) antibody showed a poorly differentiated tumor growing in a diffused fashion (Figure 1d). The tumor infiltrates the prostate as cell clusters, without glandular formation and containing TIAF1 protein aggregates (Figure 1d).

Next, hairless mice were exposed to UVB irradiation to generate skin squamous cell carcinoma (SCC).<sup>15</sup> TIAF1 is overexpressed in the sebaceous gland of the normal skin (Figure 1e). UVB rapidly increased the expression of TIAF1 in the epidermis in 12 h, followed by reduction. However, in the dermal area, TIAF1 levels were increased from 24 h to 1 month after UVB exposure. The developed SCC tumors had reduced expression of TIAF1 (Figure 1e).

### TIAF1 aggregation in the metastatic cancer cells in the brain.

TIAF1 aggregates are present in the hippocampi of both non-demented humans and patients with Alzheimer's disease.<sup>11</sup> Co-expression of TIAF1 and A $\beta$  aggregates was found in the metastatic cancer in the brain (Figures 2a and b). Conceivably, when metastatic small-cell lung cancer cells relocated to the brain, TIAF1 aggregates were deposited in the interface between cancer and brain cells or within the tumors (Figures 2a and b, Supplementary Figures S7 and S8). Fluoro-Jade C stain<sup>11</sup> demonstrated the presence of degenerating neurons (Figures 2a and b, Supplementary Figures S7 and S8). In negative controls, R48-2 peptide blocked the immunostain (Figures 2a and b, Supplementary Figures S7 and S8). Similarly, co-expression of the aggregates for TIAF1 and A $\beta$  was shown for the metastatic lung cancer, nasopharyngeal carcinoma (NPC) and colon cancer in the brain (Figure 2b, Supplementary Figures S7 and S8). Despite the presence of A $\beta$ , no apparent apoptosis was observed in the cancer cells.

Compared with TIAF1, WOX1 expression is relatively low in neurofibromatosis NF1 (Figures 2c and d). TIAF1 is overexpressed in the peritumor area (Figure 2d). Alteration of environmental cues induces TIAF1 expression and aggregation.<sup>11</sup> Presence of fibrous aggregation of TIAF1 is shown in the peritumor coat of NF1 (Figure 2e), prostate cancer (Supplementary Figure S9), many solid tumors and hippocampi of patients with Alzheimer's disease (data not

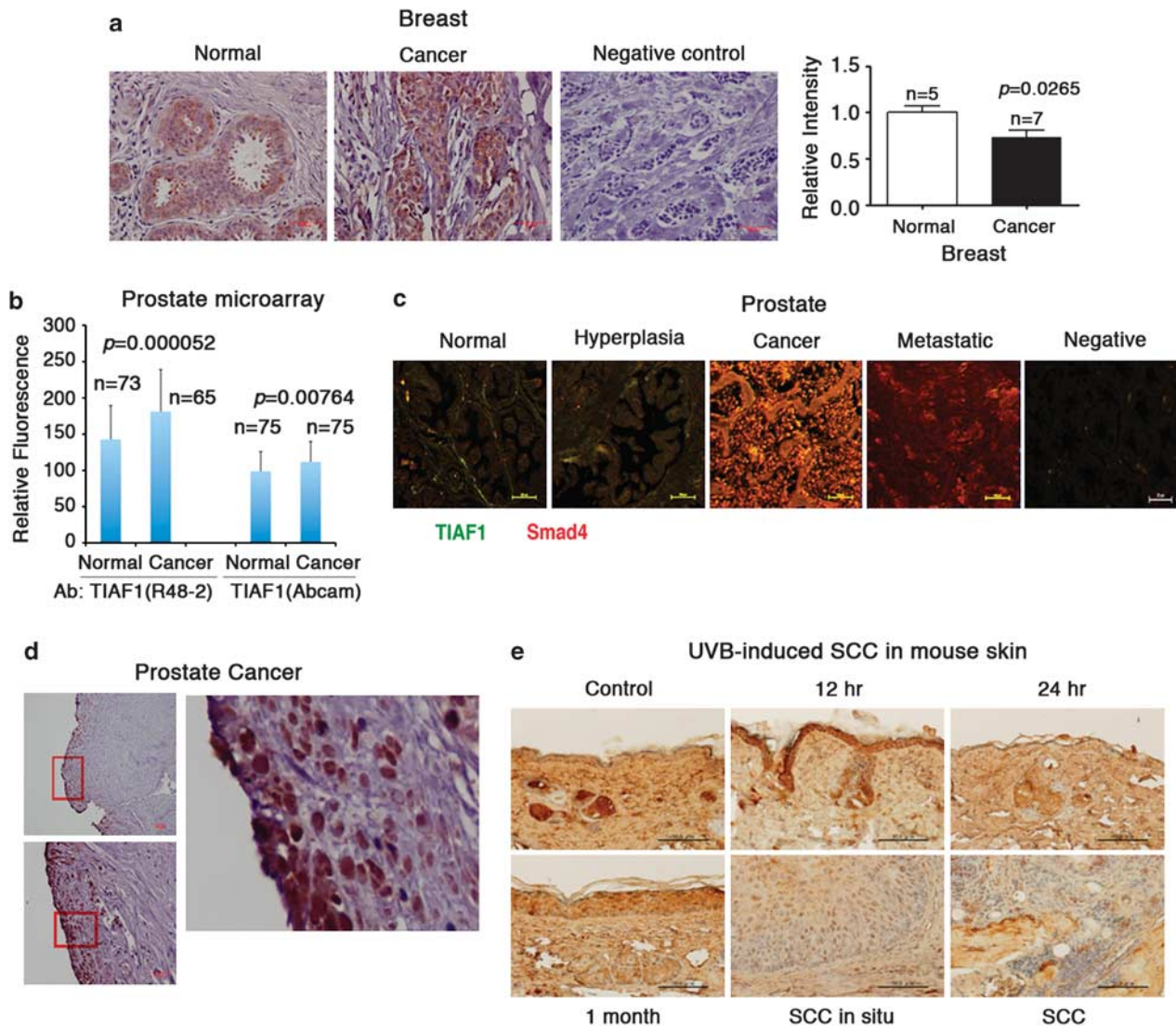


**Figure 1** TIAF1 expression in breast, prostate and skin cancers. (a) IHC staining of normal and breast cancer tissue sections revealed a significant reduction of TIAF1 in the cancer tissues, using TIAF1(R48-2) antibody (Student's *t*-test). In negative control, R48-2 peptide blocked the immunoreactivity of the antibody. Also, see additional data in Supplementary Figure S2. (b) TIAF1 protein expression is significantly increased in prostate cancer, compared with normal controls, as determined using both the TIAF1 (R48-2) antibody (left panel) and a commercial TIAF1 antibody (right panel) for immunofluorescence microscopy in prostate tissue microarray slides from NCI (Student's *t*-test).<sup>11,17,35,39</sup> Also, see data in Supplementary Figures S3, S4 and S5. (c) By immunofluorescence microscopy, significant increases (50–120%) in the TIAF1 protein expression were shown in prostate cancer tissues (three cases), as compared with samples from age-matched normal controls, prostatic hyperplasia and metastatic prostate cancer. In negative controls (Negative), non-immune serum was used for staining. Scale bar, 100  $\mu$ m;  $\times$  100 magnification. Merged images of TIAF1 (green) and Smad4 (red) are shown. Also, see detailed pictures in the Supplementary Figure S5. (d) A poorly differentiated tumor grew in the prostate as cell clusters with no glandular formation but contained TIAF1 protein aggregates. Graphs are sequentially enlarged from each red box (from top left, bottom left to right). (e) UVB irradiation induced formation of SCC in hairless mice. TIAF1 protein expression is abundant in the sebaceous gland of the normal skin. The developed SCC tumors have low levels of TIAF1. Scale bar = 50  $\mu$ m

shown). Again, R48-2 peptide blocked the immunoreactivity (Figure 2f).

When metastatic 13-06-MG glioma cells were subcutaneously inoculated in both flanks of nude mice, the cells were metastatic to the lung. Presence of high levels of TIAF1 expression is shown in the growing tumor, compared with the normal lungs of nude mice (Figure 2g).

**Extracellular matrix (ECM) proteins induce the expression and aggregation of TIAF1 and A $\beta$ , and ectopic**

**WOX1 upregulates TIAF1 expression.** To simulate the encounter of metastatic cancer cells with brain cells, neuroblastoma SK-N-SH cells were cultured on the ECM of prostate DU145 cells for 48 h.<sup>11,16</sup> SK-N-SH cells were shown to have overexpressed aggregates of TIAF1 and A $\beta$ , as determined by fluorescent immunostaining (Figures 3a and b). However, when the endogenous TIAF1 level was low, A $\beta$  expression was also low (Figure 3b). In negative controls, cells were seeded onto serum protein-coated matrix where no TIAF1 and A $\beta$  production was observed (data not shown).

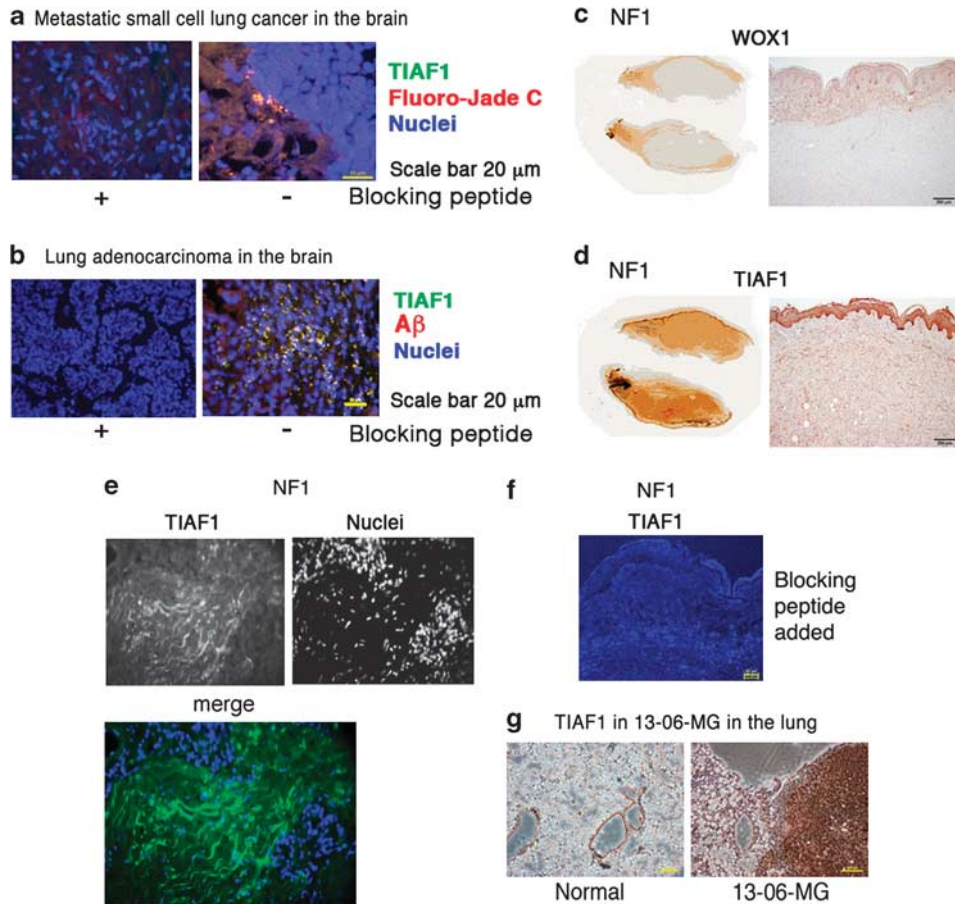


**Figure 2** TIAF1 aggregation in the interface between metastatic cancer cells and the brain tissues. **(a)** Presence of aggregated TIAF1 in the dead neurons located in the interface between the brain tissue and the metastatic small-cell lung cancer. Degenerating neurons were stained with Fluoro-Jade C (red). Nuclei were stained with DAPI. Scale bar, 20  $\mu\text{m}$ ;  $\times 400$  magnification. A merged image is of TIAF1 (green), Fluoro-Jade C (red) and DAPI (blue). The blocking R48-2 peptide was used in negative controls. Also, see Supplementary Figures S7 and S8. **(b)** TIAF1/A $\beta$  aggregates are shown in a metastatic lung adenocarcinoma in the brain. Scale bar, 20  $\mu\text{m}$ ;  $\times 400$  magnification. A merged image is of TIAF1 (green), A $\beta$  (red) and DAPI (blue). The blocking R48-2 peptide was used in negative controls. **(c and d)** In IHC staining, expression of WOX1 and TIAF1 is shown in neurofibromatosis NF1. TIAF1 is overexpressed in the peritumor area, but is less expressed in the tumor itself. Scale bar, 100  $\mu\text{m}$ . **(e)** Fibrous protein aggregates are shown in the peritumor coats of neurofibromas. TIAF1 is present in the fibrous aggregates ( $\times 400$  magnification). **(f)** R48-2 peptide was used to block the immunoreactivity in the negative control staining. **(g)** Metastatic 13-06-MG glioma cells were subcutaneously inoculated and shown to metastasize to the lung of a nude mouse. The growing tumor in the lung showed a high level expression of TIAF1 as compared with the normal lung of a nude mouse. Scale bar, 200  $\mu\text{m}$ ;  $\times 400$  magnification (IHC). A representative data set is shown from three repeats

Also, petri dishes were coated with various amounts of matrix proteins from DU145, followed by seeding with SK-N-SH cells. Two days later, SK-N-SH cells were harvested and shown to have increased levels of polymerized A $\beta$  (Figure 3c). The smallest unit of A $\beta$  is  $\sim 4$  kDa. Similar results were observed by culturing SK-N-SH cells on the matrix of many other types of cancer cells such as breast MCF7 and lung NCI-H1299 cells (data not shown).

We simulated the potential effects of brain metastatic cancer cells on neural cells by co-culturing. SK-N-SH cells were co-cultured with COS7 fibroblasts, followed by determining the expression of TIAF1. SK-N-SH cells were transiently overexpressed with enhanced cyan fluorescence protein (ECFP), and COS7 cells with EYFP. When both cells were co-cultured for 24 h, TIAF1 was not induced (Figures 3d and e). However, transiently overexpressed EYFP-WOX1

dramatically induced TIAF1 expression in COS7 cells (Figures 3d and e).

**Aggregating TIAF1 induces spontaneous activation of SMAD-responsive promoter in p53-deficient NCI-H1299 cells.** TIAF1 physically interacts with Smad4 and suppresses the SMAD-driven promoter activation.<sup>11</sup> When COS7 cells were transiently overexpressed with Smad4, in the presence of a SMAD promoter plasmid (containing green fluorescence protein (GFP) as reporter), the promoter became activated (Figure 4a). Transiently overexpressed TIAF1 blocked Smad4-induced promoter activation (Figure 4a). When p53-deficient NCI-H1299 cells were transfected with TIAF1 or WOX1, in the presence of the SMAD promoter plasmid, spontaneous activation of the promoter occurred (Figure 4b). TIAF1 was tagged with

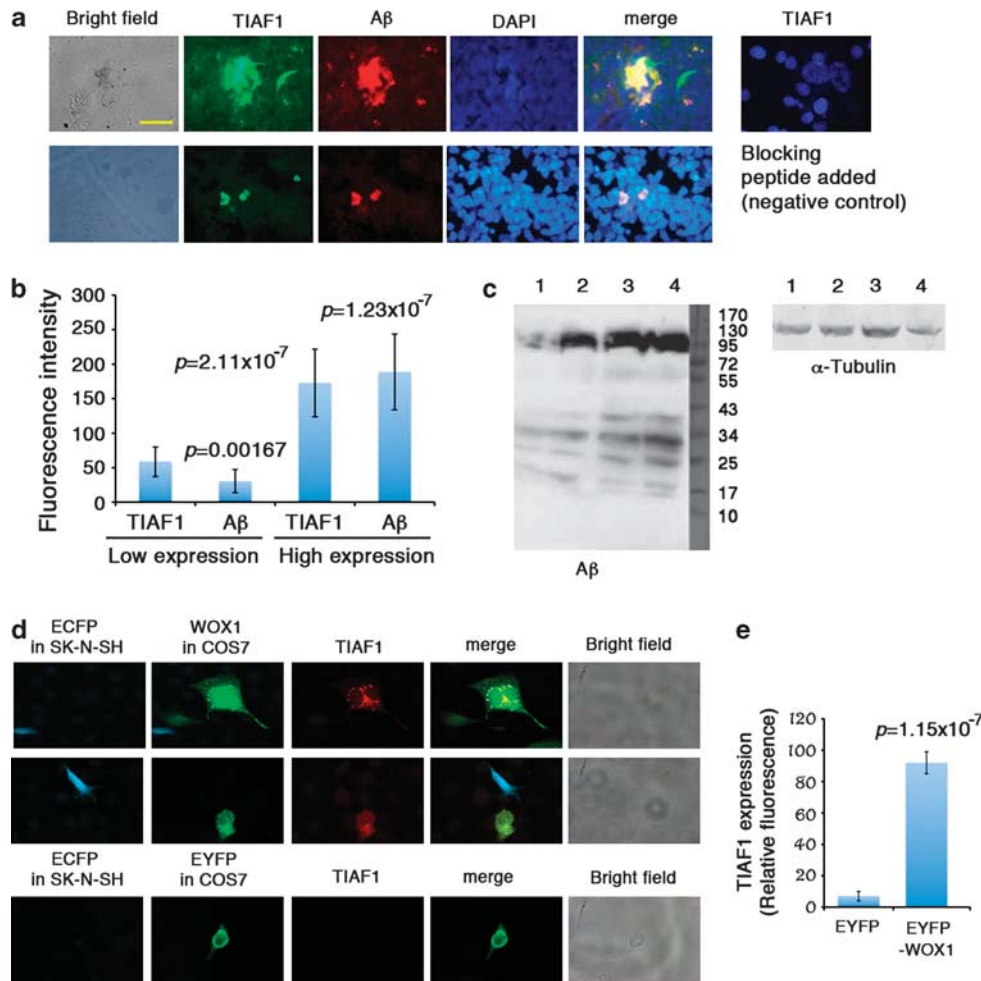


**Figure 3** ECM proteins induce the expression and aggregation of TIAF1 and A $\beta$ , and ectopic WOX1 upregulates TIAF1 expression. (a) Neuroblastoma SK-N-SH cells were cultured on the ECM of prostate DU145 cancer cells. Extracellular protein matrix from DU145 cells was prepared as described.<sup>11,16</sup> Note that TIAF1 and A $\beta$  protein aggregates are colocalized or exist alone. In negative controls, R48-2 blocking peptide was used in the immunostaining (merge of DAPI and TIAF1 images). Two representative data are shown from three experiments ( $\times 400$  magnification; 50 cells examined per experiment). (b) Data are tabulated for endogenous TIAF1 expression at low and high levels, relative to the expression of A $\beta$  (mean  $\pm$  S.D.; Student's *t*-test;  $n=3$ ; all data versus low expression TIAF1 controls).<sup>11,17,35,39</sup> In negative controls, cells were seeded onto serum proteins-coated matrix, which did not induce TIAF1 and A $\beta$  production. Fluorescence intensity was  $<25$ . (c) Petri dishes were coated with various amounts of matrix proteins from DU145, followed by seeding with SK-N-SH cells. Two days later, Western blotting for A $\beta$  expression was performed. A $\beta$  is polymerized to various sizes. The monomeric A $\beta$  is  $\sim 4$  kDa. Coated proteins: lane 1, 0  $\mu$ g; lane 2, 1  $\mu$ g; lane 3, 2  $\mu$ g; and lane 4, 4  $\mu$ g.  $\alpha$ -tubulin is regarded as protein-loading control. (d and e) SK-N-SH cells were expressed with ECFP, and COS7 cells with EYFP or EYFP-WOX1. Co-culture of ECFP-SK-N-SH and EYFP-COS7 cells did not result in induction of TIAF1 expression. However, ECFP-WOX1 alone was sufficient to induce TIAF1 expression in COS7 cells (mean  $\pm$  S.D.; Student's *t*-test;  $n=3$ ; 50 cells examined per experiment)<sup>11,17,35,39</sup>

*Discosoma species* red fluorescent protein (DsRed). However, when TIAF1 was tagged with monomeric DsRed, no spontaneous activation of the SMAD-governed promoter was observed (Figure 4b). TIAF1, tagged with DsRed, EGFP, ECFP or EYFP, tended to aggregate, whereas monomeric DsRed-TIAF1 (TIAF1dm) remained mainly as monomer.

**TIAF1 self-association induces expression of Smad4 and WOX1.** In agreement with our previous observations,<sup>11</sup> ectopic expression of TIAF1 tagged with ECFP or EYFP (ECFP-TIAF1 or EYFP-TIAF1) in breast MCF7 cells resulted in an increased self-binding, as determined by FRET (Förster resonance energy transfer) analysis (Figure 5a).<sup>11,17</sup> The TIAF1 self-binding led to an increased expression of Smad4,

and both Smad4 and TIAF1 colocalized in the cytoplasm and cellular protrusion (Supplementary Figure S10). TGF- $\beta$ 1 marginally reduced the effects (Figure 5a).

By non-reducing SDS-PAGE and western blotting, transiently overexpressed EGFP-TIAF1 induced the expression of Smad4 and WOX1 in MCF7 (Figure 5b) and other types of cancer cells (data not shown). TIAF1 self-polymerized, as the molecular sizes are  $>95$  kDa (TIAF1 monomer, 12 kDa; EGFP-TIAF1, 44 kDa). Prima-1, an activator of p53,<sup>18</sup> further increased TIAF1 polymerization by more than 200 kDa (Figure 5b). The induced Smad4 exhibited as a monomer (Figure 5b). Under the influence of ectopic TIAF1, WOX1 polymerized from a monomer  $\geq 46$  kDa (Figure 5b). In parallel, ectopic EGFP-TIAF1 formed cytoplasmic punctate aggregates, with concurrent expression of WOX1 (Figure 5c).

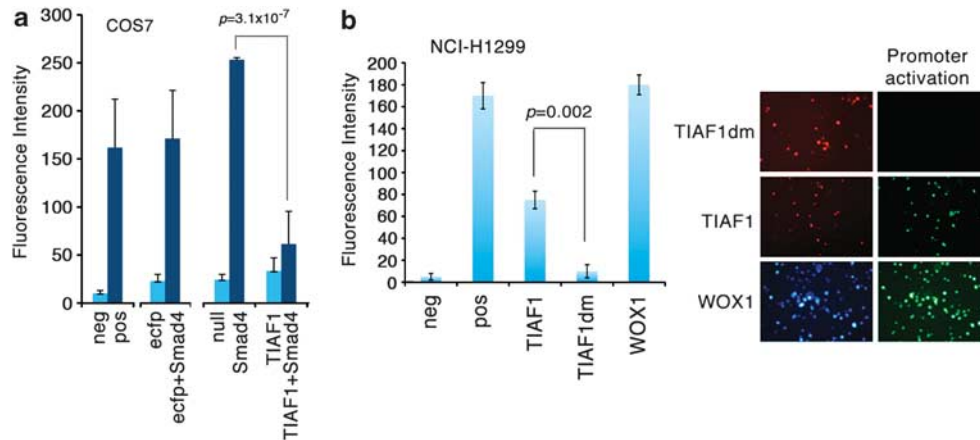


**Figure 4** TIAF1 self-aggregation is essential for causing spontaneous activation of a SMAD-responsive promoter in p53-deficient cells. **(a)** COS7 cells were transfected by liposome with plasmids for expressing ECFP, ECFP-Smad4, ECFP-TIAF1 and/or a GFP-reporting plasmid with a SMAD-responsive element.<sup>17,35</sup> In controls, cells were transfected with a negative or a positive plasmid. After 24 h, the cells were imaged by fluorescence microscopy. The extent of promoter activation was measured (mean  $\pm$  S.D.; Student's *t*-test;  $n = 3$ ).<sup>17,35</sup> Smad4 induced the promoter activation, whereas TIAF1 suppressed the effect. Similar results were observed by tagging Smad4 or TIAF1 with DsRed (data not shown). neg, negative control; pos, positive control; null, electroporation with medium only. **(b)** p53-deficient NCI-H1299 cells were transfected with DsRed-TIAF1, TIAF1dm or ECFP-WOX1, in the presence of the SMAD promoter plasmid. DsRed-TIAF1 induced spontaneous activation of the SMAD-governed promoter, whereas the monomeric DsRed had no effect. A representative set of promoter activation is shown (right panel). Both negative and positive controls were included in the experiments (mean  $\pm$  S.D.; Student's *t*-test;  $n = 3$ )

Both EGFP and dominant-negative EGFP-TIAF1<sup>11</sup> failed to induce WOX1 expression (Figure 5c). When TIAF1 was tagged with monomeric DsRed, no aggregate formation was observed (data not shown).

**Endogenous TIAF1 aggregate formation requires culturing two distinct cell types on non-self ECM.** By co-culturing both COS7 fibroblasts and neuroblastoma SK-N-SH cells on the ECM of prostate DU145 cells for 48 h, endogenous TIAF1 became punctate aggregates in the cytoplasm of both cells, as determined by using specific TIAF1(R48-2) antibody (top two rows; Figure 5d). WOX1 expression was also increased (Figure 5d). No TIAF1 aggregate formation was observed by culturing COS7 cells alone on the ECM (Figure 5d). Again, the R48-2 blocking peptide abolished the immunofluorescence (Figure 5d). The observations suggest that when two distinct types of cells encounter each other, endogenous TIAF1 aggregation may occur.

**TIAF1-/Smad4-binding induces generation of amyloid precursor protein (APP) and A $\beta$ .** p53-deficient NCI-H1299 cells were transiently overexpressed with ECFP-Smad4 and EYFP-TIAF1. The cells were treated with TGF- $\beta$ 1 for 24 h, which resulted in an increased generation of APP and A $\beta$  (Figure 5e). By FRET analysis, TGF- $\beta$ 1 increased the binding of Smad4 and TIAF1 (Figure 5e). Similar results were also obtained using p53-positive MCF7, COS7 and L929 cells (data not shown).

**TIAF1 is required for WOX1-, p53- and dominant-negative JNK1 (dnJNK1)-mediated apoptosis.** We examined whether TIAF1 participates in WOX1- and p53-mediated apoptosis. TGF- $\beta$ -sensitive mink lung epithelial Mv1Lu cells were transfected with expression constructs of WOX1 and/or

siRNA-targeting TIAF1 (TIAF1si)<sup>5,7</sup> by electroporation, followed by culturing for 48 h. In controls, a 'scrambled RNA' plasmid was used in transfection. When endogenous TIAF1 was knocked down by siRNA, WOX1-induced growth inhibition of Mv1Lu cells was blocked (Figure 6a).

Similarly, L929 cells were transfected with the expression plasmids of WOX1 and/or TIAF1si by electroporation, and were then grown in soft agarose for 3 weeks. Presence of live colonies was measured using MTS proliferation assay.<sup>7</sup> WOX1 significantly inhibited the anchorage-independent growth of L929 cells ( $P < 0.001$ ;  $n = 3$ ; Student's *t*-test), when compared with control cells transfected with the 'scrambled RNA' plasmid (Figure 6b). However, WOX1 did not inhibit the growth of TIAF1si-expressing cells ( $P > 0.05$ ;  $n = 3$ ; Student's *t*-test), suggesting that WOX1-induced growth suppression is TIAF1-dependent.

WOX1 and TIAF1 worked synergistically to induce cell death. Transient expression of low levels of WOX1 or TIAF1 did not cause L929 cell death ( $< 10\%$ ) (Figure 6c). When in combination, both WOX1 and TIAF1 significantly caused cell death ( $\sim 40\%$ ) (Figure 6c). Dominant-negative WOX1 (dnWOX1) alone did not induce cell death, in the absence or presence of TIAF1 (Figure 6c). dnWOX1 is known to block the apoptotic functions of p53 and WOX1.<sup>12-14,17</sup> Alteration of Tyr33 and Tyr61 in WOX1 abolishes its apoptotic function, and no enhancement of apoptosis occurred in the presence of TIAF1 (Figure 6c). Tyr61 is a conserved phosphorylation site and its phosphorylation status has been confirmed by specific antibody (Chang *et al.*, unpublished).

We determined whether TIAF1 or WOX1 knockdown causes resistance to p53-dependent apoptosis. L929 cells, which were stably transfected with a scramble, TIAF1si or WOX1si construct, were electroporated with an empty vector, a p53 or a dnJNK1 expression plasmid. In agreement with our previous studies,<sup>12,19,20</sup> both transiently overexpressed p53

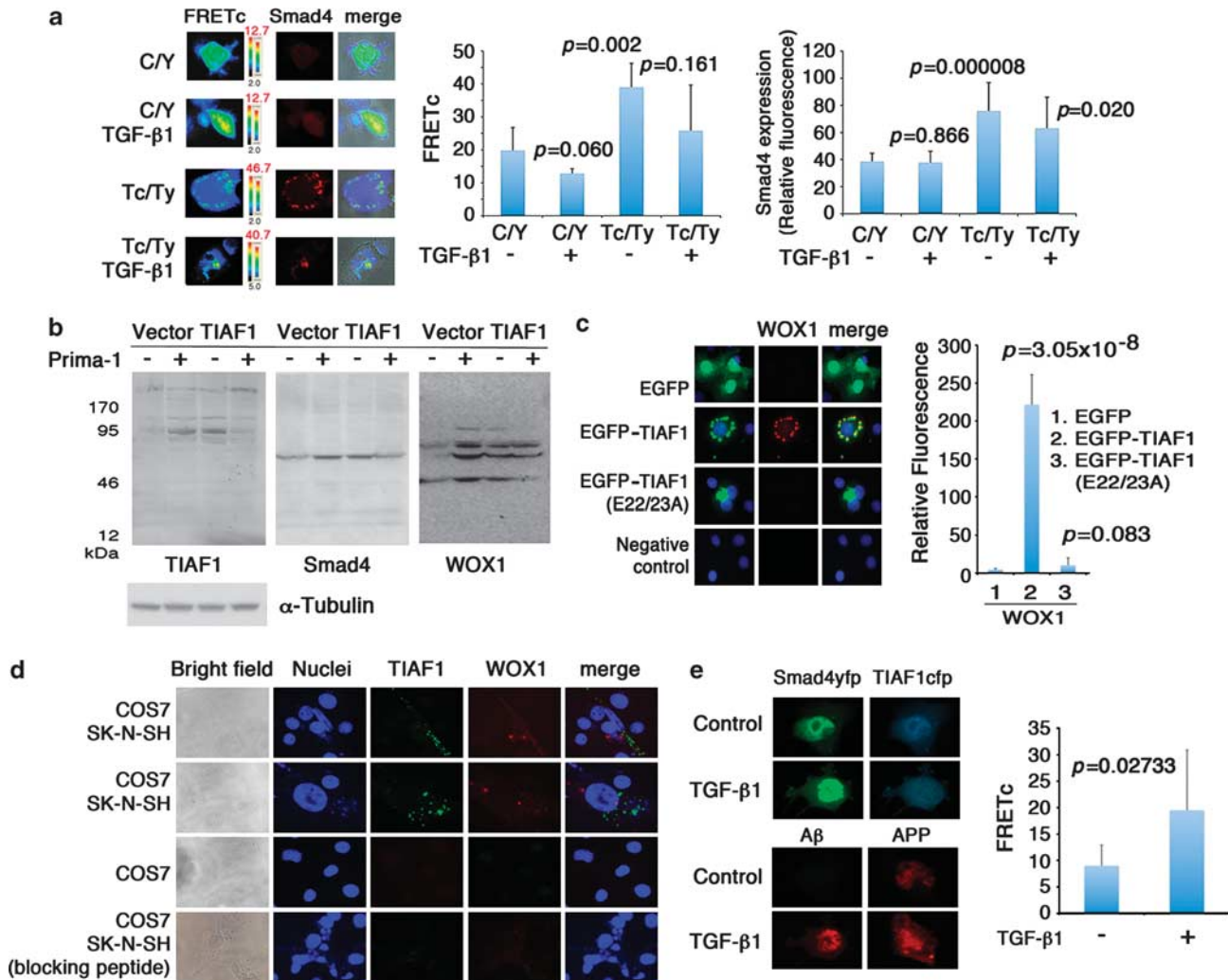


**Figure 5** TIAF1 self-association induces expression of Smad4 and WOX1. (a) MCF7 cells were transiently transfected with ECFP and EYFP (C/Y) or ECFP-TIAF1 and EYFP-TIAF1 (Tc/Ty) by liposome. The cells were treated with or without TGF- $\beta$ 1 (5 ng/ml) for 24 h. TIAF1 self-binding was analyzed by FRET microscopy.<sup>11,17,35</sup> FRETc shows the extent of protein/protein binding.<sup>11,17,35</sup> TIAF1 self-binding led to Smad4 expression, as determined by immunofluorescence staining. Statistical analysis: all tests *versus* C/Y controls; Student's *t*-test ( $n = 6$ ). The induced Smad4 colocalized with TIAF1 in the cytoplasm and the spiny protrusion ( $\times 400$  magnification; Supplementary Figure S10). (b) Transiently overexpressed EGFP-TIAF1 upregulates the expression of Smad4 and WOX1 in MCF7 (non-reducing SDS-PAGE) and other types of cancer cells (data not shown). Exposure of cells to Prima-1 (10  $\mu$ M) for 1 h to activate p53 resulted in increased polymerization of TIAF1 and WOX1, but not Smad4. (c) COS7 cells were transiently overexpressed with EGFP-TIAF1 or EGFP. Significantly increased expression of WOX1 is shown, where these proteins colocalize with TIAF1 aggregates, as determined using specific antibodies ( $n = 10$ ; mean  $\pm$  S.D.; experiments *versus* EGFP controls, Student's *t*-test). Dominant-negative TIAF1 (E22/23A) and EGFP failed to induce the indicated protein expression. (d) To stimulate endogenous TIAF1 aggregate formation, COS7 and/or SK-N-SH cells were co-cultured on the ECM of prostate DU145 cells for 48 h. Aggregate formation of endogenous TIAF1, along with WOX1 expression, is shown in the cytoplasm of both cells (top two rows). No TIAF1 aggregate formation was observed by culturing COS7 cells alone on the ECM (third row from the top). R48-2 blocking peptide abolished the immunofluorescence (bottom row). (e) NCI-H1299 cells were transiently overexpressed with ECFP-Smad4 and EYFP-TIAF1, followed by treating with TGF- $\beta$ 1 (5 ng/ml) for 24 h. Increased binding of Smad4 and TIAF1 positively correlates with upregulation of APP and A $\beta$

and dnJNK1 caused apoptosis of control cells (Figure 6d). TIAF1 or WOX1 knockdown cells resisted death caused by the transiently overexpressed p53 and dnJNK1 (Figure 6d). In contrast, when TIAF1 was knocked down in Mv1Lu cells, apoptosis caused by transiently overexpressed Smad4 was increased (subG1 phase; Figure 6e).

**TIAF1, WOX1 and p53 synergistically induce apoptosis and block anchorage-independent growth and cell migration.** We investigated whether TIAF1, WOX1 and

p53 act synergistically in causing apoptosis. L929 fibroblasts were grown on cover slips overnight, and co-transfected with non-apoptosis-inducing amounts of p53, WOX1 and/or TIAF1 plasmid constructs by the liposome-based Gene Fector (Venn Nova, Pompano Beach, FL, USA). The cells were then grown for 48 h. When in combination, TIAF1, p53 and WOX1 dramatically induced apoptosis in a synergistic manner ( $\sim 75\%$ ) (Figure 7a). The combination of TIAF1/p53, p53/WOX1 or TIAF1/WOX1 had a much less effect in inducing apoptosis (0–25%) (Figure 7a). Similar results were

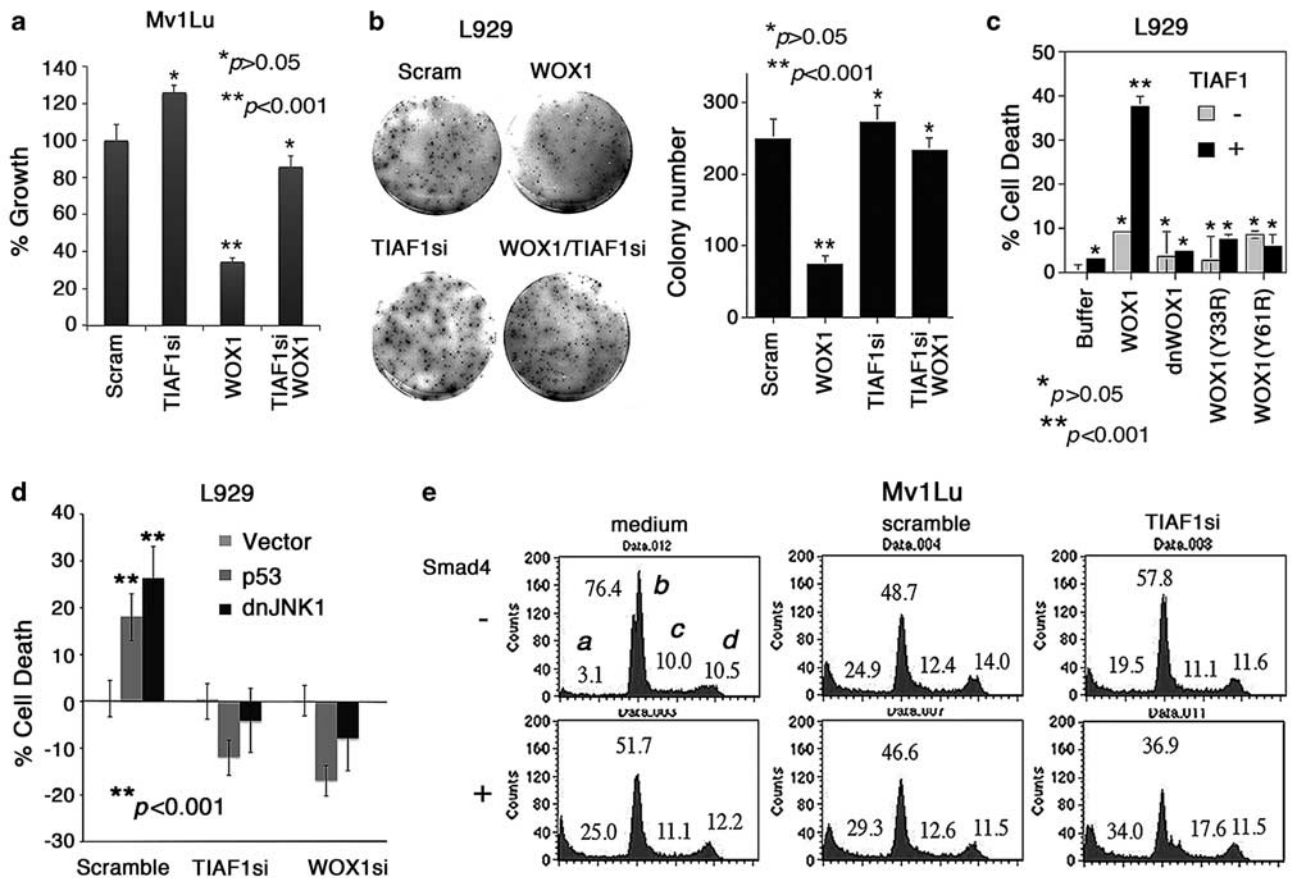


**Figure 6** TIAF1 is essential for apoptosis mediated by WOX1, p53 and dominant-negative JNK1. (a) Mv1Lu cells were transfected with expression plasmid constructs of WOX1 and/or TIAF1si by electroporation, followed by culturing for 48 h. The extent of cell growth was measured by MTS proliferation assay. TIAF1 knockdown cells resisted WOX1-induced growth inhibition ( $n = 8$ ; mean  $\pm$  S.D.; Student's *t*-test: experiments versus scramble controls). Scram = 'scrambled RNA' control plasmid. (b) L929 cells were transfected with WOX1 and/or TIAF1si plasmids, and then grown in soft agarose for 3 weeks to allow colony formation (measured by MTS proliferation assay) ( $n = 3$ ; Student's *t*-test: experiments versus scramble controls). (c) When L929 cells were transfected with WOX1 and TIAF1 plasmids ( $1.25 \mu\text{g}$  per  $10^6$  cells), both expressed proteins synergistically caused cell death ( $\sim 40\%$ ,  $n = 8$ ). Dominant-negative WOX1 (dnWOX1)<sup>17</sup> and phospho-WOX1 mutants (Y33R and Y61R)<sup>17</sup> failed to induce cell death, in the absence or presence of TIAF1 ( $n = 8$ ; Student's *t*-test: experiments versus scramble controls). (d) L929 stable transfectants, expressing a scramble, TIAF1si or WOX1si construct, were established. Transient overexpression of these cells with an empty vector, p53 or dnJNK1 construct was carried out, and the extent of cell death was measured in 48 h ( $n = 8$ ; Student's *t*-test: experiments versus scramble controls). When TIAF1 and WOX1 were knocked down, ectopic p53 and dnJNK1-induced cell death was blocked. (e) In contrast, when TIAF1 was knocked down, Smad4-induced apoptosis of Mv1Lu cells was enhanced (see subG1 phase; a representative data from two experiments). a, SubG1 phase; b, G0/G1 phase; c, S phase; d, G2/M phase

also observed in COS7, NCI-H1299 and other cells (data not shown).

When L929 cells were co-transfected with the above constructs, followed by performing anchorage-independent growth, TIAF1, p53 and WOX1 together dramatically suppressed colony formation by  $>95\%$  (Figure 7b). Each protein alone blocked colony formation by  $\sim 50\%$ , and that two proteins together increased the suppression up to 65–90% (Figure 7b). We have previously shown that p53 and TIAF1 together effectively block the anchorage-independent growth of L929 cells.<sup>7</sup>

In parallel experiments, ectopic expression of p53, WOX1 and TIAF1 significantly blocked the migration of L929 and breast MDA-MB231 cells during the observation for 16 h (Figure 7c and Supplementary Figure 11a). Non-apoptosis-inducing levels of expression plasmids for p53, WOX1 and TIAF1 were used in introducing into cells. The effect was observed by testing each protein alone or in various

combinations. Interestingly, under similar conditions, ectopic p53, WOX1 and TIAF1 in combination were less effective in blocking the migration of breast MCF7 than those of p53 and WOX1 alone (Supplementary Figure S11b).

Of particular note is that when normal cells such as fibroblasts and cardiomyocytes were expressed with p53, WOX1 and TIAF1, these cells became highly sensitive to death induced by cytokines TNF- $\alpha$  and TGF- $\beta$ 1 in 4 h (data not shown). Again, the observations suggest that p53, WOX1 and TIAF1 can act in concert to drive the cell death event.

## Discussion

In summary, we have determined that (1) TIAF1, along with Smad4 and  $A\beta$ , participates in the formation of peritumor capsules, which is crucial for solid tumor growth and protection; (2) under the stimulation of non-self ECM, endogenous TIAF1 is upregulated and undergoes

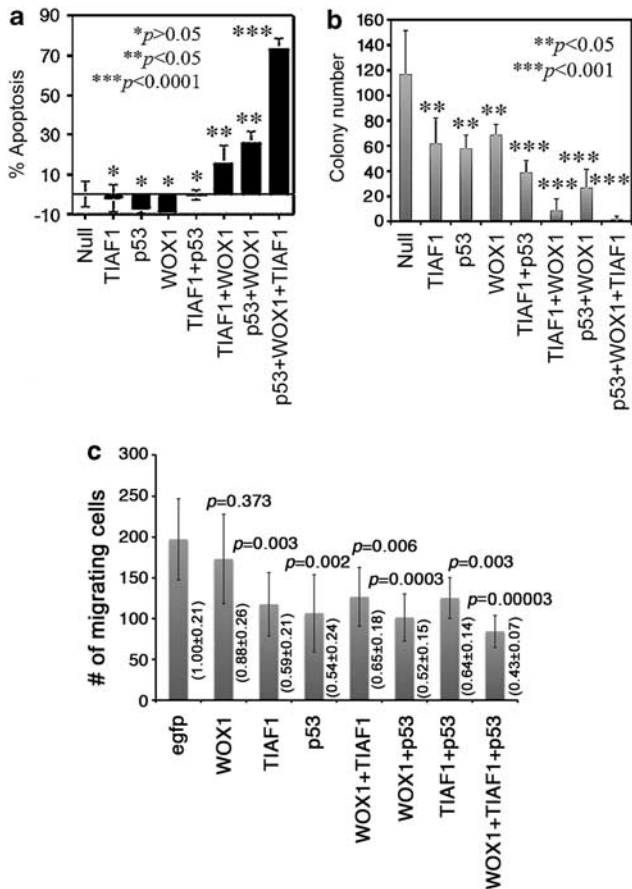


**Figure 7** TIAF1, WOX1 and p53 synergistically induce apoptosis, block cell migration and inhibit anchorage-independent growth. (a) L929 cells were co-transfected with non-apoptosis-inducing amounts of wild-type p53, WOX1 and/or TIAF1 plasmid constructs (2.5  $\mu$ g) by the liposome-based GeneFactor. The extent of cell death was measured by nuclear morphology. Nuclei were stained with DAPI (mean  $\pm$  S.D.;  $n = 8$ ; Student's *t*-test). (b) L929 cells were transfected with the above constructs by electroporation, and then subjected to performing anchorage-independent growth assay. After 3 weeks, the live cell colonies were measured by staining with the MTS proliferation assay (mean  $\pm$  S.D.;  $n = 8$ ; Student's *t*-test). (c) Under similar conditions, L929 cells were transfected with non-apoptosis-inducing amounts of wild-type p53, WOX1 and/or TIAF1 plasmid constructs. The transiently overexpressed p53, WOX1 and TIAF1, alone or in combinations, significantly blocked the migration of L929 cells (mean  $\pm$  S.D.;  $n = 3$ ; Student's *t*-test). *P* value is shown on the top of each bar. The number in each bracket is 'fold increase' in cell migration

aggregation, which binds Smad4 and blocks SMAD promoter activation;<sup>11</sup> (3) however, in the absence of p53, the aggregating TIAF1 activates the SMAD-governed promoter; (4) increased levels of TIAF1 induces WOX1 expression, and vice versa; (5) TIAF1 is essential in the p53- and WOX1-mediated cell death, and these proteins act synergistically in inducing cell death (Figure 8).

Alteration of TIAF1 levels appears to affect cancer progression. We showed that UVB-induced SCC formation in rats is associated with an initial upregulation of TIAF1, followed by reduction in the cancer. This expression profile positively correlates the expression of WOX1 protein during SCC development.<sup>15</sup> Also, TIAF1 is accumulated in developing metastatic tumor cells when growing in a new organ site.

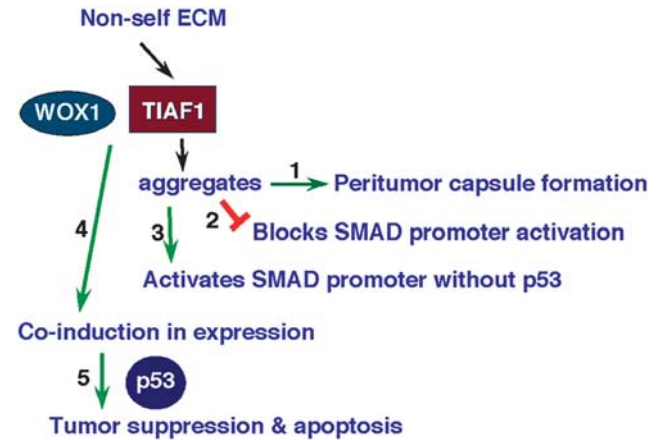


**Figure 8** TIAF1 aggregation and associated events. (1) Under environmental alterations (e.g., non-self ECM), endogenous TIAF1 is prone to aggregation, which is critical for supporting peritumor capsule formation; (2) During self-aggregation, TIAF1 binds Smad4 and blocks SMAD promoter activation; (3) Intriguingly, under p53-deficient conditions, aggregating TIAF1 supports the activation of the SMAD-governed promoter; (4) Overexpressed TIAF1 induces WOX1 expression, and vice versa; (5) TIAF1, p53 and WOX1 act synergistically in causing growth suppression and cell death

Once the metastatic solid tumors become established, TIAF1 is significantly downregulated. The observation suggests that TIAF1 is central to cancer progression. TIAF1 may exhibit as fibrous aggregates, together with Smad4, A $\beta$  and other proteins, in the stromal tissues of tumors and peritumor capsules. Also, both TIAF1 and Smad4 are co-present in the normal prostatic concretions in the lumens of prostatic glandular ducts, and they are intracellular proteins. How these proteins become secreted remains to be established. Whether the extracellular TIAF1 and Smad4 are functionally inactive is unknown.

A developing tumor circumvents pericellular and environmental challenges. It is not surprising to see dramatic upregulation or downregulation of critical proteins, either intracellular or extracellular, in a single cancer cell during division and continuous expansion.<sup>21,22</sup> For example, during metastasis, cancer cells frequently have reduced expression of tumor suppressors probably because of gene mutation or epigenetic inactivation.<sup>23,24</sup> These cells may utilize strategies by significantly increasing the production of TGF- $\beta$ , hyaluronan, hyaluronidases, metalloproteinases, gain-of-function isoforms of tumor suppressors and others to facilitate migration to target organs.<sup>25-27</sup> In contrast, at the benign stage, physical protection is built surrounding the peritumor area for allowing the growth and formation of a solid tumor.<sup>28,29</sup>

In our previous study, we have shown that TIAF1 aggregation in the hippocampus is essential for amyloid  $\beta$  deposition and formation of fibrils and plaques.<sup>11</sup> What leads to TIAF1 self-aggregation is largely unknown. We have determined that under the stress of cytokines or chemicals and/or alteration of pericellular matrix, TIAF1 becomes self-associated or aggregated.<sup>11</sup> In this study, we further demonstrated that upon co-culturing of COS7 and SK-N-SH cells on the ECM of

prostate DU145 cells, endogenous TIAF1 and WOX1 are upregulated and become aggregated. The observations support the scenario that an unfriendly environment induces endogenous TIAF1 aggregation. TGF- $\beta$  rapidly induces TIAF1 self-aggregation, which leads to apoptosis in a caspase-dependent manner in certain cells.<sup>11</sup> Overexpressed TIAF1 affects Smad signaling and transcriptional activation. TIAF1 binds Smad4 *in vivo*, and blocks Smad-dependent promoter activation. Accordingly, when TIAF1 protein expression is knocked down by siRNA, spontaneous accumulation of Smad proteins in the nucleus occurs, along with activation of the SMAD-regulated promoter.<sup>11</sup> Interestingly, TGF- $\beta$ 1 induces TIAF1 self-aggregation in a T $\beta$ RII-independent manner, and this may be related with binding of TGF- $\beta$ 1 to membrane hyaluronidase Hyal-2.<sup>17</sup> Indeed, TGF- $\beta$  is able to signal via a Smad-independent manner for activation of NF- $\kappa$ B and JNK,<sup>30</sup> induction of lymphoid enhancer-binding factor (Lef-1) transcription factor,<sup>31</sup> and terminal skeletal muscle differentiation.<sup>32</sup>

TIAF1 is a likely gatekeeper in regulating cancer progression. TIAF1 is upregulated during the early stage of SCC formation. The developed SCC tumor has reduced TIAF1 expression. In prostate cancer, TIAF1 is most upregulated in the cancerous stage, but is downregulated during cancer metastasis. Interestingly, the expression profile of tumor suppressor WOX1 exhibits similarly to that of TIAF1 during cancer progression *in vivo*.<sup>15,33,34</sup> That is, both WOX1 and TIAF1 are significantly upregulated during the early phases of benign tumor formation. However, both proteins are downregulated when tumors possess metastatic potential. We determined that ectopic WOX1 induces the expression of TIAF1. WOX1 is known to enhance the transcriptional activation of SMAD and NF- $\kappa$ B promoters,<sup>17,35</sup> suggesting that TIAF1 expression is controlled by both promoters. TIAF1 in turn induces the expression of Smad4 and A $\beta$ , depending upon the status of TIAF1 self-aggregation. TIAF1/A $\beta$  aggregates are 'natural and protective fences' for both cancer and neural cells, but are likely to induce neurodegeneration during long-term exposure.

TIAF1 self-binding is essential for increasing the expression of Smad4 and WOX1. The underlying mechanism is unknown. Interestingly, the induced Smad4 colocalizes with TIAF1, and WOX1 appears to undergo self-association or binding with other proteins. Smad4 is able to interrupt the TIAF1 aggregation.<sup>11</sup> We have shown that when cells possess a greater amount of TIAF1 than Smad4, these cells survive upon challenge with TGF- $\beta$ 1. However, when cells express a greater amount of Smad4 than TIAF1, they were highly sensitive to TGF- $\beta$ 1-induced apoptosis.<sup>11</sup> In this study, we have confirmed the observations by TIAF1 knock-down and shown increases in Smad4-mediated apoptosis. Thus, a dynamic balance between Smad4 and TIAF1 is critical for cell survival.

We provided supporting evidence that TIAF1 is essential in the p53, WOX1 and dnJNK1-mediated cell death. And, these proteins can act synergistically in inducing cell death. How TIAF1 has such crucial effects is unknown. Conceivably, a direct interaction between TIAF1 and WOX1 occurs, which further connects the binding with p53. This scenario needs further study.

## Materials and Methods

**Cell lines, prostate cancer tissue microarrays, cancer tissue sections, IHC, antibodies and synthetic peptides.** Cell lines used in the study were monkey kidney COS7 fibroblasts, murine L929 fibroblasts, mink lung Mv1Lu cells, human breast MCF7 and MDA-MB-231 cells, human lung NCI-H1299 cells, human neuroblastoma SK-N-SH cells and human prostate DU145 cells (American Type Culture Collections, Manassas, VA, USA). Purified human platelet-derived TGF- $\beta$ 1 and recombinant TGF- $\beta$ 1 were purchased from R&D Systems (Minneapolis, MN, USA) and PeproTech (Rocky Hill, NJ, USA), respectively. Prostate cancer tissue microarray slides (T-PP-2D), containing 75 samples each for control and cancer groups, respectively, were obtained from the Tissue Array Research Program, National Cancer Institute (Bethesda, MD, USA). In addition, human cancer tissue sections were obtained from the Department of Pathology, University of Colorado Health Sciences Center (by Dr. Cl Sze, before 2005). IRB approval was waived. Informed consents were obtained from the family members of the deceased patients. Also, cancer tissue sections were obtained from the MacKay Memorial Hospital, Taipei, Taiwan (by Dr. MF Chiang) with IRB approval. De-paraffinization, IHC and immunofluorescence staining were performed as described.<sup>11,36</sup> Presence of autofluorescence in each tissue section was examined by fluorescence microscopy. In most cases, we pre-blocked the autofluorescence of tissues by Sudan Black B (Sigma, St. Louis, MO, USA) before immunostaining.<sup>37</sup>

Specific homemade antibodies were against TIAF1(R48-2)<sup>5,11</sup> and WOX1.<sup>12,17,38</sup> The sequence of R48-2 peptide is NH-AAGDAGEESRVQLKNEVRR-COOH (amino acid #16–35; Genemed Synthesis, San Antonio, TX, USA). The TIAF1 (R48-2) antibody was used mainly for IHC and fluorescent immunostaining. Where indicated, this peptide (20  $\mu$ M) was used to absorb the produced TIAF1(R48-2) antibody (1  $\mu$ l) in negative control experiments for IHC and fluorescent immunostaining.<sup>36</sup> Also, we generated antibody TIAF1-R48-1 (amino acid #44–60; NH-VEQAYVDKVCVCGPSA-COOH) in rabbits, as described.<sup>12</sup> The following specific antibodies used were against: A $\beta$  (MCA2172, AbD/Serotec, Kidlington, UK),<sup>11</sup> APP (MAB348, Chemicon/Millipore, Temecula, CA, USA),<sup>11</sup> Smad4<sup>11</sup> (Santa Cruz Laboratory, Santa Cruz, CA, USA),  $\alpha$  tubulin (Sigma) and TIAF1 (Abcam).<sup>11</sup> Fluoro-Jade C (Millipore, Billerica, MA, USA) was used to stain degenerating neurons. Adobe Photoshop CS5 software was used to analyze the extent of protein expression from western blots.

**cDNA expression constructs and FRET.** TIAF1si, scrambled RNA and stable L929 cell transfectants were prepared as previously described.<sup>5,7</sup> TIAF1 and Smad4 were tagged with enhanced green fluorescence protein (EGFP; in pEGFP-C1, Clontech, Mountain View, CA, USA), ECFP in pECFP-C1 (Clontech) or DsRed in pDsRed (Clontech).<sup>5,7,17</sup> These are mammalian expression plasmids. Additional mammalian expression plasmids were WOX1, p53, dominant-negative TIAF1 (E22/23A), dnJNK1 and dnWOX1.<sup>7,12,17</sup> Where indicated, L929, MCF7, NCI-H1299 cells or other indicated cells were electroporated with the above constructs (200 V, 50 msec; Square Wave BTX ECM830, Genetronics, San Diego, CA, USA), cultured overnight and then treated with TGF- $\beta$ 1 for indicated times. Alternatively, the cells were transfected with the aforementioned DNA constructs using liposome-based GeneFactor (Venn Nova). Whole cell lysates were prepared in the presence of a cocktail of protease inhibitors (Sigma). The extent of protein expression was determined using indicated specific antibodies in each indicated experiment. FRET analysis for bimolecular interactions was carried out as described.<sup>11,17,35</sup> Briefly, cells were stimulated with an excitation wavelength of 440 nm. FRET signals were detected at an emission wavelength of 535 nm. ECFP and EYFP were used as donor and acceptor fluorescent molecules, respectively. The FRET images were corrected for background fluorescence from an area free of cells. The spectrally corrected FRET concentration (FRETc) was calculated using a software program (Image-Pro Plus 6.1, Media Cybernetics, Bethesda, MD, USA) using Youvan's equation:

$$\text{FRETc} = (\text{fret}[\text{fret}]) - \text{cf}[\text{don}] \times (\text{don} - \text{bk}[\text{don}]) - \text{cf}[\text{acc}] \times (\text{acc} - \text{bk}[\text{acc}]),$$

where fret = fret image, bk = background, cf = correction factor, don = donor image and acc = acceptor image. The equation normalizes the FRET signals to the expression levels of the fluorescent proteins.

**Quantification of fluorescent images.** Fluorescent or immunofluorescent microscopy was performed using a NIKON TE2000-U microscope (Nikon, Tokyo, Japan), as described.<sup>11,17,35,39</sup> For prostate cancer tissue microarray slides, the relative extent of protein expression in each section was quantified

using the histogram tool of the Nikon's EIS Elements BR3.2 software (Nikon). Each slide was quantified independently by two laboratory researchers. For cultured cell images, the relative fluorescence intensities of whole cells or individual punctates were quantified by Photoshop (under the Histogram and Marquee or Quick Selection tools, Adobe Photoshop CS5) and by Nikon's software. For each control or experiment, 20–100 cells were examined in 3–5 experiments. Presented data were from analyses by Photoshop.

**Cell proliferation assay and flow cytometry.** MTS tetrazolium assay (CellTiter 96 AQueous OneSolution Cell Proliferation Assay, Promega, Madison, WI, USA) was used to measure the extent of cell and colony growth.<sup>7</sup> In addition, cells were transfected with the TIAF1 or indicated constructs by electroporation and cultured for 24–48 h, followed by determining the extent of apoptosis and growth suppression by cell cycle analysis using a fluorescence-activated cell sorting/flow cytometry machine (BD, Sparks, MD, USA), as described.<sup>7,39</sup>

**UVB irradiation on hairless mouse skin.** The *in vivo* experiments were performed, as described.<sup>15</sup> An approved protocol for animal use was obtained from the Institutional Animal Care and Use Committee of the National Cheng Kung University Medical College. Briefly, hairless SKH-hr1 female mice, 6-week-old, were obtained from Charles River Laboratories (Wilmington, MA, USA). The mice were housed in individual cages in a room with a constant temperature and humidity and an alternating 12-h light and dark cycle, and fed *ad libitum* with a commercial diet and water. To examine acute response, three mice were exposed to UVB (2.16 kJ/m<sup>2</sup>; 312 nm) once using a BLE-8T312 UV lamp (Spectronics, Westbury, NY, USA), and the mice were killed 1 day later. To determine chronic response, mice were exposed to UVB thrice per week (Monday, Wednesday and Friday) starting with 0.36 kJ/m<sup>2</sup>, respectively, for 1 and 5 months ( $n = 3$ ), followed by increasing 100% weekly. After week 10, a consistent dose of UVB irradiation (2.16 kJ/m<sup>2</sup>) was given over the next 8 weeks. In a control group, mice received no UVB irradiation. Skin tissue sections were prepared<sup>15</sup> and processed for IHC staining using TIAF1(R48-2) antibody.

**Cell migration or wound healing assay.** Cell lines, including breast MDA-MB-231 and MCF cells and murine L929 fibroblasts, were transiently transfected with expression constructs for p53, TIAF1 and/or WOX1 cDNA by electroporation.<sup>5,12,17</sup> Cell migration assay was performed by using Culture-Inserts (ibidi, Verona, WI, USA) in the petridishes, as described.<sup>40</sup> A culture insert was placed on a 35-mm dish, and an equal number of cells ( $2.8 \times 10^4$  cells in 70  $\mu$ l RPMI or DMEM medium) were seeded into the two reservoirs of the same insert, so as to generate a  $500 \pm 50 \mu$ m gap between two cell populations. After 24-h incubation at 37 °C with 5% CO<sub>2</sub>, the insert was gently removed and the medium was removed. Migration experiments were then conducted under serum-free medium. The extent of cell migration was imaged for indicated times using the NIKON TE2000-U microscope.<sup>17,39</sup>

**Data analysis.** All experiments indicated above were performed 2–5 times. Data were presented as mean  $\pm$  S.D. Student's *t*-tests were performed for statistical analysis where indicated.

### Conflict of Interest

The authors declare no conflict of interest.

**Acknowledgements.** This research was supported, in part, by the Department of Defense USA (DAMD17-03-1-0736 and W81XWH-08-1-0682), the Guthrie Foundation for Education and Research the National Science Council, Taiwan, ROC (NSC96-2320-B-006-014, 98-2628-B-006-045-MY3, 98-2628-B-006-041-MY3, and 99-2320-B-006-012-MY3), the National Health Research Institute, Taiwan, ROC (NHRI-EX99-9704BI), the National Cheng Kung University Landmark Projects (C0167) and the Department of Health, Taiwan, ROC (DOH101-TD-PB-111-TM010) (to NS Chang). Technical assistance of Jane CY Lu is appreciated.

### Author Contributions

MFC, FJL, HMS and CIS provided IRB-approved clinical samples. JYC, SJC, CCH and THH carried out immunohistochemistry. MHL and LYY made DNA constructs. JYC, SRL, MHL, HH, PYC, YAC, and

NSC performed experiments. NSC conceived the project, designed experiments, performed imaging analyses, analyzed data and wrote the manuscript. YAC, PYC, HH, FJL, CIS and NSC proofread the manuscript.

1. Wahl SM, Wen J, Moutsopoulos N. TGF-beta: a mobile purveyor of immune privilege. *Immunol Rev* 2006; **213**: 213–227.
2. Mantel PY, Schmidt-Weber CB. Transforming growth factor-beta: recent advances on its role in immune tolerance. *Methods Mol Biol* 2011; **677**: 303–338.
3. Meulmeester E, Ten Dijke P. The dynamic roles of TGF- $\beta$  in cancer. *J Pathol* 2011; **223**: 205–218.
4. Tian M, Neil JR, Schiemann WP. Transforming growth factor- $\beta$  and the hallmarks of cancer. *Cell Signal* 2011; **23**: 951–962.
5. Chang NS, Mattison J, Cao H, Pratt N, Zhao Y, Lee C. Cloning and characterization of a novel transforming growth factor- $\beta$ 1-induced TIAF1 protein that inhibits tumor necrosis factor cytotoxicity. *Biochem Biophys Res Commun* 1998; **253**: 743–749.
6. Khera S, Chang NS. TIAF1 participates in the transforming growth factor  $\beta$ 1-mediated growth regulation. *Ann NY Acad Sci* 2003; **995**: 11–21.
7. Schultz L, Khera S, Sleve D, Heath J, Chang NS. TIAF1 and p53 functionally interact in mediating apoptosis and silencing of TIAF1 abolishes nuclear translocation of serine 15-phosphorylated p53. *DNA Cell Biol* 2004; **23**: 67–74.
8. van der Leij J, van den Berg A, Albrecht EW, Blokzijl T, Roozendaal R, Gouw AS *et al*. High expression of TIAF-1 in chronic kidney and liver allograft rejection and in activated T helper cells. *Transplantation* 2003; **75**: 2076–2082.
9. Pfoertner S, Jeron A, Probst-Kepper M, Guzman CA, Hansen W, Westendorf AM *et al*. Signatures of human regulatory T cells: an encounter with old friends and new players. *Genome Biol* 2006; **7**: R54.
10. Griseri P, Vos Y, Giorda R, Gimelli S, Beri S, Santamaria G *et al*. Complex pathogenesis of Hirschsprung's disease in a patient with hydrocephalus, vesico-ureteral reflux and a balanced translocation t(3;17)(p12;q11). *Eur J Hum Genet* 2009; **17**: 483–490.
11. Lee MH, Lin SR, Chang JY, Schultz L, Heath J, Hsu LJ *et al*. TGF- $\beta$  induces TIAF1 self-aggregation via type II receptor-independent signaling that leads to generation of amyloid  $\beta$  plaques in Alzheimer's disease. *Cell Death Dis* 2010; **1**: e110.
12. Chang NS, Pratt N, Heath J, Schultz L, Sleve D, Carey GB *et al*. Hyaluronidase induction of a WW domain-containing oxidoreductase that enhances tumor necrosis factor cytotoxicity. *J Biol Chem* 2001; **276**: 3361–3370.
13. Chang NS, Hsu LJ, Lin YS, Lai FJ, Sheu HM. WW domain-containing oxidoreductase: a candidate tumor suppressor. *Trends Mol Med* 2007; **13**: 12–22.
14. Chang JY, He RY, Lin HP, Hsu LJ, Lai FJ, Hong Q *et al*. Signaling from membrane receptors to tumor suppressor WW domain-containing oxidoreductase. *Exp Biol Med* 2010; **235**: 796–804.
15. Lai FJ, Cheng CL, Chen ST, Wu CH, Hsu LJ, Lee JY *et al*. WOX1 is essential for UVB irradiation-induced apoptosis and down-regulated via translational blockade in UVB-induced cutaneous squamous cell carcinoma *in vivo*. *Clin Cancer Res* 2005; **11**: 5769–5777.
16. Chang NS, Joki N, Mattison J, Dinh T, John S. Characterization of serum adhesive proteins that block tumor necrosis factor-mediated cell death. *Cell Death Differ* 1997; **4**: 779–786.
17. Hsu LJ, Schultz L, Hong Q, Van Moer K, Heath J, Li MY *et al*. Transforming growth factor beta1 signaling via interaction with cell surface Hyal-2 and recruitment of WWOX/FOX1. *J Biol Chem* 2009; **284**: 16049–16059.
18. Bykov VJ, Selivanova G, Wiman KG. Small molecules that reactivate mutant p53. *Eur J Cancer* 2003; **39**: 1828–1834.
19. Chang NS. Hyaluronidase activation of c-Jun N-terminal kinase is necessary for protection of L929 fibrosarcoma cells from staurosporine-mediated cell death. *Biochem Biophys Res Commun* 2001; **283**: 278–286.
20. Hong Q, Hsu LJ, Schultz L, Pratt N, Mattison J, Chang NS. Zfra affects TNF-mediated cell death by interacting with death domain protein TRADD and negatively regulates the activation of NF-kappaB, JNK1, p53 and WOX1 during stress response. *BMC Mol Biol* 2007; **8**: 50.
21. Di Fiore F, Sesboué R, Michel P, Sabourin JC, Frebourg T. Molecular determinants of anti-EGFR sensitivity and resistance in metastatic colorectal cancer. *Br J Cancer* 2010; **103**: 1765–1772.
22. Fröhlich E. Proteases in cutaneous malignant melanoma: relevance as biomarker and therapeutic target. *Cell Mol Life Sci* 2010; **67**: 3947–3960.
23. Golubovskaya VM, Cance W. Focal adhesion kinase and p53 signal transduction pathways in cancer. *Front Biosci* 2010; **15**: 901–912.
24. Taylor MA, Parvani JG, Schiemann WP. The pathophysiology of epithelial-mesenchymal transition induced by transforming growth factor-beta in normal and malignant mammary epithelial cells. *J Mammary Gland Biol Neoplasia* 2010; **15**: 169–190.
25. Simpson MA, Lokeshwar VB. Hyaluronan and hyaluronidase in genitourinary tumors. *Front Biosci* 2008; **13**: 5664–5680.

26. Perera M, Tsang CS, Distel RJ, Lacy JN, Ohno-Machado L, Ricchiuti V *et al*. TGF-beta1 interactome: metastasis and beyond. *Cancer Genomics Proteomics* 2010; **7**: 217–229.
27. Kraljevic Pavelic S, Sedic M, Bosnjak H, Spaventi S, Pavelic K. Metastasis: new perspectives on an old problem. *Mol Cancer* 2011; **10**: 22.
28. Schaller BJ, Buchfelder M. Neuroprotection in primary brain tumors: sense or nonsense? *Expert Rev Neurother* 2006; **6**: 723–730.
29. Stern R. Association between cancer and "acid mucopolysaccharides": an old concept comes of age, finally. *Semin Cancer Biol* 2008; **18**: 238–243.
30. Mao R, Fan Y, Mou Y, Zhang H, Fu S, Yang J. TAK1 lysine 158 is required for TGF- $\beta$ -induced TRAF6-mediated Smad-independent IKK/NF- $\kappa$ B and JNK/AP-1 activation. *Cell Signal* 2011; **23**: 222–227.
31. Cordray P, Satterwhite DJ. TGF-beta induces novel Lef-1 splice variants through a Smad-independent signaling pathway. *Dev Dyn* 2005; **232**: 969–978.
32. Droguett R, Cabello-Verrugio C, Santander C, Brandan E. TGF-beta receptors, in a Smad-independent manner, are required for terminal skeletal muscle differentiation. *Exp Cell Res* 2010; **316**: 2487–2503.
33. Watanabe A, Hippo Y, Taniguchi H, Iwanari H, Yashiro M, Hirakawa K *et al*. An opposing view on WWOX protein function as a tumor suppressor. *Cancer Res* 2003; **63**: 8629–8633.
34. Chang NS, Schultz L, Hsu LJ, Lewis J, Su M, Sze CI. 17beta-estradiol upregulates and activates WOX1/WWOXv1 and WOX2/WWOXv2 *in vitro*: potential role in cancerous progression of breast and prostate to a premetastatic state *in vivo*. *Oncogene* 2005; **24**: 714–723.
35. Li MY, Lai FJ, Hsu LJ, Lo CP, Cheng CL, Lin SR *et al*. Dramatic co-activation of WWOX/WOX1 with CREB and NF-kappaB in delayed loss of small dorsal root ganglion neurons upon sciatic nerve transection in rats. *PLoS One* 2009; **4**: e7820.
36. Chen ST, Chuang JI, Cheng CL, Hsu LJ, Chang NS. Light-induced retinal damage involves tyrosine 33 phosphorylation, mitochondrial and nuclear translocation of WW domain-containing oxidoreductase *in vivo*. *Neuroscience* 2005; **130**: 397–407.
37. Oliveira VC, Carrara RC, Simoes DL, Saggiaro FP, Carlotti CG Jr, Covas DT *et al*. Sudan Black B treatment reduces autofluorescence and improves resolution of in situ hybridization specific fluorescent signals of brain sections. *Histol Histopathol* 2010; **25**: 1017–1024.
38. Sze CI, Su M, Pugazhenthil S, Jambal P, Hsu LJ, Heath J *et al*. Down-regulation of WW domain-containing oxidoreductase induces Tau phosphorylation *in vitro*. A potential role in Alzheimer's disease. *J Biol Chem* 2004; **279**: 30498–30506.
39. Lin HP, Chang JY, Huang SS, Lin SR, Lee MH, Hsu LJ *et al*. Phorbol ester dissociates an *in vivo* MEK/WOX1 complex for switching on a novel type of apoptosis in T lymphocytes. *Genes Cancer* 2011; **2**: 550.
40. Goyal P, Behring A, Kumar A, Siess W. STK35L1 associates with nuclear actin and regulates cell cycle and migration of endothelial cells. *PLoS One* 2011; **6**: e16249.



**Cell Death and Disease** is an open-access journal published by Nature Publishing Group. This work is licensed under the Creative Commons Attribution-NonCommercial-No Derivative Works 3.0 Unported License. To view a copy of this license, visit <http://creativecommons.org/licenses/by-nc-nd/3.0/>

Supplementary Information accompanies the paper on Cell Death and Disease website (<http://www.nature.com/cddis>)